DOCTOR OF PHILOSOPHY

Sclerochronology at St Kilda

A study of late Holocene climate and hydrography on the western Scottish shelf using the shells of long-lived bivalve molluscs

Alexandroff, Stella

Award date:
2022

Awarding institution:
Bangor University

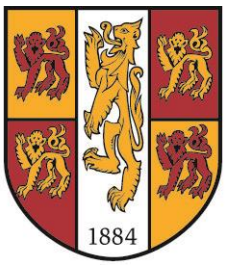

PRIFYSGOL
BANGOR
UNIVERSITY

Sclerochronology at St Kilda:

A study of late Holocene climate and hydrography on the western Scottish shelf using the shells of long-lived bivalve molluscs

A thesis submitted in fulfilment of the degree of Doctor of Philosophy

March 2022

Stella J. Alexandroff

School of Oceans Sciences, Bangor University,

Menai Bridge, Anglesey, UK, LL59 5AB

Declaration

I hereby declare that this thesis is the results of my own investigations, except where otherwise stated. All other sources are acknowledged by bibliographic references. This work has not previously been accepted in substance for any degree and is not being concurrently submitted in candidature for any degree unless, as agreed by the University, for approved dual awards.

Yr wyf drwy hyn yn datgan mai canlyniad fy ymchwil fy hun yw'r thesis hwn, ac eithrio lle nodir yn wahanol. Caiff ffynonellau eraill eu cydnabod gan droednodiadau yn rhoi cyfeiriadau eglur. Nid yw sylwedd y gwaith hwn wedi cael ei dderbyn o'r blaen ar gyfer unrhyw radd, ac nid yw'n cael ei gyflwyno ar yr un pryd mewn ymgeisiaeth am unrhyw radd oni bai ei fod, fel y cytunwyd gan y Brifysgol, am gymwysterau deuol cymeradw.

Acknowledgements

First of all, I want to thank my supervisors **Prof. James Scourse** and **Dr Paul Butler** for introducing me to the world of sclerochronology and for all their advice and support. Their enthusiasm is contagious, and the respectful, sincere and friendly way in which they treat colleagues and students is inspiring. Thank you, I could not have wished for better supervisors than you.

This work was part of the Initial Training Network ARAMACC (Annually Resolved Archives of Marine Climate Change; project 604802) funded by the EU within the framework of Marie Skłodowska-Curie Actions. The NERC Facility for Scientific Diving funded and carried out diving campaigns to retrieve additional shell samples. Many thanks to **Dr Martin Sayer** (now at Tritonia Scientific) and his team for their hard work and for bringing me all these beautiful *Arctica* shells. I thank the **crew of the RV *Prince Madog*** for the support before and during the research cruise, and all researchers aboard that helped me with the sample collection. The annual *Arctica* $\delta^{18}O$ sampling was funded by NERC and carried out at the National Environmental Isotope Facility — many thanks to **Prof. Melanie Leng** in particular. Thank you to **David Johns** from the Continuous Plankton Recorder Survey for preparing and sending me the plankton data and providing friendly advice.

Special thanks to **Prof. Bernd Schöne** for welcoming me at the Department of Palaeontology at the University of Mainz where I learned a lot about stable isotope mass spectrometry during a one-month secondment. Many thanks to **Prof. Paula Reimer**, **Ron Reimer**, and **Julia Simpson** for hosting me at the ^{14}CHRONO Centre, and for the radiocarbon analysis and friendly support.

I want to thank all supervisors and partners in ARAMACC for their friendly advice, and all my PhD colleagues in ARAMACC for the scientific exchange and the fun we had together. I particularly thank **Dr Tamara Trofimova** for being a wonderful roommate on our many science trips, and my close sclero friend with whom I can always talk about shell and life issues.

Thanks to **Dr Martyn Roberts**, **Dr Jessica Vaughan**, and **Gwyn Hughes**, for their technical support in the labs and for always brightening my day with their friendly nature. Thank you to **Sophie Slater** for her help with processing *Arctica* shells and to **Alexander Lee** for providing much of the groundwork for the *Arctica* chronology — it was a pleasure to work with both of you. Thank you **Dr Philip Hollyman** for performing Raman spectroscopy on the fossil shells and for all your kindness — you truly are golden.

Throughout my PhD, I have had the privilege of working among brilliant friends and colleagues that I could always count on when I was seeking advice or support. I thank all my PhD colleagues, all academic, administrative, and technical staff, for making the work environment at SOS Bangor an exceptionally friendly and inspiring one. Some I have already mentioned above, but special thanks also go to **Dr Alejandro Román González**, who taught me sclero lab techniques and who was always ready to lend me a hand or an ear, or tell me (pretty bad) jokes when I needed it. My friend **Dr Jennifer Jeffery (Shepperson)** was one of the reasons why I loved going to work — thank you for the coffee breaks, walks, and kitchen chats that gave me perspective and a welcome mental rest before going back to staring at shells.

I could of course not have done any of this without the loving support of **my family and friends**, to whom I am forever grateful. Thank you to **Camilo** for his constant support, encouragement, and patience throughout the years, and for helping me learn to trust my own judgement. Tack så mycket och många kramar!

Summary

The North Atlantic region is a key component of the global climate system. However, the lack of long-term observations hampers our understanding of the natural variability of this region. In recent decades, bivalve sclerochronology has emerged as a field providing high-quality proxy data that can help fill these gaps and reflect marine variability at different timescales. This thesis presents centennial-scale, annually resolved sclerochronological records of hydrographic and climatic variability at St Kilda, a volcanic archipelago on the western Scottish shelf. Two floating chronologies were constructed using fossil shells of the bivalve *Glycymeris glycymeris* and dated to the 4th millennium before present (BP). In addition, a modern chronology was built with live- and dead-collected *Arctica islandica*, spanning 1889–2015 CE. Sub-annual $\delta^{18}O_c$ data were obtained from fossil and live *G. glycymeris* and from modern *A. islandica* as a proxy for sea surface temperatures (SSTs). The growth season of both *G. glycymeris* and *A. islandica* at this location lasts from May to October, with most growth occurring before the temperature peak in August. Thus, the floating chronologies and the modern *Arctica* chronology represent late-spring and summer SSTs. The annual temperature range was 4.4 °C in the fossil shells, which is similar to the range observed today (3.8 °C). Average SSTs reconstructed from the fossil shells were similar to the late 19th century CE and 1 °C cooler than today. The similarity in growth season and temperature range between the fossil and modern specimens can be attributed to similar boundary conditions in the fourth millennium BP compared to today. In the final results chapter of this thesis, the modern *Arctica* growth chronology and an associated annually resolved $\delta^{18}O_c$ series were compared to biological and environmental data and climate indices. Significant correlations were found between *Arctica* growth variability and changes in primary production, regional SSTs, zonal wind pressure, and sea level pressure. This work thus establishes that St Kilda is appropriately sited to study large-scale marine climatic variability using bivalve sclerochronology. Moreover, the *Arctica* chronology was positively correlated with variability in population size of the Soay sheep living on Hirta, St Kilda, which demonstrates the tight coupling of the marine and terrestrial environments at this remote location.

Table of contents

Chapter 1

General introduction

Chapter 1 — General introduction

Today's climate is rapidly changing. Global surface temperatures have increased by 1 °C since the late 19th century CE, causing significant adverse impacts and losses to marine and terrestrial ecosystems (IPCC, 2022). Global warming is projected to be highly likely to exceed 1.5 °C in the near term, which would cause further, in some cases irreversible, damage to ecosystems and human societies (IPCC, 2022). These impacts and risks are becoming increasingly complex, as multiple climate hazards occur simultaneously and interact with each other across different regions and systems (IPCC, 2022). To quantify and understand the current changes and to model future changes and responses, it is indispensable to have robust evidence-based records of the natural variability of the climate and environmental systems. These records need to be sufficiently long to provide a meaningful baseline and to reflect natural variability at different timescales. However, observations are scarce, generally short, and often intermittent — this is particularly true for the ocean.

The ocean covers 71% of Earth's surface and contains 97% of Earth's water. With 50 times as much carbon and 1000 times as much heat capacity as the atmosphere, the ocean plays a dominant role in moderating the temperature of the earth at various timescales (Schmitt, 2018, and references therein). Over the past few decades, the ocean has absorbed over 90% of the global warming induced by carbon emissions (e.g., Trenberth et al., 2014; Wijffels et al., 2016). In addition to its central role in our climate system, the ocean is also a crucial source of food and ecosystem services, on which the livelihood of a large part of humankind depends (e.g., Cheung et al., 2010).

Despite its essential role in regulating global climate, the ocean has often been underrepresented in climate action and sustainability plans in the past decades. However, the most recent version of the Paris Agreement calls for a focus on ocean research (UNFCCC, 2021), and UNESCO has declared 2021–2030 to be the "United Nations Decade of Ocean Science for Sustainable Development" (IOC-UNESCO, 2021). While the scientific community has made great progress in expanding ocean observations in the past 30 years (Schmitt, 2018,

and references therein), the lack of long-term observations is a significant barrier to our understanding of the ocean's role in the natural variability of the coupled ocean-atmosphere climate system. There is, however, an increasingly significant approach to extending ocean measurements back in time: this is the use of reconstructions based on proxy data from natural (biogenic and sedimentary) marine archives.

1.1 North Atlantic climate

The North Atlantic region is a key component of the global climate system. Deep-water formation in the northern North Atlantic and Arctic seas is a major driver of the global meridional overturning circulation, often referred to as the "global conveyor belt". The Atlantic sector of this meridional overturning circulation (AMOC) plays a crucial role in the global redistribution of heat, carbon, and nutrients, and has been implicated in abrupt climatic shifts (e.g., Buckley and Marshall, 2015). The exact mechanisms of the AMOC have not yet been resolved, but they are thought to be a combination of both vertical mixing processes and wind-induced upwelling (Kuhlbrodt et al., 2007; Rahmstorf, 2015; Toggweiler and Key, 2001). The vertical mixing component of the circulation is described in the concept of "thermohaline circulation", a term that has been widely used in oceanographic literature for the past 100 years (e.g., Defant, 1929). The key features of the overturning circulation are (1) deep-water formation, (2) deep water currents, (3) upwelling of deep waters, and (4) spreading of surface and sub-surface waters through near-surface currents. A very simplified overview of these key features in the AMOC can be described as follows: (1) As warm surface waters move northward, they become denser through heat loss and sea ice formation, which causes them to sink and form the North Atlantic Deep Water (NADW) limb of the AMOC. Important areas for deep-water formation in the North Atlantic are the Greenland Sea and Norwegian Sea to the east, and the Labrador Sea to the west. (2) The dense, cold, and nutrient-rich NADW flows southward and (3) is subject to upwelling along the way, most notably in the Antarctic region. (4) Surface or near-surface currents flow northward, eventually losing heat and becoming denser and forming NADW, thus closing the flow. One of the most important surface currents is the North Atlantic Current (NAC) (Lozier et al., 1995; Rossby, 1996). Originating in the western half of the North Atlantic, the NAC flows northeastward, divided in several branches, toward the Iceland Sea and the Greenland and Norwegian seas. The NAC is unique in the sense

that it transports warm waters to much higher latitudes than any other western boundary current (Rossby, 1996). This heat transport by the NAC, in combination with westerly winds, has an ameliorating effect on European climate (Seager et al., 2002). Current strength, variability, and position is strongly associated with the North Atlantic Oscillation (NAO), the dominant pattern of atmospheric variability in the North Atlantic region (Hurrell et al., 2003; Visbeck et al., 2003). The paradigm of the NAO describes the variability in atmospheric circulation resulting from relative changes in pressure between the "Azores high" (a large region of relatively high atmospheric pressure) and the "Icelandic low" (a low-pressure region); these pressure differences are most pronounced during the cold months of the year. During a positive NAO phase, the pressure difference between the two regions is higher than on average, which results in strong westerly winds, mild and wet winters, and a storm track positioned over the British Isles. During a negative NAO phase, the pressure difference is relatively low, resulting in cold and dry winters in northwest Europe, with predominantly easterly winds, and a southward-shifted storm track. The NAO and the ocean interact with each other with varying lead–lag relationships and can be linked to the multidecadal variability in North Atlantic sea surface temperatures (SSTs), sometimes referred to as the Atlantic Multidecadal Oscillation (AMO) (Drinkwater et al., 2014; Knight et al., 2006). The complex nature of these interactions is still poorly understood and sometimes contested (Clement et al., 2016, 2015; Zhang et al., 2016).

In addition to the main North Atlantic basin, shelf seas are an integral part of the North Atlantic region. Shelf sea waters are in constant exchange with the open ocean, and are disproportionately important for primary production and the sequestration of atmospheric carbon (Chen et al., 2013). Thus, understanding of the dynamics and natural variability of the Atlantic circulation and its interactions with the adjacent shelf seas is a significant component of our understanding of past and future climate changes. The present work focusses on variability of the western Scottish shelf in particular. A more comprehensive introduction to the hydrography of the shelf is provided in Chapter 2.

1.1.1 North Atlantic climate in the 4th millennium BP

North Atlantic SSTs have been decreasing since 5700 yrs before present (BP), which is generally linked to an orbitally forced decrease in solar irradiance (e.g., Marchal et al., 2002). However, SST trends and variability in the late Holocene are temporally and spatially heterogeneous, due to processes in the different limbs of the AMOC and regional ocean-atmosphere feedbacks (e.g., Moffa-Sánchez et al., 2014; Solignac et al., 2008). In the fourth millennium BP, solar activity was relatively low, with a strong negative excursion noted at ca. 3400 cal yrs BP (Steinhilber et al., 2012, 2009). The atmospheric conditions in the fourth millennium BP are thought to have been dominated by a weakly positive NAO with several negative phases (Goslin et al., 2018; Olsen et al., 2012; Orme et al., 2017). A low-to-negative NAO is associated with a southward-shifted storm track and a southward-shifted and weaker NAC (Curry and McCartney, 2001; Taylor and Stephens, 1998). However, reconstructed long-term trends of the NAO and storm track positions cannot provide a full picture of their high-frequency variability. For example, aeolian sediment reconstructions from the Outer Hebrides, Scotland, indicate strong westerly wind activity at ca. 3300 cal yrs BP (Gilbertson et al., 1999; Orme et al., 2016), which could have caused increased Atlantic inflow on the Hebrides Shelf (see Chapter 2).

1.1.2 Studying past marine variability

Traditional palaeoceanographic studies have mainly focussed on changes over millennia (e.g., Lynch-Stieglitz et al., 2007). While terrestrial records tend to be more highly resolved due to fast sedimentation rates, marine records of equivalent resolution are rather scarce (Charman and McCarroll, 2010). However, modern instrumental observations of the AMOC show pronounced changes in the system on decadal scales, and these play a major role in the decadal-scale variability of North Atlantic climate (Robson et al., 2014; Smeed et al., 2018). Modern observations are sparse, usually intermittent, and only cover the last few decades. The RAPID programme provides the longest continuous observation of the strength and structure of the AMOC via an array of moorings that spans the entire Atlantic basin at 26° N; however, even this record only dates back to 2004 CE (www.rapid.ac.uk/rapidmoc). Thus, a dense network of

proxies for past high-frequency variability of the AMOC is required to complement existing records of past climatic changes and to build a bridge to modern observations (Ninnemann and Thornalley, 2016). Focussing in on the British Isles specifically, hydroclimatic variability in the late Holocene has predominantly occurred on the decadal-to-centennial scale, with strong links to changes in North Atlantic ocean circulation (Charman, 2010; Swindles et al., 2013). Hence, to investigate and constrain marine-terrestrial relationships further, highly resolved marine records are needed, which is where the sclerochronological archives presented here come in.

1.2 Sclerochronology

Sclerochronology … *Greek* skleros (hard), khronos (time), logia (study of)

It has long been known that mollusc shells and other biominerals may exhibit periodic layers that provide information on the life history of the organism. An early mention of this can be found in Aristotle's "History of Animals", written over 2300 years ago (Aristotle, ca. 350 BCE/1910). Many centuries later, Leonardo da Vinci noted that we can count *"(…) in the shells of cockles and snails, the years and months of their life, as we do in the horns of bulls and oxen, and in the branches of plants (…)"* (da Vinci, 1510/1970). By the 20th century, technology and scientific methods had advanced sufficiently for scientists to (1) accurately age and date organisms based on their calcified growth structures, (2) quantify the variability in growth throughout their lifetime, and (3) extract environmental information based on their geochemical properties.

The term "sclerochronology" was coined in a study on coral skeleton by Buddemeier et al. (1974) and reflects the analogy to the long-established field of dendrochronology. However, while dendrochronology specifically refers to the dating and study of growth variation based on tree rings, the term sclerochronology is commonly used in a wider sense, representing both the study of growth variation and the study of geochemical composition within the skeletal matrix (sometimes referred to as sclerochemistry). The most recent definition of

sclerochronology was formulated at the 1st International Sclerochronology Conference in St. Petersburg, FL, USA, in 2007 as "the study of physical and chemical variations in the accretionary hard tissues of organisms, and the temporal context in which they formed (…)" (Oschmann, 2009). The studied structures include coral skeletons (e.g., Hudson et al., 1976; Knutson et al., 1972), mollusc shells (e.g., Jones, 1980; Surge et al., 2013), otoliths (e.g., Campana, 1999; Devereux, 1967), coralline algae (e.g., Halfar et al., 2000), and statoliths (e.g., Hollyman et al., 2018), among others. The focus may be on the life history of the studied specimen, or on the history of the environment that the specimen lived in.

The diversity and global distribution of sclerochronological archives entails that they can be used to study environmental changes in many different environments across all climate zones. Coral studies were long dominating high-resolution marine climate research, leading to a bias towards tropical and subtropical regions. In recent decades, marine molluscs — and to a lesser extent coralline algae — have become more and more prominent as climate archives in extratropical environments. Bivalves, in particular, have emerged as the most widely used sclerochronological archive for past climate in mid- to high latitudes (e.g., Jones, 1983; Schöne et al., 2005). The annual growth bands in long-lived bivalves reflect the environment the animals live in and can be crossmatched between specimens to construct multicentennial chronologies (e.g., Butler et al., 2010). The North Atlantic is a hotspot for sclerochronological research of past marine climate, with *Arctica islandica* being the dominating species in the literature (e.g., Butler et al., 2013, 2010; Schöne et al., 2005; Wanamaker, Jr. et al., 2011; Witbaard et al., 1997). Other taxa of long-lived bivalves increasingly used in sclerochronological studies include *Glycymeris* in the North Atlantic and adjacent seas (Brocas et al., 2013; Bušelić et al., 2015), *Tridacna* in the Indo-Pacific (Elliot et al., 2009; Warter and Müller, 2017), and *Panopea generosa* (Pacific geoduck) in the northeastern Pacific (Black et al., 2009; Strom et al., 2005).

A brief historical overview of "firsts" in bivalve sclerochronology

The idea to correlate shell growth patterns between different specimens was first introduced by Clark (1968), in a study on surface striae in *Pecten diagensis*. A decade later, Jones and Thompson led ground-breaking research by sectioning shells and studying the internal growth patterns of *Spisula solidissima* and *Arctica islandica* (Jones, 1981, 1980; Jones et al., 1978).

This work provided the methodological basis for bivalve sclerochronology and the application of dendrochronological statistical techniques to standardize ontogenetic growth trends in shells (Jones, 1981). This was also the point at which *Arctica islandica* was established as a sclerochronological archive (Jones, 1980; Thompson and Jones, 1977; Thompson et al., 1980). A glimpse into the development of this early work is provided in Jones (1983).

About 20 years later, Witbaard et al. (1997a) published a 110-year chronology built with *A. islandica* from the North Sea, marking the first centennial-scale *A. islandica* chronology. While this chronology was built with live-collected specimens (Witbaard et al., 1997a), Marchitto et al. (2000) were the first to incorporate dead-collected shells into a chronology, and postulated that a 1000-year chronology would be feasible. Today, we know this to be true — thirteen years after the study by Marchitto et al. (2000), Butler et al. (2013) published a 1357-year chronology built with *A. islandica* from the North Icelandic Shelf. This proved that bivalves can be used to construct millennial-scale, absolutely dated, annually resolved, replicated records of past marine variability (Butler et al., 2013). However, if dead-collected shells can be crossmatched with live-collected material, it should also be possible to build chronologies exclusively with fossil shells. This would result in "floating" chronologies, i.e. chronologies that are not anchored in time and therefore are not assigned absolute calendar dates. Indeed, Scourse et al. (2006) provided a proof of concept when they built the first floating bivalve chronology using fossil *A. islandica* from the North Sea, which at the same time was the first floating chronology built entirely with marine fossil material.

Temperature reconstructions using $\delta^{18}O$

Pioneering work by Harold C. Urey and colleagues laid the foundations for temperature reconstructions based on oxygen isotope values ($\delta^{18}O$) in calcium carbonates (Epstein et al., 1953; Urey, 1947; Urey et al., 1951). Today, $\delta^{18}O$ is still the most widely used proxy for past ocean temperatures. When applied to the highly resolved layers in sclerochronological archives, and assuming the $\delta^{18}O$ of the ambient water is known or can be estimated, $\delta^{18}O$ values can be used to reconstruct environmental temperature variability and/or life history of the studied organism (e.g., Devereux, 1967; Weidman et al., 1994).

In this thesis, $\delta^{18}O_c$ (with a subscript "c") is used to refer specifically to $\delta^{18}O$ in shell carbonate.

Dating uncertainty and replication in sclerochronological records

When live-collected specimens are incorporated into a chronology, the absolute calendar year of each annual band is known and, through accurate crossmatching, dating uncertainties within the record can be virtually eliminated (Black et al., 2019). However, when working with fossil shells, it is not always possible to incorporate live-collected specimens into the chronology. Instead, as mentioned above, crossmatched fossil shells build a "floating chronology", which is not anchored in time (Scourse et al., 2006). While this means that dating uncertainty of the overall time series is still a limiting factor in floating chronologies, the growth series are annually resolved and, most importantly, replicated. Thus, floating chronologies provide valuable and robust high-resolution records of past environmental variability.

1.3 Target species

The research in this thesis is based on specimens of two bivalve species, *Arctica islandica* and *Glycymeris glycymeris*. While *A. islandica* is the most widely used bivalve in sclerochronological palaeoclimate studies and has been the target of research for several decades, *G. glycymeris* emerged as a marine climate archive less than ten years ago (Brocas et al., 2013; Reynolds et al., 2013; Royer et al., 2013). Both species have proven to be reliable recorders of past marine variability and suitable for crossmatching, and their habitat preferences complement each other.

1.3.1 *Arctica islandica* (Linnaeus, 1767)

With a maximum recorded lifespan of 507 years, *Arctica islandica* (common names: ocean quahog, Icelandic clam), is the longest-living animal of which the exact age has been determined (Butler et al., 2013). *A. islandica* is a boreal species that is widely distributed on the eastern and western continental shelves of the temperate and boreal North Atlantic (Dahlgren et al., 2000, and references therein). It has been found at depths of 4 m to 256 m, where it lives buried in fine sediments, preferably mud or sand (Morton, 2011; Thórarinsdóttir

and Einarsson, 1996). The cross-lamellar shell of *A. islandica* is close-to-circular and covered in periostracum, an organic layer that protects the shell from dissolution and microbial activity (Schöne, 2013).

A. islandica are categorised as suspension filter feeders or as deposit feeders, and possess relatively short siphons; food intake occurs therefore at the water-sediment interface (Morton, 2011; Schöne, 2013, and references therein). Once buried, *A. islandica* stay practically motionless, close to the surface (Morton, 2011). They can, however, burrow several centimetres into the substrate, where they intermittently stay between one and seven days and respire anaerobically (Taylor, 1976).

A. islandica is without a doubt a valuable archive of marine environmental variability, as is shown by its prominent role in extratropical sclerochronological literature. A review of *A. islandica* as a palaeoenvironmental archive is provided by Schöne (2013).

1.3.2 *Glycymeris glycymeris* (Linnaeus, 1758)

Previous studies have demonstrated that the long-lived bivalve *Glycymeris glycymeris* (common name: dog cockle) is a potential target for reconstructing climate variability in the North Atlantic region (Brocas et al., 2013; Reynolds et al., 2013). *G. glycymeris* can live for almost 200 years (Reynolds et al., 2013) in shallow shelf seas off northwest Africa and Europe at depths up to 100 m (Hayward and Ryland, 1995; Thomas, 1975). *G. glycymeris* is a rheophilic species, i.e. it inhabits environments with much water movement, and often occurs in sparse, tide-swept areas (Holme, 1966). Although they may occur in muddy sediment (Tebble, 1966), *G. glycymeris* prefer gravel, gravelly sand or sand (Thomas, 1975, and references therein).

Glycymerids are slow and relatively inefficient burrowers; however, they are able to move around considerably on the surface, due to their "exceptionally muscular foot" (Thomas, 1975). Thomas (1975) argued that the circular shape of *Glycymeris* indicates an evolutionary need for

high mobility, as this shape allows the animal to rock back and forth and thereby move faster. *G. glycymeris* has a very thick cross-lamellar shell that is penetrated by many microscopic channels, i.e. microtubuli (Böhm et al., 2016; Crippa, 2013). The outer shell layer consists of simple crossed lamellae, and a "zebra pattern" is visible on the outside of the shell under the periostracum (Crippa, 2013) (see Figure 3.3 in Chapter 3).

Shell growth occurs synchronously among specimens or populations that are exposed to the same environmental factors, which renders sclerochronological studies possible (Brocas et al., 2013; Reynolds et al., 2013). Growth lines are formed each year when shell growth slows down drastically shortly after the temperature peak (Berthou et al., 1986; Reynolds et al., 2017). Studies from the Irish Sea showed that *G. glycymeris* chronologies (Brocas et al., 2013) seem to be more strongly correlated with SSTs than *A. islandica* chronologies (Butler et al., 2010) in this region.

1.3.3 Annual growth increments

Whether shell growth continues at a very slow rate throughout the "off season" or ceases completely at one point is not known, but any information that might be stored in the annual lines is inaccessible to current sampling techniques. Consequently, "annual" *G. glycymeris* and *A. islandica* growth series do not represent the entire year but are instead biased towards the warmer months of the year. This seasonal bias is a common characteristic of bivalve chronologies at mid- to high latitudes (Killam and Clapham, 2018), and is usually regarded as a limitation. However, many climatic patterns and shifts result from processes that are also seasonally biased, and annual averages of past climatic and environmental conditions mask such seasonal-scale variability. Thus, seasonal bias in the growth series can potentially be used as an asset when the exact timing of the growth season is known. The growth season can be determined through sub-annual oxygen isotope samples of the shell carbonate ($\delta^{18}O_c$), which are calibrated against instrumental temperature records (e.g., Weidman et al., 1994). Furthermore, the sub-annual $\delta^{18}O_c$ series can provide insight into inter-annual variability of the respective growth season through time (Schöne and Fiebig, 2009; Wanamaker et al., 2011)

1.4 Scope and aim of this thesis

Background and author's note

The original main objective of my PhD project was to develop a modern chronology for St Kilda covering the past 200–300 years or more. We expected to find *Arctica islandica* during the research cruise in 2014, since records of this species had previously been recorded for this site (National Biodiversity Network; nbn.org.uk). This chronology was intended to complement other chronologies that were being built at the same time, off the Faroe Islands and northern Norway (the site was later changed to Viking Bank, North Sea), as part of an EU-funded Marie [Skłodowska] Curie Initial Training Network. These sample sites were strategically placed along a south-north gradient and in different environments influenced by the various branches of the North Atlantic Current. However, the scope of a study that is based on field work and natural archives is ultimately determined by what we find. In the present case, our research cruise yielded an unexpected, yet exciting collection — no *A. islandica* were found, but instead several hundred valves of *G. glycymeris*, of which there were no previous records at this site. A second, even bigger, surprise came when radiocarbon dating indicated that these shells, which were in very good condition, had in fact died over 3000 years ago. Modern *A. islandica* were later collected during a subsequent diving campaign, but by that time, the main scope of this thesis had shifted towards the fossil material (Chapter 5 and 6).

1.4.1 Scope and context

Natural archives and proxy records are needed to study natural variability, establish baselines, and advance our understanding of the marine system. Recent and ongoing debate about trends and variability in AMOC strength shows the need for high-quality proxy data that allow us to study this system at various spatial and temporal scales (see Kilbourne et al., 2022, in response to Caesar et al., 2021). While sclerochronological records have limitations when it comes to capturing low-frequency variability, they can be combined with other proxies, e.g., sediment cores, into composite records that reflect ocean variability more accurately (e.g., Cunningham et al., 2013; Reynolds et al., 2018). The bivalve chronologies presented in this thesis are part of a larger, growing network of sclerochronologies in the North Atlantic (e.g., Bonitz et al.,

2017; Mette et al., 2021; Reynolds et al., 2017; Wanamaker et al., 2011). As such, this work provides an important piece of the overall puzzle and contributes to our knowledge of this complex system.

The location of St Kilda, in particular, makes the records presented in this thesis unique. Highly resolved proxy series have been published for the inner western Scottish shelf; a 200-year *G. glycymeris* chronology was constructed for the Tiree Passage (Reynolds et al., 2017; Reynolds et al., 2013) and a decadal-scale record of marine variability covering the last millennium was constructed with benthic foraminifera from Loch Sunart (Cage and Austin, 2010). Similar records are, however, missing for the outer western Scottish shelf. As will be discussed in Chapter 2 and further demonstrated in Chapter 4, the hydrography of the outer shelf differs considerably from that on the inner shelf, as conditions are more marine and less impacted by coastal influences. The western Scottish shelf exchanges water with the open ocean via Atlantic inflow and downwelling (see Chapter 2). Being located far out on the shelf, St Kilda is thus considered a suitable site to study the variability of North Atlantic climate. Furthermore, records from shelf seas are tightly coupled with the adjacent terrestrial environment, which provides exciting opportunities to study marine-terrestrial interactions.

1.4.2 Aim and objectives

The overall aim of this work is to provide a characterisation of past marine variability in the late Holocene on the western Scottish shelf using sclerochronological methods.

The following objectives were conceived to achieve this aim:

- to build centennial-scale sclerochronologies for St Kilda using
    - fossil *G. glycymeris* shells dated to the 4th millennium BP and
    - live- and dead collected modern *A. islandica*
- to determine the growth season of these bivalves through sub-annual $\delta^{18}O_c$ sampling
- to calculate past seasonal and average seawater temperatures based on $\delta^{18}O_c$

- to test whether seasonality and seasonal temperature range differs between the 4th millennium BP and today
- to analyse the modern chronology and investigate how it relates to environmental variability

1.5 Thesis structure

This thesis is written in traditional format and consists of one general introduction (current chapter), one introductory chapter about the oceanographic setting (Chapter 2), one chapter introducing the methods and materials used (Chapter 3), four results chapters including chapter-specific discussion (Chapter 4–7), and the final chapter summarising the main findings and conclusions (Chapter 8). I chose to write this thesis in monograph style because it better represents the way in which the results were obtained — each chapter builds on the previous ones. An overview of the chapters is given below.

Chapter 1 — General introduction

Chapter 2 — Oceanography, geology, and biology of St Kilda

This chapter provides an introduction to the oceanography, geography, and biology of St Kilda. The chapter starts out with a general overview of the oceanographic setting and describes the Atlantic inflow, shelf–ocean exchange, and shelf currents that influence the western Scottish shelf. The most important temperature datasets available for the outer western Scottish shelf are then introduced. The last section of the chapter focusses on St Kilda specifically and provides insight into what makes this location special — the offshore setting, geological and physical characteristics, the harsh and stormy environment, and its (former) human and animal inhabitants.

Chapter 3 — Material and methods

This chapter introduces the shell material and all methods used in subsequent results chapters. The outline of this chapter follows the structure of the overall thesis; it begins by describing the methods used to test which instrumental data are most appropriate, followed by an introduction to the shell material. Then, the methods used for shell processing, increment

measuring, chronology construction, and analysis are described. After that, radiocarbon dating techniques and analyses as well as Raman spectroscopy, used to evaluate the fossil shell material, are explained. Lastly, sub-annual and annual oxygen isotope sampling methods and analysis are described.

Chapter 4 — Evaluating *in-situ* and gridded surface temperature data

This is a brief chapter that builds on the introduction to the hydrography of the western Scottish shelf in Chapter 2. Due to the lack of local data at St Kilda and the intermittent nature of *in-situ* data on the outer western Scottish shelf in general, gridded temperature data are used for comparisons with proxy data in this thesis. Chapter 4 investigates the question which of three data products (OISSTv.2, ERSSTv.5, HadISST1) is the most skilful at representing regional SSTs on the outer shelf by comparing them to available (yet scarce) *in-situ* temperature series.

Chapter 5 — Radiocarbon dates and taphonomy

This chapter lays the foundation of the sclerochronological work of this thesis. The shell material that is later used to build chronologies (see Chapter 6) is described here in detail. The majority of the shell material consisted of fossil *G. glycymeris* and modern *A. islandica*. In addition, ten live, albeit young, *G. glycymeris* were found. In all, 308 specimens were measured, weighed, and their condition was assessed. A scoring system was applied to systematically evaluate five taphonomic variables — the condition of periostracum, ligament, margin, and nacre, and the level of bioerosion. Fourteen fossil *G. glycymeris* were radiocarbon dated, whereof 12 were assigned dates in the 4th millennium BP; the other two shells yielded younger dates. The fact that approximate dates were known for these 14 shells provided a good opportunity to investigate whether any relationship could be found between how much time had passed since their death and the condition they were in, using the taphonomic scoring system mentioned above.

Chapter 6 — Master chronologies and sub-annual oxygen isotopes: growth variability, growth season, and seasonal temperatures in the late Holocene

This chapter represents the core of the sclerochronological work of this thesis. Two floating chronologies built with fossil *G. glycymeris* (referred to as the *Misfits* chronology and the *St Kilda Seven* chronology), and one modern chronology built with live- and dead-collected *A. islandica* are introduced. Statistics and frequency domain analyses are presented for each of

the three chronologies. A Bayesian chronological model was used to constrain the radiocarbon dates of the *St Kilda Seven* fossil chronology, placing it at 3500–3300 cal yr BP.

In the second part of this chapter, the growth season for *G. glycymeris* and *A. islandica* is established through sub-annual $\delta^{18}O_c$ profiles, and seasonal and average seawater temperatures are calculated for the fossil shells from 3500–3300 cal yr BP and compared to modern conditions.

Chapter 7 — The modern *Arctica* chronology and other data: environmental records, spatial correlations, and Soay sheep

The final results chapter focusses on the modern chronology built with *A. islandica* shells collected during a diving campaign in 2016. The *Arctica* chronology that was introduced in Chapter 6 is now compared to local, regional, and basin-wide environmental and biological proxy data. Correlations with climate indices and local food web dynamics are discussed, with special focus on plankton and Soay sheep.

Chapter 8 — General discussion

This chapter provides a brief summary of the four results chapters (Chapter 4–7) before discussing the limitations of $\delta^{18}O_c$-based temperature reconstructions and presenting the main conclusions. The chapter ends with suggestions for future research directions and complementary studies at St Kilda.

Parts of this thesis have been published in:

Alexandroff, S.J., Butler, P.G., Hollyman, P.R., Schöne, B.R., Scourse, J.D., 2021. Late Holocene seasonal temperature variability of the western Scottish shelf (St Kilda) recorded in fossil shells of the bivalve Glycymeris glycymeris. Palaeogeogr. Palaeoclimatol. Palaeoecol. 562, 110146. https://doi.org/10.1016/j.palaeo.2020.110146

I have the rights to reuse the figures, tables, and text in this thesis.

The text and results figures throughout this thesis, including the parts previously published in the paper cited above, are my own and original work. The only exception is Figure 5.2, which

was provided by my co-author Dr Philip Hollyman, who performed the Raman spectrometry analysis in the fossil shells (see sections 3.5 and 5.2.2). Dr Hollyman also helped draft early versions of the text in sections 3.5 (Raman spectrometry methods) and 5.2.2 (Raman spectrometry results), which were subsequently revised by me. My co-authors of the cited paper provided helpful comments, corrections, and suggestions to improve it.

Chapter 2

Oceanography, geology, and biology of St Kilda

Chapter 2 — Oceanography, geology, and biology of St Kilda

2.1. Introduction

The western Scottish shelf is a highly complex system affected by both coastal and oceanic influences. The Atlantic water on the shelf has its origin in the European Slope Current (see Section 2.2), which in turn consists of similar water masses to those in the upper layers of the Rockall Trough (Figure 2.1a). The main contributor to water composition in the Rockall Trough is the relatively warm and saline Eastern North Atlantic Water (ENAW), entering from the south. In addition, albeit in smaller quantities, relatively cool and fresh Western North Atlantic Water (WNAW) is advected to the trough via the North Atlantic Current. Lastly, North Atlantic Water (NAW) from the European Slope Current also mixes with the upper layers in the Rockall Trough. It is known that salinity, temperature, and nutrient contents in the upper waters of the Rockall Trough are subject to multiyear variability that is distinguishable from seasonal variability (Holliday, 2003; Holliday et al., 2000; Johnson et al., 2013). Interannual variation of temperature is of the order of ±0.5 °C, while that of salinity is ±0.05 (Holliday, 2003; Holliday et al., 2000). This variability is influenced by a dynamic system of different atmospheric and oceanic indicators, of which the exact driving and forcing mechanisms have yet to be disentangled (Hughes et al., 2012). It is, however, evident that the North Atlantic wind stress field and the strength of the Subpolar Gyre (SPG) play an important role in the hydrographic variability of the Rockall Trough (Holliday, 2003; Holliday et al., 2008; Hughes et al., 2012). A strong SPG circulation is thought to increase inflow of fresh and cool WNAW, whereas a weak SPG results in warmer and more saline upper waters as the dominance of ENAW becomes stronger (e.g., Hátún et al., 2005; but see Foukal and Lozier, 2017).

It is thought that the western Scottish shelf is subject to similar interannual variability (e.g., Inall et al., 2009). However, explaining the temporal and spatial variability on the shelf, and its interactions with the open ocean, has proven difficult (Jones, 2016; and references therein). The western Scottish shelf is particularly complex, due to the interplay of different currents coupled with a convoluted coastline, and it presents a strong longitudinal gradient in

temperature and salinity (e.g., Ellett, 1979; Inall et al., 2009; Jones, 2016). At ca. 55.5° N, a portion of the European Slope Current branches off and flows onto the Malin Shelf, forming the Atlantic Inflow Current, which supplies the shelf with saline and nutrient-rich water (see Section 2.3.1). The Scottish Coastal Current, on the other hand, carries fresher shelf water northwards, providing the entire western Scottish shelf with coastal influences (see Section 2.3.2; Figure 2.1).

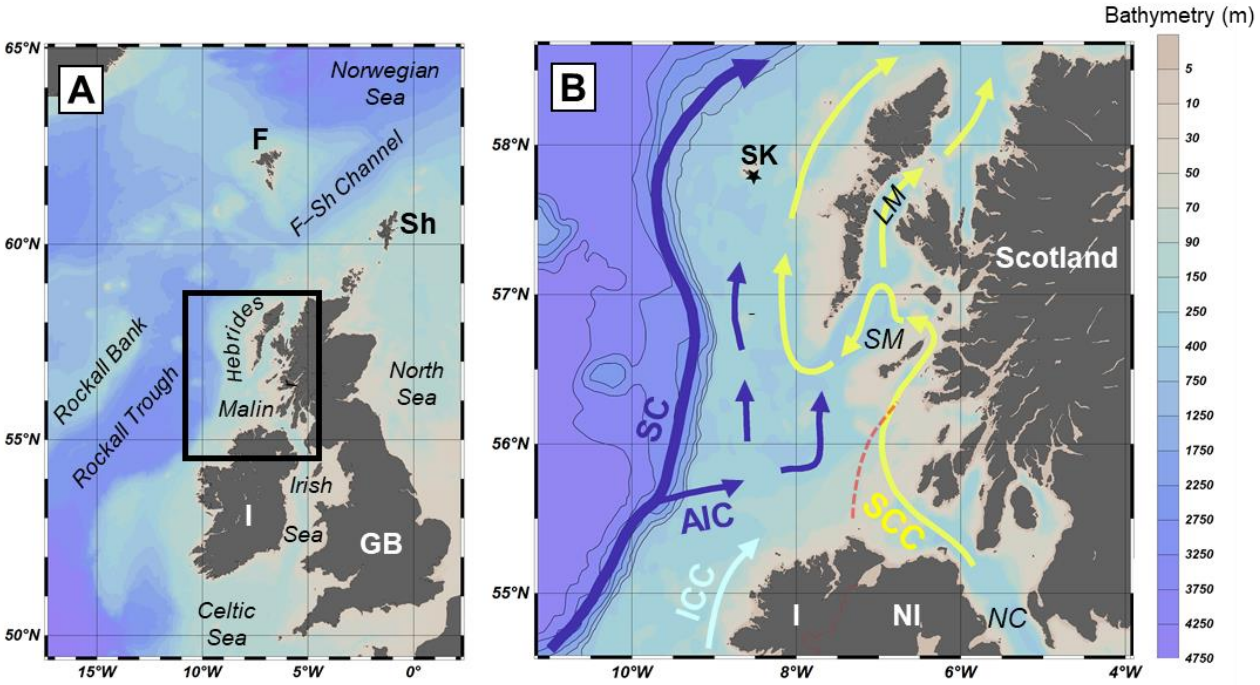

Figure 2.1: Western Scottish shelf and location of St Kilda, Scotland. **(A)** Overview map. Colours indicate bathymetry according to the legend to the right. Land masses are labelled with "I" = Ireland, "GB" = Great Britain, "F" = Faroe, "Sh" = Shetland. Abbreviations: Hebrides = Hebrides Shelf, Malin = Malin Shelf, F-Sh Channel = Faroe-Shetland Channel. The black rectangle indicates the location of the detail shown in map B. **(B)** Detail of map A. Sample location (black star) at St Kilda, Outer Hebrides, Scotland. The yellow arrows indicate the approximate circulation of the Scottish Coastal Current (SCC). The dark blue arrows indicate the flow of the slope current (SC) and Atlantic Inflow Current (AIC) transporting Atlantic water. The light blue arrow indicates the Irish Coastal Current (ICC). Background colours denote bathymetry according to the legend to the right. Depth contours for the shelf margin and open ocean are drawn in black lines. The shelf margin is indicated by depth contours starting from 200 m. Approximate positions of currents were taken from Inall et al. (2009), Turrell et al. (1996), and Porter et al. (2018).The dashed red line denotes the Islay Front (Simpson et al., 1979). NC = North Channel, SM = South Minch, LM = Little Minch. Land masses are labelled with "Scotland", "SK" = St Kilda, "I" = Ireland, and "NI" = Northern Ireland. (Ocean Data View; Schlitzer, 2020)

Atlantic water dominates on the outer shelf at depths below 100 m (Bailey et al., 2011; Painter et al., 2016). At shallower depths, the Atlantic signal weakens, and further inshore, the system is predominantly influenced by the coastal waters. Salinities decrease and temperatures

increase from the shelf edge to the inner coastline (Painter et al., 2016; see Figure 2.2). Temperature shows a strong seasonal cycle on the shelf similar to the cycle in the Rockall Trough. However, the amplitude is higher near the coast than on the outer shelf and at the shelf edge (Inall et al., 2009). Annual temperature cycles at depth depend on whether and to what degree waters are stratified. On the inner Scottish shelf, the sea is generally well mixed throughout the year, due to strong tidal mixing in shallow water. Here, bottom water temperatures follow a similar annual cycle as sea surface temperatures. On the outer shelf, however, the sea is deeper, and tides are weaker; surface heating in spring and summer leads to a decrease in density in the upper layer and the formation of a thermocline. Water masses beneath the thermocline present an attenuated annual temperature cycle, with a slower warming during spring and summer. In autumn, wind stirring causes heat from the surface to mix with the deeper layers (Ellett and Edwards, 1983).

Several studies have suggested that strong westerly winds cause increased Atlantic inflow to the shelf (e.g., Burrows et al., 1999; Inall et al., 2009). Jones et al. (2018) studied the variability in salinity on the western Scottish shelf to trace the different currents influencing this area. The authors found that the western Scottish shelf is a highly variable environment, which is especially true for the inner shelf, where interannual salinity anomaly is considerable (see Figure 2.3, adapted from Jones et al. 2018). Jones et al. (2018) also concluded that the hydrographic state can switch quickly from Atlantic-water dominance to coastal-water dominance, and vice versa, following strong wind events. In a state of strong westerly winds, the inner shelf sea may be composed of 62% Atlantic water and 38% coastal water on average, while during prevailing easterly winds, the mix may be made up of 6% Atlantic water and 94% coastal water on average (Jones et al., 2018). These numbers were calculated for the inner Malin shelf and will likely be different on the outer shelf, where interannual salinity anomaly is smaller (Figure 2.3, Jones et al. 2018). However, they clearly demonstrate the variable nature of the shelf system west of Scotland.

The amount of oceanic water that is advected onto the shelf has important effects on the ecosystem (e.g., Adams et al., 2013; Gowen et al., 1998; Reid et al., 2001; Whyte et al., 2014). Primary productivity is limited by nitrate and phosphate (Smith et al 2014); the main source of these nutrients on the shelf is the open ocean (Proctor et al., 2003). Thus, studying the influx and distribution patterns of these nutrients is a prerequisite for understanding biological processes on the shelf. Section 2.3.2 explains the role of the Atlantic Inflow Current in nutrient supply specifically.

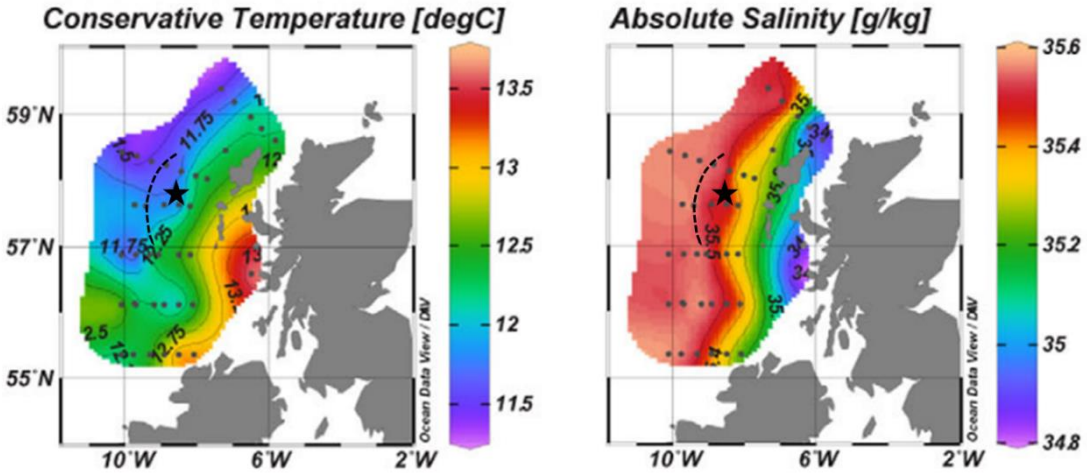

Figure 2.2: Surface contour map showing average temperature (left) and salinity profiles (right) in October/November 2014, adapted from Painter et al. (2016). The approximate position of St Kilda is marked by a star. The shelf edge at the latitude of St Kilda is indicated by a dashed line. Please note that salinity is given in g/kg, while practical salinity is used in the main text of this thesis.

St Kilda (Lat: 57.82° N, Long: 08.59° W; Figure 2.1b) is located on the Hebrides Shelf, a region of the western Scottish shelf at a latitude of ca. 56° N to 60° N (see Figure 2.1a). In this thesis, "Hebrides Shelf" refers to the outer portion of the shelf only (excluding the Minch), which is bordered by the Outer Hebrides island chain to the east and the Rockall Trough to the west. The maximum depth of the Hebrides Shelf sea is ca. 200 m; the adjacent Rockall Trough reaches a depth of 2000 m at this latitude. To the south lies the Malin Shelf (see Figure 2.1a). While the Hebrides Shelf only accounts for ca. 7% of the overall NW European continental shelf, it plays an important role in water–mass exchange between the open ocean and the continental shelf (Painter et al., 2016). The role of the Hebrides Shelf as a carbon sink is explained in Section 2.2.1.

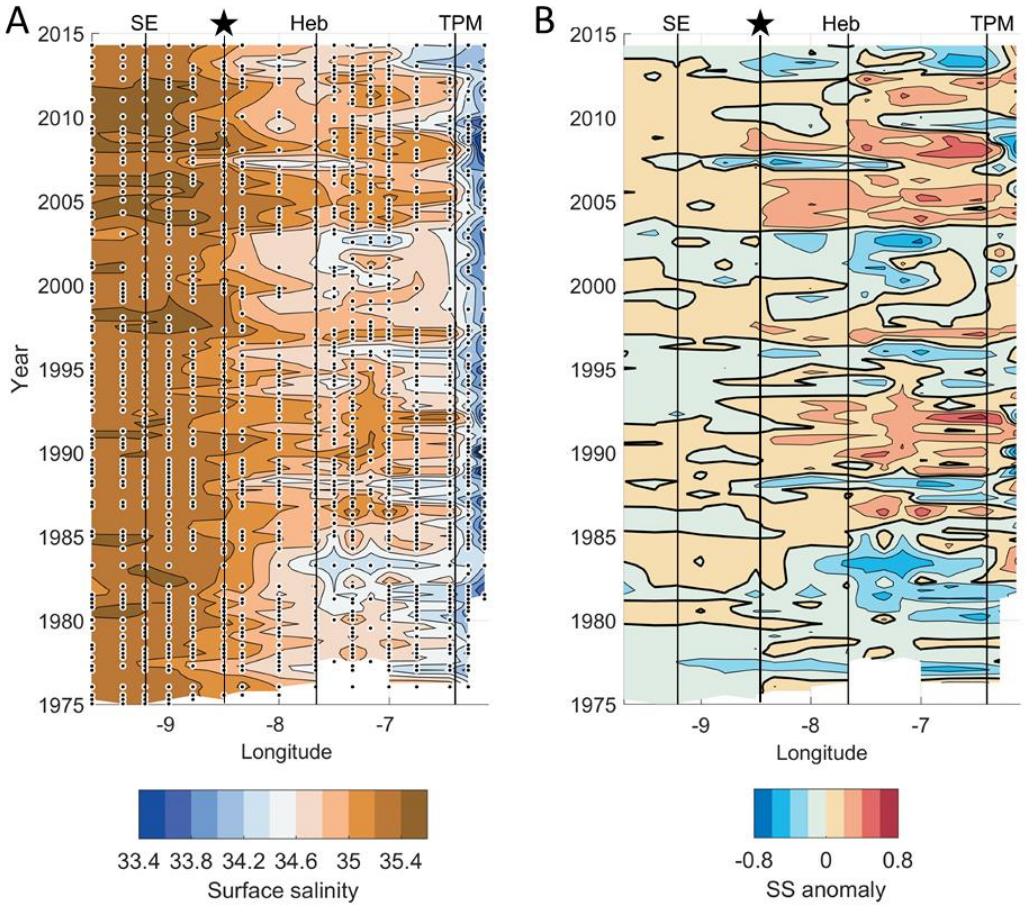

Figure 2.3: Hovmöller plot of the surface salinity along the Ellett line stations, adapted from Jones et al. (2018). SE = Shelf edge (Station R); Heb = southern tip of the Outer Hebrides, TPM = Tiree Passage Mooring site. The black star indicates Ellett station 15G, located at the same longitude as St Kilda, 100 km to the south. (A) Surface salinity through time. (B) Surface salinity anomaly through time.

2.2 The slope current and shelf-edge exchange

The European Slope Current (hereafter simply called "slope current") flows poleward for 1600 km along the continental shelf break, from the Goban Spur to north of the Shetland Islands (Burrows and Thorpe, 1999; Pingree et al., 1999; Souza et al., 2001). The slope current is of similar origin to the upper waters in the eastern Rockall Trough and its characteristics and variability can therefore be considered as the same as that of the Rockall Trough (see Section 2.1 above). However, it should be noted that the water in the slope current (NAW) is slightly

warmer, saltier, and less dense than the otherwise very similar ENAW at the latitude of the Rockall Trough (Holliday et al., 2000; Johnson et al., 2013).

The driver of the slope current is the north-south density gradient resulting from the decrease in temperature in the upper water column with increasing latitude. As a typical slope current, it is controlled by a process known as the Joint Effect of Baroclinity and Relief (JEBAR; Huthnance, 1984; Souza et al., 2001), and thus bathymetrically controlled. The current flows between the 200 m and 900 m isobaths, with its high-salinity core situated above the 200–300 m isobaths. It is a steady barotropic current, i.e. its poleward flow is a consequence of density change as well as the sloping topography (Pingree et al., 1999; Souza et al., 2001). Due to its strong and steady flow along the steep edge, the slope current acts as an insulator to exchange between the ocean and the continental shelf (Pingree et al., 1999; Souza et al., 2001). Notwithstanding this insulating effect, there are several processes through which water masses are exchanged between the open ocean and the shelf. The slope current is subject to temporal and spatial "weak points", in which leakage occurs. Firstly, while the current is the strongest in winter, the poleward flow becomes weaker in other seasons, and might even be reversed (i.e. equator-ward) in the early spring (Pingree et al., 1999). Secondly, abrupt topographical changes in the slope lead to a breakdown of the current, and thus oceanic water intrudes onto the shelf (Pingree et al., 1999). Most importantly, the slope current itself is an integral part of the shelf–ocean exchange that takes place through downwelling processes — the poleward-flowing current and the prevailing wind direction generate on-shelf transport of oceanic surface water as well as local Ekman drains from the shelf down the slope (Holt et al., 2009; Simpson and McCandliss, 2013; Souza et al., 2001). Further downwelling occurs through winter cascades, where deep saline water cools down during winter, becoming denser and consequently forming a gravity current (Shapiro et al., 2003; Shapiro and Hill, 1997). Drifters released by Burrows and Thorpe (1999) crossed the Hebrides Shelf edge at several locations, confirming dispersion and cross-shelf fluxes.

2.2.1 Shelf–ocean carbon exchange

The NW European continental shelf plays an important role as a carbon sink, by fixing atmospheric CO_2 and transporting it to deep layers of the open ocean through the downwelling processes mentioned above (Burrows and Thorpe, 1999; Holt et al., 2009; Huthnance, 1992;

Inall et al., 2009; Jones et al., 2018; Painter et al., 2016; Shapiro et al., 2003; Simpson and McCandliss, 2013; Souza et al., 2001). Wind-driven surface water flows onshore, which is compensated by a down-slope flow of shelf bottom water with a flux of 1 Sv (Holt et al., 2009; Wakelin et al., 2012). A hydrodynamic model simulation by Holt et al. (2009) showed that 40% of the carbon sequestered in one growing season had been transported off the NW European shelf by the start of the next growing season. Out of these 40% of transported carbon, 52% were moved below the permanent pycnocline. However, these processes are spatially heterogeneous. Painter et al. (2016) studied the carbon exchange between the open ocean and the Hebrides Shelf specifically and found a net offshelf transport of particulate organic carbon (POC), with fluxes that are three to five times larger than the global mean. Thus, this area is a potentially significant source of POC to the slope current and the benthos in the neighbouring open ocean.

2.3 Shelf currents influencing the Hebrides Shelf

The outer western Scottish shelf is mainly influenced by two shelf currents, (1) the Atlantic Inflow Current, providing the shelf with water from the open ocean, (2) and the Scottish Coastal Current, carrying fresh water from coastal areas.

2.3.1 Atlantic Inflow Current

As described in Section 2.2, the slope current has several “weak points”, where its insulating effect breaks down and Atlantic water flows onto the shelf. Most recently, the advection of slope current water onto the shelf at ca. 55.5° N has been identified as a distinct current, called Atlantic Inflow Current (AIC) (Figure 2.1b; Porter et al., 2018). The AIC transports nutrient-rich slope current water onto the shelf, where it mixes with the fresher and cooler Irish Coastal Current (ICC) flowing northward (Figure 2.1b; Porter et al., 2018). Now carrying Atlantic and ICC water, the AIC continues eastward along the northern coast of Ireland. The eastern extent of the AIC is likely limited by the Islay Front (see dashed red line in Figure 2.1b; Simpson et al., 1979). The Islay Front is a shelf-sea tidal mixing front between the Irish and Scottish coast west of Islay. During summer, the Islay Front marks the boundary between seasonally stratified water on the outer shelf and tidally mixed water on the inner shelf (Simpson et al., 1979).

However, the front persists throughout the year, even when stratification on the outer shelf breaks down. This can partially be explained by the strong contrast in salinity between the Atlantic water to the west and the water flowing out of the Irish Sea to the east, which leads to horizontal density gradients that prohibit mixing (Ellett and Edwards, 1983; Jones, 2016). Porter et al. (2018) used shallow drifters to track the AIC and concluded that a weaker Islay Front will result in a more eastward extension of the current and inflow into the Minch, i.e. the channel between mainland Scotland and the Outer Hebrides. Conversely, when the Islay Front is strong, the AIC is blocked and deflected back to the outer shelf. Both pathways eventually lead to the North Sea (Porter et al., 2018).

Porter et al. (2018) estimated that the AIC may be responsible for a nitrate flux of up to 74 kg/s and a phosphate flux of up to 7.6 kg/s onto the shelf. These numbers are even larger than previous estimates (Proctor et al., 2003). Both nitrate and phosphate are limiting factors for primary productivity, thus, the on-shelf transport of these nutrients by the AIC may play an important role in stimulating phytoplankton growth (Smith et al., 2014). In addition, the AIC could transport phytoplankton seed populations directly from the open ocean onto the shelf (Porter et al., 2018). Satellite images show bands of high chlorophyll concentration associated with the AIC, confirming its influence on phytoplankton abundance on the shelf (Porter et al., 2018).

2.3.2 Scottish Coastal Current (SCC)

The SCC is a buoyancy-driven current that potentially influences the entire western Scottish shelf (Figure 2.1b). It flows northwards through the North Channel (see “NC” in Figure 2.1b), carrying relatively fresh Irish Sea water, and receives further freshwater input from the Clyde Sea and the many sea lochs along the western Scottish coast (Ellett and Edwards, 1983; Inall et al., 2009, and references therein). As a buoyancy-driven current, the SCC flows parallel to the coastline, with the land to its right due to the Coriolis force (Simpson, 1997). However, the flow is complicated by tides, winds, waves, and shelf-sea fronts. The current meanders at the southern entrance to the Minch (i.e. South Minch, see “SM” in Figure 2.1b), where saline Atlantic water causes horizontal density gradients (Hill et al., 1997). The baroclinic conditions force the SSC to bifurcate (Hill et al., 1997). One portion continues northward along the eastern side of the channel and passes through the Little Minch (see “LM” in Figure 2.1b). The other portion turns westward, crosses the channel, recirculates southward and flows around Barra,

and then turns northward to the west of the Outer Hebrides island chain, thus transporting coastal influences to the outer shelf (Hill et al., 1997; Inall et al., 2009; Jones et al., 2018; Simpson and Hill, 1986).

2.4 Instrumental data

2.4.1 *In-situ* oceanographic data

There are two important datasets of seawater temperature and salinity data for western Scottish shelf seas which are considered in this thesis:

(1) **The Ellett Line:** The Ellett Line is a hydrographic section that was launched by David Ellett in 1975 and is managed by the Scottish Association for Marine Science (SAMS), Oban, and the National Oceanography Centre (NOC), Southampton (Holliday and Gary, 2014). The project is aimed at providing a long data series of the hydrography of the eastern subpolar North Atlantic. The transect stretches from the western Scottish coast westward across the Rockall Trough and was extended to Iceland in 1996 (also referred to as "The Extended Ellett Line"). Measurements along the Ellett Line reach back as far as 1948, however annual observations did not start until 1975. The frequency of observations varies between stations and years, with up to six observations per station and year in the 1970s and 1980s, and mostly only one observation per station approximately every two years from the 1990s onwards. All in all, the extended section consists of 69 stations, however not all stations are sampled in each year. In this thesis, we focus on two stations:

1. Station 15G (Lat: 56.88° N, Long: 08.5° W; Figure 2.4): This station is located ca. 100 km south of St Kilda, on the Scottish shelf. The hydrographic conditions at this site are thus considered very similar to those at St Kilda. It is, however, not as frequently sampled as some other stations on the Ellett Line. Temperature and salinity have been measured 16 times in the period 1977–2008. Surface and bottom water data are available. The maximum water depth is 150 m.
2. Station Q (Lat: 57.05° N, Long: 09.21° W; Figure 2.4): Station Q is located on the outer shelf edge, bisecting the slope current. The local series consists of 69

measurements spanning 1975–2010 and thus provides more data than most other stations, including 15G. Surface and bottom water data are available. The maximum water depth is 350 m.

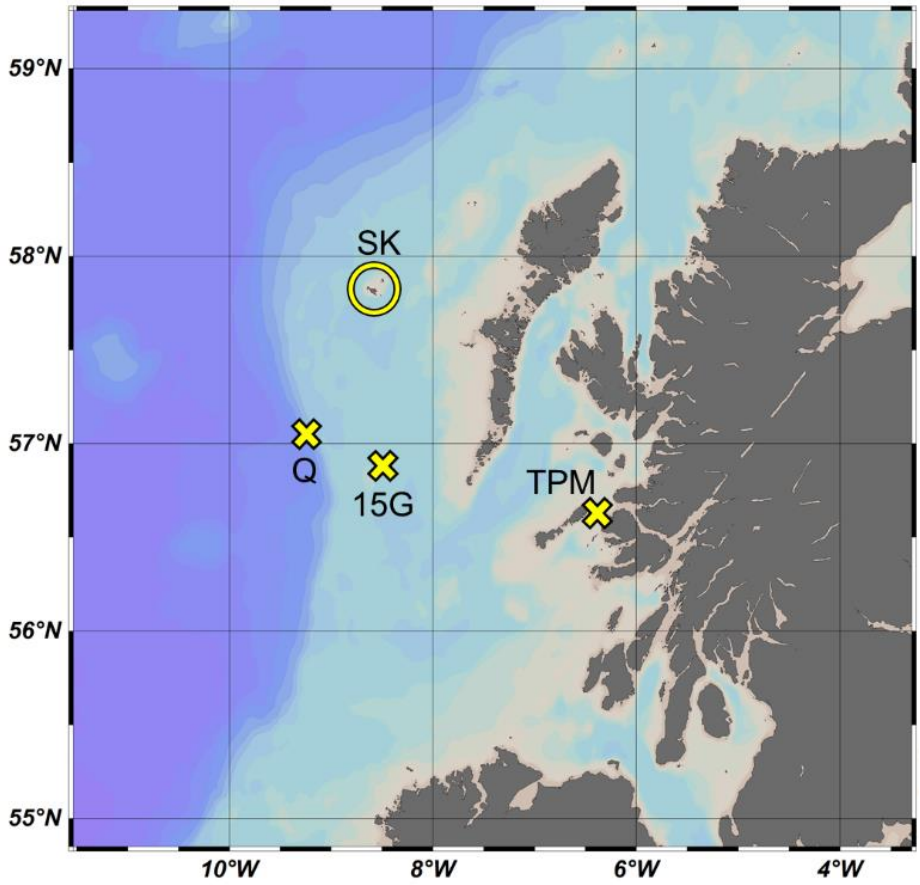

Figure 2.4: Hydrographic stations. Ellett line stations Q and 15G, and the Tiree Passage Mooring site (TPM) are marked with yellow crosses. St Kilda is marked with a circle (SK). (Ocean Data View; Schlitzer, 2020)

(2) **The Tiree Passage mooring** (Lat: 56.62° N, Long: 06.4° W; Figure 2.4): Being located in the Inner Hebrides between the islands of Coll and Mull, the Tiree Passage mooring (TPM) provides coastal data. The TPM is managed by SAMS and features hourly temperature and current measurements since 1981, as well as hourly salinity measurements since 2002. There are numerous gaps in the series, due to equipment failure and temporary lack of funding, among other reasons. Surface and bottom water data are available. The maximum water depth is 45 m.

In addition to the datasets mentioned above, the International Council for the Exploration of the Sea (ICES) provides bottle data and CTD data on their website (http://www.ices.dk/marine-data/data-portals). The ICES data stem from different cruises and different teams; thus the locations, methods, sampled time of year, and sampling frequency vary considerably over time. However, these data can be used to complement the two data series described above.

The longest coastal seawater temperature series in Scotland is located at Millport (Lat: 55.75° N, Long: 4.9° W) in the Firth of Clyde. Monthly-to-weekly data are available from March 1909 (with the years 1927–1948 missing), provided by the Scottish Government agency Marine Scotland (https://marine.gov.scot/information/coastal-monitoring-site-millport). Millport is under strong influence of the Scottish Coastal Current and coastal freshwater sources and is therefore not further discussed in this thesis.

In-situ data at St Kilda

There are no mooring sites at St Kilda, and the only hydrographic data available for this location are from bottle data obtained on individual cruises. Bottle data are available to download on the ICES website (http://www.ices.dk/marine-data/data-portals), but they yield only four data points for St Kilda, in July 1936, August 1938, June 1949, and June 1952 (Table 2.1). All measurements were taken at a depth of ca. 30 m.

Table 2.1: Four seawater temperature measurements at St Kilda, provided by ICES, for the 2nd July 1936, 5th August 1938, 2nd June 1949, and 23rd June 1952. Sample depths are between 29 and 35 m.

	T °C
July 1936	11.49
August 1938	12.34
June 1949	9.98
June 1952	10.52

2.4.2 Gridded sea surface temperature products

As *in-situ* data are scarce, gridded SST data products are the best alternative for proxy-data calibration at St Kilda. Three commonly used and freely available gridded temperature data products were considered for this thesis:

1. HadISST1 (Rayner et al., 2003): Met Office Hadley Centre's sea ice and sea surface temperature dataset; developed by the UK Meteorological Office
2. ERSST V5 (Huang et al., 2017): Extended Reconstruction Sea Surface Temperature Version 5; developed by the US National Oceanic and Atmospheric Administration (NOAA);
3. OISST V2 (Reynolds et al., 2002): Optimal Interpolation SST; NOAA

These data products offer interpolated global SST data, taking sea ice concentration into account in higher latitudes. The data products differ from each other in many ways; they are based on different raw data sources and offer different series lengths and different temporal and spatial resolution (see Table 2.2 for an overview). Perhaps most importantly, all three products use different interpolation techniques to bridge spatial and temporal gaps in the data. In addition, the two longer series, HadISST1 and ERSST V5, use reconstruction techniques in the data-scarce period before 1948. While both are based on empirical orthogonal functions (EOFs), the techniques differ between the two products. OISST V2 is the shortest series, however it offers the highest temporal resolution with weekly updates and a high-spatial resolution version of 1/4° by 1/4° is available (not discussed here). ERSST V5 does not contain any satellite SST data; incorporation of satellite data in earlier versions proved to bias the dataset towards colder temperatures. It is important to consider all these factors when choosing one product for proxy calibration. Previous studies have compared the three products regarding their ability to capture long-term trends over large spatial scales (Rayner et al., 2003; Reynolds et al., 2002). However, in biological and environmental studies, local or regional annual-to-decadal variability is often of more interest than macro-scale trends. Hughes *et al*. (2009) proposed a method to calculate how well each product represents the local *in-situ* data. The proposed method was used in this thesis as well (see Section 3.1 for the methods, Section 4.1.1 for the results, and Section 4.3.2 for further discussion).

Table 2.2: A selection of key features of the three gridded temperature products HadISST1, ERSST V5, and OISST V2. Abbreviations: ICOADS (previously COADS) = International Comprehensive Ocean-Atmosphere Data Set; MDB = Met Office Marine Data Bank; GTS = Global Telecommunication System; AVHRR = Advanced Very High Resolution Radiometer.

	HadISST1	**ERSST V5**	**OISST V2**
First complete year	1871	1854	1982
Spatial resolution	1° X 1°	2° X 2°	1° X 1°
Temporal resolution	Monthly	Monthly	Weekly
***In-situ* SST datasets**	ICOADS (1871–1995), MDB (including GTS from 1998)	ICOADS 3.0 (1854–2015), GTS (from 2016), and Argo SST	ICOADS (1981–1998), GTS (from 1998)
Satellite SST	AVHRR since 1982 (bias adjusted)	none	AVHRR (bias adjusted)

2.4.3 Meteorological data

The UK Met Office has been recording meteorological conditions at the Stornoway Airport (Lat: 58.21° N, Long: 06.32° W) in the Outer Hebrides, ca. 100 km northeast of St Kilda, since 1873. Hallett et al. (2004) found that the meteorological data from Stornoway captures the local conditions at St Kilda well when comparing winter data from 2000–2002 (temperature, $r = 0.92$; gust speed, $r = 0.82$; rainfall, $r = 0.78$). Access to the Stornoway series can be requested at http://archive.ceda.ac.uk/.

2.5 The St Kilda archipelago

St Kilda is an isolated volcanic archipelago, composed of four islands and several stacks, far out on the Hebrides Shelf (Figure 2.1, Figure 2.5). It forms the westernmost point of the Outer Hebrides, Scotland, and is located 64 km west-northwest of the nearest inhabited land, North Uist. Hirta is the biggest island with a circumference of 14 km, and it is the only island of the archipelago that has been inhabited. The other major islands are Dùn, Soay, and Boreray.

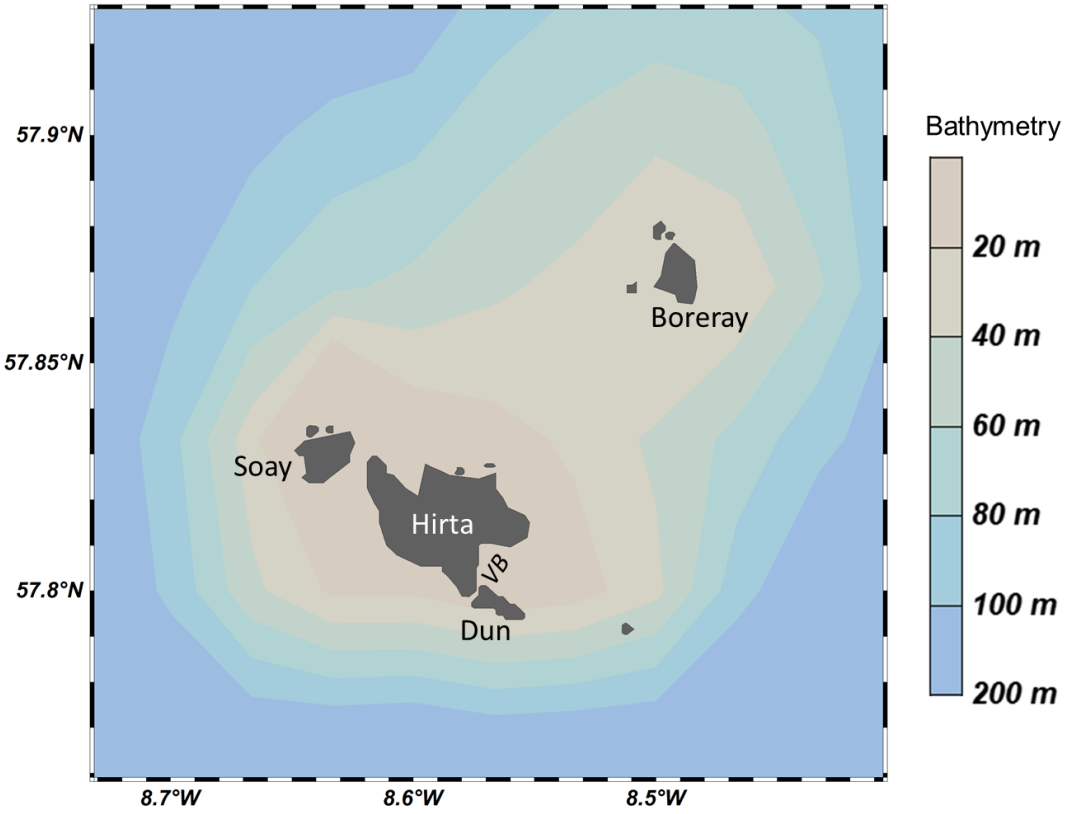

Figure 2.5: The St Kilda archipelago. The four main islands are labelled (Hirta, Soay, Dùn, Boreray). VB = Village Bay. Rough bathymetry contours are shown in colours as indicated in the legend to the right. (Ocean Data View; Schlitzer, 2020)

St Kilda is owned and managed by the National Trust for Scotland (NTS) and considered a near-pristine environment due to the low level of human interference and pollution (National Trust for Scotland, 2012). The archipelago has been uninhabited since the 1930s; however, it is not completely devoid of human presence. The Ministry of Defence maintains a small base on Hirta, and during the summer NTS rangers, scientists, and tourist groups visit the island.

2.5.1 Geological setting

The archipelago is situated on an outcrop of bedrock, referred to as the St Kilda Platform, and consists of intrusive igneous rocks. The coastlines are dominated by dramatic features, including the highest cliff (Conachair, 430 m) as well as the highest sea stack (Stac an Armin, 191 m) in Great Britain and Ireland (Scottish Executive, 2003). The cliff lines have been shaped by glaciation-deglaciation processes and sea-level changes, high-energy wave erosion, weathering, and other influences.

The cliff line of St Kilda plunges steeply into the sea until it is interrupted by a platform with several sub-surfaces and steps between 40 m and 80 m depth (Sutherland, 1984). These surfaces are thought to have been formed at about 12.6–11.5 kyr BP, during the abrupt cooling of the Younger Dryas or Loch Lomond Stadial (Bowen et al., 1986; Sutherland et al., 1984). They were mainly cut by frost shattering and sea ice, and were subsequently drowned due to melting of the ice sheet. At 120 m below the current sea level, another platform is present, which was most likely formed during the Last Glacial Maximum about 22–19 kyr BP (Sutherland et al., 1984; NB: More recent studies place the global Last Glacial Maximum at 26–19 kyr BP, e.g., Clark et al., 2009) . The surrounding shelf to the north, west, and south is marginally deeper (up to 140 m) than the lowest platform, while it gradually shoals to the east.

Marine sediment

The St Kilda Platform is characterised by exposed bedrock. Where sediment is present, it is usually a veneer of gravel, sandy gravel, or gravelly sand of less than 10 cm thickness. The finest sediment found at St Kilda is sand, mainly located at Village Bay (Hirta), and on the eastern and southwestern flanks of the platform. Silt is deposited infrequently and only in small sheltered areas, e.g., in caves and tunnels, or under boulders and under rocks on the sea bed (Ellis et al., 1995).

2.5.2 The marine environment at St Kilda

"One particularly severe storm left us deaf for a week – incredible but true. The noise of the wind, the pounding of the heavy sea, were indescribable."

—Mary Cameron, one of the last inhabitants of St Kilda; cited in Steel, 1975 (2011 edn., p. 29)

Waves and Storms

Due to its exposed offshore location close to the shelf margin, St Kilda is subjected to high-energy swell and wind waves throughout the year. The local wave conditions are dominated by swell waves generated in the open ocean. However, storms and storm waves affect St Kilda from all directions. Even Village Bay, one of the most sheltered sites at St Kilda, is exposed to storms arriving from south-easterly directions, with a fetch of 110 km (Sutherland, 1984). As the sea shallows abruptly above the platform close to the coastline of St Kilda, high-energy

swell waves move freely and break onto the coastline. The mean annual significant wave height at St Kilda is 3.06 m, which is close to nearby open-ocean wave heights of 3.2 m and significantly higher than coastal wave heights off the Inner Hebrides of mostly below 1.5 m (https://marinescotland.atkinsgeospatial.com/nmpi/). Maximum significant wave heights exceed 5 m and occur for 10% of the year (Scottish Executive, 2003). High-speed winds of 110 km/h occur regularly; on the clifftops wind speeds can reach 185 km/h (Scottish Executive, 2003).

Marine flora and fauna

As an offshore archipelago, St Kilda is subject to the *island mass effect*, a term coined by Doty and Oguri (1956) in a study on Hawaii, referring to the observed increase in primary production around oceanic islands. Located on the outer shelf in seasonally stratified waters, the archipelago causes tidal stirring and a breakdown of the stratification, which brings nutrient-rich bottom waters to the surface (Simpson and Tett, 1986). Simpson and Tett (1986) reported that the cold-water upwelling and mixing at St Kilda results in an increase in column phytoplankton production of 40% over an area of 5000 km^3. Consequently, the mixing caused by St Kilda has an important effect on the food chain beyond the local ecosystem, including large regions of spawning and nursing grounds for fish (Ellis et al., 2010). An abundance of fish naturally attracts predators such as seabirds and the Atlantic grey seal (*Halichoerus grypus*).

Marine life at St Kilda is not as well-documented as that of neighbouring islands of the Outer Hebrides. However, the literature provides insight into the taxonomic composition of marine algae (e.g., Watling et al., 1970), marine fauna (e.g., Ellis et al., 1995), and sandy beach fauna (e.g., Scott, 1960). Ellis et al. (1995) comprehensively studied the marine fauna of St Kilda using several different methods such as scuba diving, benthic trawling, line angling and intertidal collection. All in all, they found 296 species, including rare elements such as the anthozoan *Phellia gausapata* (Ellis et al., 1995). It is noteworthy that the authors marked the presence of *A. islandica*, but did not list *G. glycymeris* among the species found at St Kilda (Ellis et al., 1995).

The upper sublittoral flora is dominated by kelp species that are adapted to high-energy wave and surge exposure, such as dabberlocks (*Alaria esculenta;* Watling et al., 1970). Due to the oceanic conditions and low turbidity, sun light reaches deeper than in coastal areas, and dense

kelp forests occur at depths of up to 30–40 m (Scottish Executive, 2003). At depths of 60–80 m, the wave-base motion still influences the ecosystem, as well as currents and eddies. Here, rocky outcrops and boulders are abundant, often covered by coralline algae and encrusting animals, but also by erect sponges and bryozoans (Scottish Executive, 2003).

Only a few tourist and fishing vessels anchor at St Kilda each year. Commercial fishing at this site mainly consists of creel fishing for lobsters and crabs (Harris et al., 2018). While fishing activity is small, it is unknown whether catch levels of crabs and lobsters are sustainable (National Trust for Scotland, 2012). Ellis et al. (1995) hypothesised that overfishing of lobsters and crayfish may have occurred at this site as lobsters were only found in low numbers and crayfish were completely absent.

Village Bay

Village Bay is 1.2 km wide and located on the south-eastern coast of Hirta (Figure 2.5, Figure 2.6). The storm beach at Village Bay is 500 m long and 30–35 m wide at low tide; it is composed of boulders above a sandy beach (Scott, 1960; Watling et al., 1970). The sandy beach is exposed at low tide only and represents one of the few sandy patches at St Kilda (Scott, 1960; Watling et al., 1970). A small stream, *Amhuinn mhor*, divides the beach into two halves, close to where the island of Hirta is divided into a northern part characterised by granophyre, and a southern part characterised by dolerite. This division is evident in the rocks on the stormy beach; buff-coloured coarse rocks are dominant in the granophyre zone north-east of the stream, whereas blue-coloured, fine-grained small rocks dominate the dolerite zone south-west of the stream (Watling et al., 1970). Village Bay is one of the most sheltered areas of the archipelago, due to its eastward orientation and the protection provided by Dùn to the south; nonetheless, it is still exposed to storm waves and wind. Scott (1960) studied the fauna of the sandy beach and found that both taxonomic richness and numbers of specimens were low, with one notable exception being the abundant isopod *Eurydice pulchra*. Scott (1960) attributed the scarcity of species and individuals to two factors: (1) The observed quick drainage of the beach, caused by the angular and jagged shape of the sand particles, and (2) the impermanence of the sand, which is stripped from the beach each winter. A study by Ellis et al. (1995) confirmed the dynamic nature of the beach and its labile fauna, as they noted a complete absence of *Eurydice pulchra*, which had been abundant in Scott's study only 35 years prior (Scott, 1960).

Figure 2.6: Village Bay, viewed from Hirta. Cleits and remains of the village can be seen in the foreground. On the left are the military base and jetty. The neighbouring island Dùn is in the background to the right. The largest vessel in the middle of the bay is the RV *Prince Madog*. (Photo by Paul Butler)

2.5.3 Seabirds, humans, and Soay sheep

St Kilda is known not only for its dramatic cliffs and geological features, but also for its distinctive island biology and human history. While taxonomic richness of flora and fauna is generally low, the high abundance of seabirds each spring and summer is striking. The archipelago is a breeding site for 17 seabird species, with up to a million birds at the height of the breeding season, making it the largest seabird colony in northern Europe (Scottish Executive, 2003). St Kilda is home to the largest colony of the northern gannet (*Morus bassanus*) in the world, and hosts 94% of the UK breeding population of Leach's storm petrel (*Hydrobates leucorhous*) (Department of Energy and Climate Change, 2016; Kober et al., 2010). Other important breeding colonies include the Atlantic puffin (*Fratercula arctica*), northern fulmar (*Fulmarus glacialis*), European storm petrel (*Hydrobates pelagicus*), razorbill

(*Alca torda*), common guillemot (*Uria aalge*) and kittiwake (*Rissa tridactyla*) (Harris and Murray, 1989; Kober et al., 2010).

Archaeological evidence suggests that humans settled on Hirta as far back as the Neolithic (4000 to 2500 BCE) (Fleming, 1995). The St Kildans lived in one single village at Village Bay, in a tight-knit community that never surpassed more than 200 people at any given time (Steel, 1975/2011). They kept sheep and few cattle, and harvested meagre crops, but their most important source of food were seabirds and seabird eggs (Figure 2.7). The birds and eggs were harvested in great numbers and at great risk by climbing the steep cliffs. In 1697 CE, Martin Martin visited the island and estimated that the 180 inhabitants at the time had consumed 48,000 seabird eggs within three weeks (Martin, 1698/1753). Between the years 1829 and 1843, the 100 islanders slaughtered about 12,000 fulmars and 5000 gannets every year (Steel, 1975/2011). Life at St Kilda was harsh; the islanders were exposed to wind, storms and salt spray, far away from the next inhabited land. Over the course of the 19th century, contact between the St Kildans and the mainland increased, which changed the community structure and decimated the population through imported diseases (Steel, 1975/2011). By the early 20th century, the number of islanders had declined drastically, and they were struggling to survive. The last 36 islanders remaining on Hirta were evacuated in 1930.

While the evacuation marked the end of an extraordinary chapter of Scottish history, it also opened the door to a range of biological studies. When the St Kildans left, so did the domesticated blackface sheep that had been kept on Hirta. However, to maintain the grazing pressure on the island, a flock of feral sheep from the neighbouring island Soay was established on Hirta two years after the evacuation (Boyd et al., 1964). Soay sheep are thought to be the direct descendants of the first sheep brought to St Kilda, and the most primitive breed of domestic sheep in Europe (Boyd et al., 1964). The Soay sheep on St Kilda are unmanaged and entirely exposed to the weather. There are no trees or buildings that provide shelter, apart from abandoned storage buildings made of stone (i.e. *cleits*; Fleming, 1995). Other than the occasional case of a seabird attacking lambs, there are no predators, and given the isolated nature of St Kilda, there is no migration either. As a consequence, the survival and fitness of the sheep are intrinsically tied to their physical environment, e.g., temperature, precipitation, and wind speed. Thus, the Soay sheep population on Hirta is the subject of scientific studies on population dynamics and evolution due to its exposure to weather and climate (e.g., Boyd et al., 1964; Coulson et al., 2001). Continuous and highly resolved data on sheep individuals,

mortality, morphology, and other parameters, are available since 1985, thanks to the St Kilda Soay Sheep project (https://soaysheep.bio.ed.ac.uk/).

Figure 2.7: Top: A St Kildan family during fulmar harvest. Bottom: Two St Kildan men with Soay sheep. (National Trust for Scotland, retrieved from https://kildaprojet.com/2016/11/25/st-kilda-old-memories/)

Chapter 3

Material and methods

Chapter 3 — Material and methods

3.1 Oceanographic data

Instrumental hydrographic data are scarce on the Scottish western shelf – this is particularly true for non-coastal environments like St Kilda. Therefore, gridded data are the best option for calibrating proxy records and tracking changes through time. For a detailed description of the three gridded data products OISSTv.2, HadISST1 and ERSSTv.5, see Section 2.4. Ideally, the gridded SST datasets should be compared to *in-situ* data to ensure that the best-fitting dataset is used for the specific location (see Hughes et al., 2009). Hughes et al. (2009) compared the three products OISSTv.2, HadISST1, and ERSSTv.3 to *in-situ* data of six locations in the Northeast Atlantic region, including one site in the Faroe-Shetland Channel, which was the one closest and most similar to St Kilda. Overall, OISSTv.2 and HadISST1 performed the best in that study, including at the Faroe-Shetland site, where HadISST1 provided the closest match.

Unfortunately, *in-situ* data at St Kilda are too scarce for any such comparisons. The closest stations with hydrographic data are station Q and 15G of the Ellett line (see Figure 2.4 in the previous chapter). While station Q has a higher resolution of measurements (69 measurements 1975–2010) than station 15G (16 measurements 1977–2008), it is located on the shelf margin, and thus not ideally suited to assess how well the gridded data represent local conditions at St Kilda. Station 15G is located south of St Kilda and has a similar oceanographic setting and thus provides the most representative, yet poorly resolved, data. Therefore, an *in-situ* data ensemble was built by combining the few local data points (mainly bottle data, see Section 2.4.1) for St Kilda and the data points obtained from station 15G. Where there was only one data point for a specific calendar month in a year, that data point was included in the ensemble. Where there were more than two data points from one or both locations within the same calendar month, the average was calculated and included in the ensemble. The gridded data products were then compared to the *in-situ* ensemble data following the same steps as outlined in Hughes et al. (2009):

1) Annual temperature data for the OISSTv.2 product are available from 1982 onwards, however, there are no *in-situ* data for that year. Hence, all data series were cut off before 1983 and the resulting period of comparison spanned 33 years (1983–2015).
2) As the growth season of *A. islandica* at this location is May–October (see Results section 4.4.2.2) and *in-situ* data are very scarce during the rest of the year, only those six months were considered in this comparison.
3) *In-situ* data are partially depth-averaged and thus they are not expected to fit the absolute sea surface temperatures. Therefore, monthly temperature anomalies were calculated by subtracting the average temperature for 1983–2015 from each year to compare the variability between the datasets.
4) To decrease the effect of the differences in sampling frequency, three-year annual means were calculated and used for all further analysis.
5) The Pearson correlation as well as the root-mean-square-error (RMSE) between each gridded dataset and the *in-situ* ensemble were calculated. A high Pearson correlation coefficient and low RMSE means higher similarity between datasets.
6) In addition to point 5 above, a Skill score was calculated for each gridded product using the standard deviation and Pearson correlation. This Skill score *S* measures how well the scale of variability matches between datasets. The equation for calculating *S* was developed by Taylor (2001):

$$S = \frac{4(1+r)^4}{\left(\hat{\sigma}_g + \frac{1}{\hat{\sigma}_t}\right)^2 (1+r_0)^4} \qquad (1)$$

where r is the Pearson correlation coefficient between gridded data and *in-situ* data, r_0 is the highest attainable correlation ($r_0 = 1$), σ_g is the standard deviation of the gridded satellite data, and σ_t is the standard deviation of the *in-situ* data.

The chosen grid was Lat: 57–58° N/Long: 8–9° W for OISSTv.2 and HadISST1, and Lat: 57–59° N/Long: 7–9° W for ERSSTv.5.

In a second round, data points from station Q were added into the *in-situ* ensemble dataset to include more data points, albeit from a larger area. The same comparison with gridded datasets as outlined in the six steps above was performed again.

3.2 Sample collection

3.2.1 Sampling overview

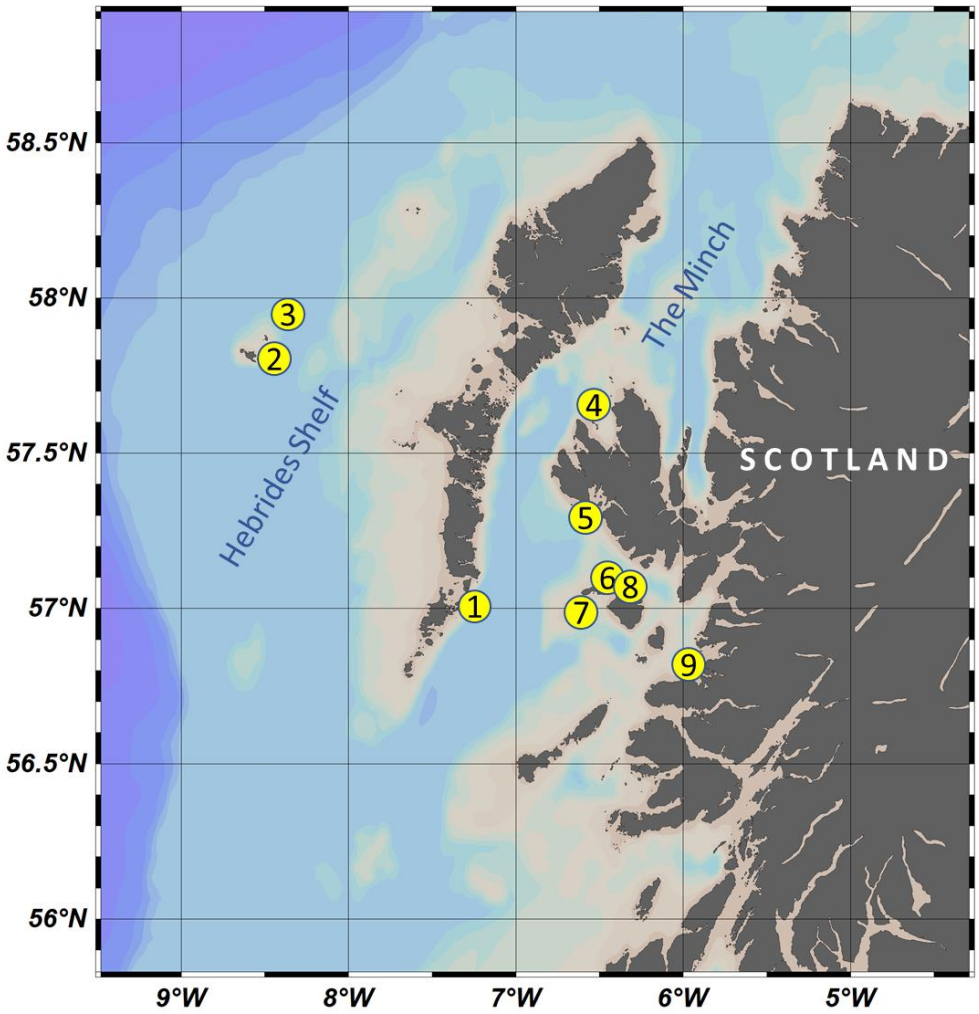

Figure 3.1: Sample sites of the Hebrides cruise aboard the RV *Prince Madog*. Yellow circles indicate sample sites where dredging took place; they are numbered in chronological order. 1 = Barra, 2 = St Kilda/Village Bay, 3 = St Kilda platform north, 4 = Skye north, 5 = Skye south, 6 = Canna north, 7 = Canna south, 8 = Rhum, 9 = Ardnamurchan.

The material for this study was collected on two occasions using different methods: (1) By dredging during a research cruise off the Hebrides in May 2014, and (2) by manual collection by SCUBA divers at St Kilda in April 2016. During the cruise aboard the RV *Prince Madog* to the Inner and Outer Hebrides, numerous shell valves and live specimens of *Glycymeris glycymeris* and *Arctica islandica* were collected using a customised "Arctica dredge". The dredge is 1 m wide, covered with a 1.5 x 1.5-cm mesh and equipped with two sets of 10 cm-long teeth to dig into the sediment. At every sample site, a side-scan sonar was towed at 2 knots to examine the entire potential transect. Patches with large boulders or exposed bedrock were

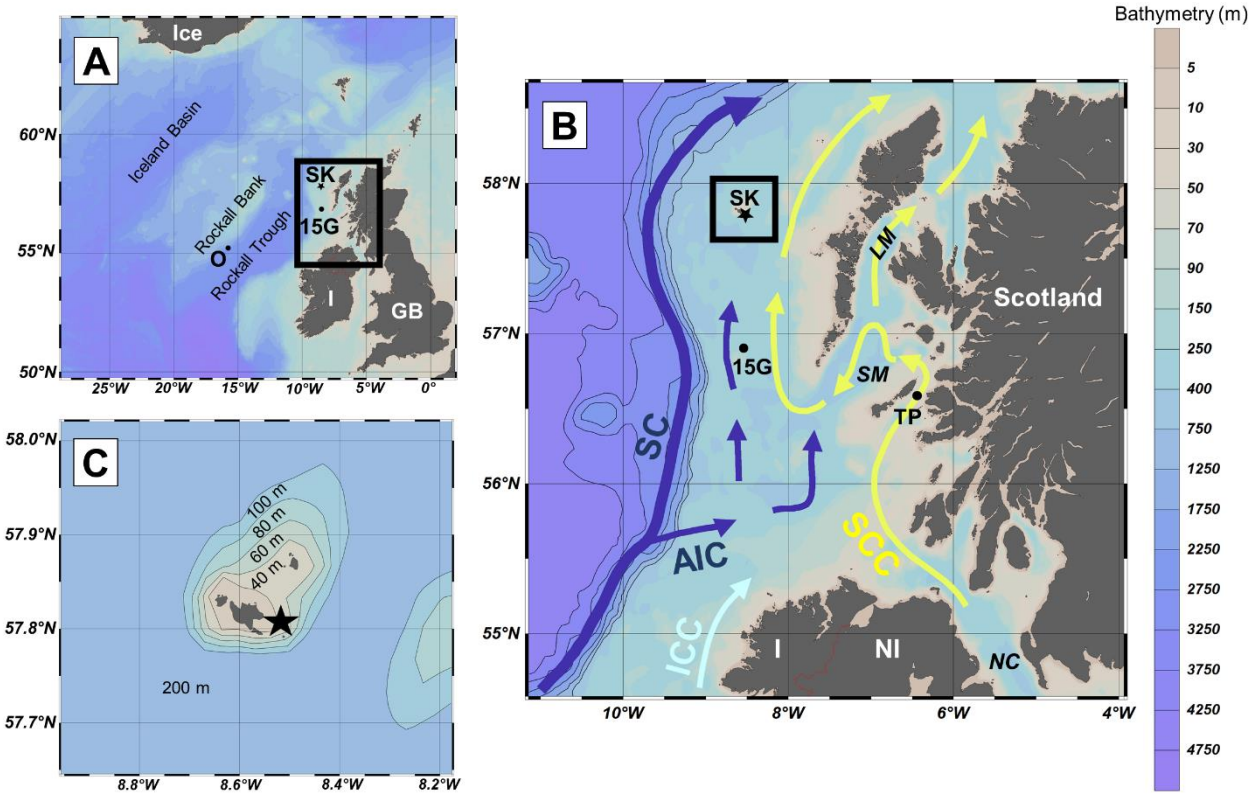

Figure 3.2: Location of the sample site at St Kilda, Scotland. **(A)** Overview map. Colours indicate bathymetry according to the legend to the right. Land masses are labelled with "Ice" = Iceland, "I" = Ireland, "UK" = United Kingdom. "SK" = St Kilda. "15G" = Ellett line station 15G, marked with a dot. "O" = Location of $\delta^{18}O_w$ measurement (Östlund and Grall, 2001) referred to in Methods section 3.6.5, marked with a dot. The black rectangle indicates the location of the detail shown in map B. **(B)** Detail of map A. Sample location (black star) at St Kilda, Outer Hebrides, Scotland. The yellow arrows indicate the approximate circulation of the Scottish Coastal Current (SCC). The dark blue arrows indicate the flow of the slope current (SC) and Atlantic Inflow Current (AIC) transporting Atlantic water. The light blue arrow indicates the Irish Coastal Current (ICC). Background colours denote bathymetry according to the legend to the right. Depth contours for the shelf margin and open ocean are drawn in black lines. The shelf margin is indicated by depth contours starting from 200 m. Approximate positions of currents were taken from Inall et al. (2009), Turrell et al. (1996), and Porter et al. (2018). TP = Tiree Passage mooring station. NC = North Channel, SM = South Minch, LM = Little Minch. Land masses are labelled with "Scotland", "SK" = St Kilda, "I" = Ireland, and "NI" = Northern Ireland. The black rectangle indicates the location of the detail in map C. **(C)** Detail of map B. Shown is the archipelago of St Kilda with the surrounding bathymetry. The respective depths are indicated within each depth contour line. The black star marks the sample site of this study. (Ocean Data View; Schlitzer, 2020)

noted in the logbook. Once the seabed was scanned, the Arctica dredge was deployed and dragged at 4 knots for 10–15 min, avoiding rocky areas (Appendix B).

The cruise route was planned in an effort to include both coastal sites from the Inner Hebrides and also offshore sites at St Kilda (Figure 3.1). The rationale was that chronologies produced with shells from the Inner Hebrides would complement existing chronologies from comparable sites in the Irish Sea (Butler et al., 2010) and the Tiree Passage (Reynolds et al., 2013), while chronologies from the offshore locations at St Kilda, Outer Hebrides, could be used to study signals that represent the North Atlantic open ocean. Before selecting sample sites, we checked the National Biodiversity Network website (NBN, nbn.org.uk) for previous records of *A. islandica* and *G. glycymeris*. These presence data on NBN do not always indicate whether there is a healthy population at the site or whether only individual specimens were found. Thus, two additional criteria were applied to select suitable areas for sampling and enhance the likelihood of finding enough shells for sclerochronological studies: (1) The water depth should be between 20–150 m (also due to the limited wire length of the winch that the Arctica dredge is attached to), and (2) the sediment type should range between muddy sand and gravelly sand. Most of the material was collected at Village Bay, St Kilda (hereafter called "Village Bay" or VB); north of Skye ("Skye North", SN); and northeast of Canna ("Canna North", CN). An overview of all shells collected at the three main sites is given in Table 3.1.

This thesis focuses on St Kilda; its offshore location close to the shelf margin makes it a highly valuable site for palaeoceanographic reconstructions (Figure 3.2, see Chapter 2). Apart from seven young live *G. glycymeris* specimens, the vast majority of the material retrieved at Village Bay during the cruise aboard the *Prince Madog* were single *G. glycymeris* valves, dredged at 40–65 m depth (Table 3.1). In a subsequent campaign, divers from the UK NERC National Facility for Scientific Diving (NFSD) were deployed at Village Bay in April 2016; in this campaign, a very large *A. islandica* population was found, of which a hundred live specimens and more than 60 valves were recovered at 24 m depth. Additional diving at greater depths, where we expected to find live *G. glycymeris*, was not possible due to bad weather.

During the research cruise in 2014, all live samples were frozen aboard immediately after collection and later thawed and shucked in the laboratory at Bangor University. During the diving campaign in 2016, the live samples could not be frozen on board due to limited space

in the freezer. Instead, they were kept in a cool place and shucked immediately after arrival at Bangor University.

Table 3.1: Number of shells collected at the different sampling locations. St Kilda 16 = Collection through divers in 2016. All other locations were dredged in 2014.

	Coordinates (Lat, Long)	***Arctica* live**	***Arctica* dead**	***Glycymeris* live**	***Glycymeris* dead**	**Depth**
St Kilda	57.82° N, 08.59° W	-	4	12	645	40–65 m
St Kilda 16	57.82° N, 08.59° W	c. 100	c. 100	-	-	24 m
Canna North	57.06° N, 06.47° W	28	16	1	-	72–119 m
Skye North	57.61° N, 06.52° W	18	52	3	58	45–65 m

3.2.2 Shell condition and properties

The dead-collected *G. glycymeris* shells from Village Bay were in variable condition, ranging from heavily bored and faded in colour to well preserved with the external shell pattern intact (Figure 3.3). Most of the heavily bored *G. glycymeris* shells were excluded from this study and curated in storage boxes immediately after being cleaned and dried. The dead-collected *A. islandica* from Village Bay were mostly in good condition, having been handpicked by divers. All the other sample locations yielded live and dead material in variable condition; however, only a small amount of this material was used in this thesis.

Figure 3.3: *G. glycymeris* valve from St Kilda (specimen 14G0VB031). The shell is intact and the typical external shell markings are still visible. Scale bar = 1 cm.

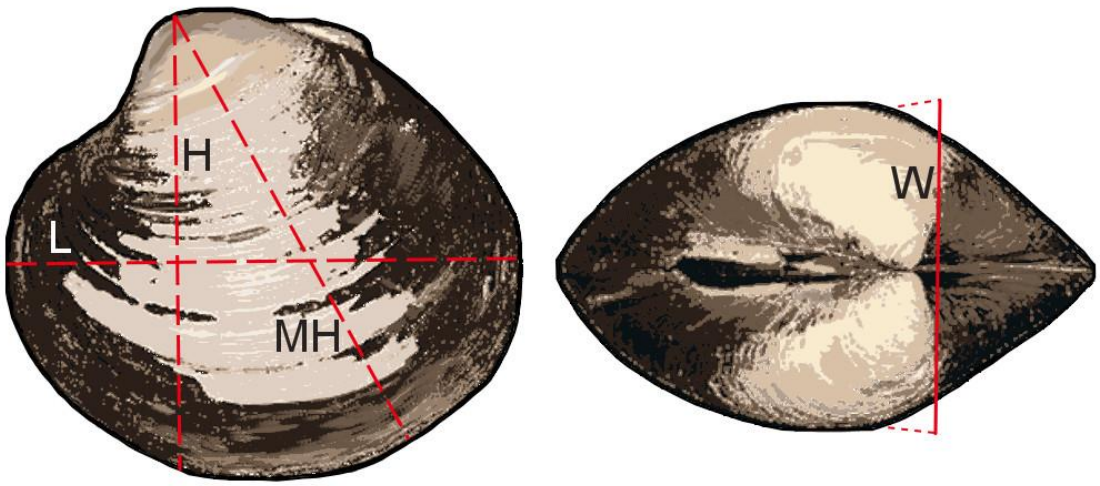

Figure 3.4: Measurement axes in *A. islandica*. L = Length, H = Height perpendicular to length, MH = Maximum height along axis of maximum growth, W = Width. *G. glycymeris* were measured along the same four axes.

Shells that were considered usable for sclerochronological studies (i.e. expected to be above an age of 30 years, not too heavily eroded, with either hinge plate or shell margin or both still intact) were measured along different axes as shown in Figure 3.4 and weighed (Appendix A). The dead-collected *G. glycymeris* from Village Bay had a strikingly asynchronous shape (Figure 3.5), which was not found in shells at other locations. All in all, 187 *G. glycymeris* shells (of which 169 were from Village Bay) and 106 *A. islandica* shells (66 from Village Bay) were measured, evaluated taphonomically, and processed as described in Section 3.3.1.

After measurement, the condition of each shell was assessed following a scoring system as described in Table 3.2. The purpose of the system is to rank dead-collected material based on its taphonomic condition, presupposing that live-caught animals would receive the highest scores in every category. Hence, mainly dead-collected shells were evaluated, apart from a few live-caught shells for reference.

Table 3.2: Scoring scale of shell condition. The table shows the lowest and highest possible of a range of scores.

	Lowest		Highest
Periostracum	1 No periostracum	⟷	5 Covers whole shell
Ligament	1 No ligament	⟷	4 Fully preserved
Margin	1 Worn, heavy abrasion	⟷	4 Sharp and intact
Bioerosion	1 Whole shell heavily bored	⟷	4 No bioerosion
Nacre	1 Worn or matt with blisters	⟷	3 Shimmery and smooth

3.3 Chronologies

3.3.1 Shell preparation

Crossmatching was carried out using magnified images taken from acetate peel replicas of the acid-etched surface of sectioned shells as described by Kennish et al. (1980) and Ropes (1987). A summary of the exact methods used in the present thesis is given below.

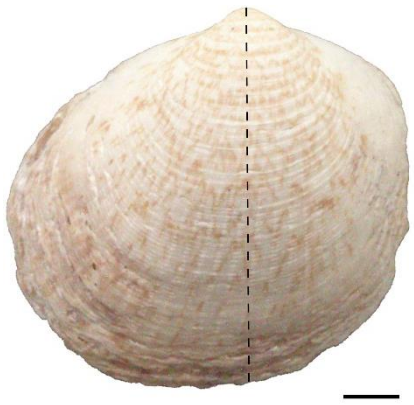

Figure 3.5: Specimen 14G0VB020, a single valve collected at Village Bay, St Kilda. The dashed line indicates the shell height, highlighting the asynchronous shape of the shell. Scale bar = 1 cm.

For *Arctica islandica*, the left valve was chosen for processing, if available and intact. This allows for additional measuring in the hinge plate tooth that is present only in the left valve of this species. *G. glycymeris* has no such tooth, but to be consistent the left valve was chosen where possible, by checking the orientation of the beak and anterior hinge line. In both cases,

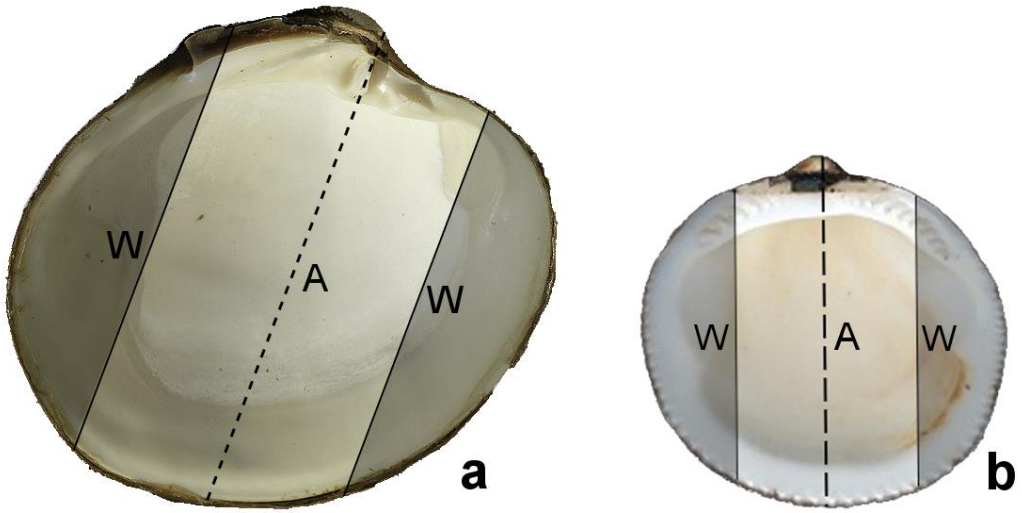

Figure 3.6: Cutting lines along the axis of maximum growth for the cross section (A) and along the "wings" to fit the shell in the embedding mould (W). (a) *A. islandica*, (b) *G. glycymeris.*

the "wings" of the valve (Figure 3.6) were cut off with a rough diamond saw to leave a central section that was small enough to fit the silicon mould used for embedding. The trimmed valves were embedded in resin, using MetPrep's Kleer-Set FF polyester casting resin and hardener. The resin and hardener were mixed (ratio: 6 drops of hardener to 10 ml of resin) by slowly stirring the two liquids together in a paper cup, using a wooden stick. Mixing the polyester resin and hardener initiates an exothermic chemical reaction, which means that the liquid initially heats up and expands, before it cools down again while setting and hardening. Embedding was carried out in three layers (base layer, middle layer with shell, top layer), with at least one hour given between each layer to let it set. The first layer was poured into the empty mould to make sure that the entire shell will be covered by resin once embedded. Then, after at least one hour, the trimmed shell sample was placed on top of the base layer, and small paper labels with the shell ID were placed next to the shell. Then, the second layer of resin was poured into the mould. This second layer was thick enough to cover the whole shell. After waiting for at least another hour, two more paper labels were placed on each side of the shell, on top of the

second resin layer, and a thin (ca 5 mm) third resin layer was poured into the mould. This method of embedding the shell in three steps allowed for labels to be embedded between layers and decreased the risk of air pockets developing. Once fully embedded, the resin blocks were left to harden for at least 24 h before sectioning. The shells were sectioned along the axis of maximum growth (Figure 3.6) with a Buehler IsoMet 5000 precision saw. The cutting line of the blade was slightly offset from the axis of maximum growth in order to ensure that it would be exposed after grinding and polishing. The sectioned blocks were then ground using silicon carbon paper mounted on a grinding machine with rotating disks. First, coarse silicon carbon pads of grit size P80 or P120 were used to grind off any sharp edges of the blocks that could damage finer pads at later stages. Then, the cut surface of each block that exposed the sectioned shell was ground using a series of successively finer pads with grit sizes of P400, P1200, P2500 and P4000 for at least 2 min each, depending on the sample. Finally, the ground surface was polished with the Presi Mecapol P230 polishing machine at 270 rpm using a self-adhesive polishing cloth coated in Presi Mexaprex GH diamond paste of 3 µm grit size mixed with lubricant of the same brand. After bathing the blocks in soapy water to remove the diamond paste, and rinsing them with clear water, they were left to dry before etching. The blocks were then etched in either 0.1 M or 0.01 M hydrochloric acid (HCl). Etching enhances the contrast between annual growth increments and the organic-rich growth lines as the latter form etch-resistant ridges (e.g., Schöne et al., 2002). However, etching also enhances other patterns in the shell, such as the crossed-lamellar structures and microtubuli that are present in *G. glycymeris* shells (Böhm et al., 2016), which in turn may obstruct the annual lines. Thus, most dead-collected *G. glycymeris* specimens had to be etched in a weaker acid than other specimens. Table 3.3 shows a general overview of the etching procedures for different shell types; there were a few exceptions that had to be determined by trial and error and are not shown in the table.

Table 3.3: Etching procedures for live- and dead-collected *A. islandica* and *G. glycymeris*. The weaker acid (0.01 M HCl) was used for most dead-collected *G. glycymeris*.

	***Arctica* live**	***Arctica* dead**	***Glycymeris* live**	***Glycymeris* dead**
0.1 M HCl	1.5-2.0 min	1.5-2.0 min	1.0-1.5 min	
0.01 M HCl				40 min

After rinsing the blocks with water, they were left to dry overnight. Leaving enough time for the samples to dry is crucial because the polyester resin contracts when it hardens, creating microscopic crevices between shell and resin in which water can accumulate and eventually spoil the acetate peel. Once dry, the polished surface was coated with ethyl acetate and covered with a cellulose acetate sheet (Agar Scientific). After at least 2 h of drying, the sheet was peeled off and squeezed between two microscope slides to make it as flat as possible for the photographic imaging.

3.3.2 Imaging and measuring

The acetate peels were photographed using a Meiji MT8100 microscope in combination with a Lumenera Infinity 3 microscope camera and the software ImagePro Premier 9.1. As the camera frame only covered a small portion of the peel at once, individual frames were photographed and stitched together using the tools provided by ImagePro Premier. In the case of specimens destined for isotope sampling, thick sections of the etched blocks were photographed as well. Table 3.4 shows the various imaging settings used.

Table 3.4: Microscope and imaging settings for resin blocks and peel photography

	Light	ImagePro stitching	Microscope lens
Thick section (whole shell)	Reflective (Olympus highlight 3001 lamp and desk lamp)	Manual	2.5x
Peel (margin)	Transmitting	Automatic	2.5x
Peel (hinge plate)	Transmitting	Automatic	5x

The first task after creating the microscope pictures is to find common growth patterns among the specimens by eye. The best way to achieve this is by looking for marker years, i.e. annual bands that are considerably wider or narrower than neighbouring years. This method worked well in the case of *A. islandica* as (1) the annual growth variability is high in this species and (2) live-collected specimens, where absolute calendar dates were known, could be used to establish marker years. Later, dead shells were scanned for the same patterns as seen in the live-caught specimens to determine whether their lifespans potentially overlap. This approach was also attempted for *G. glycymeris*, but given the more complacent nature of the banding in

this species (i.e. no strong marker years; pers. observation) and the fact that all *G. glycymeris* shells from St Kilda used for crossmatching were dead-collected, it did not prove successful and was thus abandoned.

G. glycymeris were measured in the hinge plate, where banding patterns are much clearer than in the margin. Because the annual variability in growth is rather small, each increment was measured three times along slightly offset axes and the average value was used to reduce measurement error (Figure 3.7a). In contrast, *A. islandica* produce clear images in the margin area and show higher annual growth variability, and were therefore measured in the margin (Figure 3.7b). All measurements were taken with the measuring tool in ImagePro Premier and exported to Microsoft Excel, where they were arranged in a two-column format (calendar year, increment width) and saved as individual tab-delimited files.

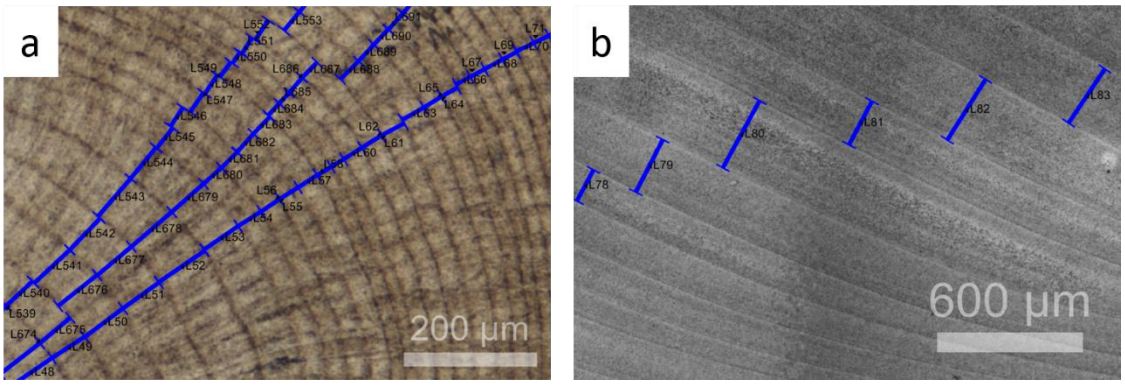

Figure 3.7: ImagePro images of acetate peels of (a) *G. glycymeris*, hinge plate, and (b) *A. islandica*, margin. The blue lines show the measurement axes.

3.3.3 Crossmatching

Correlations between the shells were visualised and quantified using the MATLAB script SHELLCORR (written by Ian Harris, UEA; Scourse et al., 2006), which is a graphical version of the dendrochronological programme COFECHA (Holmes, 1983). The tab-delimited files described above were loaded into the script and analysed pairwise after log-transforming and normalising the measurements and taking residuals from a 15-yr spline. This high-pass filter is applied to remove the low-frequency ontogenetic growth trend of the shell, where increment

width decreases with age. The removal of these growth trends enables the comparison of high-frequency variability between specimens. The correlation plot in SHELLCORR illustrates the correlation between two shells through time in a moving window that was set to 21 years and helps localise measuring errors (e.g., missed years or falsely added years) and offsets between life spans (Figure 3.8). Where SHELLCORR suggested a measuring error, the acetate peel image was examined again and remeasured if a likely source of the error could be observed on the microscope image (Butler et al., 2009a).

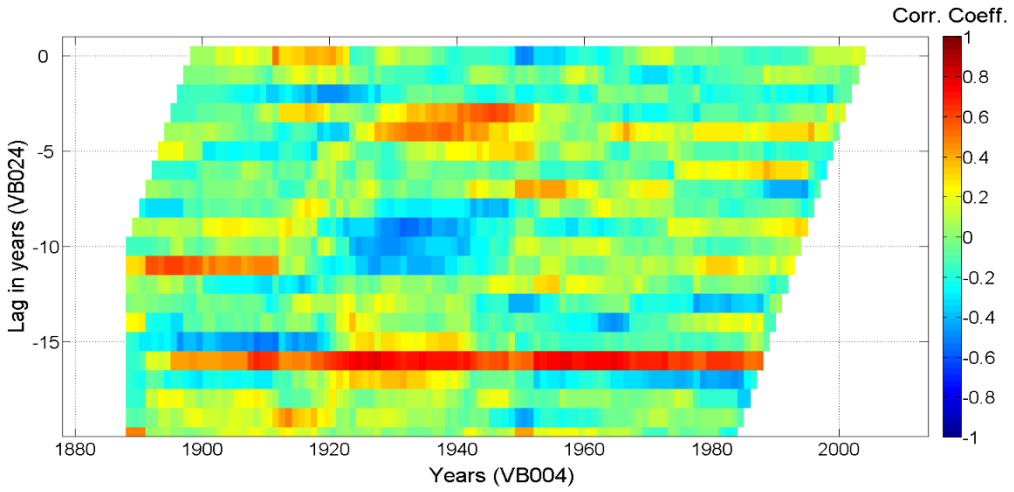

Figure 3.8: SHELLCORR plot showing a strong positive correlation between 14G0VB004 (reference shell, x-axis) and 14G0VB024 (y-axis) for >80 years with an offset of 16 years (i.e., VB024 died 16 years earlier than VB004). Calendar years on the x-axis are preliminarily assigned and not correct.

3.3.4 Master chronologies

Once the shells were successfully crossmatched, a master chronology was built using the dendrochronology programme ARSTAN (Cook, 1985; Cook and Krusic, 2005).

ARSTAN was developed as a tool to remove non-climatic growth trends in tree rings and combine tree-ring series into mean chronologies. Both tree-ring series and bivalve growth series are highly autocorrelated, which can mask the year-to-year variation. Therefore, ARSTAN applies an autoregressive model to the measurement series to remove persistence in band widths and to enhance the common signal.

3.3.4.1 Standardisation of time series

Growth increment series in bivalve shells possess similar ontogenetic and geometrical growth trends to tree-ring series, which have to be approximated and removed (detrended) prior to chronology construction. In addition to detrending, ARSTAN also creates dimensionless indices of each series with a mean value of 1. The creation of these standardised growth indices (SGIs) through detrending and indexing is referred to as standardisation (Cook, 1985). The resulting SGIs quantify the deviation of individual increments from the estimated value for that year. A value larger than 1 indicates that the shell grew more than estimated, while a value smaller than 1 indicates less growth. One major challenge faced during this process is the 'segment length curse' (Cook et al., 1995), which describes the loss of low-frequency climatic signals during standardisation. When removing age trends, other mid- to low-frequency signals are generally removed as well. The resulting chronology thus fails to capture climate oscillations with wavelengths that exceed the length of the individual time series. In the past few decades, a subfield of dendroclimatology has dedicated itself to studying ways to preserve low-frequency signals. Although no definite solution has been found, regional curve standardization (RCS; Briffa et al., 1992; Cook et al., 1995) and related RCS-type methods (for an overview, see Helama et al., 2017) have been shown to retain low frequencies better than conventional methods. The regular RCS method applies one single reference curve to all time series (i.e. bivalve specimens) of one location, based on the mean ontogenetic growth curve. The mean curve is estimated by aligning all individual series by biological age and then calculating a bi-weight robust mean of the aligned series. The mean curve is then smoothed by fitting a cubic spline with a 50% frequency-response cut-off equal to 10% of the series length (Esper et al., 2003). This leads to better retention of low-frequency variability compared to methods that fit a separate curve to each individual series (Cook et al., 1995). However, RCS requires a large sample size and high series replication due to decreased shared variance among specimens, and to ensure that the curve is derived from an equal number of specimens throughout all time periods. Therefore, this method was not suitable for the present study and a negative exponential curve was fitted to each series instead. The negative exponential function is a deterministic approach, i.e. it fits an *a priori* mathematically defined function to the series, which models the geometry of growth and its effect on increment widths (Cook et al., 1990). The equation used here to determine the growth trend G_t was first proposed by Fritts (1963):

$$G_t = a * e^{-bt} + k \qquad (2)$$

where *a*, *b* and *k* are coefficients of the regression function, all being a function of time (*t*), and describing the initial increment width, concavity of the curve and limiting (minimum) increment width, respectively.

3.3.4.2 Chronology strength — Rbar and EPS

Two values are used to quantify the quality of the chronology: The series inter-correlation (Rbar) and the expressed population signal (EPS; Wigley et al., 1984).

The Rbar measures the mean correlation between all detrended series, and thus the strength of the signal common to all time series in the chronology. More sensitive species will show stronger common signals among specimens and generally yield a higher Rbar. However, the Rbar does not by itself indicate how well environmental factors are represented, thus even chronologies with a low Rbar of 0.4–0.5 can be valuable proxies.

The EPS measures how well the chronology signal represents the population signal. It is defined as

$$EPS \equiv (\bar{R}_N)^2 \approx \frac{N \times Rbar}{1+(N-1)\times Rbar} \qquad (3)$$

where N is the number of series in the chronology, and $\bar{R}_N$ is the expected correlation between an N-series average and the population average (Wigley et al., 1984). As the equation illustrates, both a high Rbar and a high number of series increase the EPS. Therefore, to be regarded as reliable, a chronology with low inter-series correlation will need to have more series incorporated than a chronology with a high Rbar. Wigley et al., (1984) recommended a minimum EPS of 0.85 to ensure that the chronology is reliable. However, just like the Rbar, the EPS does not per se indicate whether a chronology is suitable to reconstruct climate (Buras, 2017).

3.3.4.3 Using ARSTAN to build chronologies

The tab-delimited files created for SHELLCORR were combined into one compact file using the programme FMT (http://www.ltrr.arizona.edu/pub/dpl-mac/68k/dpl.txt) and loaded into ARSTAN. The raw series were power-transformed, detrended by fitting a negative exponential curve and stacked in a composite ("master") chronology using a bi-weight robust mean function (Cook et al., 1990). The correlation between the master chronology and each individual series was calculated based on moving 30-year windows with 15 years overlap.

The two floating fossil *G. glycymeris* chronologies consisted of seven (referred to informally as "St Kilda Seven chronology") and two shells (referred to informally as "Misfits chronology"), respectively. The modern *A. islandica* chronology consisted of six shells.

3.3.5 Analysis of chronologies

3.3.5.1 Spectral analysis

We analyse the spectra of frequencies to find dominant patterns and periodicities in time series. However, it is important to bear in mind that the underlying processes of time series in climate and environmental studies are dynamic. Here, three different methods were chosen, using the free software PAST (Hammer et al., 2001) and KSpectra (SpectraWorks, version 3.4.3): (1) Singular Spectrum Analysis (SSA; Vautard et al., 1992), (2) the Multitaper Method (MTM; Lees and Park, 1995; Thomson, 1982), and (3) Continuous Wavelet Transform Analysis (CWT) with Morlet (wavenumber 6) as mother wavelet (Torrence and Compo, 1998). SSA is a linear analysis and prediction tool with data-adaptive character, and is meant to perform well for short and noisy time series (Vaughan et al., 2011). It decomposes time series into a sum of components. Vaughan et al. (2011) developed algorithms for noise reduction, detrending, and identifying oscillatory components for SSA. To account for dynamic processes, SSA relies on reconstructed components rather than simply averaging over entire time windows. Similarly, MTM was developed to improve the conventional Fourier transform method, especially with regard to biases introduced through finite and small sample sizes (Thomson, 1982). It uses weighted averages of direct-spectrum estimates based on orthogonal windows, and thus creates

multiple independent estimates for each sample to reduce smoothing of the data. CWT is particularly useful to analyse non-stationary data as it plots changes in dominant patterns through time along the x-axis. In all three analyses (SSA, MTM, and CWT), significance tests ($p = 0.05$) were performed against a red-noise background spectrum (autoregressive lag-1).

3.3.5.2 Comparison with other datasets

The *Arctica* chronology was compared to instrumental data, climate indices, and biological data to investigate correlations and potential relationships.

Plankton data

Plankton records were obtained from the Continuous Plankton Recorder (CPR) Survey at Plymouth, United Kingdom. The data request was made through an online form (https://www.cprsurvey.org/). The CPR project provides sub-surface plankton data from across the North Atlantic, using consistent sampling methods since its conception by Alister Hardy in the 1920s (Reid et al., 2003; Richardson et al., 2006). Sampling has been virtually unbroken with a monthly resolution since 1948, although data availability and length of record vary greatly from region to region, as the sampling routes have changed and expanded over time (Reid et al., 2003). The requested dataset (Johns, 2021) for this thesis spanned the years 1958–2015 and contained abundance data from the CPR standard areas C4 (Scottish shelf) and C5 (open ocean; see Edwards et al., 2016 for a map) for the following groups: small copepods, large copepods, Decapoda larvae, euphausiids, dinoflagellates, diatoms. In addition to these abundance data, an index for phytoplankton colour was given, divided into four categories (0, 1, 2, 6.5), depending on the level of "greenness" of the sample. Annual average values covering (1) the whole calendar year, (2) May to September (i.e. the main growth season of *A. islandica* at this location, see Results section 4.4.2), and (3) the seasons winter, spring, summer, and autumn, were calculated for each group. Then, the plankton data were compared to the *A. islandica* growth index series by visual wiggle-matching and with the Pearson correlation method. The data of the two standard areas C4 and C5 were (1) analysed separately, (2) analysed after dividing them into smaller areas, and (3) analysed after combining the two. The results presented in Section 7.1 are based on data from the C4 area only (ca. Lat: 54°–60° N,

Long: 3°–10° W), as no significant correlations were found between *A. islandica* growth and open-ocean plankton data in standard area C5.

SST, AMO index, and NAO index

The *Arctica* growth series was compared to regional HadISST1 data (see Section 3.1), the Atlantic Multidecadal Oscillation (AMO) index, and the North Atlantic Oscillation (NAO) index. Monthly data for the climate indices were obtained from the KNMI Climate Explorer website (https://climexp.knmi.nl, Trouet and Van Oldenborgh, 2013) and combined into seasonal averages (Dec–Feb for winter, Mar–June for spring, July–Aug for summer, Sep–Nov for autumn). Comparison was done by eye, and statistically using the Pearson correlation method.

Spatial correlations

Correlations between the *Arctica* growth series and meteorological and atmospheric data in different regions across the North Atlantic were investigated using the online tools in the KNMI Climate Explorer (https://climexp.knmi.nl, Trouet and Van Oldenborgh, 2013). The chosen area ranged from 20° N to 70° N and from 90° W to 10° E. The datasets used for sea surface temperatures were OISSTv.2 (1980–2015; Reynolds et al., 2002) and ERSSTv.5 (1890–2015; Huang et al., 2017). Reanalysis data of zonal wind stress at 200 mbar (ERA5; Hersbach et al., 2020) and sea level pressure (MERRA; Rienecker et al., 2011) were also compared to the *Arctica* growth series.

Soay sheep population data

In 1932, some of the Soay sheep that had been living on the eponymous island of Soay were moved to Hirta (Clutton-Brock and Pemberton, 2004). The last human inhabitants had left Hirta two years earlier (see Section 2.5.3), and thus the sheep were left to live and survive on their own without human interference. Being of great interest to ecologists and other scientists, the population dynamics of the sheep population on Hirta has been closely followed for decades. A precise record of mortality, breeding success, growth, and other factors of virtually all sheep on Hirta is available since 1985. For this thesis, a record of the total annual number of sheep

between 1985 and 2013 was obtained from Hunter et al. (2018) and compared to the *Arctica* growth series using the Pearson correlation method.

3.4. Radiocarbon analysis

3.4.1 Laboratory techniques

All samples were radiocarbon dated using accelerator mass spectrometry (AMS), a direct measurement method through which radioactive ^{14}C atoms are counted relative to the stable carbon isotopes ^{12}C and ^{13}C. Compared to conventional gas-proportional or liquid scintillation dating, AMS is more expensive, but faster, and it requires considerably less sample to reach a similar level of precision. As indicated by its name, AMS accelerates ions to high kinetic energies before mass analysis. Before AMS can be conducted, the sample carbonate has to be converted into graphite targets to load the ion source of the accelerator as summarised below.

Shell selection and initial preparation

After the first six shells had been crossmatched in two floating chronologies, five of them were sent to Beta Analytic for AMS radiocarbon sampling (Table 3.5). It was originally thought, based on the good condition of the shells, that the specimens had died within the last century and thus the more mature parts of the shell potentially carried signals of the marine radiocarbon bomb pulse (Scourse et al., 2012), which would allow for more exact dating. As the shells had already been embedded in polyester resin for crossmatching as described in Section 3.3.1, the resin had to be removed using a rough diamond saw and grinding pads. A small (<2 mm^3) piece of the tip of the margin, integrating roughly 50 years, of each shell was then cut off and sent to Beta Analytic in labelled bags for analysis. An alternative method was to drill into the shells and extract powder samples, which would allow for more precise sampling of fewer increments. This method was, however, dismissed due to an increased risk of atmospheric CO_2 being absorbed by the sample (Darden Hood, pers. comm.; Darrell Kaufmann, pers. comm.).

A further nine specimens (Table 3.5), which had not yet been crossmatched, but which showed similar taphonomic characteristics to the first five shells, were also radiocarbon dated. These

shells were prepared in the same way as described above and analysed using the AMS at the ^{14}Chrono Centre at the Queen's University in Belfast.

Table 3.5: List of specimens sent to either Beta Analytic or the ^{14}Chrono Centre for radiocarbon dating. Plus sign: Specimens had been crossmatched in two floating chronologies prior to dating. Double plus sign: Specimens were crossmatched after dating.

Beta Analytic	^{14}Chrono Centre
14G0VB003^{+}	14G0VB005
14G0VB004^{+}	14G0VB006^{++}
14G0VB020^{+}	14G0VB007
14G0VB024^{+}	14G0VB008
14G0VB019^{+}	14G0VB021^{++}
	14G0VB028
	14G0VB031
	14G0VB043
	14G0VB050

Pre-treatment and graphitisation

Both laboratories that analysed our samples use tandem accelerators. These are loaded with samples that have been converted into graphite targets. To obtain these targets, shell carbonate is reduced to graphite in the presence of a metal catalyst. A brief overview of this process as performed at the ^{14}C Chrono Centre is given below.

First, the shell samples were leached in HCl to etch away ca. 25% of the material and remove all contaminant secondary carbonates. The shell samples were then further acidified in phosphoric acid (H_3PO_4) to convert shell carbonate into a CO_2 sample by hydrolysis. The extracted CO_2 was separated from any non-condensable gases by freezing the gas sample for at least 30 seconds using liquid nitrogen. After this pre-treatment, the purified CO_2 was graphitised using the hydrogen reduction method, with iron powder functioning as catalyst (Vogel et al., 1984). Hydrogen (H_2) was introduced to the frozen CO_2 samples in a ratio of 2:1. Once the gases had sublimed, they were heated to 560 °C in the presence of pre-cleaned iron powder. The heating induced the last step of graphitisation, reducing CO_2 to carbon monoxide (CO) and then further to elemental carbon, which adhered to the iron powder. The obtained graphite was collected and pressed into a target wheel.

AMS measuring

The following paragraph briefly outlines the key features of the AMS method at the ^{14}C Chrono Centre. For a more detailed description see Reimer et al. (2015).

The target wheels are filled with graphite samples, standards, secondary standards and backgrounds (i.e. blanks that do not contain ^{14}C), and loaded into the ion source of the accelerator (NEC 0.5 MV compact accelerator). An accelerated caesium-ion (Cs^+) beam is then sputtered onto the targets to create carbon ions (C^-). These C^- ions, in turn, are repelled by the negatively charged target holder and accelerated along the beam line. Bending magnets are applied to deflect the accelerated ions, dividing the C^- ions into three beams corresponding to the different atomic masses. Lighter isotopes will be deflected more strongly than heavier isotopes, resulting in a more curved beam. Molecular ions are stripped and positively charged ions are filtered out through electrostatic analysers. The $^{12}C^-$ and $^{13}C^-$ ions are detected by Faraday cups, while the $^{14}C^-$ ions are counted separately in a ^{14}C particle detector. Both $^{14}C/^{12}C$ and $^{13}C/^{12}C$ ($\delta^{13}C$) ratios are recorded by AMS; the former is used for age calculation, whereas $\delta^{13}C$ is used to correct for natural and machine-generated isotope fractionation. The $^{14}C/^{12}C$ ratio is background corrected based on values obtained from blanks that have been pre-treated and graphitised in the same way as the samples. Lastly, the corrected $^{14}C/^{12}C$ value is normalised to the oxalic acid II standard (SRM 4990C, National Institute of Standards and Technology) and converted into a Conventional Radiocarbon Age using the Libby half-life (5568 years).

3.4.2 Data analysis

3.4.2.1 Calibration of radiocarbon dates

All radiocarbon dates were calibrated using the MARINE20 calibration curve (Heaton et al., 2020). The calibration curve automatically applies an age-dependent, "global" average marine reservoir correction of approximately 400 ^{14}C yrs based on the spatially averaged modelled value for the surface mixed layer of the ocean. Apart from the general marine reservoir effect (ΔR), local and regional effects that can influence carbon isotope ratios in the water, represented by deviation above or below the ΔR value (Stuiver and Braziunas, 1993), also have to be taken into account. The closest sampled ΔR values available for St Kilda are from the

Irish Sea, Inner Hebrides, and Faroe Islands (Table 3.6, source: calib.org/marine). A weighted mean for that region was calculated based on the ten closest stations (Table 3.6) and yielded a ΔR of −117 ± 41 ^{14}C yrs. It is worth noting that the samples used to calculate all existing ΔR values were collected at coastal sites, whereas St Kilda is heavily influenced by the open ocean (see Chapter 2). Moreover, ΔR in some cases varied substantially at the same location (see Loch Broom and Belfast Lough, Table 3.6).

Time-dependent changes in ΔR have been reported for this region and linked to climatic shifts such as the 8.2 ka event (e.g., Ascough et al., 2004, 2007, 2016). Conversely, Russell et al. (2015) could not detect any significant changes through time for this region when re-evaluating data used in Ascough et al. (2004, 2007) and other publications. To our knowledge, there are no studies that investigate time dependency of ΔR in the Northeast Atlantic during the 4th millennium BP specifically. Reimer et al. (2002) recommend a ΔR value of –33 ± 93 ^{14}C yrs for the Scottish and Irish west coasts for the past 5900 years, however, this recommendation is outdated since new calibration curves have been published. Therefore, the calculated average ΔR of −117 ± 41 ^{14}C yrs is applied in this thesis.

Table 3.6: Measured local ΔR deviation at the ten closest locations.. Map no = Reference number on calib.org/marine. All values based on bivalve samples.

Location	Lat (°)	Long (°)	Local ΔR	ΔR Error	Map no.	Reference
Hebrides, Scotland	58.12	−6.46	−127	35	1988	Lo Giudice Cappelli and Austin (2020)
Hebrides, Scotland	58.12	−6.46	−128	35	1993	Lo Giudice Cappelli and Austin (2020)
Minch, Scotland	58.06	-−6.29	−152	35	1996	Lo Giudice Cappelli and Austin (2020)
Minch, Scotland	58.18	−6.13	−52	35	1986	Lo Giudice Cappelli and Austin (2020)
Minch, Scotland	58.18	−6.13	−156	35	1987	Lo Giudice Cappelli and Austin (2020)
Minch, Scotland	58.18	-−6.13	−72	35	1998	Lo Giudice Cappelli and Austin (2020)
Minch, Scotland	58.18	−6.13	−98	39	1999	Lo Giudice Cappelli and Austin (2020) (2020)
Northern Ireland	55.17	−6.78	−91	50	545	Harkness (1983)
Northwest Scotland	55.83	−5.33	−171	29	531	Harkness (1983)
Northwest Scotland	57.83	−5.33	−87	34	532	Harkness (1983)

3.4.2.2 Constraining radiocarbon dating uncertainties

To constrain dating uncertainties, the radiocarbon dates and the chronological information derived from crossmatching were entered into the Bayesian tree-ring sequence model in OXCAL 4.4 (Bronk Ramsey et al., 2001; Bronk Ramsey, 2009; Bronk Ramsey, 2021). The calibrated radiocarbon dates plus the known gaps between samples (i.e. the absolute number of years between the death of one specimen and that of another) are combined and fit to the calibration curve to calculate a probability density for the age of each sample. MARINE20 was again chosen as calibration curve.

3.5 Raman spectroscopy

Aragonitic shells like *G. glycymeris* and *A islandica* may undergo diagenesis and turn into calcite, which can alter the oxygen isotopic composition and thus impact palaeotemperature reconstructions (Cochran et al., 2010; Pederson et al., 2019; Urey et al., 1951). Raman spectroscopy can be used to distinguish between the different polymorphs of calcium carbonate, as it produces different spectra specific to each crystal structure (De La Pierre et al., 2014). In order to confirm that aragonite in the fossil shells had not been converted to calcite, micro-Raman spectroscopy was performed on fossil shell specimens at the Diamond Light Source, Oxford. A 473 nm laser at a power of 15 mW with a magnification of 20x was used for the analysis. Raman spectra were acquired from each visible shell layer. As all shell layers displayed coincident peaks, only the spectra from the outer outer shell layer (see Section 3.6.2) are presented in this thesis. Spectra between 135 and 1100 cm^{-1} are described, as these wavelengths are used to distinguish between calcium carbonate polymorphs (Parker *et al*., 2010; Wehrmeister *et al*., 2010). Synthetic calcite and speleothem aragonite were used as reference material to compare key interpretative bands (synthetic calcite and speleothem aragonite, Brinza et al. 2014).

3.6 Stable isotope analysis

There are different ways to sample and analyse stable isotope ratios in shell carbonate; here, shell carbonate powder was extracted through micromilling (Dettman and Lohmann, 1995) and analysed the samples using continuous-flow isotope ratio mass spectrometry (CF-IRMS).

3.6.1 Shell preparation

All specimens, except for modern *G. glycymeris*, had been measured and added to a chronology prior to isotope sampling. The shells were processed as described in Section 3.3.1. The etched surfaces of the sectioned blocks were ground and polished to remove any acid and acetate. The blocks were then photographed as described in Section 3.3.2. Due to poor visibility with the micromill camera, a dissecting microscope was used to examine the shells beforehand and mark annual lines on the resin block to facilitate accurate sampling.

3.6.2 Milling techniques

The samples were mainly microdrilled, and in some cases also micromilled, using an ESI New Wave robotic micromill fitted with an Olympus SZ61 camera and loaded with a 300 µm drill bit. We refer to micromilling when the drill is moved horizontally along the shell surface, as opposed to strictly vertical microdrilling (Figure 3.9 and Figure 3.10a). One of the advantages of vertical drilling is that time-averaging and cross-contamination between neighbouring sample spots are easier to gauge and control (personal observation). This advantage, however, only applies when the increments are wide enough for several sub-samples to be taken. The ideal number of samples per increment obtained by microdrilling depends on the research question; here, we considered a minimum of five samples per increment as tolerable and a minimum of ten samples as ideal. Micromilling becomes a necessity (1) when "annual" samples are taken (i.e. only one sample integrating the whole increment), or (2) when the increments are so narrow that a sample spot of 300 µm would contain too large a portion of the growth year. To obtain annual samples, the drill is moved in the direction of shell growth, from one growth line to the next (Figure 3.9 and Figure 3.10b). In the case of sub-annual milling,

the drill moves parallel to growth lines, in overlapping paths (Figure 3.9 and Figure 3.10c). By milling along overlapping, parallel lines, we firstly avoid using the full diameter of the drill bit and thus decrease the amount of time averaged in one sample. Secondly, milling along a line instead of drilling one vertical spot allows us to collect enough carbonate for isotope analysis without having to penetrate deep into the shell. Due to the curvature of the shell, the time-averaging effect will increase with depth of penetration.

An alternative to milling on overlapping paths is using a finer drill bit and leaving space between the lines. This, however, could not be tested as it has proven difficult to find drill bits of less than 300 µm diameter that fit the chuck of the robotic micromill. Attempts were made to use drill bits of 200 µm diameter fitted to the chuck with an adapter. However, the increased length of the drill bit (due to addition of the adapter) interfered with the micromill software and led to a limited use of its features. This decreased control over the micromill in combination with the fact that finer drill bits break more easily led to abandonment of this method altogether.

The shells consist of an inner (ISL) and an outer shell layer (Crippa, 2013). The outer shell layer is further divided into an inner portion (iOSL) and an outer portion of the outer layer (oOSL) (Figure 3.9). As isotopic fractionation differs between the layers (Trofimova et al., 2018), it is important to stay within the same layer while sampling. All robotically milled and drilled samples in this study were taken in the oOSL.

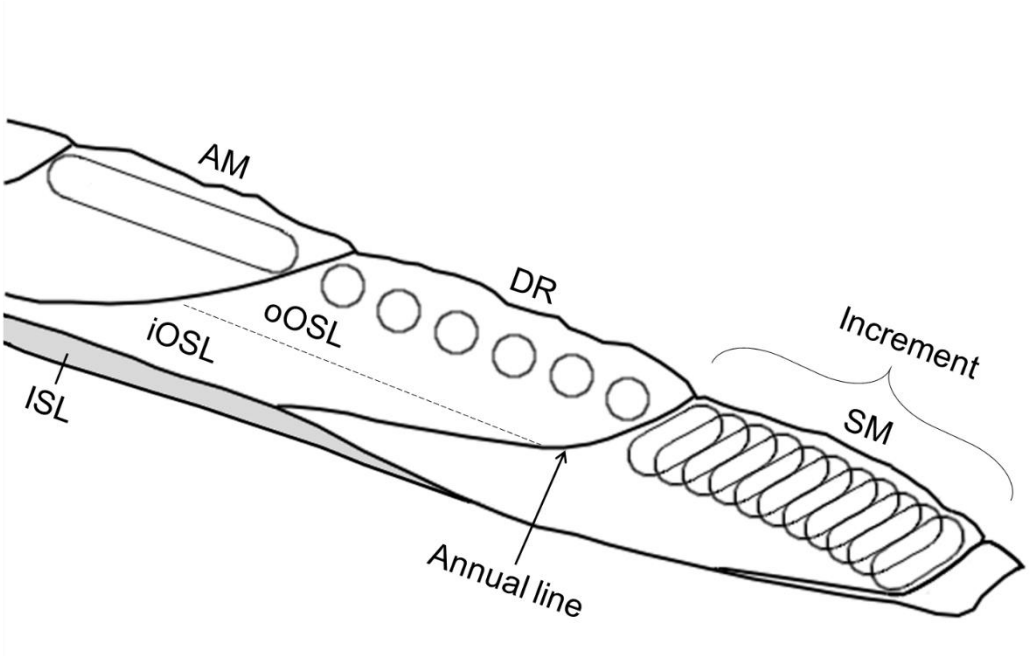

Figure 3.9: Different sampling techniques. AM = Annual micromilling (not used here), DR = Microdrilling, SM = Sub-annual micromilling. oOSL = Outer portion of the outer shell layer; iOSL = Inner portion of the outer shell layer; ISL = Inner shell layer. The annual line is indicated by an arrow. Increment = portion between two annual lines.

3.6.3 Sampling strategy

Specimens of both *G. glycymeris* and *A. islandica* were sampled sub-annually in the juvenile increments of the shell margin. This yielded isotope data from three time periods (Table 3.7):

(1) 2003–2013: The data was replicated across four live-collected *G. glycymeris*.

(2) 1885–1895: Isotope series were produced from two live-collected *A. islandica* and spanned from 1885-1895 with two years overlap between the specimens.

(3) Five 10-yr windows in the 4th millennium BP: Seven crossmatched, dead-collected *G. glycymeris* were sampled. Three specimens had settled within eight years of each other, allowing for sampling of the same calendar years in all three shells and thus replication of isotope values for one of the five 10-yr windows. The other four 10-yr windows contain data from only one specimen each.

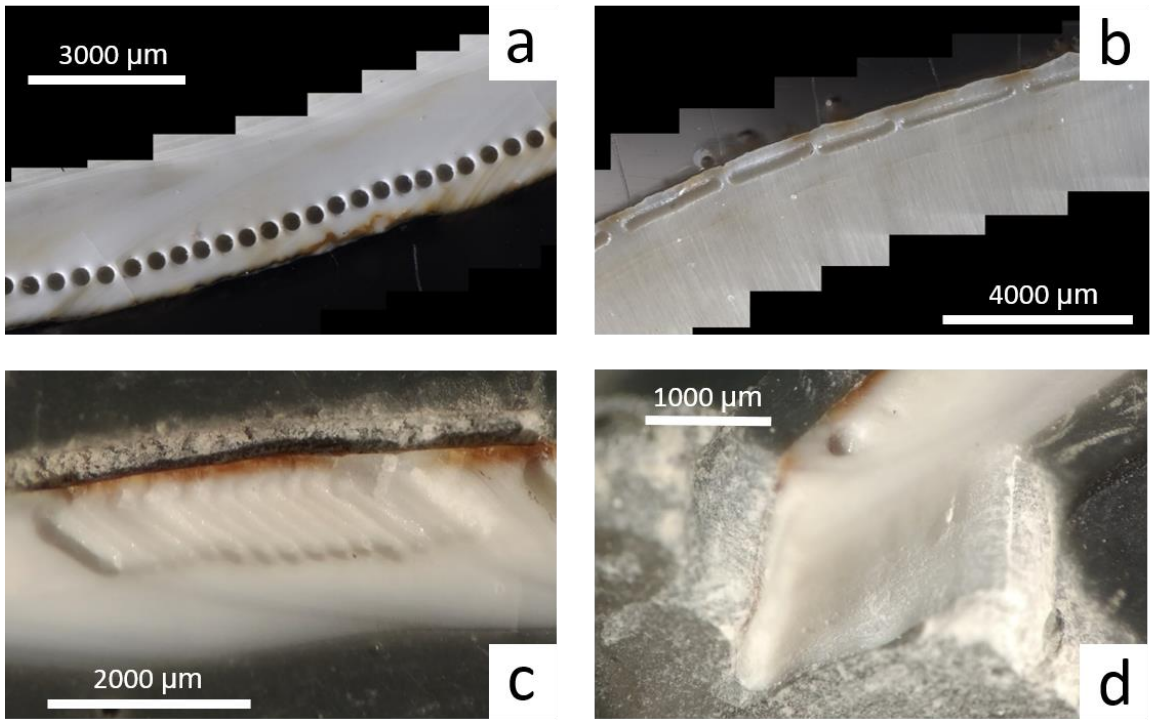

Figure 3.10: Different isotope sampling techniques. (a) Drilling. (b) Annual milling, (c) Sub-annual milling, (d) Manual milling (results not included in this thesis).

Table 3.7: Overview of samples per time period

Modern *G. glycymeris*	***A. islandica***	**St Kilda 7 – Fossil *G. glycymeris***
2003–2013	**1888–1898**	**4th mill BP**
14G2VB132	16A2VB007	14G0VB003
14G2VB135	16A2VB010	14G0VB004
14G2VB136		14G0VB006
14G2VB137		14G0VB020
		14G0VB021
		14G0VB023
		14G0VB024

Drilling was the preferred method in this study. As almost all sampled increments were from the juvenile stage, most of them were wide enough for six samples or more (in some cases >15 samples per increment) to be taken.

Sub-annual milling was additionally performed on the modern *G. glycymeris* to compare sampling methods (as described in Section 3.6.2).

3.6.4 Mass spectrometry

3.6.4.1 Sample preparation

The carbonate powder samples obtained through micromilling were weighed to ensure that they were within the optimal range for the spectrometer (30–120 µg in this case). Where the mass was too low, two samples had to be combined. Where the mass was too high, the sample had to be divided.

Each sample was put into a labelled Exetainer glass vial. Sixty samples were prepared for each run and fed into the spectrometer.

3.6.4.2 Sample analysis

The powder samples were analysed with a Finnigan MAT 253 isotope ratio mass spectrometer (IRMS) coupled to a Finnigan GasBench II at the University of Mainz.

Isotope ratios are reported based on the VPDB (Vienna Peedee Belemnite) δ-scale as defined by the IAEA (International Atomic Energy Agency, Vienna). The original carbonate source for the internationally agreed zero point, PDB, has been exhausted. Instead, the NBS-19 values of –2.20‰ for $\delta^{18}O$ and 1.95‰ for $\delta^{13}C$ are now used as reference. In this study, the isotope ratios were calibrated against an NBS-19 calibrated IVA Carrara marble ($\delta^{13}C$ = 2.01‰, $\delta^{18}O$ = –1.91‰) and measured to an average internal precision (1σ) of 0.05‰ for $\delta^{13}C$ and 0.07‰ for $\delta^{18}O$.

In continuous-flow gas IRMS, single gases are produced from the source material and ionised under a vacuum. Here, CO_2 was derived from the aragonite sample for analysis of oxygen and carbon isotope ratios. The gas flows through a curved magnetic field and is separated into different ion beams. Ion beams containing heavier isotopes bend at a bigger radius than beams containing lighter isotopes. The content of each ion beam is finally collected and measured in Faraday cups.

3.6.5 Data analysis

As a first step, all samples outside the given interpretable signal intensity range for each run were removed from the isotope series. Then, each isotope series was divided into annual segments based on microscope pictures, notes and sketches taken during microdrilling, indicating the annual lines. Where possible (modern *G. glycymeris* and *A. islandica*), calendar years were assigned to all segments. The fossil *St Kilda 7* isotope series stem from a floating chronology in the 4th millennium BP and could thus not be assigned absolute calendar dates. Instead, the ontogenetic years sampled were related to their positions in the floating chronology to evaluate where individual series overlap (see Results section 4.4.1.1, Figure 4.34).

The oxygen isotope ratios of the modern samples were calibrated against temperature data. The modern *G. glycymeris* and *A. islandica* isotope series were paired up with the Met Office HadISST 1.1 series (Rayner et al., 2003) for the 1x1-degree grid cell that St Kilda falls within (57–58° N, 8–9° W), using AnalySeries 2.0.8 (Paillard et al., 1996). To align the $\delta^{18}O$ series with the temperature series, the annual lines within the $\delta^{18}O$ series had to be identified, and the series was inverted to obtain a positive correlation with the temperature series. Then, each annual peak in the $\delta^{18}O$ series was aligned with the peak in the corresponding calendar year of the temperature series. All $\delta^{18}O$ data points to the left and to the right of each peak were fit to the remaining temperature series.

The same procedure was done after converting the $\delta^{18}O$ series into seawater temperatures (see Section 3.6.5.1), where again the peaks were aligned first, followed by aligning matching temperature values on either side. Peaks were always aligned, even in cases where the $\delta^{18}O$-derived temperatures were higher or lower than the HadISST1 values. I justify this by (1) the fact that sampling resolution is lowest in this part of the increment (i.e. less growth during the warmest time of the year compared to earlier in spring) and thus time-averaging will be stronger here, which makes it less likely to have exactly matching temperature values, and (2) pointing out that in order to align the absolute temperature of the peak in the $\delta^{18}O$ series with the corresponding absolute temperature in the HadISST1 series, we would have to make the decision to put the data point either before or after the temperature peak, which would be speculative.

3.6.5.1 Palaeotemperature equation

Seawater temperatures were obtained from the $\delta^{18}O$ series using the palaeotemperature equation for aragonitic shells developed by Grossman and Ku (1986) with a PDB-VMOW scale correction of −0.27 ‰ (Dettman et al., 1999; Gonfiantini et al., 1995; Hut, 1987):

$$T\,°C = 20.6 - 4.34\,(\delta^{18}O_{ar} - (\delta^{18}O_{w} - 0.27)) \qquad (4)$$

…where $\delta^{18}O_{ar}$ is the $\delta^{18}O$ (PDB) of aragonitic shell, and $\delta^{18}O_{w}$ is the $\delta^{18}O$ (SMOW) of the water.

As no local $\delta^{18}O_{w}$ values are available for St Kilda, the NASA Global Seawater Oxygen-18 Database (Schmidt et al., 1999) was used to find the closest available value. The closest and oceanographically most similar location where $\delta^{18}O_{w}$ has been measured is at Lat: 55.3° N and Long: 15.6° W, with a value of 0.38‰ (Östlund and Grall, 2001; see Figure 3.2). This measurement was taken in an offshore environment in the Rockall Trough area at a depth of 46 m, and therefore deemed an appropriate value for St Kilda. In this study, it was assumed that $\delta^{18}O_{w}$ has remained constant over the last four millennia at our sample site, and thus 0.38‰ was used for all time periods.

3.6.5.2 Seasonality

All inter-specimen isotope and isotope-to-temperature alignments were done both by manual manipulation in Excel and with the age-depth correlation tool in AnalySeries 2.0.8 (Paillard et al., 1996).

For comparison of seasonality between the different species and time windows, all isotope series had to be detrended with a high-pass filter and resampled (see Schöne and Fiebig, 2009; Wanamaker et al., 2011). This resampling corrects the bias introduced by sampling increments from different ontogenetic stages with different growth rates. Following the methods used by Wanamaker et al. (2011), a linear regression model was fitted to each isotope series to calculate the low-frequency trend, and the trend was subtracted from the raw $\delta^{18}O$ values. The resulting

normalised series were divided into individual years (i.e. shell increments). Wanamaker et al. (2011) resampled all increments with seven or more samples using a 7-point model, arguing that it would still account for the annual seawater temperature cycle. In the present study, a 6-point model was used instead, as a higher number than six would exclude all increments with six or fewer sample spots, and thus leave too few for analysis. As *A. islandica* and *G. glycymeris* at Village Bay mainly grow from May to October (see Results section 4.4.2), a 6-point model was deemed to provide sufficient resolution. All increments with more than six oxygen isotope values were fitted to a cubic spline model and downsampled to six samples per increment using the fitting tool in AnalySeries 2.0.8. Subsequently, the average annual $\delta^{18}O$ range recorded by the shells in each of the three time periods (see Section 3.6.3) was calculated. For the 1888–1898 *Arctica* series, shells 16A2VB007 and 16A2VB010 were combined into one averaged isotope series (arithmetic mean). Among the fossil *G. glycymeris* shells from the 4th millennium BP, specimens 14G0VB004 and 14G0VB021 overlap in time and were therefore also averaged into one series. For the modern *G. glycymeris* record, specimens 14G2VB132, 14G2VB136 and 14G2VB137 were combined into one average series. Then, for each increment with six samples (by default or by downsampling) within one specimen, $\delta^{18}O_{min}$ values were subtracted from $\delta^{18}O_{max}$ values to calculate the range ($\Delta\delta^{18}O$). The average range was then calculated based on the individual annual values. The overall average $\Delta\delta^{18}O$ value of the fossil St Kilda Seven *G. glycymeris* group was calculated based on specimens 14G0VB006, 14G0VB020, 14G0VB023, and the combined 14G0VB004+14G0VB021 series (see figure 3.12 for a visual representation of the isotope series). Specimens 14G0VB003 and 14GVB024 from the fossil *G. glycymeris* group and modern *G. glycymeris* specimen 14G2VB135 were excluded from this analysis because too few of their increments fulfilled the criterion of providing six or more isotope samples.

Scaling factor

Downsampling the data to fit a 6-point model might attenuate the signal and decrease the temperature range captured by $\delta^{18}O_{shell}$. This is particularly true in cases where sampling resolution is considerably higher than six samples per year. Therefore, the results had to be scaled using modern temperature data to facilitate meaningful comparisons between time periods. Following Wanamaker et al. (2011), a scaling factor was calculated based on the modern *G. glycymeris* samples and instrumental data, and then applied to all time periods. First, the average temperature range for May–October in the years 2003–2013 CE was calculated

using HadISST1 data. Secondly, the average temperature range derived from the *G. glycymeris* $\delta^{18}O_{shell}$ data, covering 2003–2013 CE, was calculated. Lastly, the instrumental temperature range was divided by the shell-derived temperature range to calculate the scaling factor. The $\delta^{18}O$-derived temperature ranges of all three time periods (4th millennium cal yr BP, late 19th century CE, 2003–2013 CE; see Section 3.6.3) were multiplied by the scaling factor.

3.6.5.3 Average temperatures

To obtain comparable mean temperatures for each time interval, the $\delta^{18}O$ series were again resampled by fitting them to a cubic spline 6-point model, this time without detrending the data. The same shells were used as in the section above, and again only increments with six or more isotope samples were considered.

3.6.5.4 Annual $\delta^{18}O$ data in *Arctica islandica*

In addition to the seasonal milling described above, annual sampling was performed across two specimens (16A2VB006, 16A2VB010) of the modern *Arctica* chronology. The annual series was calculated by averaging the replicated years. A schematic representation of annual milling is given in Figure 3.9 ("AM") and Figure 3.10b. The samples were processed at the Stable Isotope Facility of the British Geological Survey (BGS) in Keyworth, UK. Seawater temperatures were calculated with the equation by Grossman & Ku given above (Equation 4).

3.6.5.5 Comparison with other data

The annual *Arctica* $\delta^{18}O$ series was compared to regional HadISST1 data (see Section 3.1) and the phytocolour index series (see Section 3.3.5.2) using the Pearson correlation method. Spatial correlation analysis was undertaken with the KNMI Climate Explorer software, using the HadISST1 dataset for SSTs and the EN4 dataset for sea surface salinity (Good et al., 2013).

Chapter 4

Evaluating *in-situ* and gridded SST data

Chapter 4 — Evaluating *in-situ* and gridded SST data

St Kilda's oceanographic setting is difficult to characterise, due to the dynamic interactions between oceanic and coastal influences, local upwelling, and lack of *in-situ* measurements (see Chapter 2). Therefore, a fundamental question before interpreting sclerochronological data is which instrumental datasets best represent this location. This question is explored in the following chapter.

Section 4.1 presents *in-situ* temperature and salinity data from the inner shelf, the outer shelf, and the shelf margin. The objective is to compare temporal variability in different environments on the western Scottish shelf from May to October (i.e. during the growth season of *A. islandica* and *G. glycymeris*; see Chapter 6).
In a subsequent part of this chapter (Section 4.2), gridded surface data are then compared to *in-situ* temperature records from the outer shelf. The objective here is to test how accurately different gridded data products represent SSTs on the outer shelf, and which data product should ultimately be chosen for comparisons with sclerochronological data from this region.

4.1. *In-situ* data in different oceanographic settings

Data from three different hydrographic stations on the western Scottish shelf are compared. Figure 4.1 shows sea surface temperature (SST) measurements from the Tiree passage mooring site (TPM) and the Ellett line stations Q and 15G for 1983–2014 CE. Station Q is located on the shelf margin, station 15G is located south of St Kilda, and TPM is located in the Tiree Passage between the islands Tiree and Mull in the Inner Hebrides (see Section 2.4 for a description of all stations). 15G and Q show a high similarity in SST values, especially in June–August, while TPM records cooler SSTs in May–August, and warmer SSTs in September and October (Figure 4.1, Figure 4.2).

Practical salinity data between May and October groups 15G and Q together with average values of 35.1 and 35.3, respectively, while the Tiree Passage is considerably fresher with an average value of 34.4 (Figure 4.3, Figure 4.4). It should be noted, however, that salinity has been recorded at TPM only from 2002 onwards, while few data points are available for 15G and Q during that time interval.

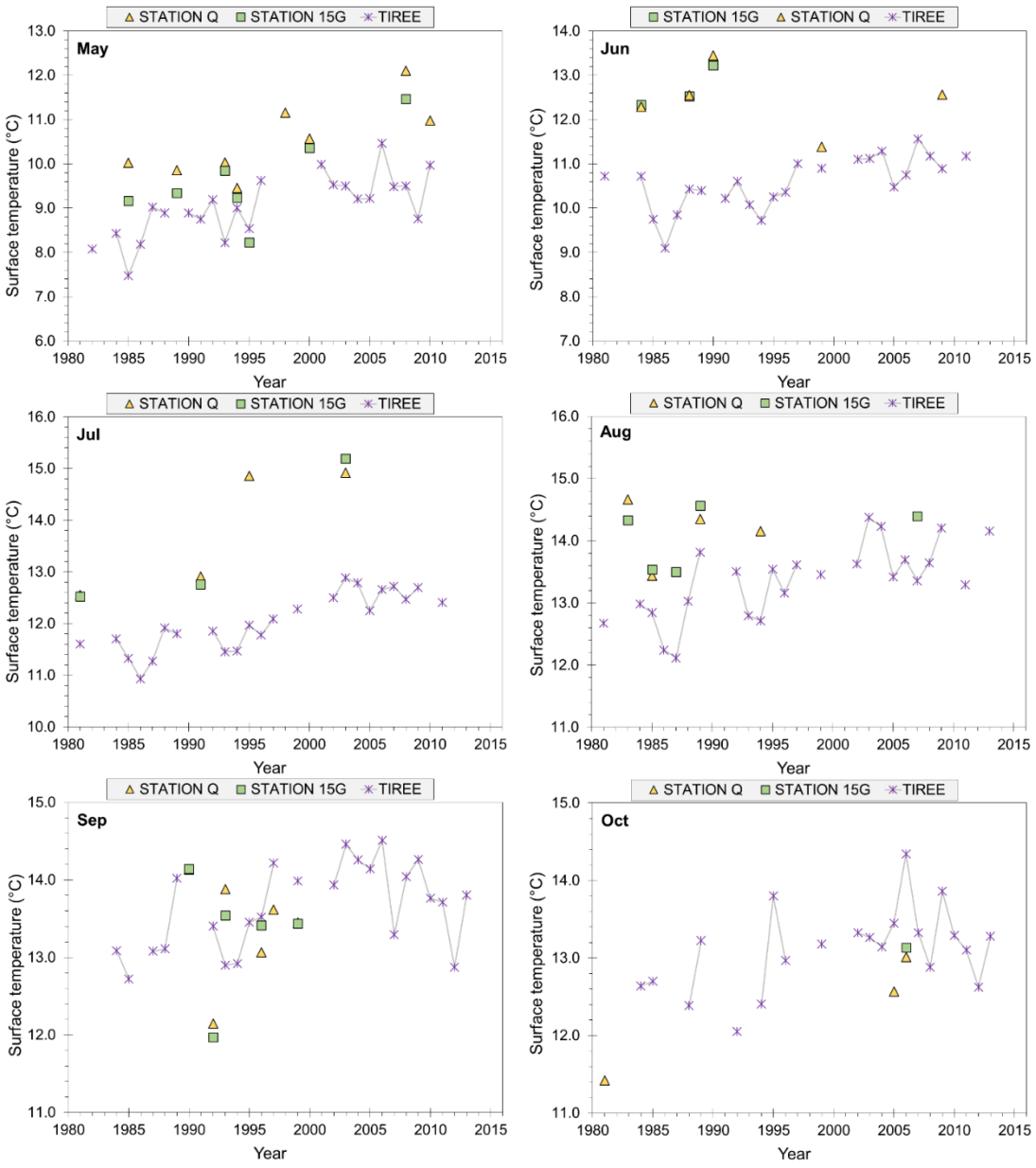

Figure 4.1: Monthly SST data from Ellett line stations Q (yellow triangle), 15G (green square), and the Tiree Passage mooring station (purple cross).

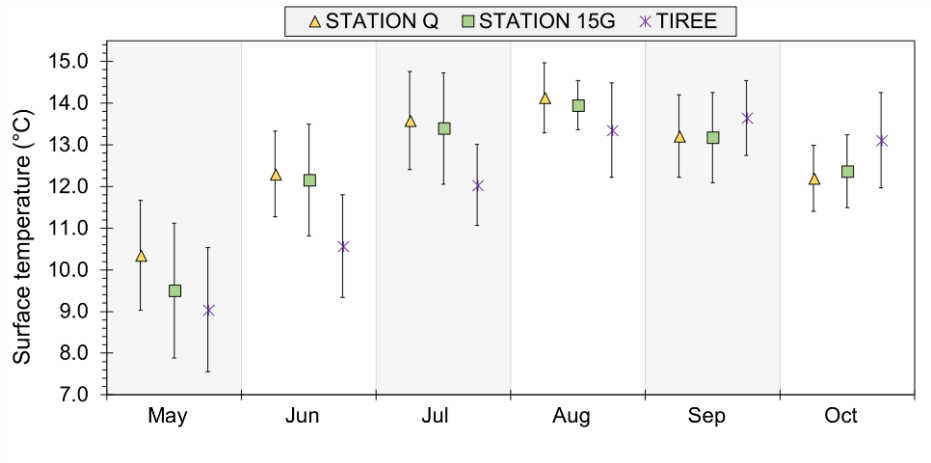

Figure 4.2: Average monthly SST data from Ellett line stations Q (yellow triangle), 15G (green square), and the Tiree Passage mooring station (purple cross) between 1983 and 2014. Same input data as in Figure 4.1. Error bars indicate the full range of measurements.

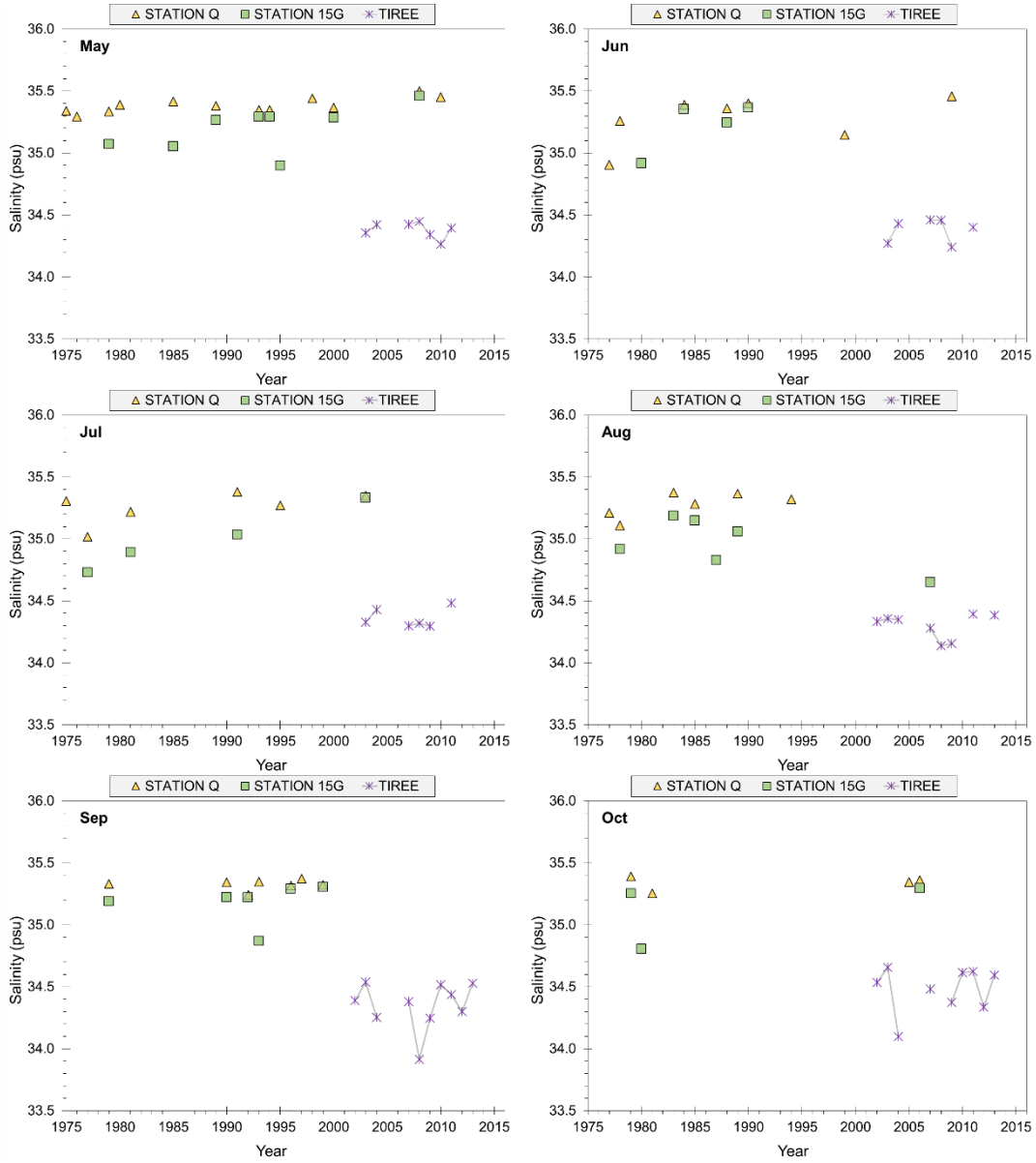

Figure 4.3: Monthly salinity data from Ellett line stations Q (yellow triangle), 15G (green square), and the Tiree Passage mooring station (purple cross).

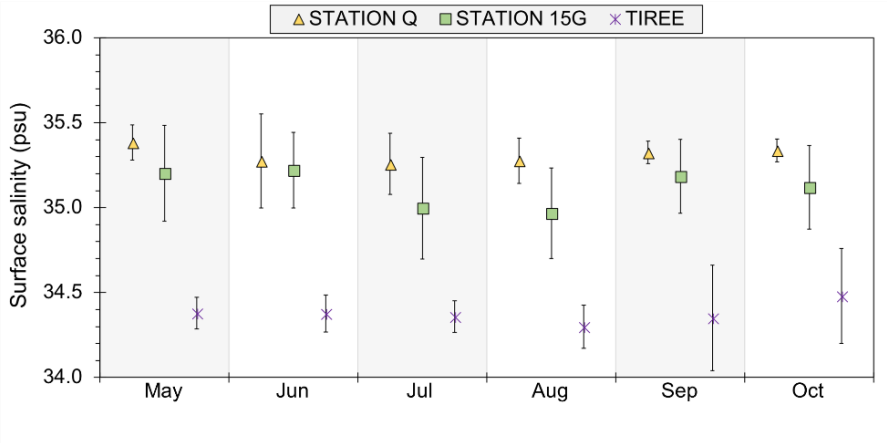

Figure 4.4: Average monthly salinity data from Ellett line stations Q (yellow triangle), 15G (green square), and the Tiree Passage mooring station (purple cross) from 1975–2013. The input data is the same as in Figure 4.3. Error bars indicate the full range of measurements. Note that the TPM data only ranges 2002–2013.

4.2 Gridded sea surface temperature data

This section presents comparisons between *in-situ* data on the Scottish shelf and gridded data products. The *in-situ* data consists of Ellett line stations 15G and Q, as well as ICES bottle and CTD data on the outer western Scottish shelf between 57° N and 59° N and 7.5° W and 9.5° W (see Section 2.4). The average SST values for May to October were calculated for each year (Table 4.1). However, as sampling did not take place in the same months every year, there are discrepancies in which months are incorporated in the average values per year. This has to be taken into account when calculating the standard deviation. Thus, as a control, each month was considered individually as well (Table 4.1). The corresponding data of monthly SSTs are also presented for the three gridded data products HadISST1, ERSSTv.5, and OISSTv.2. All raw *in-situ* measurements and monthly gridded data are presented in Figure 4.5.

The CTD and bottle data obtained from ICES presents the lowest average temperatures of all datasets.

Table 4.1: Maximum and minimum temperatures and standard deviations by month for the three *in-situ* data series and the three gridded SST products for 1983–2015. ICES = CTD and bottle data for Long = 57 –59° N and Lat = 7.5 to 9.5° W; 15G = Station 15G on the Ellett line; Q = Station Q on the Ellet line.

	ICES				***15G***				***Q***			
	***Max* °C**	***Min* °C**	***Avr* °C**	***σ***	***Max* °C**	***Min* °C**	***Avr* °C**	***σ***	***Max* °C**	***Min* °C**	***Avr* °C**	***σ***
May	9.09	8.43	8.67	0.25	11.47	8.23	9.67	0.95	12.10	9.46	10.52	0.80
Jun	12.23	10.85	11.48	0.57	13.23	10.54	12.70	0.38	13.44	11.39	12.45	0.66
Jul	11.51	10.99	11.18	0.23	15.19	12.53	13.98	1.22	14.92	12.91	14.23	0.93
Aug	13.36	12.03	12.70	0.67	14.56	13.39	14.06	0.45	14.94	13.43	14.15	0.45
Sep	14.19	11.57	13.31	1.23	14.14	11.97	13.30	0.72	14.13	12.15	13.38	0.64
Oct	12.63	11.66	12.11	0.40	13.14	11.39	13.14	n.a.	13.01	12.57	12.79	0.22

	HadISST1				**ERSSTv.5**				**OISSTv.2**			
	***Max* °C**	***Min* °C**	***Avr* °C**	***σ***	***Max* °C**	***Min* °C**	***Avr* °C**	***σ***	***Max* °C**	***Min* °C**	***Avr* °C**	***σ***
May	11.35	9.60	10.31	0.40	11.14	8.98	10.08	0.45	11.48	9.56	10.29	0.46
Jun	13.33	10.85	12.00	0.55	12.80	10.54	11.48	0.54	12.87	10.55	11.80	0.60
Jul	14.93	12.21	13.40	0.51	14.28	11.91	12.95	0.50	14.58	12.02	13.21	0.55
Aug	15.18	12.95	14.18	0.50	14.96	12.33	13.66	0.61	15.22	12.58	14.01	0.61
Sep	13.98	12.29	13.24	0.45	14.31	11.92	13.13	0.56	14.31	12.25	13.42	0.55
Oct	12.88	11.27	12.11	0.41	12.81	11.05	11.98	0.48	13.17	11.42	12.28	0.45

Pearson correlation analysis between the anomalies of the three gridded satellite data and the anomalies of *in-situ* subsurface data (≤ 60 m depth) resulted in similar values for all three products (Table 4.2). OISSTv.2 has the lowest Pearson correlation coefficient (r = 0.74), and the second-highest root-mean square error (RMSE = 0.23). HadISST1 and ERSSTv.5 have similar correlation coefficients, however, the RMSE is considerably lower for HadISST1 than for ERSSTv.5 (Table 4.2). Thus, based on the Pearson correlation and RMSE alone, HadISST1 outperforms the other two data products. However, when the standard deviation of each product is taken into account, ERSSTv.5 and OISSTv.2 show higher similarities to *in-situ* data than HadISST1. This is also reflected in higher Skill scores for the products, calculated based on the Pearson correlation and the standard deviation (see Methods section 3.1).

Correlation coefficient, RMSE, and Skill score increase slightly when station Q is included in the *in-situ* data ensemble (Table 4.2). However, the rankings of gridded products remain the same; HadISST1 has the highest Pearson correlation and lowest RMSE, while ERSSTv.5 achieves the highest Skill score.

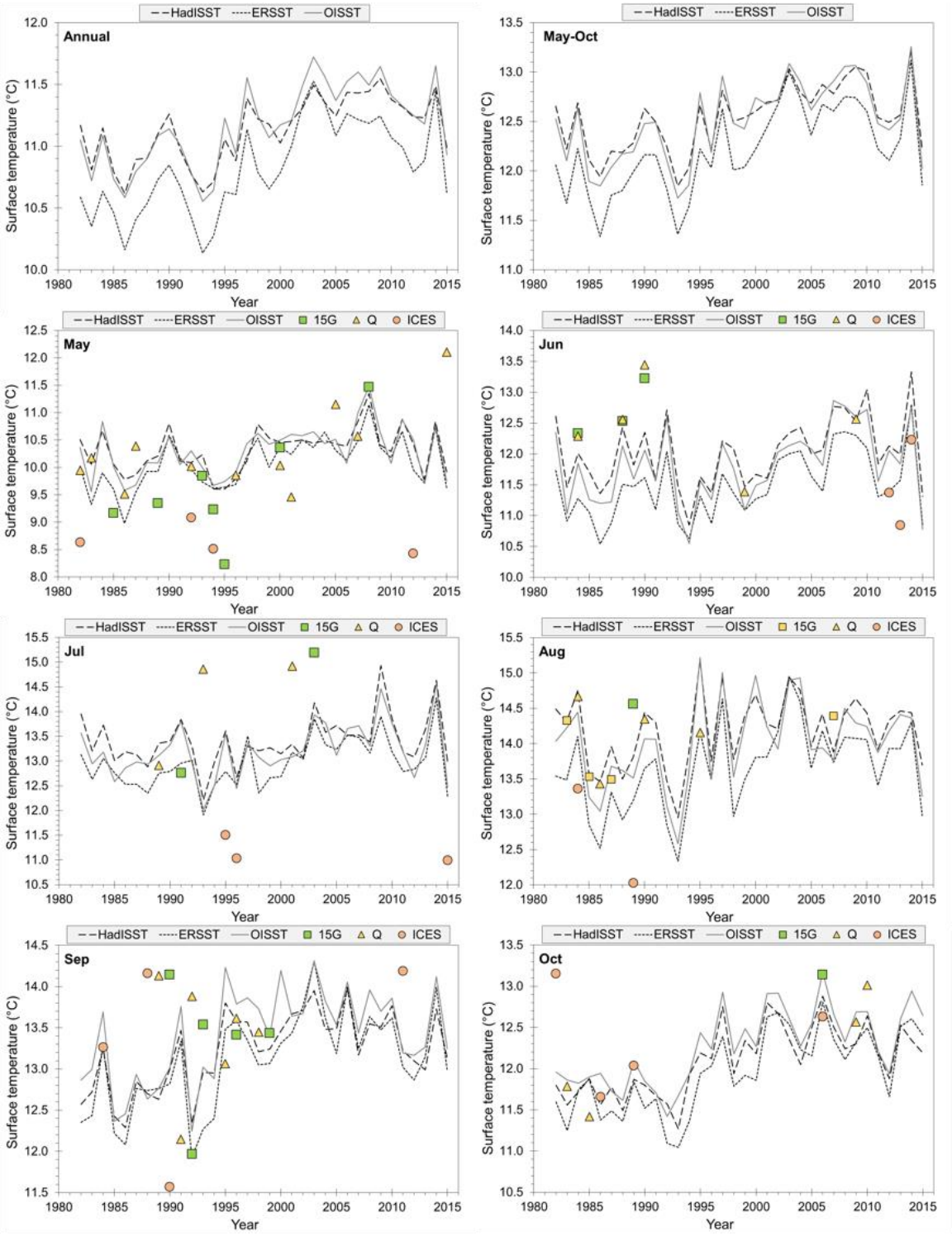

Figure 4.5: Gridded SST data (HadISST1, ERSSTv.5, OISSTv.2) and *in-situ* temperature data. The top two panels show monthly gridded SST data averaged over a calendar year (left) and over the main growth season of *G. glycymeris* at St Kilda (May–Oct, right). The bottom six panels show monthly gridded SST data and *in-situ* temperature data from the Ellett line stations 15G and Q (surface temperatures) and CTD and bottle data obtained by ICES. Please note changes of scale on the y-axes.

Table 4.2: Statistics for each of the gridded SST products (HadISST1, ERSSTv.5, OISSTv.2) compared to *in-situ* SST data measured at St Kilda and Ellett Line station 15G. Given are the Pearson correlation coefficient r, the root-square mean error (RMSE), the standard deviation σ, and the Skill score (calculated based on Pearson correlation and the standard deviation).

	ICES and 15G				***ICES, 15G, and Q***			
	Pearson r	**RMSE**	**σ**	**Skill score**	**Pearson r**	**RMSE**	**σ**	**Skill score**
HadISST1	0.82	0.21	0.29	0.32	0.81	0.19	0.29	0.36
ERSSTv.5	0.82	0.28	0.40	0.49	0.81	0.31	0.40	0.52
OISSTv.2	0.79	0.26	0.35	0.39	0.78	0.24	0.35	0.43

4.3 Discussion

As stated in the introduction to this chapter, the objectives were to (1) present May–October salinity and temperature data from different environments on the western Scottish shelf, (2) provide an overview of instrumental data available at St Kilda, and (3) test which gridded dataset represents the *in-situ* conditions at St Kilda most accurately. It is important to note that the data above are not an attempt to provide a full and detailed oceanographic characterisation of the western Scottish shelf, as that would be beyond the scope of this thesis. The spatial and temporal variability of the physical and chemical environment on the shelf has been studied in detail elsewhere (e.g., Ellett, 1979; Inall et al., 2009; Jones et al., 2018; Painter et al., 2016), and is briefly discussed in Chapter 2.

4.3.1 Hydrographic stations Q and 15G compared with the TPM

When interpreting sclerochronological data, it is important that the properties of the surrounding waters are known. St Kilda is a challenging location to characterise, since it is positioned in a highly dynamic environment, impacted by storms and swell, strong tidal currents (Cartwright, 1969), upwelling (Simpson and Tett, 1986), and a variable mixture of oceanic and coastal water (see Chapter 2). Moreover, local hydrographic instrumental data are scarce, as sampling on the outer shelf is complicated by the rough conditions.

As discussed in Chapter 2, the closest hydrographic station is 15G of the Ellett line, located on the outer shelf ca. 100 km south of St Kilda (Section 2.4.1, Figure 2.4). Temperature and salinity data of station 15G was compared to that of the open ocean (station Q) and the Inner Hebrides (Tiree Passage, TPM) to assess differences in temperature and salinity between the outer shelf, the open ocean, and a coastal environment. A clear east-west gradient in SST and salinity across the western Scottish shelf is reflected in Figures 4.1 and 4.3. Stations Q and 15G have similar monthly temperature profiles, especially between June and October, when the average temperature difference between the two sites is 0.1 °C (Figure 4.1). In contrast, temperatures recorded at TPM are significantly cooler during the summer months. The difference in SSTs can partially be explained by the strong tidal dynamics causing vertical mixing at TPM, whereas the outer shelf and open ocean begin to stratify in spring (see Chapter 2). However, salinity is a better tracer of oceanic vs. coastal water masses than temperature, as

it is more conservative and sensitive to advection (Jones et al., 2018; Young and Holt, 2007). Notwithstanding that the TPM salinity data hardly overlaps with the Q and 15G series in time, it is evident that the TPM is located in a fresher environment; the Scottish Coastal Current and other coastal influences are stronger at TPM than at 15G (Figure 4.3 and Figure 4.4). Yet, coastal influences are present on the outer shelf as well. The dominance of Atlantic vs. shelf waters at 15G and St Kilda varies between years and is linked to the NAO (Jones et al., 2020; see Chapter 2).

While 15G data was used here to characterize the conditions at St Kilda, there are two important caveats that need to be taken into account. Firstly, 15G station data is intermittent and therefore of limited use. Secondly, while St Kilda is surrounded by waters of relatively uniform depths, it is subject to upwelling of cold bottom water due to the "island mass effect" (see Section 2.5.2). Hence, local surface temperature and salinity at St Kilda might differ from the surrounding waters on the outer shelf (Simpson and Tett, 1986). Previous studies have characterised the tidal regime (Cartwright, 1969; Cartwright et al., 1980), local upwelling and island-stirring effect (Simpson and Tett, 1986), and marine geology (Sutherland, 1984) at St Kilda. These studies provide valuable insights into the physical and geological environment at the archipelago, and demonstrate its complexity. However, long-term *in-situ* data are indispensable for a better understanding of the unique environment at St Kilda, and to what extent it represents or differs from the surrounding shelf.

4.3.2 Gridded data products compared to *in-situ* data

Gridded data products are the best option for establishing an SST baseline at St Kilda. However, different gridded data products use different raw data and interpolation methods, resulting in different outputs (see Section 2.4.2). Thus, these datasets will differ in their skill to represent any given environment. In addition, as gridded data are spatially smoothed in contrast to local conditions, it is important to have a good understanding of the oceanography of the sample site and choose the grid and kernel size accordingly, to avoid introducing additional error by averaging across different oceanographic regimes.

Here, *in-situ* data from the outer shelf were compared to the three products HadISST1 (Rayner et al., 2003), ERSSTv.5 (Huang et al., 2017), and OISST V2 (Reynolds et al., 2002) to assess

their respective performance. Because station 15G provides only few data points, the *in-situ* data were complemented by ICES bottle and CTD data from surface waters on the outer western shelf. All in all, the correlation coefficient was relatively high across all data products, while Skill scores were generally low. ERSST V5 yielded the highest Skill score, which can be attributed to the higher standard deviation in the ERSST series compared to the other two data products. Thus, one possible interpretation is that ERSST V5 is better at reflecting regional temperature anomalies. While the ERSST V5 dataset has a lower resolution than OISST V2 and HadISST1, Hughes et al. (2009) found that the difference between 2° grids and 1° grids are negligible. The authors further state that the grid size of the data products does not necessarily reflect the true resolution of the embedded data (Hughes et al., 2009). Thus, the lower resolution does not necessarily make ERSST V5 less suitable for studies at St Kilda. However, the RMSE was the highest when using ERSST V5.

One major source of uncertainty in the comparison between *in-situ* data and gridded products are the *in-situ* data themselves. As mentioned above, Ellett line hydrographic data (stations 15G and Q) are intermittent, which may complicate interpretation. The ICES dataset was added to the *in-situ* data ensemble to increase the number of data points; however, it comprises different locations and methods used by different teams, and might therefore introduce error. All gridded products performed better when station Q was included in the *in-situ* data ensemble. One possible reason for the better performance might be the increase in the number of data points achieved by incorporating station Q. Another possible reason is that the spatially and temporally smoothed gridded SST data do not fully represent regional conditions on the shelf, and instead incorporate open-ocean signals.

Hughes et al. (2009) assessed the performance of the three products OISST V2, HadISST1, and ERSST V3 (Smith et al., 2008) at six locations in the Northeast Atlantic region (see Methods section 3.1). HadISST1 performed best at the Faroe-Shetland channel, which was the most similar and closest location to St Kilda (Hughes et al., 2009). Similarly, Boehme et al. (2014) tested the performance of the three gridded datasets (using ERSST V3) as proxies for ecological variation by comparing them to *in-situ* temperature data from the Norwegian Sea and annual-cohort growth data of Atlantic salmon (*Salmo salar)* from northern and eastern Scotland. The authors recommend HadISST for similar studies that pre-date 1982, and OISST V2 for more recent studies, although the latter might underperform in high-latitude regions where sea ice is prevalent (Boehme et al., 2014). Conversely, the authors advise against

using ERSST for anomaly studies and recommend its use beyond the mesoscale only (Boehme et al., 2014).

While ERSSTv.5 had the highest Skill scores in the present study, HadISST1 yielded a lower RMSE (Table 4.2). Thus, given that the comparison of *in-situ* data and gridded products did not yield clear results in the present study, this thesis follows the recommendations by Hughes et al. (2009) and Boehme et al. (2014) to use HadISST1 for proxy-temperature comparisons.

Chapter 5

Radiocarbon dates and taphonomy

Chapter 5 — Radiocarbon dates and taphonomy

The following chapter introduces the sclerochronological part of this thesis and provides an overview of the collected shell material on which the subsequent result chapters are based.

The samples collected at St Kilda, including dead-collected shells and live specimens, are described in Section 5.1. The preservational state of *A. islandica* and *G. glycymeris* shells was systematically assessed using a scoring system.

In Section 5.2, the taphonomy of 14 radiocarbon-dated *G. glycymeris* shells is presented in more detail. Since their approximate death dates are known, these specimens were used to study the relationship between taphonomy and passage of time. A linear link between taphonomic processes and time would enable sclerochronologists to determine whether fossil shells were approximately coeval and, consequently, whether they are suitable for crossmatching. This would represent a low-resource alternative to radiometric or AMS dating, and thus provide new opportunities in palaeoceanographic studies using bivalve shells.

5.1 Sample description

We collected 874 specimens during the research cruise aboard RV *Prince Madog* in 2014, of which the vast majority were single valves of *G. glycymeris* from St Kilda (see Methods section 3.2.1). During the 2016 diving campaign, ca. 100 live and ca. 100 dead *A. islandica* were collected at Village Bay, St Kilda. All in all, 192 *G. glycymeris* and 116 *A. islandica* specimens were processed as described in Methods section 3.3.1, and assigned scores based on their taphonomic condition (see Methods section 3.2.2 for the criteria for selecting shells and the scoring system). The average scores assigned to live and dead *G. glycymeris* and *A. islandica* samples are presented in Table 5.1. Live *G. glycymeris* reached the highest scores in all categories, while the periostracum of live *A. islandica* were showing signs of degradation. Live- and dead-collected samples mainly differed in the condition of periostracum and

ligament, which were absent or considerably degraded in dead samples. The intactness of the margin also differed between live and dead samples. In contrast, bioerosion yielded similar scores for both live- and dead-collected specimens. The hand-collected dead samples were in a better condition than those collected by dredging, and yielded scores that were similar to live samples. The biggest difference between live *A. islandica* and hand-collected dead *A. islandica* was the condition of the ligament.

Table 5.1: Average scores for dead- and live-collected *G. glycymeris* and *A. islandica* from all sample sites of the 2014 research cruise and the 2016 diving campaign. The scores for live samples were the same for dredged and manually collected specimens.

			n	***Perio-stracum*** *(1–5)*	***Liga-ment*** *(1–4)*	***Margin*** *(1–4)*	***Erosion*** *(1–4)*	***Nacre*** *(1–3)*
Live	Dredge or divers	*G. glycymeris*	10	5	4	4	4	3
		A. islandica	53	3	4	4	4	3
Dead	Dredge	*G. glycymeris*	182	1	1	2	3	2
		A. islandica	6	1	1	1	4	2
	Divers	*A. islandica*	30	2	2	3	4	2

5.2 Radiocarbon ages and taphonomy of *G. glycymeris*

Fourteen *G. glycymeris* valves from St Kilda were radiocarbon dated. Six of these specimens had already been crossmatched with each other, while a seventh shell crossmatched with another specimen not included in the radiocarbon analysis. These crossmatched shells thus form two independent floating (i.e. not absolutely dated) chronologies. Table 5.2 shows all radiocarbon dates with a local marine reservoir correction. Twelve out of the 14 specimens dated back to the 4th millennium BP, including all seven shells that are integrated in the two floating chronologies. The remaining two specimens yielded younger radiocarbon dates, placing them at ca. 820 yr BP and ca. 440 yr BP, respectively. The calibrated radiocarbon dates had 2-sigma uncertainty ranges of between 328 years and 500 years after a local reservoir correction of $\Delta R = -117 \pm 41$ was applied (see Methods section 3.4.2).

Table 5.2: Conventional and calibrated radiocarbon dates for all dated shell samples with a local marine reservoir correction of ΔR = –117 ± 41. Calibrations were made using the MARINE20 calibration curve (Heaton et al., 2020). Specimens marked with an *S* crossmatched and are incorporated in the *St Kilda Seven* chronology, the specimen marked with an *M* is one of two specimens in the *Misfits* chronology (see Chapter 6).

Specimen	Lab ID	Conventional ^{14}C age (yrs BP)	1 σ (68%) calibrated age (cal yrs BP)	2 σ (95%) calibrated age (cal yrs BP)
14G0VB003 [S]	Beta-408875	3650 ± 30	3466–3322	3546–3239
14G0VB004 [S]	Beta-408876	3630 ± 30	3448–3300	3518–3210
14G0VB005	UBA-29385	3680 ± 30	3490–3570	3570–3276
14G0VB006 [S]	UBA-29386	3700 ± 30	3516–3375	3605–3314
14G0VB007	UBA-29387	3560 ± 30	3359–3215	3430–3142
14G0VB008	UBA-29388	3500 ± 30	3310–3154	3365–3064
14G0VB019 [M]	Beta-408877	3480 ± 30	3280–3108	3351–3028
14G0VB020 [S]	Beta-408878	3700 ± 30	3522–3373	3615–3308
14G0VB021 [S]	UBA-29389	3550 ± 30	3354–3209	3427–3131
14G0VB024 [S]	Beta-408879	3710 ± 30	3535–3385	3624–3320
14G0VB028	UBA-29390	820 ± 30	336–204	430–130
14G0VB031	UBA-29391	3600 ± 30	3405–3259	3470–3183
14G0VB043	UBA-29384	3710 ± 30	3537–3392	3620–3331
14G0VB050	UBA-29392	440 ± 30	55–na	113–na

5.2.1 Taphonomic scores

A comparison of dead-collected *G. glycymeris* from different time periods is presented in Table 5.3. The samples from the three oldest time periods included in this table have been radiocarbon dated and thus an approximate geological age is known. The exact year of death is known for the most recent shell (2013 CE) because it has been crossmatched with live-caught specimens (crossmatching results not included in this thesis). This shell was collected at Skye North during the 2014 research cruise and presented a complete increment for 2013, thus it had died less than one year before collection. There are no significant differences in scores between the specimens from ca. 3700–3400 yr before present (BP = 1950 CE), ca. 820 yr BP, and ca. 440 yr BP. The most recent specimen, from 2013 CE, yielded higher scores than the earlier specimens for its ligament, margin, and nacre. The periostracum was missing in all specimens, including the most recent one. None of the specimens showed signs of bioerosion, except for the most recent specimen.

Table 5.3: Scores for *G. glycymeris* from different time periods. The 3710-3480 yr BP group consists of twelve shells and thus the average scores are presented here. The 2013 CE shell is a specimen from Skye North that crossmatched with live shells from the same location (results not shown in this thesis) and thus the exact death date is known.

Death date	***Perio-stracum*** *(1–5)*	***Liga-ment*** *(1–4)*	***Margin*** *(1–4)*	***Bioerosion*** *(1–4)*	***Nacre*** *(1–3)*
ca. ***3710-3480 yr BP*** *(n=12)*	1	1	2	4	2
ca. ***820 yr BP*** *(n=1)*	1	1	1	4	1
ca. ***440 yr BP*** *(n=1)*	1	1	2	4	2
2013 CE *(n=1)*	1	3	4	2	3

Figure 5.1 presents one of the specimens dated to the 4th millennium BP (14G0VB031) and the specimen dated to ca. 440 yr BP (14G0VB050). Despite the age difference, both shells yielded similar scores, the younger shell from ca. 440 yr BP performing slightly worse due to the abraded margin. The pattern on the outside of the shell that is typical for *G. glycymeris* is better preserved in the older shell (Figure 5.1). However, these patterns were not included in the scoring system and not assessed systematically.

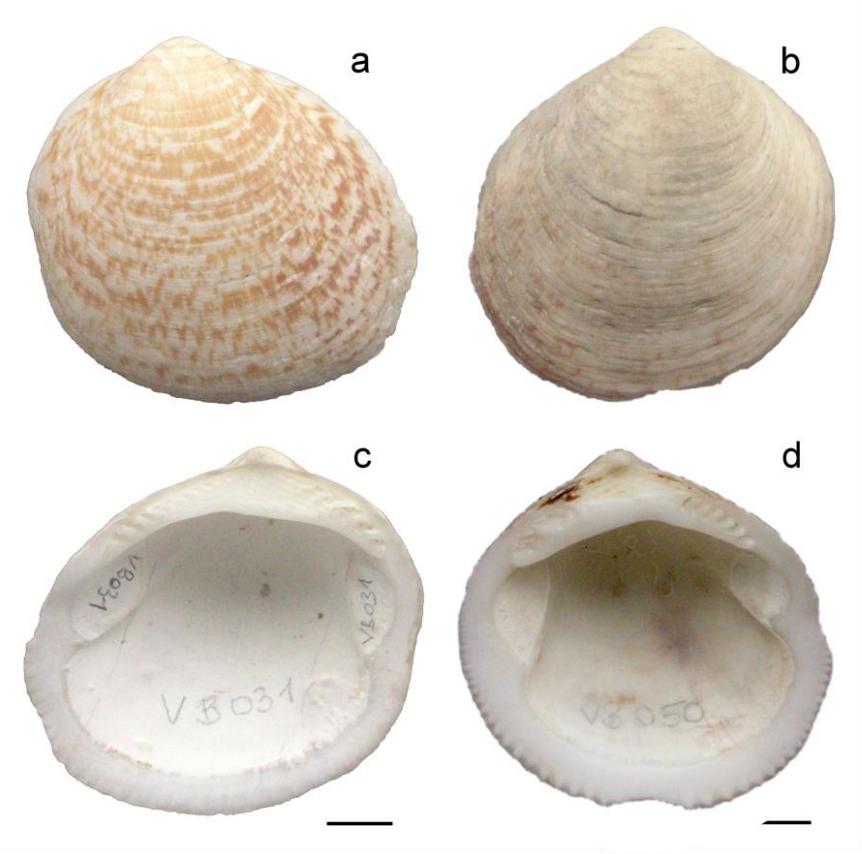

Figure 5.1: *G. glycymeris* valves dredged at St Kilda. Specimen 14G0VB031 to the left (a, c) is ca. 3000 years older than specimen 14G0VB050 to the right (b, d). The black scale bars represent 1 cm.

All shells from the 4th millennium BP were matt white on the inside, while live-collected shells had a glossy inside. This characteristic was not assessed systematically.

5.2.2 Raman spectroscopy

The fossil shells showed no signs of diagenesis, all Raman spectra of the fossil shells being consistent with those of aragonite (Figure 5.2). Clear characteristic aragonite peaks were identified at 153, 181, 206 and 702–706 cm^{-1} (Parker *et al*., 2010) along with a characteristic calcium carbonate peak at 1085 cm^{-1} (Wehrmeister *et al*., 2010). No characteristic calcite peaks were identified in any spectra acquired from fossil *G. glycymeris*.

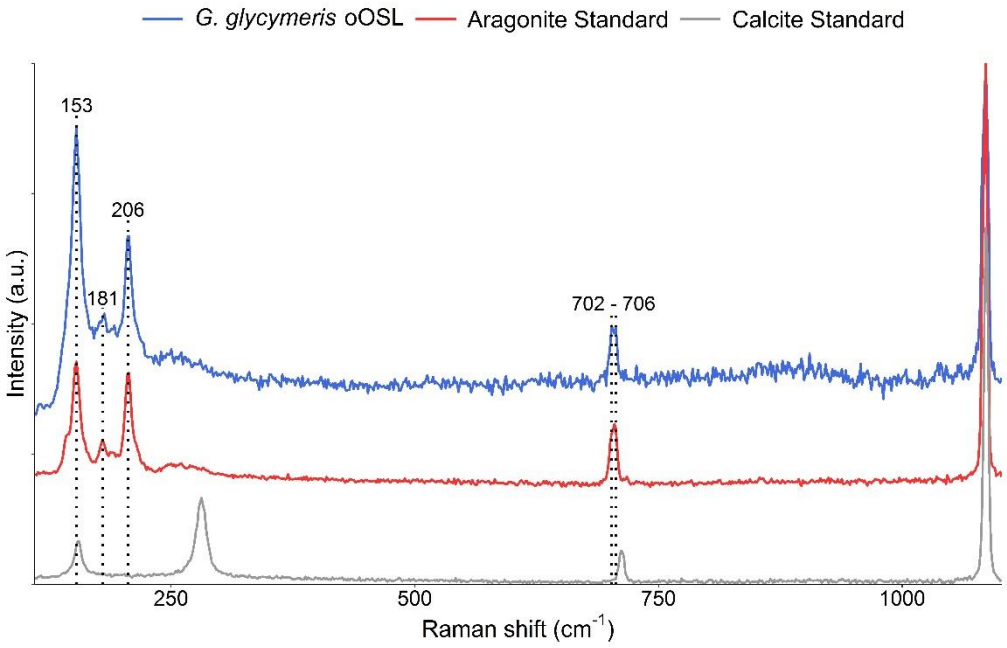

Figure 5.2: Raman spectra acquired between 135 and 1100 cm-1 for the oOSL of a fossil *G. glycymeris* along with spectra from speleothem aragonite and synthetic calcite. Characteristic peaks in the spectra are indicated (dotted lines) for coincident peaks in the shell and speleothem aragonite. A clear matching peak at 1085 cm^{-1} is visible for all samples. The y-axis is displayed as arbitrary units of intensity. Data and figure kindly provided by Philip Hollyman.

5.3 Discussion

5.3.1 Taphonomic scores

Shell condition was methodically assessed following a scoring system used by the Sclerochronology group at Bangor University (Butler et al., 2020; see Methods section 3.2.2). These data are collected systematically for all processed shell material and saved for future reference and potential studies. The same taphonomic scoring system was applied to both *A. islandica* and *G. glycymeris*. However, previous taphonomic studies on *G. glycymeris* have used additional variables, including the abrasion of ornamentation and colour patterns of the exterior shell (Cabral and Martins, 2016; Rogalla and Amler, 2007).

5.3.1.1 Live-collected material (*A. islandica* and *G. glycymeris*)

One might expect that live specimens generally obtain the highest possible score in each category (periostracum, ligament, bioerosion, nacre, margin). However, this does not have to be the case. Shell condition may deteriorate while the animal is still alive; this is particularly true for the periostracum, which is often found to be abraded or eroded in older parts of bivalve shells. To provide a baseline for *G. glycymeris* and *A. islandica*, a simple overview of both live and dead specimens and their average taphonomic scores is presented in Table 5.1. Each sample site was initially considered individually to account for possible local environmental influences that may affect shells differently. However, no major differences were found between the live specimens sampled at Village Bay (St Kilda), Skye, Canna, and Rhum; thus, all data were grouped as presented above (see Appendix A for individual scores).

Ten live-collected *G. glycymeris* specimens were assessed, of which seven had been collected at Village Bay, St Kilda, and three north of Skye. All live *G. glycymeris* obtained the highest possible score in every category (Table 5.1). It is noteworthy that all ten specimens were fully covered in periostracum; this thin organic layer is often eroded during the lifetime of a specimen, persisting only as a narrow rim at the ventral margin (Rogalla and Amler, 2007, see Introduction section 1.5). The preservation of the periostracum may be partially explained by the water depth that the specimens were collected at (45–65 m at Village Bay, 42–64 m at Skye). Even though strong wave-base motion is still present at these depths at Village Bay,

abrasion processes are much slower here than in the surf zone (Driscoll, 1967). Moreover, all live-caught *G. glycymeris* were relatively young at the time of capture; the seven specimens from St Kilda were around 15 years old and all three specimens from Skye were younger than 40 years old. Thus, since the fossil specimens were considerably older at their time of death (around 100 years), it is conceivable that they may have shown signs of periostracum erosion during their lifetime even though their modern counterparts did not.

In contrast, live specimens of *A. islandica* were often only covered to ca. 50% by periostracum. These specimens were generally collected at shallower depths (e.g., 26 m at Village Bay) and considerably older (where age was assessed) than the *G. glycymeris* samples. Consequently, the *A. islandica* specimens had been more exposed to physical abrasion and chemical erosion. Apart from the lower scores for periostracum cover, live *A. islandica* obtained the highest possible score in every category.

5.3.1.2 Fossil *G. glycymeris* from different time intervals

While a relatively large number of *G. glycymeris* shells was retrieved from Village Bay, St Kilda, only 14 specimens were radiocarbon dated (Table 5.2). The overall number of shells that could be used to study the relationship between shell condition and time was limited to these 14 radiocarbon-dated specimens plus one shell from north of Skye that had died less than a year before it was collected (Table 5.3). Apart from the group assigned to the 4th millennium BP (n = 12), all time intervals in Table 5.3 are represented by only one specimen. The results presented in this chapter do therefore not allow any general conclusions to be drawn and the following discussion is to be taken with caution.

Ligament and periostracum

Preservation of ligament clearly set the recently dead specimen (2013 CE) apart from other groups (Table 5.3). This is unsurprising, since organic material decays faster than the calcareous shell material and can therefore be expected to be largely absent in fossil material (see also Butler et al., 2020). However, while presence of organic material may suggest a relatively recent death of the specimen, absence of such organic-rich material does not automatically allow for the opposite conclusion to be made. This seems to be particularly true for the periostracum, which, as mentioned above, often is eroded or abraded during the lifetime of a specimen and was completely absent in the specimen that had died in 2013 CE (Table 5.3).

Nacre and margin

The condition of nacre and margin was better in the recently dead specimen compared to older samples. However, there was a high variation in scores among the coeval specimens from the 4th millennium BP, indicating that their exposure to the physical and biotic environment differed (Appendix A). Thus, no clear trends could be detected.

Bioerosion

There is an important caveat when assessing bioerosion in material pre-selected for sclerochronological studies. Because it is difficult to crossmatch specimens that are heavily bored, these shells are of less interest to sclerochronologists and were the first ones to be removed from the sample pool presented in this thesis. Put differently, the shells that were processed, assessed, and radiocarbon dated were not chosen randomly. Instead, the most intact shells with negligible bioerosion were picked, where possible, to ensure that the subsequent microscope images would be clear enough for crossmatching. This has two major implications: (1) There is a bias towards more intact shells in the fossil sample material presented above, and (2) even if bioerosion was a discriminatory factor between shells from different time intervals, this finding would be devalued by the fact that heavily bored shells are only of limited use. Notwithstanding this caveat to using bioerosion scores, the following paragraph will provide a short discussion of the results in Table 5.3.

Bioerosion was not a discriminating factor between shells from different groups. In fact, the most recent dead-collected specimen had the lowest score in this category (Table 5.3). Given the lack of bioerosion in the shells dated to the fourth millennium BP, they must have remained buried in the sediment after their death (e.g., Flessa et al., 1993). In an experimental study on shell destruction, Driscoll (1970) found that, in low-energy environments, the main cause of destruction in shells above the sediment-water interface is boring, while the main destructive agent beneath the interface is chemical dissolution. Thus, bioerosion might be more indicative of how the shells have been preserved in the sea, rather than for how long. Indeed, bioerosion — particularly microboring — is a well-known indicator of rapid burial in palaeontological studies (Lescinsky et al., 2011; Vogel et al., 2000).

Summary of findings in comparison with existing literature

All in all, the scoring system was not sufficient to discriminate between dead-collected material from different time periods in this study, i.e. it was not possible to determine whether a

specimen had died 500 years ago or 3500 years ago. While the small sample size prevents definite conclusions to be drawn, the findings are in good accordance with the existing literature. For example, in a study on *Chione* spp. from the Gulf of California, Flessa et al. (1993) found significant time-averaging in surficial shell lags (up to 3500 years), and taphonomic grades were not a reliable indicator of time since death. In a comprehensive study on abrasion processes in over 500 *G. glycymeris* shells, Rogalla and Amler (2007) distinguished nine taphonomic characteristics: valve outline and shape, ornamentation of exterior shell surface, colour and periostracum of the exterior shell surface, beak/umbo depression, beak/umbo facets, hinge plate condition, ligamental area condition, internal shell surface within pallial line and adductor scars, and crenulation of inner ventral margin. Each of these nine characters were divided into six to ten abrasion stages (Rogalla and Amler, 2007). The authors concluded that abrasion processes in *G. glycymeris* are "mosaic-like", i.e. noncontinuous and nonlinear (Rogalla and Amler, 2007). The study by Rogalla and Amler (2007) thus provides further evidence supporting the finding that the antiquity of a shell cannot be quantified through its exterior condition; however, it should be noted that their study was based on shells collected in the intertidal. In contrast, the St Kilda shells were collected at depths below 46 m, and are thus more representative of a low-energy environment than an intertidal or surf-zone environment. This is an important distinction to make when comparing results from different studies, since shell destruction is 150 to 1000 times faster in the surf zone compared to low-energy sublittoral environments, and mostly caused by abrasion (Driscoll, 1970). Arguably the most relevant study for this discussion was published recently by Butler et al. (2020), in which the authors assessed the taphonomic condition of 277 radiocarbon-dated *A. islandica* shells from the North Sea. The study design was similar to the one described in this chapter, as the same dredge and the same taphonomic scoring system were applied (Butler et al., 2020; see Methods chapter). The shells were divided into four different groups based on their radiocarbon dates: modern (post bomb pulse), 0–500 cal yr BP, 500–1500 cal yr BP, and early Holocene/late Glacial (EHLG, ~6000–14,000 cal yr BP) (Butler et al., 2020). The authors then tried to assign the shells to the correct radiocarbon groups based on their taphonomic variable scores, using discriminant analysis and principal component analysis. Only the modern shells were placed in the correct group to a high enough degree, whereas in other age groups the portion of correctly placed shells could be as low as 20%; the authors thus concluded that shell condition and taphonomy cannot be used to triage shells for chronology construction (Butler et al., 2020).

5.3.2 Comparability of fossil *G. glycymeris* and modern shells

As described above, the fossil shells used for chronology building were in very good condition, and Raman spectroscopy showed no diagenetic alterations (Figure 5.2). This makes them suitable for sclerochronological studies and comparison with live specimens. Once that is known, the remaining question is whether the fossil specimens lived in the same location as they were found, and in similar depths as the live specimens. Here, the distinctive topography of St Kilda is helpful (see Section 2.5.1) — the steep sub-surfaces and the lack of sediment on most of the platform suggest that the fossil shells lived at Village Bay, at similar depths as the live specimens. Relative sea-level change does not have to be considered in this study, as sea-level rise in this region has been smaller than 2 m in the last 4000 years (Gehrels, 2010).

5.3.3 Conclusions and implications for future studies

The radiocarbon ages of the dated shells (Table 5.2) are mainly clustered in the 4th millennium BP. This bias can be partially explained by the fact that six of the dated shells had been crossmatched with each other prior to radiocarbon dating; consequently, they were expected to be contemporaneous (*St Kilda Seven* chronology, see Chapter 6). In addition, six other specimens also yielded similar radiocarbon dates, placing them at approximately 3700–3500 yr BP. However, the remaining two shells were considerably younger (820 yr BP and 440 yr BP). This offers the possibility to build floating chronologies with shells from different time windows, or perhaps even a continuous record over the past three or four millennia. Decadal-scale $\delta^{13}C$ and $\delta^{18}O$ records spanning the last millennium have been published for Loch Sunart, NW Scotland, based on benthic foraminifera (Cage and Austin, 2010). Similarly, a *G. glycymeris* chronology spanning the last millennium has been constructed for the Tiree Passage (unpublished data, pers. comm. David Reynolds), as an extension of the previously published chronology for the same site (Reynolds et al., 2013). Both these locations are situated in proximity to each other on the inner Malin shelf, and no comparable chronologies are available for the outer shelf. As discussed in Chapter 2 and Chapter 4, the Scottish shelf exhibits a strong longitudinal gradient in salinity content, salinity anomaly, SST amplitudes, and water chemistry, as coastal influences are considerably stronger on the inner shelf (e.g., Figure 2.2, 2.3). A multi-millennial high-resolution record of an offshore environment like St Kilda would therefore be invaluable and novel information. However, to properly assess whether a continuous chronology linking the fossil shells to modern specimens is possible, the

approximate ages of the existing shell material need to be known. During the research cruise in 2014, only seven young *G. glycymeris* were found live (see Methods chapter), and during a survey of marine fauna at Village Bay around 20 years earlier, no *Glycymeris* at all were recorded (Ellis et al., 1995). Either the main population was missed in both instances, which is plausible, or *G. glycymeris* were completely absent at Village Bay during some time and only resettled there very recently. Answering this question would require a considerable amount of additional funding; consequently, the potential of a continuous multi-centennial-to-millennial *G. glycymeris* chronology at this location remains uncertain.

Building a shell-based chronology is generally time-intensive, even when live-collected specimens are used. Given that specimens found in the same shell lag can have age differences of thousands of years (Table 5.2; Flessa et al., 1993; Butler et al., 2009), any attempt to crossmatch fossil shells from a shell lag is likely to be many times more time-consuming and a potentially fruitless task, especially since spurious correlations may be found between specimens whose lifespans did not overlap in time. Therefore, the age of the used shell material should ideally be constrained before crossmatching is attempted. Currently, radiometric or AMS dating are the most common methods used to identify whether shells were approximately coeval. However, these techniques require additional resources and are age-limited; they might therefore not always be feasible. The search for alternative methods to constrain ages of fossil shell material was recently highlighted as a priority research question in sclerochronology in a horizon-scanning survey (Trofimova et al., 2020). As described above, taphonomic variable scores are most likely unsuitable as an alternative method of triaging shells; thus, the search for alternative sampling strategies in fossil material must continue.

Chapter 6

Master chronologies and sub-annual oxygen isotopes: growth variability, growth season, and seasonal temperatures in the late Holocene

Chapter 6 — Master chronologies and sub-annual oxygen isotopes: growth variability, growth season, and seasonal temperatures in the late Holocene

This chapter presents all master chronologies used in this thesis as well as sub-annual oxygen isotopes. The choice was made to combine all these results into one single chapter because their discussion is strongly linked. The crossmatched growth increments define annually resolved time series that allows the interpretation of seasonal oxygen isotopes in the first place. Conversely, the seasonal signal of the oxygen isotopes enables us to determine during which time of the year the growth increments were formed, thus providing more information on the chronologies themselves. Lastly, seawater temperatures can be calculated once the chronologies are built, assuming the oxygen isotope signal of seawater can be constrained. Thus, to allow for a fluid discussion of results that build on one another, all these data are presented together.

Master chronologies

Three chronologies were constructed: one modern *Arctica* chronology spanning 125 years, and two floating *Glycymeris* chronologies, spanning 141 years and 187 years respectively. The two floating chronologies (referred to as the *St Kilda Seven* and the *Misfits* chronologies) were assigned radiocarbon dates in the 4th millennium BP (Table 5.2 in the previous chapter). The following subsections introduce all three chronologies (Section 6.1 and Section 6.2).

The focus of this chapter is on the floating *Glycymeris* chronologies and the 4th millennium BP. The modern *Arctica* chronology is presented for comparison, but further analysis of the modern chronology and correlations with instrumental data is given in Chapter 7.

Seasonal oxygen isotopes

Section 6.3 presents sub-annual oxygen isotope profiles in the fossil *St Kilda Seven* shells and two modern *Arctica* chronology specimens. Growth season, seasonality, and mean temperatures are inferred from the oxygen isotope series of both the 4th millennium BP and the modern chronology.

NB: Parts of the results (Section 6.1.2 and Section 6.3) and discussion (Section 6.4.1.1 and Section 6.4.3) have been published in the journal Palaeogeography, Palaeoclimatology, Palaeoecology, in a research article titled "Late Holocene seasonal temperature variability of the western Scottish shelf (St Kilda) recorded in fossil shells of the bivalve Glycymeris glycymeris" (Alexandroff et al., 2021).

6.1 Floating *Glycymeris* chronologies – 4th millennium BP

Both chronologies presented in this subsection were constructed with dead-collected *G. glycymeris* from St Kilda and have been radiocarbon dated to the fourth millennium BP (Table 5.2). Their respective conventional radiocarbon ages separate these two chronologies by ca. 100 to 200 years, the *Misfits* chronology being slightly younger (3400 yr BP) than the *St Kilda Seven* chronology (3700–3500 yr BP). Because these chronologies are floating, i.e. not absolutely dated, their time axes are reported in chronology years.

6.1.1 Misfits chronology

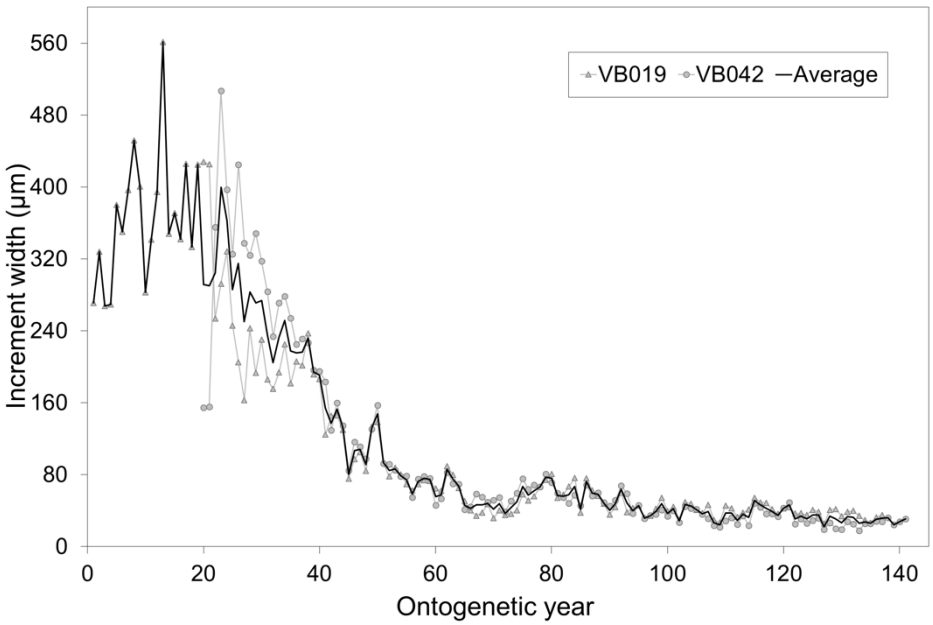

Figure 6.1: Raw increment widths of the two *Misfits* chronology shells (grey lines), measured in the hinge plate. The black line shows the arithmetic mean of the raw (i.e. not yet standardised) series.

The *Misfits* chronology consists of only two specimens (Figure 6.1) with lifespans of 127 and 112 years, respectively. Specimen 14G0VB019 was assigned radiocarbon dates that place the chronology in the mid- to late fourth millennium BP (Table 5.2).

The increments were measured in the hinge plate; thus, both series begin with small increments (Figure 6.1). These small increments in the most juvenile part of the hinge plate often presented doublet annual lines and were therefore difficult to read and crossmatch. After the first 10 to 20 years of life, the growth curve shows the expected negative exponential trend (Figure 6.1).

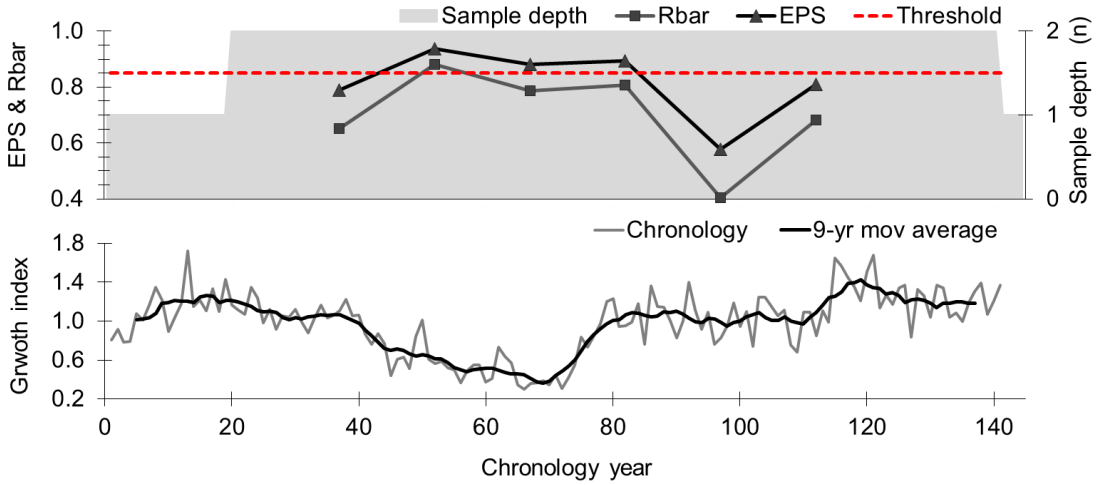

Figure 6.2: *Misfits* chronology. The bottom panel shows the standardised annual growth indices (grey line) and a 9-year moving average (black line). The top panel shows sample depth (grey shaded area), EPS (black triangles), and Rbar (black squares) of the chronology. The red dashed line is the 0.85 EPS threshold as suggested by Wigley et al. (1984).

The resulting chronology presented in Figure 6.2 spans 141 years, however only 118 years of the chronology contain data from both specimens. The inter-series correlation between the two specimens is high enough to offset the low sample number and produce an EPS higher than 0.85 for a duration of over 40 years (Figure 6.2). This 40-year period of high EPS (> 0.85) and Rbar (> 0.75) coincides with a strong negative growth trend followed by a quick recovery (Figure 6.2). The EPS and Rbar drop rapidly during the following decades (chronology years 80 to 110, EPS = 0.58, Rbar = 0.41), which show no trend and are dominated by high-frequency variability only. Towards the end of the chronology a clear positive growth trend can be observed and the EPS (0.81) and Rbar (0.68) increase again.

Wavelet spectrum

The *Misfits* chronology yielded high-frequency signals (2 to 6 years) in the earliest and latest part of the chronology, based on CWT analysis with a red-noise background (Figure 6.3). Gaps with no significant periods are dominant in the years 20 to 80.

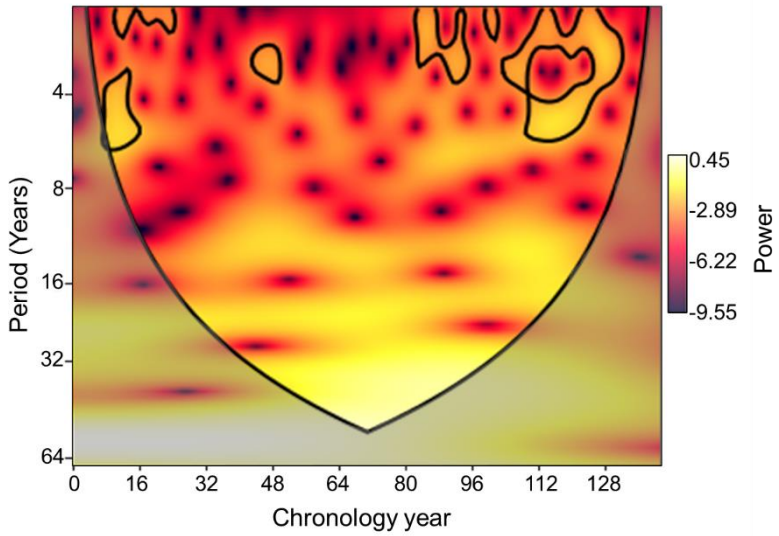

Figure 6.3: Wavelet spectrum for the floating *St Kilda Misfits* chronology using Morlet (wavenumber 6) as mother wavelet (Torrence and Compo, 1998). The legend indicates the power. The greyed area is the cone of influence, where edge effects due to zero padding may become important. The black contours represent regions of significance (p=0.05) using a red-noise background with lag-1 (autoregressive) of 0.82, calculated following the Box-Jenkins methods (Box et al., 1994).

Singular Spectrum Analysis and Multitaper Method

SSA of the *Misfits* chronology shows a significant period of 3 years ($p \leq 0.01$). Additional periods found through SSA and MTM were at $x = 0.01$ and $x \approx 0$, respectively, and have to be excluded because they approach the total length of the *Misfits* series (Figure 6.4).

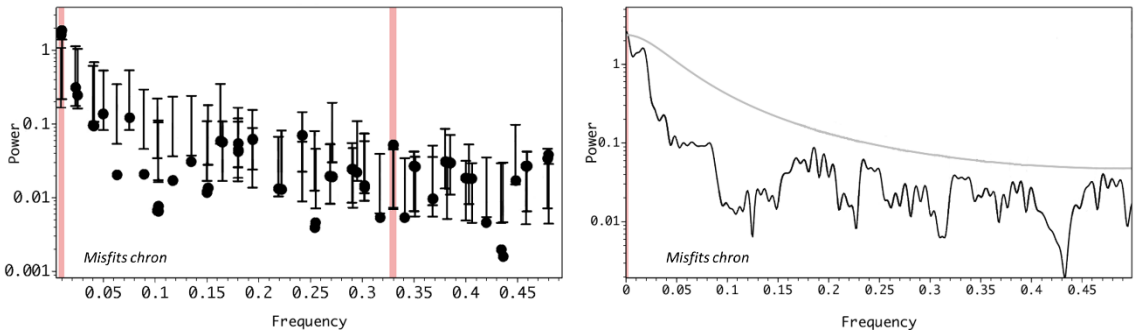

Figure 6.4: Spectral analysis of the *Misfits* chronology using a red-noise background (autoregressive lag 1). ***Left panel****:* Singular Spectrum Analysis (SSA). The vertical bars represent the 0.01 significance level. Significant periods (highlighted in pink): 100 years (x = 0.01), 3 years (x = 0.33). ***Right panel****:* Multitaper method (K = 3). The grey line represents the 0.01 significance level. The significant period is x ≈ 0.

6.1.2 St Kilda Seven chronology

The *St Kilda Seven* chronology is the focus of this thesis, next to the modern *Arctica* chronology, and provides the basis for stable isotope analysis presented in Section 6.3.

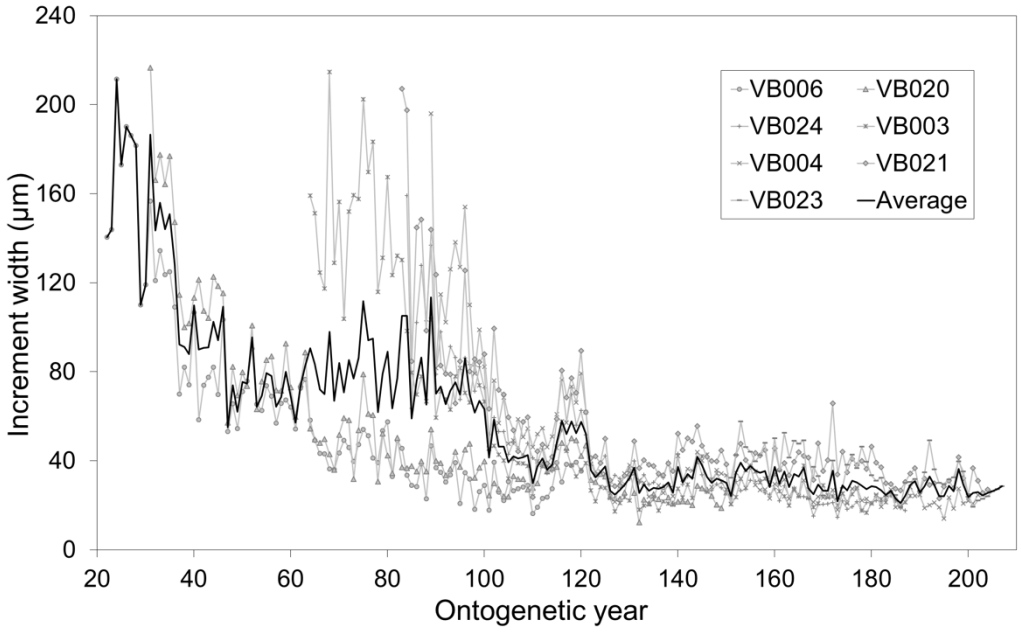

Figure 6.5: Raw increment widths of the *St Kilda Seven* chronology shells (grey lines), measured in the hinge plate. The black line shows the arithmetic mean of the raw (not yet standardised) series. The first 20 years of growth were removed in all series.

The chronology consists of seven shells and spans 207 years in total. However, the first 20 years of each specimen were removed, resulting in a chronology of 187 years (Figure 6.5, Figure 6.6). The increments were measured in the hinge plate. Similar to the *Misfits* chronology, the individual series show small increments in the first 10–20 ontogenetic years that often present doublet annual lines which are difficult to crossmatch. These smaller increments are followed by a set of large increments that then decrease in size exponentially (Figure 6.5).

The chronology is statistically robust or close-to-robust for ca. 110 years, with an EPS above 0.85, apart from a short period at around year 80 where the EPS dips below 0.80 (EPS = 0.77, Figure 6.6). Apart from the period mentioned above with a lower EPS, the years 30 to 140 show relatively high values for EPS (0.80 to 0.92) and Rbar (0.47 to 0.72). The first ten years of the chronology consist of only one specimen and should thus be treated with caution when interpreting the growth index series or when comparing it to other datasets. The following period between years 11 and 43 yielded high EPS and Rbar values despite the low sample depth (n = 2). Here, and in the following ca 100 years, the growth index series shows a low-frequency variability of ca 20–30 years. This pattern ends at around year 150. The EPS and Rbar decrease rapidly at around year 140 and continue to do so towards the end of the chronology, coinciding with the mentioned change in variability patterns.

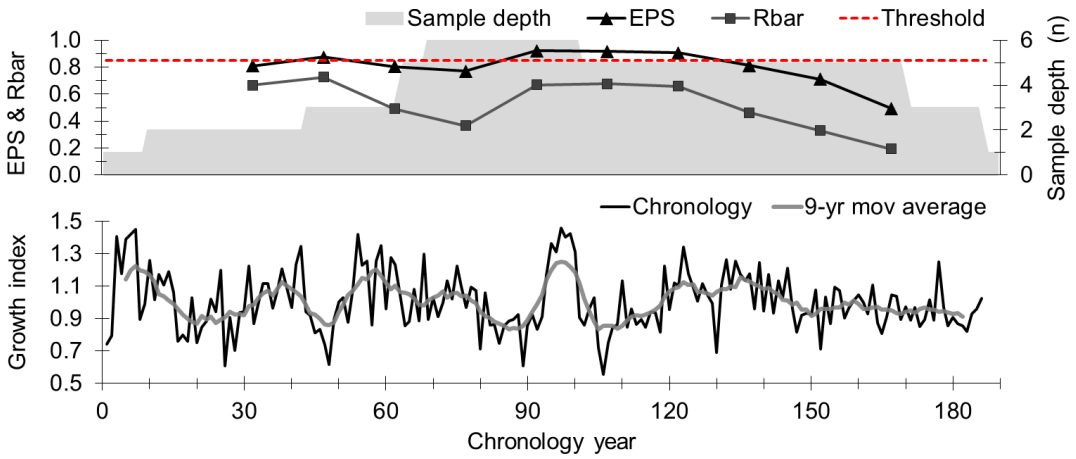

Figure 6.6: *St Kilda Seven* chronology. The top panel shows the standardised annual growth indices (grey line) and a 9-year moving average (black line). The first 20 years of growth were removed in all series, hence the chronology starting at year 21. The bottom panel shows sample depth, EPS and Rbar of the chronology. The red dashed line is the 0.85 EPS threshold as suggested by Wigley et al. (1984).

Wavelet spectrum

CWT analysis for the *St Kilda Seven* chronology produces significant periods fluctuating between 2 and 6 years for almost the entire length of the chronology (Figure 6.7). In addition to these short periods, a significant period of ca 10 to 24 years is present in the middle of the chronology, at around year 80 to 140.

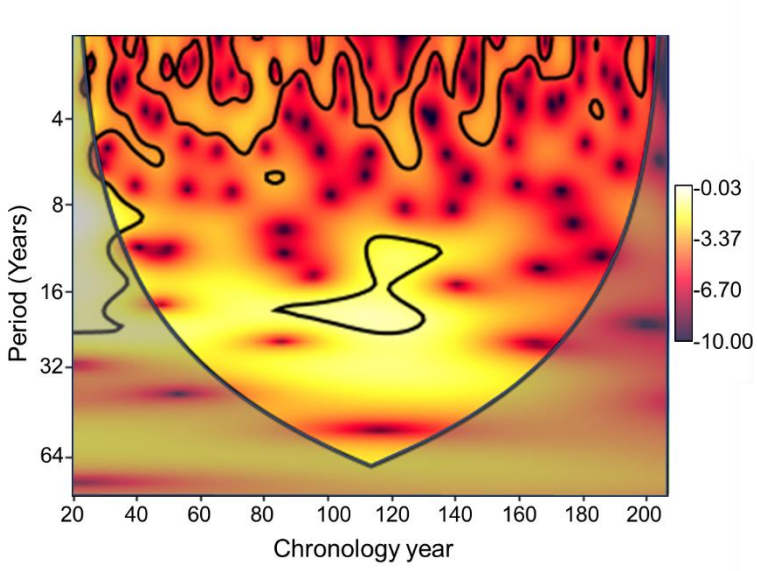

Figure 6.7: Wavelet spectrum for the floating *St Kilda Seven* chronology using Morlet (wavenumber 6) as mother wavelet (Torrence and Compo, 1998). The greyed area is the cone of influence, where edge effects due to zero padding may become important. The black contours represent regions of significance (p = 0.05) using a red-noise background with lag-1 (autoregressive) of 0.81, calculated following the Box-Jenkins methods (Box et al., 1994).

Singular Spectrum Analysis and Multitaper Method

SSA shows several persistent periods in the *St Kilda Seven* chronology (Figure 6.8). Significant results ($p \leq 0.01$) were obtained both for shorter periods of 2.4 years and 4 years, as well as for longer periods of 20 years and 33.3 years. The MTM results are consistent with SSA and produced significant periods of 2.4 years and 25 years.

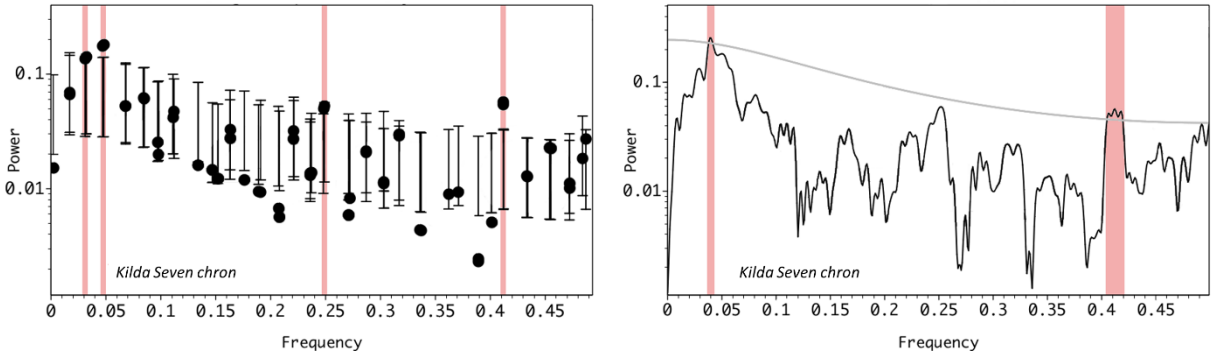

Figure 6.8: Spectral analysis of the St *Kilda Seven* chronology using a red-noise background (autoregressive lag 1). ***Left panel:*** Singular Spectrum Analysis (SSA). The vertical bars represent the 0.01 significance level. Significant periods (highlighted in pink): 33.3 years (x = 0.03), 20 years (x = 0.05), 4 years (x = 0.25), 2.4 years (x = 0.41). ***Right panel:*** Multitaper method (K = 3). The grey line represents the 0.01 significance level. Significant periods (highlighted in pink): 25 years (x = 0.04), 2.4 years (x = 0.41).

6.1.2.1 Constraining the age uncertainty of the St Kilda 7 chronology

Six specimens (i.e., all but 14G0V023) of the *St Kilda Seven* chronology were radiocarbon dated, placing the chronology in the fourth millennium BP. When the local marine reservoir effect offset is taken into account, the calibration of the radiocarbon dates produces 2-sigma uncertainties of ca. 300 years (Table 6.1). These uncertainties were constrained through a chronological model, i.e., by taking both the radiocarbon calibration curve and the stratigraphic information obtained through crossmatching into account (Table 6.1, see Methods section 3.4.2).

Table 6.1: Radiocarbon ages of the *St Kilda Seven* shells. The unmodelled and modelled dates with a 95.4% probability (2-σ) are given after a regional ΔR correction of −117 ± 93 has been applied. Modelled dates refer to dates output by the chronological model (Bayesian defined sequence model in OXCAL 4.4). Lab IDs of each specimen are given in Table 5.2.

Specimen	***Unmodelled (cal yr BP)***	***Modelled (cal yr BP)***
14G0VB006	3605–3314	3515–3405
14G0VB020	3615–3308	3475–3365
14G0VB024	3624–3320	3445–3335
14G0VB003	3546–3239	3444–3334
14G0VB004	3518–3210	3429–3319
14G0VB021	3427–3131	3428–3318

Table 6.1 includes all dates of the six *St Kilda Seven* specimens that were radiocarbon dated, before and after applying the Bayesian chronological model. The modelled dates range from 3515 to 3318 cal yr BP, which reduced the unmodelled range (3624–3131 cal yr BP) by 296 years.

The Bayesian model places the *St Kilda Seven* chronology in the mid-fourth millennium BP with probability density peaks clustered around 3500–3300 cal yr BP (Figure 6.9).

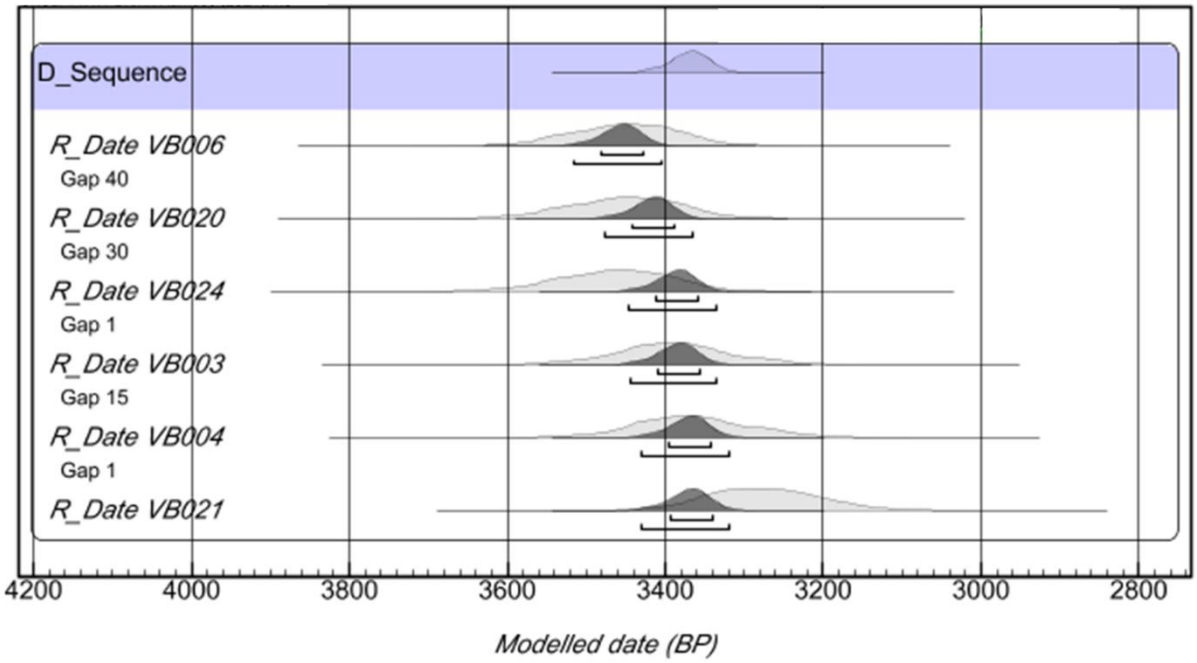

Figure 6.9: Probability densities of the death dates of six *St Kilda Seven* specimens and the combined series (D_Sequence), applying a ΔR correction of –117 ± 41. The sample IDs and gaps between each specimen as derived from crossmatching are given in the left column. The pale grey distribution curves represent the radiocarbon calibration probability distribution. The dark grey distribution curves are the resulting probability distributions obtained by the chronological model, after the gaps between each specimen are considered. The square brackets indicate a 95.4% probability. The top distribution curve (D_Sequence) is the result of wiggle-matching the crossmatched series to the radiocarbon calibration curve using the χ^2 test.

6.2 Modern *Arctica* chronology

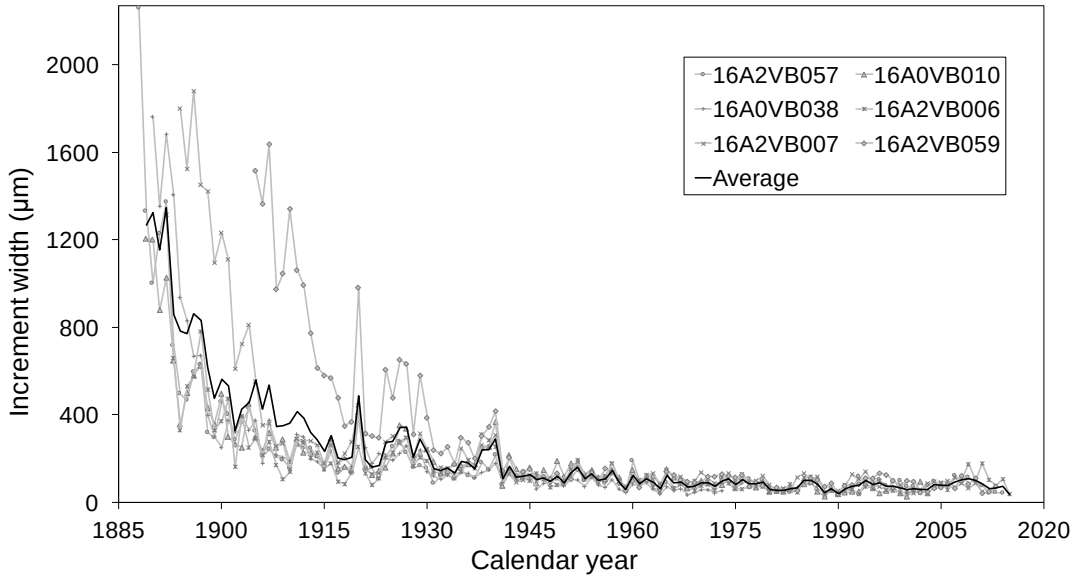

Figure 6.10: Raw increment widths of the six *A. islandica* chronology shells (grey lines), measured in the margin. The black line shows the arithmetic mean of the raw (i.e. not yet standardised) series.

Four live- and two dead-collected *A. islandica* shells were crossmatched and stacked into a chronology. The individual series ranged from 84 to 127 years, and the increment widths in the margins ranged from 26 µm in mature shell parts to 2260 µm in juvenile parts (Figure 6.10). The increments were measured in the margin. The undetrended growth series shown in Figure 6.10 follow a negative exponential growth trend. The resulting chronology spanned 1889–2015 CE in total, however, the year 1889 is only represented by one specimen. Therefore, that year was removed, shortening the chronology to 1890–2015 CE (Figure 6.11). The chronology is statistically robust in 1921–1981 CE with an EPS of > 0.85 and an Rbar of > 0.55. Both the EPS and the Rbar decrease rapidly towards the end of the chronology and are at the lowest level at year 1995 (EPS = 0.76, Rbar = 0.39). There are no statistics on the period before year 1921 CE because the EPS and Rbar were calculated based on 30-year windows (see Methods section 3.3.4).

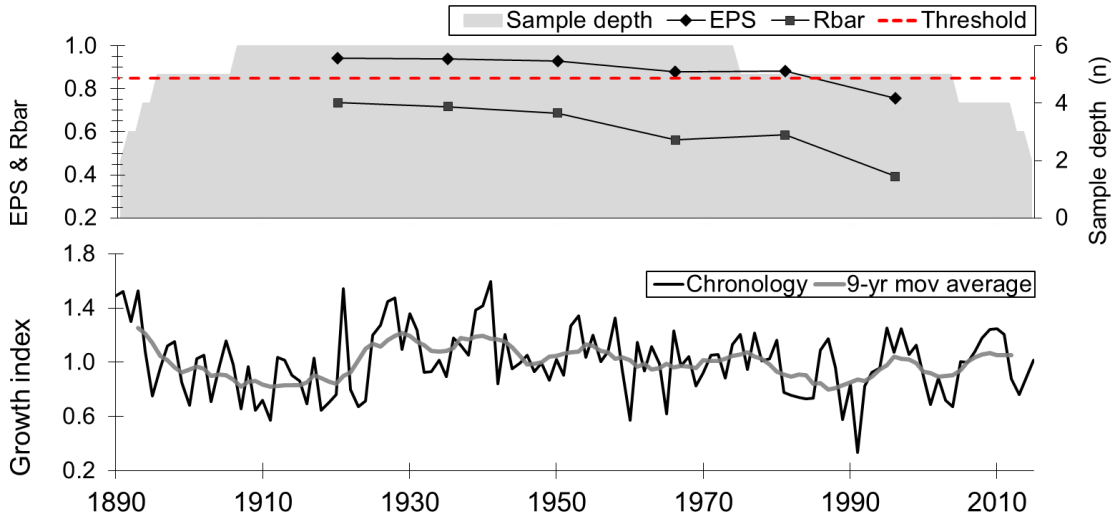

Figure 6.11: *Arctica islandica* chronology. The bottom panel shows the standardised annual growth indices (grey line) and a 9-year moving average (black line). The top panel shows sample depth, EPS and Rbar of the chronology. The red dashed line is the 0.85 EPS threshold as suggested by Wigley et al. (1984).

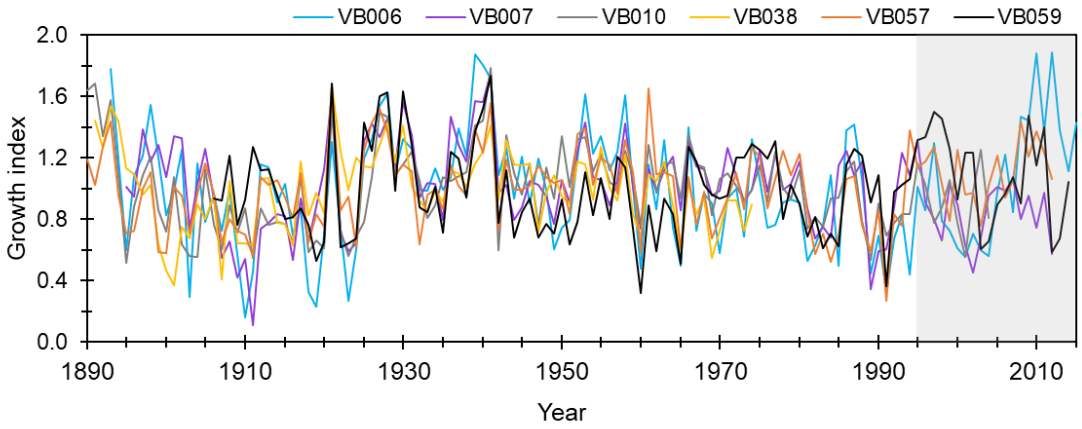

Figure 6.12: Detrended series of all six shells in the *Arctica* chronology. The grey shaded area indicates the part of the chronology with the lowest EPS and Rbar.

Wavelet spectrum

Continuous wavelet transform (CWT) analysis of the *Arctica* chronology presents significant periods of between 2 and 6 years throughout the chronology until 2002 CE, and additional quasi-decadal periods in different parts of the chronology (Figure 6.13).

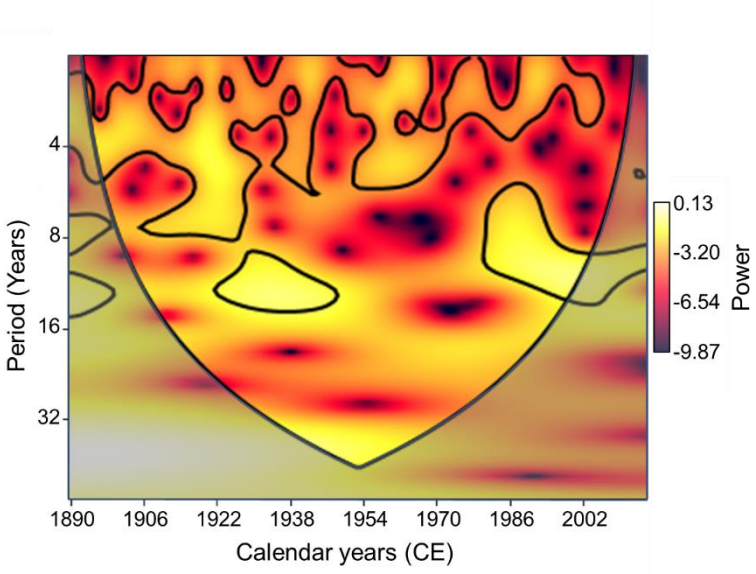

Figure 6.13: Wavelet spectrum for the modern *A. islandica* chronology using Morlet (wavenumber 6) as mother wavelet (Torrence and Compo, 1998). The greyed area is the cone of influence, where edge effects due to zero padding may become important. The black contours represent regions of significance (p = 0.05) using a red-noise background with lag-1 (autoregressive) of 0.85, calculated following the Box-Jenkins methods (Box et al., 1994).

Singular Spectrum Analysis and Multitaper Method

Figure 6.14 illustrates the analysis of persistent patterns in the chronology. While Singular Spectrum Analysis (SSA) yielded no significant periods, the Multitaper Method (MTM) showed a significant period of 2.2 years (p = 0.01).

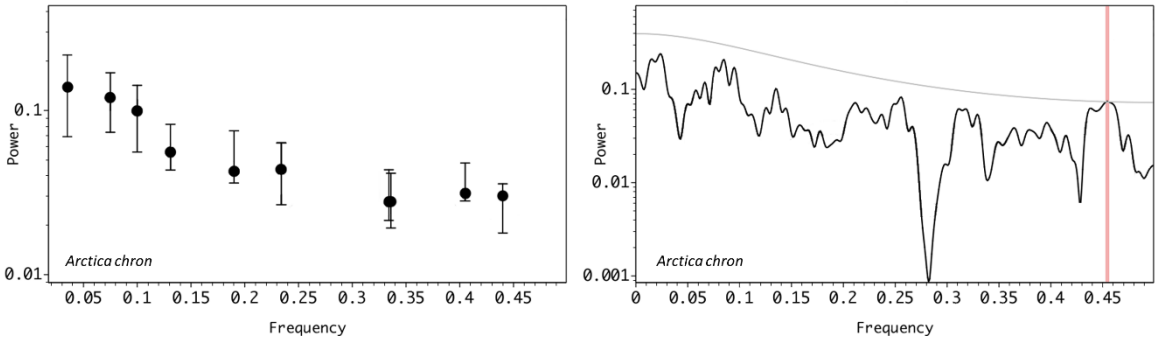

Figure 6.14: Spectral analysis of the *Arctica* chronology using a red-noise background (autoregressive lag1). ***Left panel:*** Singular Spectrum Analysis (SSA). The vertical bars represent the 0.01 significance level. ***Right panel:*** Multitaper method (K=3). The grey line represents the 0.01 significance level. Significant period (highlighted in pink): 2.2 years (x=0.455).

6.3 Seasonal oxygen isotopes

6.3.1 Raw $\delta^{18}O$ series

6.3.1.1 *Glycymeris glycymeris*

Oxygen isotope values are presented for three live-collected shells (2005–2013 CE) and five fossil shells from the floating chronology (3515–3318 cal yr BP). The three modern shells yielded sub-annual $\delta^{18}O_c$ for between 8 and 11 growth seasons (i.e. 'annual' increments) and were averaged into one combined series spanning 2005–2013 CE. The average sampling resolution in the modern specimens was six samples per year, with a minimum of five and a maximum of nine samples per year.

All seven fossil shells from the floating chronology were sampled; however, two shells (14G0VB003 and 14G0VB024) were excluded from further analysis due to low sampling resolution. Figure 6.15 shows the position of each of the remaining five fossil $\delta^{18}O_c$ series in the floating chronology, which span between 11 and 14 growth seasons each. The average sampling resolution of the five fossil shells was five samples per year, with a minimum of two and a maximum of nine samples per year. Specimens 14G0VB004 and 14G0VB021 were combined into one average series due to their overlap in time. Thus, there are four windows in the floating chronology: Two separate series at the beginning of the chronology (14G0VB006, 14G0VB020), one combined series in the middle of the chronology (14G0VB004 and

14G0VB021), and one series at around year 140 (14G0VB023). All modern and fossil shells showed a clear seasonal signal (Figure 6.16). The isotope series of the two coeval fossil specimens presented a warming trend (14G0VB004 and 14G0VB021; Figure 6.16).

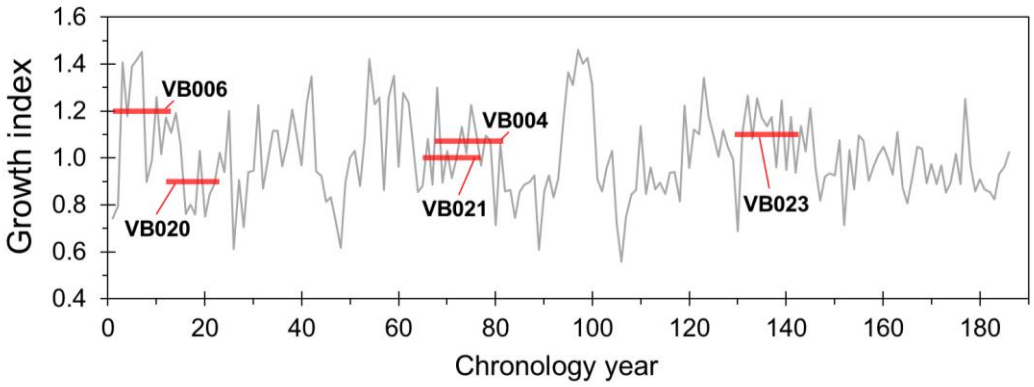

Figure 6.15: Positions of the fossil $\delta^{18}O_c$ series in the floating chronology.

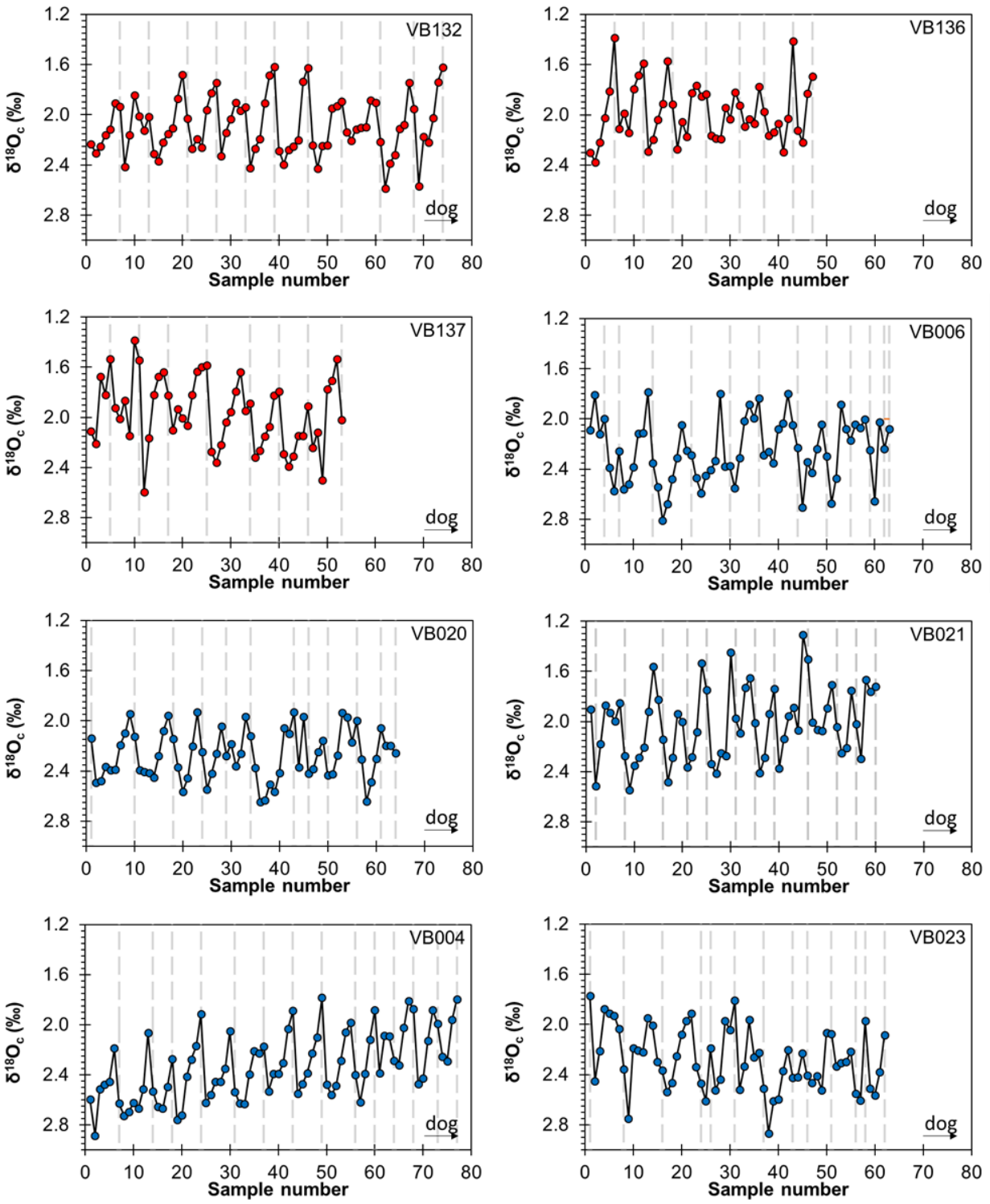

Figure 6.16: $\delta^{18}O_c$ values for the modern (red dots; 14G2VB132, 14G2VB136, 14G2VB137) and the fossil *G. glycymeris* shells (blue dots; 14G0VB006, 14G0VB020, 14G0VB004, 14G0VB021, 14G0VB023). The sample direction followed the direction of growth (dog), from the ontogenetically youngest increments towards the more mature increments. The dashed vertical lines coincide with the last sample of each growth season. Note that the y-axes are inverted, thus, peaks in the plots correspond to temperature peaks. Each sample spot has a 300 μm diameter.

6.3.1.2 *Arctica islandica*

Two shells of the *A. islandica* chronology were sampled (16A2VB007, 16A0VB010, see Figure 6.17). Specimen 16A2VB007 provided an average sampling resolution of 12 samples per year, with a minimum of five and maximum of 17 per year. Specimen 16A0VB010 provided a resolution of eight samples per year, with a minimum of three and a maximum of 14 samples per year. Similar to *G. glycymeris*, a clear seasonal signal is visible in both *A. islandica* specimens (Figure 6.17).

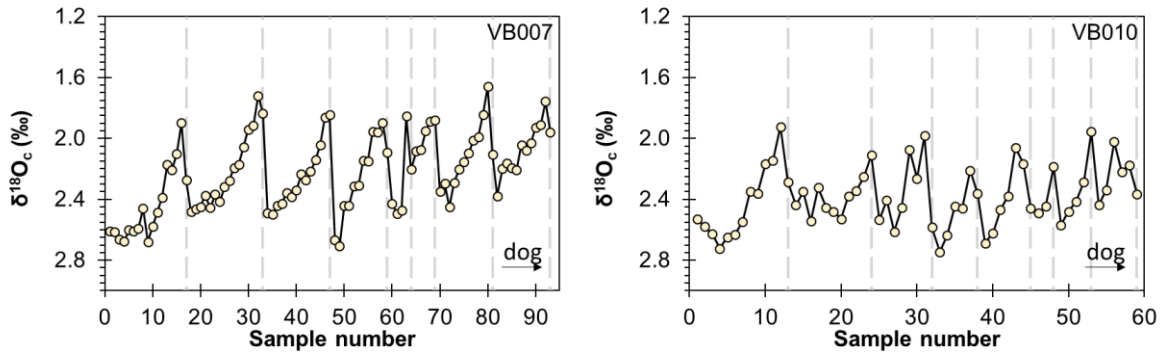

Figure 6.17: $\delta^{18}O_c$ values for the *A. islandica* shells (16A2VB007, 16A0VB010). The sample direction followed the direction of growth (dog), from the ontogenetically youngest increments towards the more mature increments. The dashed vertical lines coincide with the last sample of each growth season. Note that the y-axes are inverted, thus, peaks in the plots correspond to temperature peaks. Each sample spot has a 300 µm diameter.

6.3.2 Growth season and calibration with instrumental data

The $\delta^{18}O_c$ series were converted into temperatures using a palaeotemperature equation (see Methods section 3.6.5, Equation 4).

6.3.2.1 Live-collected *Glycymeris glycymeris*

Figure 6.18 shows the $\delta^{18}O_c$-derived seawater temperatures obtained by microdrilling modern *G. glycymeris* (14G2VB132, 14G2VB136, 14G2VB137), aligned with gridded SSTs for 2005–2013 CE. The shell-derived temperature peaks match the peaks of the gridded dataset well in

most years, with the exception of 2007, 2009, and 2010 CE where there is a difference of up to 0.8° C between the two series.

The reconstructed temperatures indicate a main growth season of *G. glycymeris* from May to September/October (Figure 6.18, Figure 6.20).

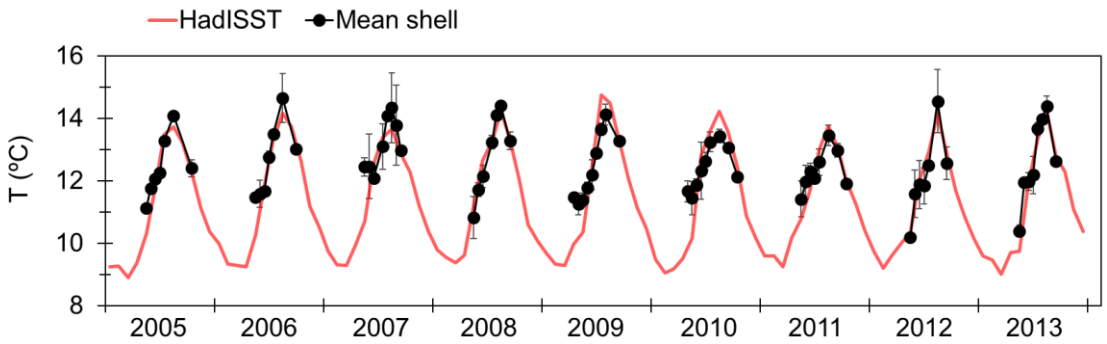

Figure 6.18: Average sub-annual temperature series derived from oxygen isotopes in three live-collected *G. glycymeris* shells (black dots), compared to monthly gridded sea surface temperature data (HadISST1, red line) for 2005–2013 CE. Error bars represent the standard deviation.

6.3.2.2 Crossmatched *Arctica islandica*

Specimen 16A2VB007 provided the highest sample resolution (see Section 6.3.1.2) and is therefore used here to determine the growth season. Figure 6.19 shows the shell-derived temperatures obtained from specimen 16A2VB007 aligned with HadISST1 reanalysis data for each respective year. Based on these results, *A. islandica* present a similar main growth season as *G. glycymeris* at St Kilda, from May to September/October. The shell-derived peak temperatures align well with the HadISST1 data in some years (1892, 1897, 1898 CE), while they fall below the HadISST1 peak in other years, in some cases with more than 1 °C difference (1891, 1893 CE; Figure 6.20).

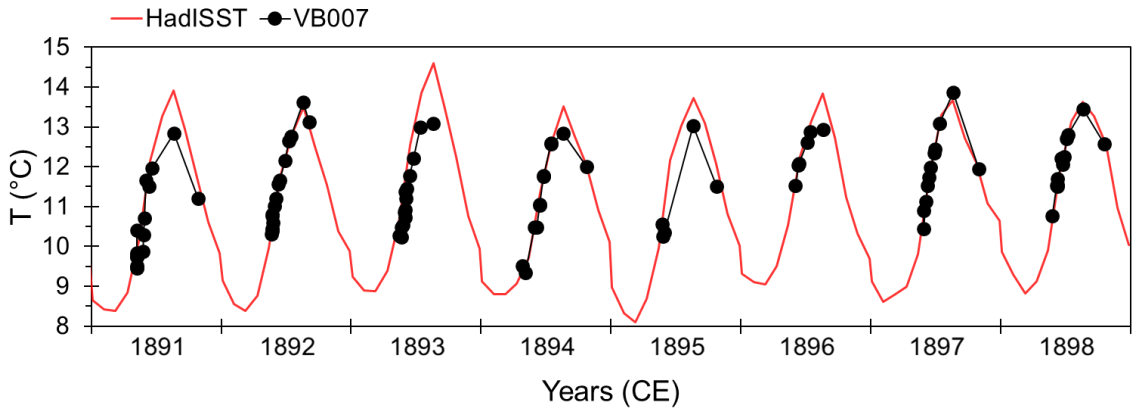

Figure 6.19: Sub-annual temperature series derived from oxygen isotopes in one *A. islandica* shell (16A2VB007, black dots), compared to monthly gridded sea surface temperature data (HadISST1, red line) for 2005–2013 CE.

6.3.3 Seasonality and average temperatures across time

Downsampling

All isotope series (fossil *G. glycymeris*, averaged modern *G. glycymeris*, averaged *A. islandica*) were resampled by fitting a 6-point cubic spline prior to any further analysis to allow for a better comparison. Figure 6.20 presents data from three calendar years (2008, 2011, 2012 CE) in the three modern *G. glycymeris* specimens, comparing results obtained by micromilling and microdrilling, and the resampled series obtained by fitting a 6-point cubic spline. These three years were chosen because they provided the best sampling resolution across all three specimens. As the figure shows, all sample techniques yielded similar results, indicating a main growth season of *G. glycymeris* at St Kilda from May to September/October, with a bias towards the late spring and summer months.

Figure 6.21 shows $\delta^{18}O_c$ data of the *A. islandica* specimen 16A2VB007 in three years (1892, 1897, 1898 CE) before and after a 6-point cubic spline has been fitted. These three years were chosen because they matched the respective HadISST1 data the best.
Whilst resampling the $\delta^{18}O_c$ series yielded similar results as the original $\delta^{18}O_c$ data, it caused a decrease in the temperature range overall (Figure 6.20, Figure 6.21).

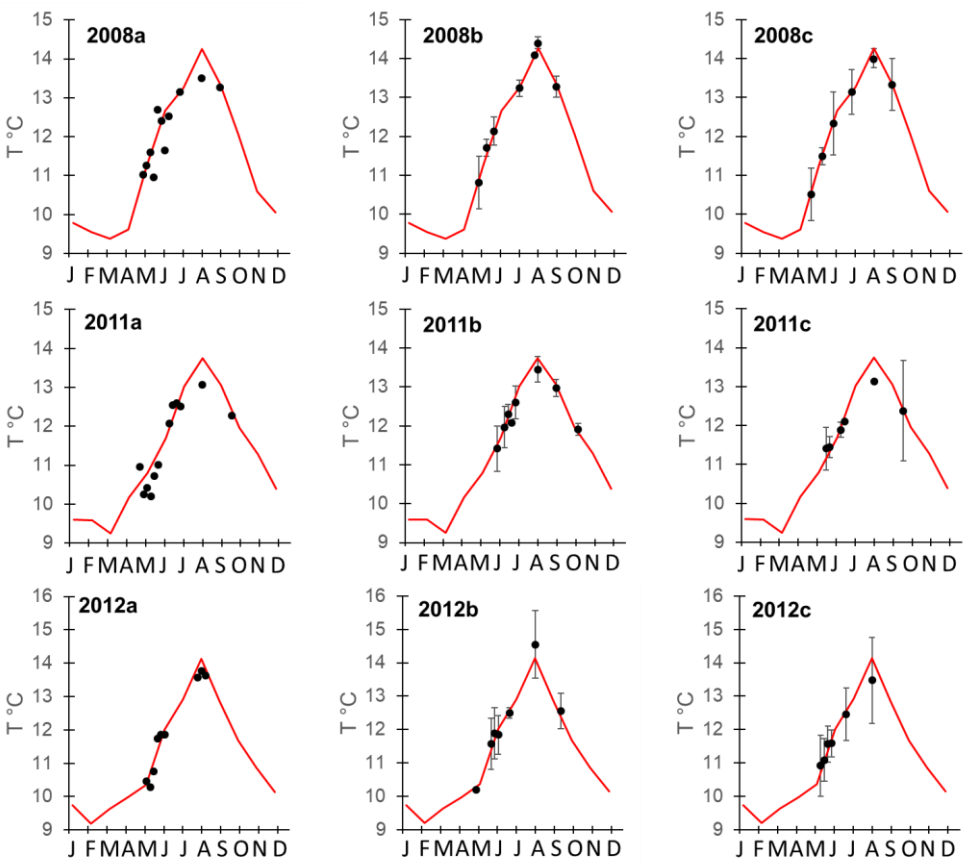

Figure 6.20: Sub-annual temperature series for 2008 CE (top row), 2011 CE (middle row), and 2012 CE (bottom row) in live-collected *G. glycymeris*. Red line: Monthly HadISST1 data. Black dots: $\delta^{18}O_c$-derived seawater temperatures. The left column (a) shows micromilled samples from one specimen (14G0VB132); the middle column (b) shows the combined series of three microdrilled specimens (same data as in Figure 6.18); the right column (c) shows the average series of the resampled microdrilled samples after a 6-point cubic spline has been fitted. Error bars indicate the standard deviation. The corresponding months are given on the x-axis for each year, starting with J = January.

Scaling factor

The scaling factor calculated from modern *G. glycymeris* and HadISST data from 2003–2013 CE was 1.55 (see Methods section 3.6.5). This means that the instrumental temperature range was 1.55 times higher than the shell-derived temperature range for the months May–October. In addition, a scaling factor of 1.62 was calculated for *A. islandica* based on reconstructed HadISST data from 1888–1898 CE to check for any discrepancies between the two species. The difference between the two scaling factors (1.62 − 1.55 = 0.7) represents 0.2 °C. Thus, both scaling factors are in good agreement with each other. However, the HadISST reanalysis data from 1888–1898 CE has to be treated with caution as it is not based on observations, in contrast to the 2003–2013 CE data. Because of this higher uncertainty in the

19th century HadISST data, and for the sake of consistency, the *G. glycymeris* scaling factor was applied to all three sample groups (fossil *Glycymeris*, *Arctica*, and modern *Glycymeris*).

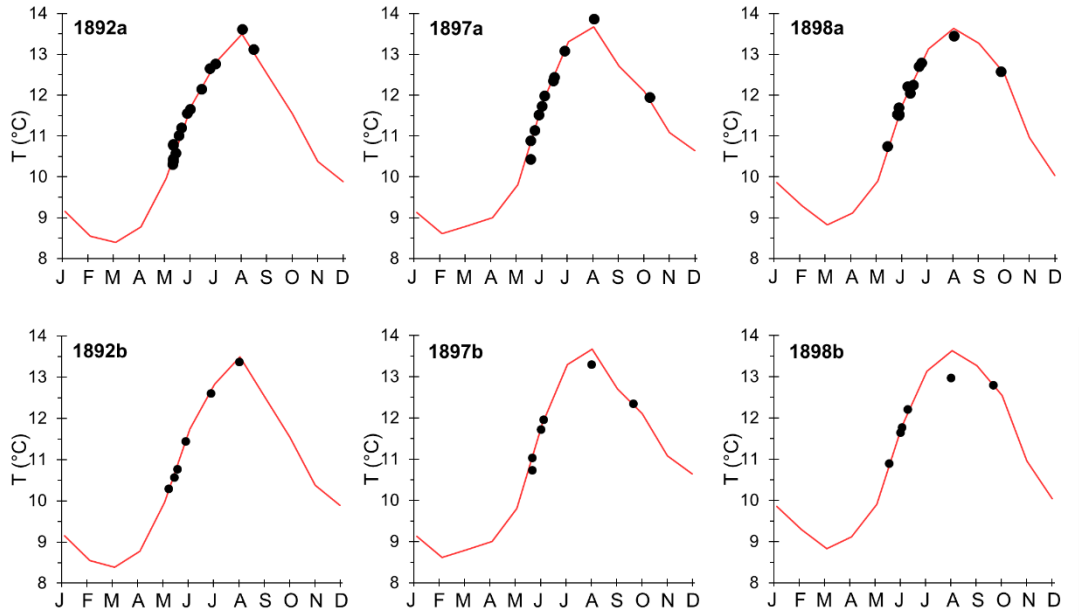

Figure 6.21: Sub-annual temperature series derived from $\delta^{18}O_c$ in one *A. islandica* shell (16A2VB007, black line), compared to monthly gridded sea surface temperature data (HadISST1) for 2005–2013 CE. Error bars represent the standard deviation. Sub-annual temperature series for 1892 CE (left), 1897 CE (middle), and 1898 CE (right). Red line: Monthly HadISST1 reanalysis data. Black dots: $\delta^{18}O_c$-derived seawater temperatures. The upper row (a) shows microdrilled samples from one specimen (16A2VB007); the bottom row (b) shows the resampled microdrilled samples after a 6-point cubic spline has been fitted. The corresponding months are given on the x-axis for each year, starting with J = January.

Seasonality

The average annual temperature range was calculated based on the resampled and detrended $\delta^{18}O_c$ series of all sample groups. Both the unscaled and the scaled seasonality (i.e. temperature range after applying a scaling factor) are presented in Table 6.2. The scaled seasonality was slightly higher in the 4th millennium BP (4.4 °C ± 1.0 °C) compared to the late 19th century (3.5 °C ± 0.7 °C) and to 2003–2013 CE (3.8 °C ± 1.0 °C; Table 6.2).

Table 6.2: Average $\Delta\delta^{18}O_c$ and spring and summer seasonality (detrended values, left), and average $\delta^{18}O$ and derived average temperatures per time period for the annual growth season (undetrended values, right). Individual series of the floating chronology are shown in the top four rows. The three bottom rows show the mean value for the floating chronology (3500–3300 yr BP avr), for *A. islandica* specimens 16A2VB007 and 16A2VB010 (1891–1898 CE), and for the combined series of the live-caught *G. glycymeris* shells (2003–2013 CE). $\Delta\delta^{18}O_c$ = Mean range in $\delta^{18}O_c$ for that time interval. T range = Temperature range calculated from $\delta^{18}O_c$. Scaled T range = Temperature range multiplied by a scaling factor of 1.55. $\delta^{18}O_{avr}$ = Average $\delta^{18}O_c$ per time period based on resampled but undetrended data. Average T = Average temperature per time period calculated from $\delta^{18}O_{avr}$. The given errors represent one standard deviation.

	Species	***Seasonality (detrended $\delta^{18}O_c$ series)***			***Averages (undetrended)***	
		$\Delta\delta^{18}O_c$ (‰)	***T range (°C)***	***Scaled T range (°C)***	***$\delta^{18}O_{avr}$ (‰)***	***Average T (°C)***
14G0VB006	*G. glycymeris*	0.59 ± 0.15	2.6 ± 0.7	4.0 ± 1.0	2.27 ± 0.13	11.2 ± 0.6
14G0VB020	*G. glycymeris*	0.56 ± 0.10	2.4 ± 0.4	3.7 ± 0.7	2.26 ± 0.08	11.3 ± 0.4
14G0VB004+021	*G. glycymeris*	0.67 ± 0.16	2.9 ± 0.7	4.5 ± 1.0	2.26 ± 0.17	11.3 ± 0.7
14G0VB023	*G. glycymeris*	0.68 ± 0.11	2.9 ± 0.5	4.6 ± 0.7	2.29 ± 0.14	11.1 ± 0.6
3500–3300 yr BP avr	*G. glycymeris*	**0.65 ± 0.14**	**2.8 ± 0.6**	**4.4 ± 1.0**	**2.27 ± 0.19**	**11.2 ± 0.8**
1891–1898 CE	*A. islandica*	**0.52 ± 0.10**	**2.3 ± 0.5**	**3.5 ± 0.7**	**2.29 ± 0.12**	**11.2 ± 0.5**
2003–2013 CE	*G. glycymeris*	**0.57 ± 0.14**	**2.5 ± 0.6**	**3.8 ± 1.0**	**2.04 ± 0.07**	**12.2 ± 0.3**

Average temperature

The average annual temperature was calculated based on the resampled $\delta^{18}O_c$ series of all sample groups (Table 6.2). The average temperature recorded in the fossil *G. glycymeris* and the *A. islandica* shells was 11.2 ± 0.8 °C and 11.2 ± 0.5 °C, respectively (Table 6.2). In contrast, the average temperature recorded in the modern *G. glycymeris* was 12.2 ± 0.3 °C.

6.4 Discussion

6.4.1 Floating *G. glycymeris* chronologies

Two floating chronologies were constructed, and later radiocarbon dated. The radiocarbon dates confirmed the sclerochronological results by consistently placing all dated crossmatched specimens in the 4th millennium BP. The conventional radiocarbon dates of the two chronologies are separated by ca. 100 years. Given that this gap approximates the lifespan of one single specimen (see Figure 6.1, Figure 6.5), it seems feasible that the two floating chronologies could be combined into a longer chronology by incorporating additional shells. However, efforts to link the two chronologies with each other have so far remained unsuccessful. As discussed in Section 5.3.3, crossmatching fossil shells is a time-consuming task, and range-finding methods are needed to preselect samples that might overlap in time and avoid spurious crossmatching. Thus, additional resources would be needed to assess the possibility of linking the two floating chronologies with each other.

6.4.1.1 The Hebrides Shelf in the fourth millennium BP

The *St Kilda Seven* chronology was constrained with a Bayesian chronological model (Figure 6.9). The *Misfits* chronology, on the other hand, could not be constrained, since the chronology consists of two shells, of which only one has been radiocarbon dated. The following discussion thus focuses on the *St Kilda Seven* chronology.

The probability distribution in Figure 6.9 presents high-density peaks at 3500–3300 cal yr BP, most likely placing the *St Kilda Seven* floating chronology in this time range. This period covers a regional climatic shift on the British Isles from dry to wet conditions, with terrestrial records of this shift grouped around ca. 3600 cal yr BP and ca. 3300 cal yr BP (see Charman, 2010, and references therein). Charman (2010) notes that the wet phase largely coincided with strong solar anomalies and a drop in SSTs south of Iceland at ca. 3600–3500 cal yr BP and 3400–3300 cal yr BP (Berner et al., 2008). Several periods of enhanced precipitation-evaporation (P-E) have been recorded for the British Isles since the mid-Holocene, which are thought to be linked with variability in solar activity and changes in the meridional overturning

circulation (Barber and Charman, 2003; Charman, 2010). However, the role of the ocean in the 3600 cal yr BP and 3300 cal yr BP events is unknown, as there is no evidence for changes in ocean circulation at that time. Charman (2010) hypothesized that the 3600 cal yr BP regional P-E shift and the observed decrease in SSTs might have been induced through atmospheric processes alone. In a study on dinocyst assemblages from the Celtic Sea, Marret et al. (2004) found an increase in oceanic species at 3600 cal yr BP, and evidence of decreased seasonality due to milder winters from 3600 cal yr BP onwards. These findings would support the hypothesis of stronger westerlies and increased Atlantic inflow on the shelf, which might also have caused wetter conditions on the British Isles (Marret et al., 2004). The 3300 cal yr BP coincides with a reconstructed negative NAO phase and records of increased storminess in Scotland (Orme et al., 2016, and references therein), which could have caused increased Atlantic inflow (see Chapter 2; Jones et al., 2018).

6.4.1.2 *Glycymeris* growth variability and spectral analysis

Due to the lack of long-lived live-collected specimens, no comparisons between *G. glycymeris* shell growth variability and physical and biological data or climate indices can be made for this location. Several studies have linked shell growth in *G. glycymeris* to SST variability (Brocas et al., 2013; Reynolds et al., 2013; Royer et al., 2013). However, this relationship is likely secondary, since shell growth can be assumed to be primarily influenced by the quality and availability of food (Reynolds et al., 2017). Food availability, in turn, is linked to water circulation and temperature. At St Kilda, the local food web will likely be affected by upwelling processes (Simpson and Tett, 1986) and the variability in Atlantic vs. shelf water dominance, as different water masses present different chlorophyll distribution patterns (Holligan, 1986) and distinct phytoplankton communities (Aiken et al., 1977).

Spectral analysis indicates significant periods of 2–6 years in both fossil chronologies (Figure 6.2, Figure 6.6), which is consistent with a relationship with the NAO (Hurrell et al., 2003). Previous studies of *A. islandica* in the North Atlantic have yielded similar spectral results in the 2-to-6-year range (Butler et al., 2013, 2010; Schöne et al., 2005; Wanamaker et al., 2009). More directly, shell growth variability in *A. islandica* (e.g., Schöne et al., 2003) and *G. glycymeris* (e.g., Brocas et al., 2013) has previously been linked to hydrographic changes related to the NAO. Changes in the NAO are linked with changes in the northeast Atlantic

circulation (e.g., Bersch, 2002) and in marine ecosystems at all trophic levels including phytoplankton and zooplankton abundance (Drinkwater et al., 2003; Fromentin and Planque, 1996; Ottersen et al., 2001). However, regional dynamics can potentially mask NAO signals in bivalve growth records (Witbaard et al., 2003).

On the Hebrides shelf, Atlantic water is more likely to be dominant during winter NAO-positive conditions, which are associated with strong westerly winds (Jones et al., 2018). Conversely, winter NAO-negative conditions are more likely to coincide with increased flow of coastal water out of the Irish Sea onto the outer shelf (Jones et al., 2018). It is therefore tempting to hypothesise that shell growth on the western Scottish shelf is linked to the NAO and its effect on water mass dominance and food availability. However, no direct comparison with instrumental data is possible for the fossil chronologies (but see Section 7.1.3 for *A. islandica* growth and the NAO), and their spectra must be interpreted with caution. While the NAO spectrum resembles a near-white noise process, it also exhibits a weakly red, i.e. Brownian, character (Gámiz-Fortis et al., 2002). Consequently, any (autocorrelated) time series with a red spectral character may present periods that are similar to that of the NAO, even where there is no direct correlation (Wunsch, 1999).

In summary, the existing link between the NAO and hydrographic variability on the western Scottish shelf suggests that there could also be a link between the NAO and shell growth. However, if such a link exists, it could potentially be masked by other (e.g., regional) signals, or it could be too weak to be "readable" in the shell chronology. Moreover, it is not known whether shell growth drivers are constant or variable through time (see Trofimova et al., 2020, for a discussion). Spectral analysis alone does not provide direct evidence for a correlation between the chronology and the NAO.

6.4.2 Modern *Arctica* chronology

The modern *Arctica* chronology is statistically robust until the 1990s, at which point the EPS drops rapidly (Figure 6.10). This interval of low EPS roughly coincides with a decrease in sample size, which can negatively affect the EPS. However, the Rbar shows a similar drop, which indicates that inter-series correlation decreased in this part of the chronology. This is also evident when assessing the individual detrended series by eye (Figure 6.10). There are

many possible reasons for the decreased synchronicity in the last three decades of the chronology. The most trivial possible explanation is reader error. Growth increments are very narrow in this portion of the shell, which makes it more difficult to correctly identify and measure growth bands. As shown in a simulation by Black et al. (2016), falsely added or missed bands can have a significant impact on the relationship between sclerochronologies and environmental time series. Even at an error rate of only 1% (i.e., 1 out of 100 bands is missed or falsely added), this error can propagate throughout the time series and blur or attenuate signals and cause the EPS to drop prematurely (Black et al., 2016). The growth lines were identified independently by two different readers (Alexander Lee and Stella Alexandroff) and discussed with Dr Paul Butler after identifying the years flagged by SHELLCORR as potentially erroneous (see Methods chapter 3.3.3). Thus, great care was taken during the construction of the time series and possible reading errors were re-evaluated. The ultimate decision on whether or not to count a growth line must be made upon visual inspection and cannot be dictated by statistical methods alone (Holmes, 1983). However, the possibility of reader error cannot be dismissed. In the same context, a possible explanation for decreased synchronicity may be (1) increased occurrence of or (2) increased misinterpretation of disturbance lines from the 1980s or 1990s onwards. Disturbance lines can be caused by natural causes, such as storms or spawning, or by anthropological influences like fishing (Richardson, 2001). Storms are frequent at St Kilda and can be assumed to be the main potential cause for disturbance lines; however, no trends in storminess (i.e. maximum gust speed) have been detected in the UK over the last five decades (Kendon et al., 2019). Disturbance lines in bivalves can be distinguished from annual lines by examining the microstructure of the increment (i.e. the shell material between lines) using an electron scanning microscope (SEM; Karney et al., 2011), or by assessing the width of daily growth lines before and after the annual or disturbance line (Schöne and Gillikin, 2013). However, in the ontogenetically oldest parts of the shell, growth increments are very narrow; consequently, daily growth lines were not visible in the metallurgical microscope used for this thesis. Indeed, other authors have previously described disturbance lines as indistinguishable from "real" annual growth lines (Butler et al., 2009a; Richardson, 2001).

Another potential explanation for the low EPS towards the end of the chronology is that inter-specimen synchronicity may vary through time due to changing environmental factors. Similarly to *G. glycymeris*, food availability and temperature, as well as light intensity, have been linked to shell growth in *A. islandica* (Ballesta-Artero et al., 2017; Schöne et al., 2005;

Witbaard et al., 2003, 1994). However, drivers of shell growth and inter-specimen covariance among bivalves are still poorly understood. In fact, disentangling the combined effect of shell growth drivers and their variability through time has recently been identified as one of 50 research priorities by sclerochronologists in a horizon-scanning survey (Trofimova et al., 2020). Marali and Schöne (2015) studied the variability of inter-species correlation among *A. islandica* specimens from Northwest Iceland and found that growth synchrony was highest during times when the Irminger Current and the East Iceland Current alternated in dominance, causing highly variable conditions. Conversely, inter-species correlation dropped significantly when only one of the major currents dominated over a long time interval, resulting in a less variable environment. However, no analogous scenario can be constructed for the western Scottish shelf, as it has remained highly variable over the last four decades, with alternating dominance of Atlantic and shelf waters (Jones et al., 2018). Thus, while we cannot exclude that the drop in EPS observed in the 1990s are caused by environmental factors, there is no evidence supporting this hypothesis.

Spectral analysis

Spectral analysis of the *Arctica* chronology (Figure 6.13) yielded similar results to the fossil *Glycymeris* chronologies. Significant periods are mainly found in the range of 2 to 8 years. This high-frequency signal is however lost towards the end of the chronology, which may be linked to the lower EPS and indicate that there is a reader error in this part of the chronology, as discussed above (see also Black et al., 2016). In addition to the 2-to-8-year frequency, quasi-decadal periods are present in the middle and towards the end of the chronology.

As mentioned in Section 6.4.1.2, spectral analysis should be interpreted with caution (Wunsch, 1999). While the spectral character of the modern chronology resembles that of the NAO, only direct comparison of the two records can determine whether they are indeed correlated. Comparisons between the chronology and the NAO as well as other instrumental records are presented in Chapter 7.

6.4.3 Seasonal oxygen isotopes

Parts of the following discussion have been published in Alexandroff et al. (2021).

6.4.3.1 Growth season and calibration of modern samples

The results presented in Section 6.3.2 suggest that *G. glycymeris* and *A. islandica* mainly grow their shells from late spring to early or mid-autumn at St Kilda, with greatest growth from May to July/August (Figure 6.20, Figure 6.21). The onset of growth in May coincides with the annual onset of coccolithophore blooms on the outer shelf (Holligan, 1986). Similar growth seasons have been reported for both species in nearby habitats, e.g., for *G. glycymeris* in the Tiree Passage (Reynolds et al., 2017) and for *A. islandica* on the Faroe Shelf (Bonitz et al., 2017).

Shell growth in *G. glycymeris* (Reynolds et al., 2017) and *A. islandica* (Schöne, 2013) is likely nonlinear. Because of this bias towards certain periods within the growth season, weighted means should be used when reporting average seasonal temperatures (Schöne, 2013). However, due to low sampling resolution as well as insufficient resolution of temperature data, a 6-point cubic spline model was applied instead to ensure that the data bias in the modern shells and the fossil shells are comparable (Wanamaker et al., 2011).

Microdrilling was the preferred method in this study, as it allows for more control than micromilling, and ensures that the samples are all taken from the same portion of the outer shell layer (see Section 3.6). Figure 6.20 shows that the two different sampling techniques yielded similar results. While micromilling provided a higher resolution, it did not always capture the temperature peak. This might be due to time-averaging effects or contamination from the iOSL (inner outer shell layer, see Figure 3.9). Microdrilling was a time-efficient technique that was used to obtain replicated data across three specimens, for which the averaged (Figure 6.18, Figure 6.20b) and modelled (Figure 6.20c) series in *G. glycymeris* matched the instrumental temperature peaks in most years. In the case of *A. islandica*, the shell-derived temperature peaks are lower than the HadISST temperature peaks in five out of eight years (Figure 6.19). There are several potential explanations for this discrepancy: (1) the seawater temperatures recorded by *A. islandica* were indeed lower than SSTs at this location; (2) the HadISST reanalysis data are inaccurate; or (3) the sampling resolution was too low and attenuated the signal (i.e., time-averaging). Out of these three potential reasons, the latter two should receive

the most attention. Since the *A. islandica* specimen was collected at 26 m depth in a highly dynamic environment, it can be assumed that it represents surface water conditions. Moreover, the modern *G. glycymeris* temperature series matched the HadISST temperature peaks, even though they were collected below 45 m further out in the same bay. It should also be noted that there is no constant offset between the *A. islandica* temperature series and the HadISST series — in fact, in three different years, the two series match each other (Figure 6.19). However, gridded data pre-1950 should be treated with caution, since they have only few observational data incorporated, which decreases the overall quality of the dataset (Hughes et al., 2009). Lastly, time-averaging effects introduced during sampling are likely to be at least in part responsible for the low temperature peaks in the *A. islandica* series. While sampling resolution was higher than in the *G. glycymeris* series, the *A. islandica* series presented in Figures 6.19 and 6.21 are based on only one specimen. Due to the nonlinear shell growth within one growth season, with the highest growth rates during late spring and early summer, there is a relatively high risk of "missing" the temperature peak and thus attenuating the signal.

In summary, the results presented in Section 6.3.3 clearly confirm that $\delta^{18}O_c$ from *G. glycymeris* and *A. islandica* at St Kilda is a faithful palaeothermometer for seawater temperatures on the Hebrides shelf. The full annual temperature range recorded in the shells might, however, be partially masked in the obtained data due to sampling resolution. Replication of data across several specimens can improve the accuracy of the reconstructed seasonality.

6.4.3.2 Seasonality in the fossil shell record

Because the growth season of *G. glycymeris* does not include winter months, the results in Section 6.3.3 do not represent full seasonality. However, the data give an indication of whether the temperature range within the growth season has changed between ca. 3500–3300 cal yr BP and today. As shown in Table 6.2, the seasonal temperature range in the fossil shells were similar to the modern range. Hence, there is no evidence of differences in spring-to-summer seasonality on the Hebrides shelf between the fossil and the modern record.

When investigating past seasonal shelf sea temperatures, possible changes in stratification must be considered. In stratified water, the warm surface layer is separated from the cold bottom

layer by the thermocline during the summer. Consequently, the difference between summer SSTs and sea bottom temperatures is higher in stratified water than in vertically mixed water, and summer bottom waters are colder in stratified than in mixed sectors (Elliott et al., 1991). It is therefore essential to know (1) whether the shelf-sea fronts (i.e. fronts between mixed and seasonally stratified waters) have moved position and (2) which depths the fossil material represents. Numerical tidal models and proxy studies have shown that stratification on the NW European shelf started at 10,000–8000 yr BP and progressed over the following millennia until 6000–5000 yr BP (Scourse et al., 2002; Uehara et al., 2006; Ward et al., 2016). The reconstructed temperatures from St Kilda do not indicate that any major change has taken place between the mid-fourth millennium BP and today, which is consistent with data from the Celtic Sea (Austin and Scourse, 1997; Marret et al., 2004; Scourse et al., 2002). Stratification and the evolution of shelf-sea fronts is of high interest as they exert a major influence on primary productivity. Conditions are favourable for productivity along shelf-sea fronts, where nutrient renewal occurs due to mixing by wind and tide (Pingree et al., 1978). This may in turn affect the growth width chronology, since shell growth is tightly linked to food availability and quality. Due to the local topography at St Kilda (Chapter 2), it can be assumed that the fossil shells lived at similar depths as the live-caught specimens, representing a shallow tidally mixed habitat. Due to the shallow sampling depths, tidal mixing, and the local upwelling system at St Kilda (Simpson and Tett, 1986), it is likely that both the fossil and modern material represent mixed water conditions and are hence more tightly coupled to SSTs and surface air temperature than would be the case if they represented stratified conditions.

As shown in Chapter 5, Raman spectroscopy determined that there were no diagenetic alterations in the fossil shells. Thus, the palaeothermometry equation for aragonitic shells applies to the fossil specimens as well.

6.4.3.3 Average temperatures in the fossil shell record compared to modern temperatures

Previous studies using summer SST proxies have found evidence of a pronounced cold interval south of Iceland at 4000–2000 cal yr BP, while records of this cooling are absent in the Norwegian Sea (e.g., Berner et al., 2008; Orme et al., 2018, and references therein; Van Nieuwenhove et al., 2018). Orme et al. (2018) hypothesize that the colder SSTs might have

been caused either by enhanced Arctic outflow or enhanced ice melt from East Greenland, both associated with negative NAO circulation. A weakening of the NAC linked to the low NAO could provide another explanation for the cooling, although this hypothesis is not supported by much evidence (Orme et al., 2018). The reconstructed late spring and summer SSTs for the Hebrides Shelf at ca. 3500–3300 cal yr BP were 1 °C lower than today (Table 6.2). However, the data presented in this thesis are not evidence of a distinct cooling event or interval. A major limitation of the data is the relatively short time interval covered by the fossil isotope record, which does not provide the context of the preceding warmer periods in the mid-Holocene. The temporal context is important though, as a warming of ca. 1 °C in annual SSTs has occurred in UK waters over the last 100 years (Hughes et al., 2017; see HadISST reanalysis data by Rayner et al., 2003). This recent warming is also reflected in the $\delta^{18}O_c$ data presented in Table 6.2, since reconstructed temperatures in the *A. islandica* shells (1891–1898 CE) were 1° C lower than today. Thus, the reconstructed temperatures for ca. 3500–3300 cal yr BP are similar to regional spring and summer SSTs in the early 20th century CE.

Chapter 7

The modern *Arctica* chronology in context: environmental records, spatial correlations, and Soay sheep

Chapter 7 — The modern *Arctica* chronology in context: environmental records, spatial correlations, and Soay sheep

The previous chapter introduced the *Arctica islandica* chronology and described its characteristics (Section 6.2). In this chapter, the same chronology will be further analysed through comparisons with climate indices, instrumental data, and proxy data. In addition, an annually resolved $\delta^{18}O_c$ series based on the chronology is presented and compared to the growth chronology.

7.1 Correlations with the *Arctica* growth chronology

7.1.1 Plankton data

There is a significant positive correlation between the *Arctica* chronology and the regional May-to-September phytocolour index (1958–2015; $p = 0.007$, $r = 0.35$). Figure 7.1 shows the two series in comparison. The positive correlation between the two series breaks down intermittently and turns negative, most notably in the early 1970s and early 2000s (Figure 7.2a–c).

No significant correlations were found between the growth chronology and any of the taxonomic phyto- and zooplankton groups (e.g., diatoms, copepods, etc.; see Methods section 3.3.5.2).

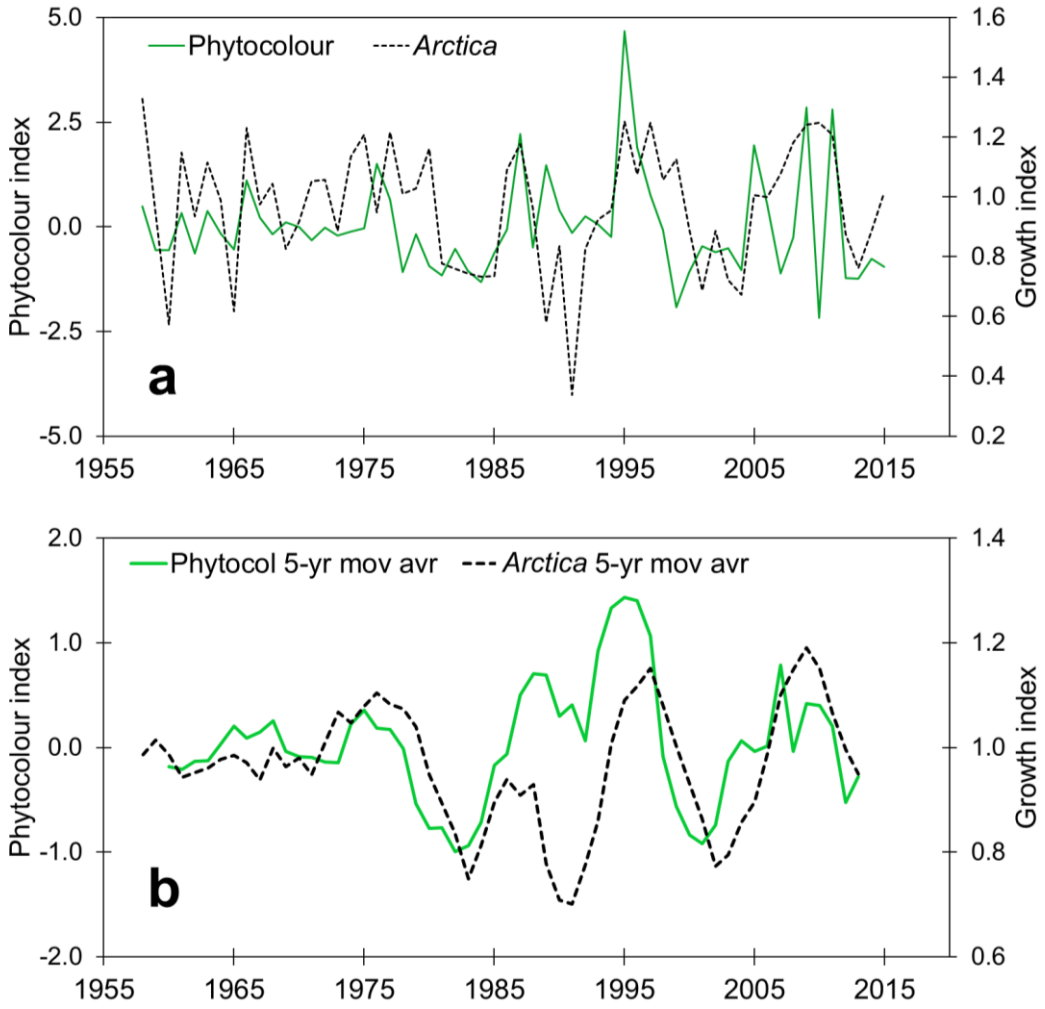

Figure 7.1: Comparison of the (a) annual records and (b) 5-year moving averages of *A. islandica* growth (dashed black line) and the regional phytocolour index (green line).

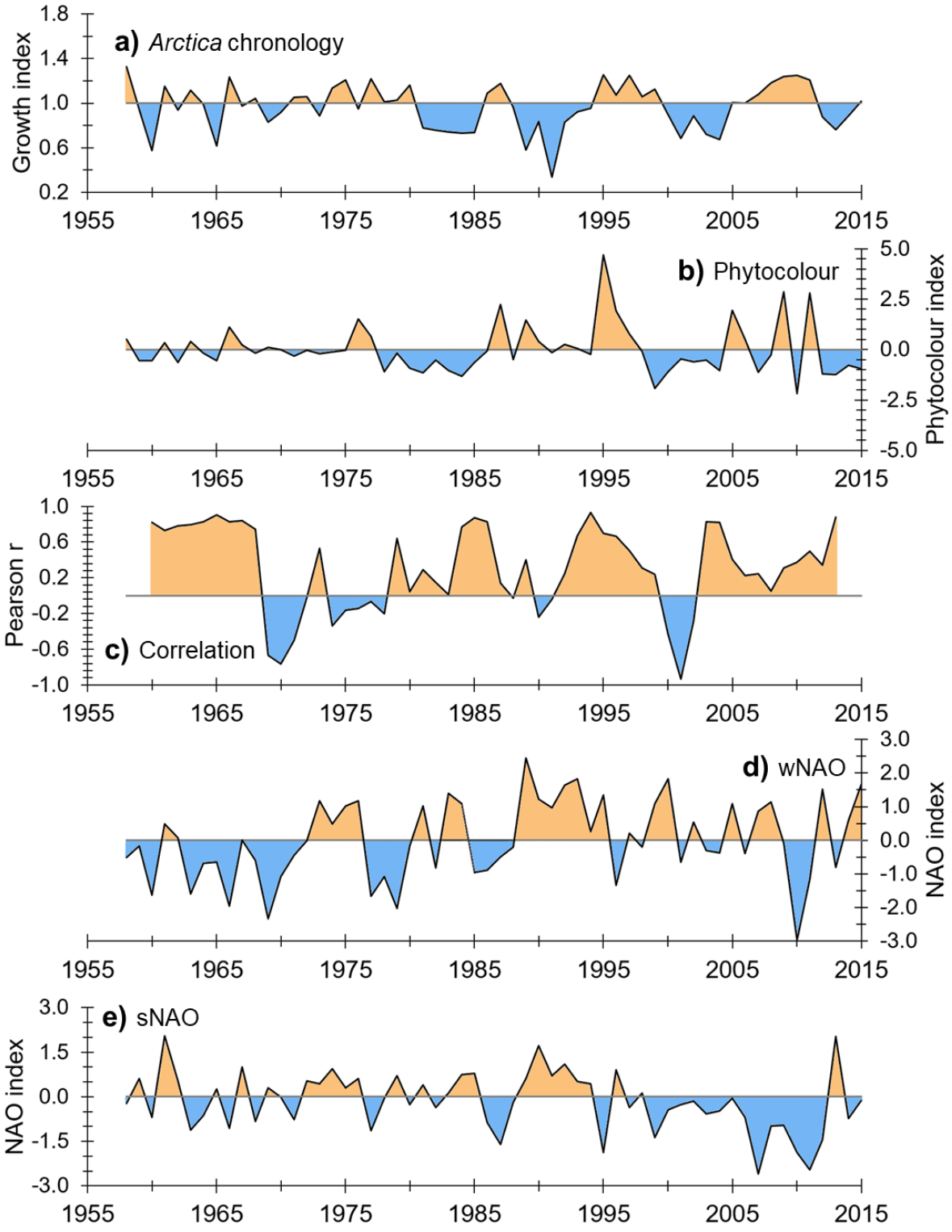

Figure 7.2: Comparison of the (a) *Arctica* chronology and (b) phytocolour index, with their (c) 5-year running correlation. Given are also the (d) winter NAO and (e) summer NAO index for additional information.

7.1.2 Sea surface temperatures

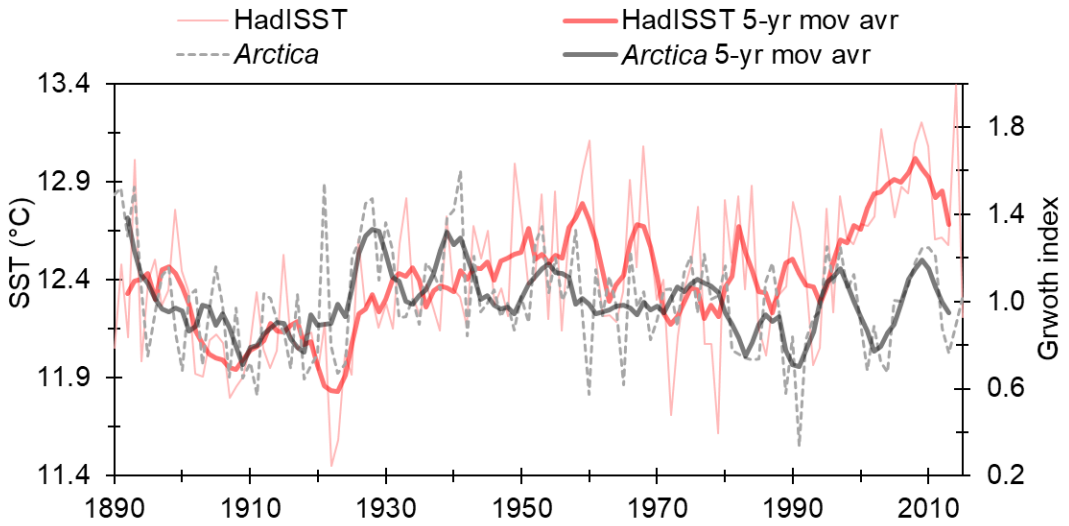

Figure 7.3: Comparison of the *Arctica* chronology (grey) and HadISST data (red) from May to September. Given are the annual series (thin lines) and their 5-year moving averages (thick lines).

The intermittent nature of *in-situ* temperature data on the outer western Scottish shelf prevents meaningful comparison with the *Arctica* growth chronology (see Section 4.1). Therefore, the growth chronology was compared to regional HadISST data (Lat: 57–58° N, Long: 8–9° W) instead. Figure 7.3 shows the May-to-September HadISST data in comparison with the *Arctica* chronology. Both series display a similar low-frequency trend between 1890 and 1940; however, there is no apparent covariance from the second half of the 20th century onwards. Pearson cross-correlation did not produce any significant results apart from a weak positive correlation of r = 0.20 with the HadISST series lagging the *Arctica* chronology by three years (Table 7.1).

Table 7.1: Pearson cross-correlation between the *Arctica* chronology and the HadISST1 product for 1890–2015 CE. The r and p values are given for the growth season (May to September), spring (Mar–May), and summer (Jun–Aug). A positive lag means that HadISST is leading, a negative lag means the chronology is leading. Significant results are in bold.

	HadISST					
	May–Sep		***Spring***		***Summer***	
Lag	**r**	**p**	**r**	**p**	**r**	**p**
-3	**0.20**	**0.03**	0.16	0.08	0.17	0.06
-2	0.16	0.08	-0.08	0.40	0.03	0.72
-1	-0.02	0.81	0.06	0.47	0.09	0.30
0	0.08	0.35	0.00	0.99	-0.03	0.74
1	-0.02	0.86	-0.06	0.54	-0.05	0.56
2	0.05	0.57	-0.02	0.81	-0.04	0.69
3	0.01	0.94	0.02	0.84	0.01	0.93

7.1.3 Atlantic Multidecadal Oscillation (AMO) and North Atlantic Oscillation (NAO)

The *Arctica* chronology was compared to the two climate indices AMO and NAO (Table 7.2).

Table 7.2: Pearson cross-correlation between the *Arctica* chronology and the PC-based NAO index from 1899–2015. R-values and p-values are given for the annual NAO, winter NAO (Dec–Feb), spring NAO (March–May), summer NAO (June–August, and the autumn NAO (Sep–Nov). A positive lag means that the index is leading, a negative lag means the chronology is leading. Significant results are in bold.

	AMO						***NAO***					
	Winter		***Summer***		***Annual***		***Winter***		***Summer***		***Annual***	
Lag	**r**	**p**	**r**	**p**	**r**	**p**	**r**	**p**	**r**	**p**	**r**	**p**
-3	**0.26**	**0.004**	**0.30**	**0.001**	**0.35**	**<0.001**	-0.07	0.47	-0.09	0.36	-0.18	0.05
-2	**0.22**	**0.02**	**0.25**	**0.005**	**0.27**	**0.002**	**-0.21**	**0.02**	-0.05	0.64	-0.17	0.07
-1	**0.22**	**0.02**	**0.20**	**0.02**	**0.24**	**0.007**	-0.14	0.13	-0.07	0.47	-0.16	0.09
0	0.16	0.07	0.12	0.17	**0.18**	**0.04**	**-0.18**	**0.05**	0.03	0.73	-0.14	0.13
1	**0.28**	**0.002**	0.15	0.11	**0.19**	**0.03**	-0.15	0.11	0.04	0.67	-0.03	0.77
2	**0.26**	**0.003**	0.08	0.36	**0.19**	**0.04**	-0.04	0.67	0.13	0.16	0.00	0.97
3	**0.31**	**0.001**	0.12	0.19	**0.24**	**0.008**	0.07	0.46	**0.21**	**0.03**	0.10	0.27
	AMO 5-yr moving average						**NAO 5-yr moving average**					
	Winter		***Summer***		***Annual***		***Winter***		***Summer***		***Annual***	
Lag	**r**	**p**	**r**	**p**	**r**	**p**	**r**	**p**	**r**	**p**	**r**	**p**
0	**0.50**	**<0.001**	**0.41**	**<0.001**	**0.47**	**<0.001**	**-0.35**	**<0.001**	-0.02	0.795	**-0.38**	**<0.001**

Significant positive correlations were found between the chronology and the winter, summer, and annual AMO index with various leads and lags (Table 7.2). Figure 7.4 illustrates a clear covariance between the AMO index and the *Arctica* chronology for the first half of the record, whereas this covariance is less evident in the second half. Between 1960 and 1980, the *Arctica* chronology shows less pronounced variability with smaller amplitudes, and from ca. 1980 onwards a decadal variability is dominant. On a bidecadal scale, the covariance between the AMO index and the *A. islandica* chronology seems to persist throughout the length of the chronology, with the AMO index leading by several years from the 1960s onwards (Figure 7.5).

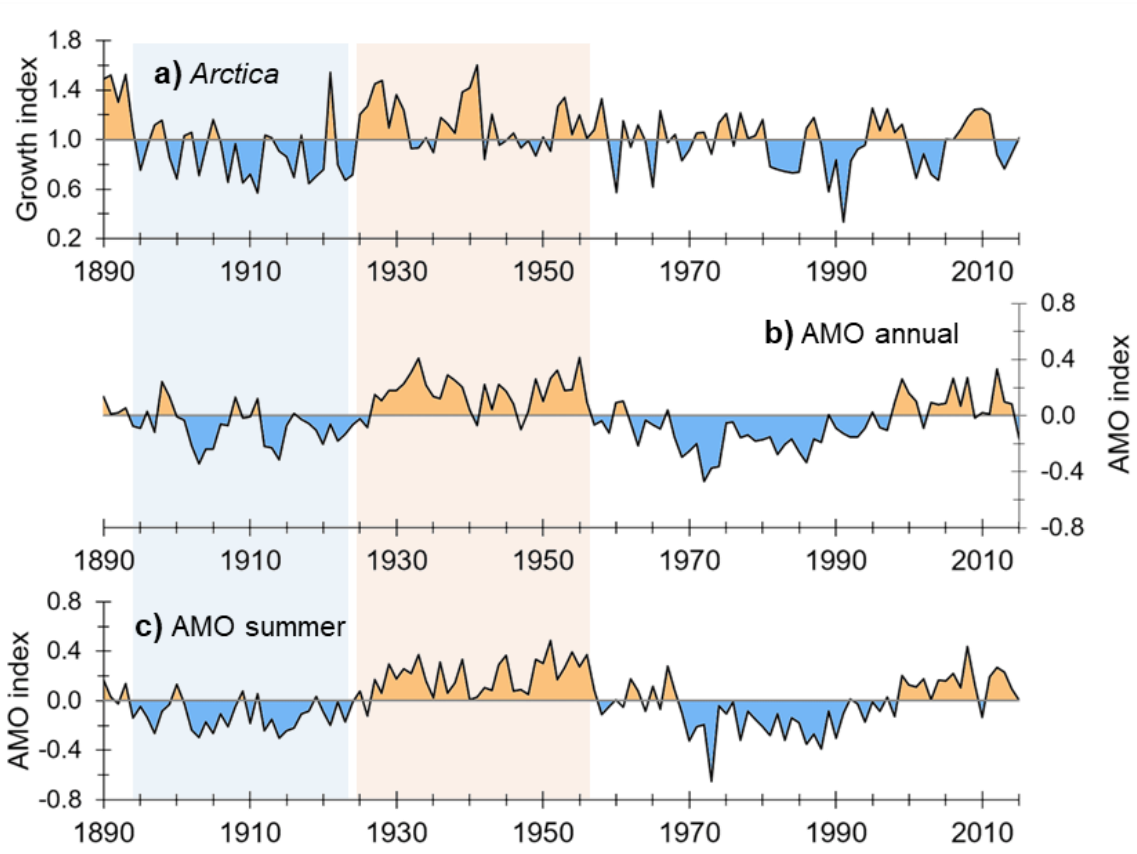

Figure 7.4: Comparison of the (a) *Arctica* chronology, (b) the annual AMO and (c) the summer AMO index. Lower-than-average values are coloured blue, higher-than-average values are coloured orange. The blue-shaded column indicates an interval where values were lower-than-average across all three series, the orange-shaded column indicates an interval where values were higher-than-average across all three series.

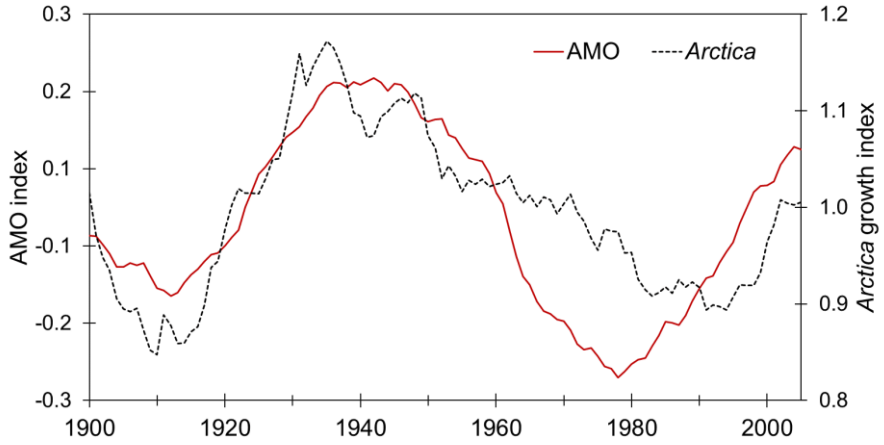

Figure 7.5: 21-year moving average of the AMO index (red solid line) and the *A. islandica* growth chronology (black dashed line)

A weak negative correlation is found between the *Arctica* growth chronology and the winter NAO index (wNAO) between 1899–2015, with the chronology leading by two years. Conversely, there is a positive correlation between the chronology and the summer NAO (sNAO) index, with the sNAO leading three years (Table 7.2). A highly significant negative correlation between the wNAO and the chronology is found when applying a five-point moving average filter ($r = -35$; $p < 0.001$; Table 7.2; Figure 7.6).

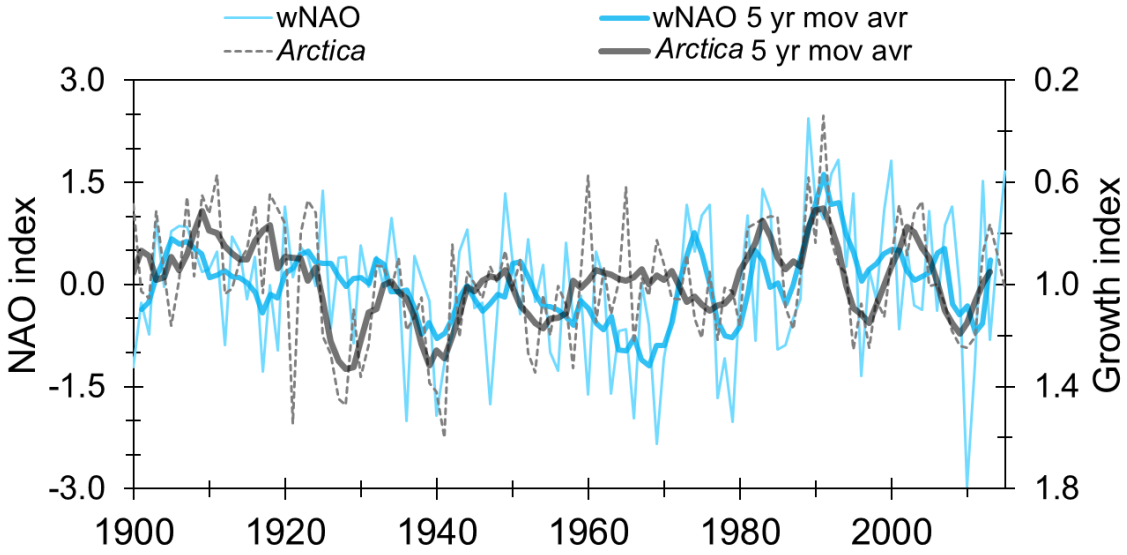

Figure 7.6: Comparison of the *Arctica* chronology (grey) and the winter NAO index (blue). Given are the annual series (thin lines) and their 5-year moving averages (thick lines). The y-values of the *Arctica* chronology have been inverted.

The summer HadISST series and climate indices (NAO, AMO) shown above are also presented in Figure 7.7 and Figure 7.8 along with the *Arctica* chronology for direct comparison.

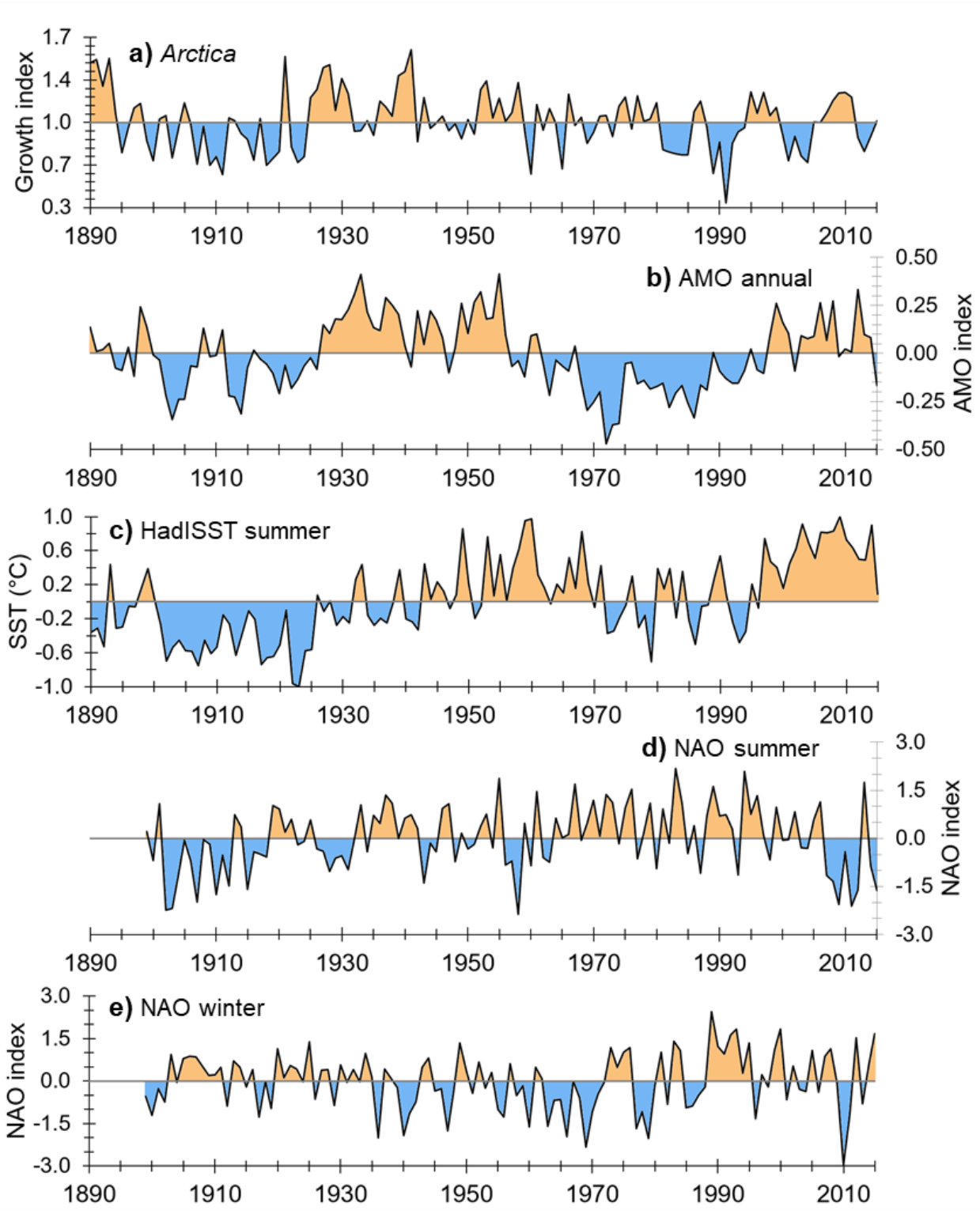

Figure 7.7: Annual records of (a) the *Arctica* chronology, (b) the annual AMO index, (c) summer SSTs (HadISST), (d) the PC-based summer NAO index, (e) the PC-based winter NAO index.

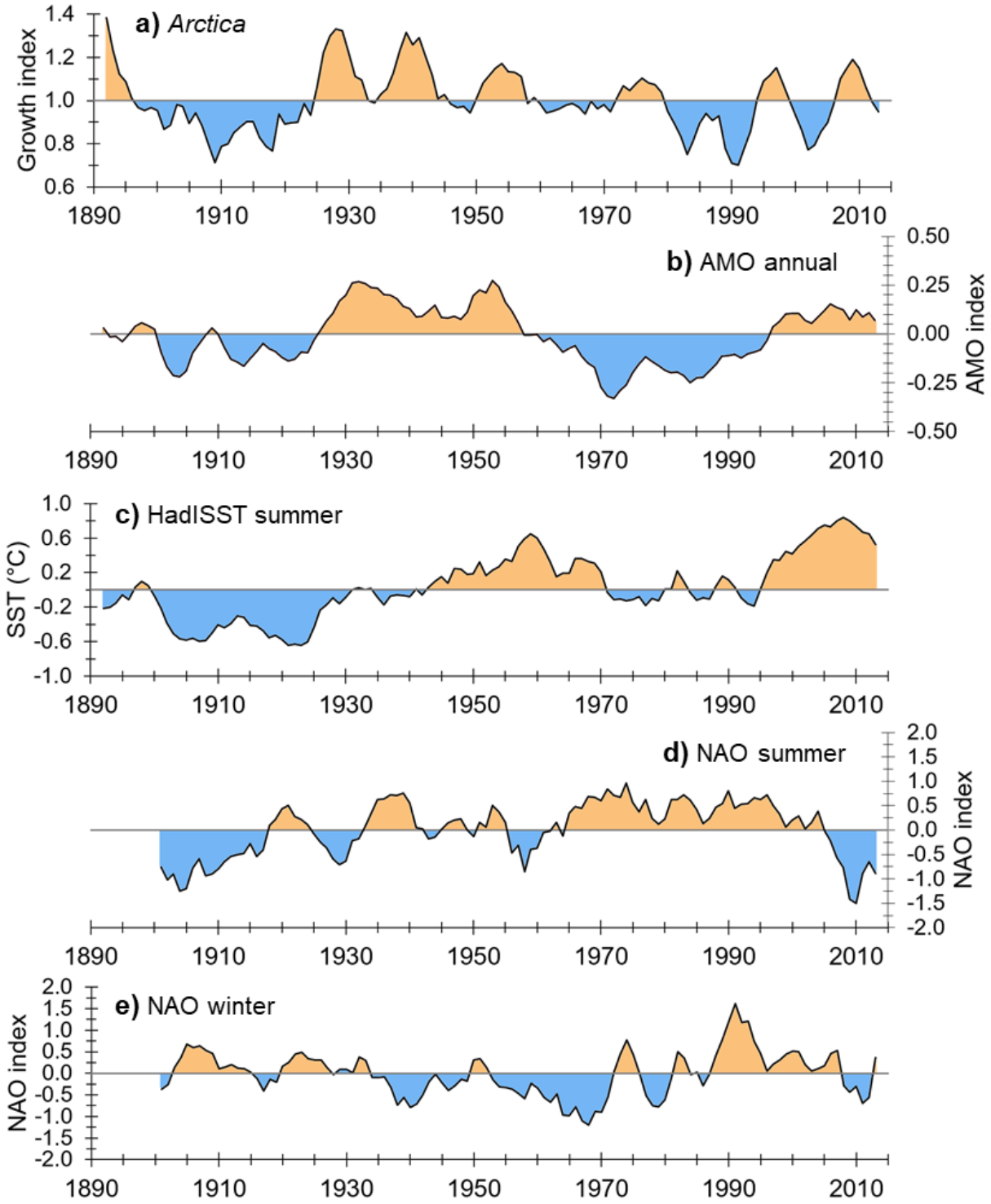

Figure 7.8: A five-point moving average filter has been applied to the series shown in Figure 7.7. (a) Arctica chronology, (b) annual AMO index, (c) summer SSTs (HadISST), (d) PC-based summer NAO index, (e) PC-based winter NAO index.

7.1.4 Spatial correlations

Sea surface temperatures

The *Arctica* growth chronology correlates positively with May-to-September SSTs in the subpolar gyre (SPG) region and along the east Atlantic coast over the last three decades (Figure 7.9). Conversely, negative correlations are found in the subtropical gyre (SPT) region (Figure 7.9a–d). When the entire length of the chronology (1890–2015) is compared to ERSST reanalysis data, only the positive correlation with SPG SSTs persists (Figure 7.9h).

Sea level pressure and zonal wind

Significant correlations were found between the *Arctica* chronology and atmospheric patterns. Figure 7.10a shows a negative correlation between the chronology and zonal wind pressure at 200 mbar in winter at a latitude of ca. 50–60° N, and a positive correlation at a latitude of ca. 25–40° N. These correlations were found for the winter of the year preceding the year of increment formation (e.g., Jan–Feb 2013 correlated with *A. islandica* growth season 2014; Figure 7.10a), and for the winter immediately following increment formation (e.g., Dec–Jan 2014/2015 correlated with *A. islandica* growth season 2014; not shown here). The *Arctica* chronology also correlates with winter sea level pressure over a large area in the North Atlantic region in a dipole pattern (Figure 7.10b).

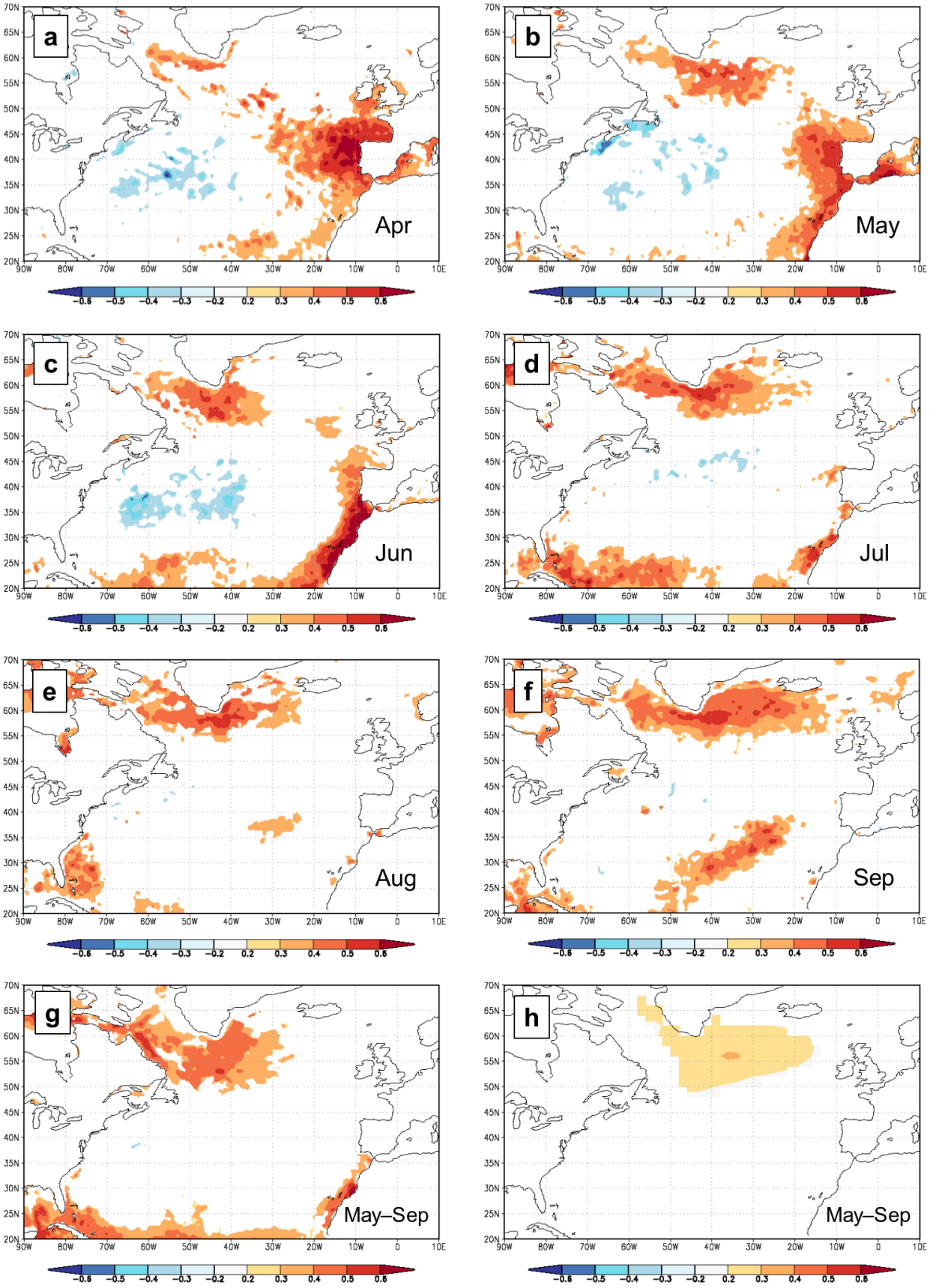

Figure 7.9: Spatial correlations between the *Arctica* growth chronology and monthly NCEP OIv2 1/4 sea surface temperatures 1981–2015 in (a) April, (b), May, (c) June, (d) July, (e) August, (f) September, and (g) averaged over the growth season May–September. (h) Spatial correlations between the *Arctica* growth chronology and ERSST v5 sea surface temperatures in May–September 1890–2015. Correlation coefficients are indicated by colour and defined in the legend below each figure. $p < 0.1$. Calculated with KNMI Climate Explorer (Trouet and Van Oldenborgh, 2013).

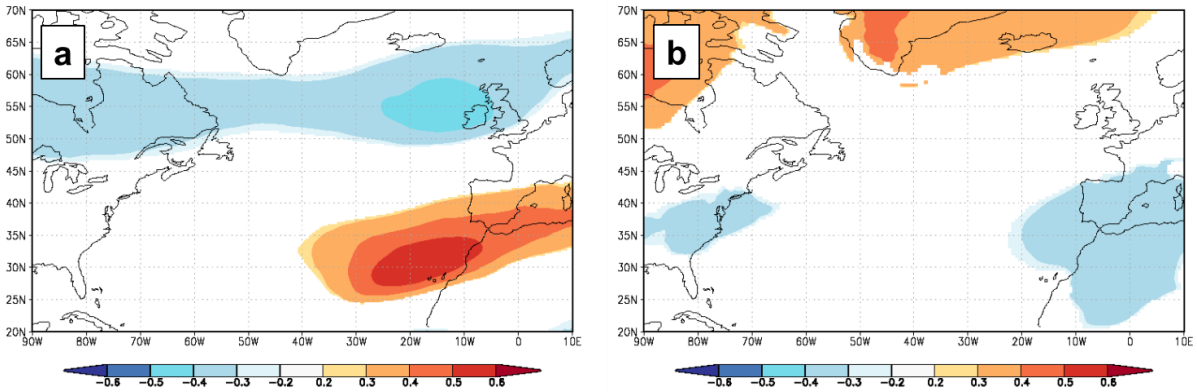

Figure 7.10: Spatial correlations between the *Arctica* growth chronology and (a) ERA5 zonal wind stress at 200 mbar from 1979 to 2015 in winter (Jan–Feb) of the previous year and (b) and MERRA sea level pressure from 1980 to 2015 in (a) the previous winter (Dec–Feb). Correlation coefficients are indicated by colour and defined in the legend below each figure. $p < 0.1$. Calculated with KNMI Climate Explorer (Trouet and Van Oldenborgh, 2013).

7.1.5 Soay sheep at St Kilda

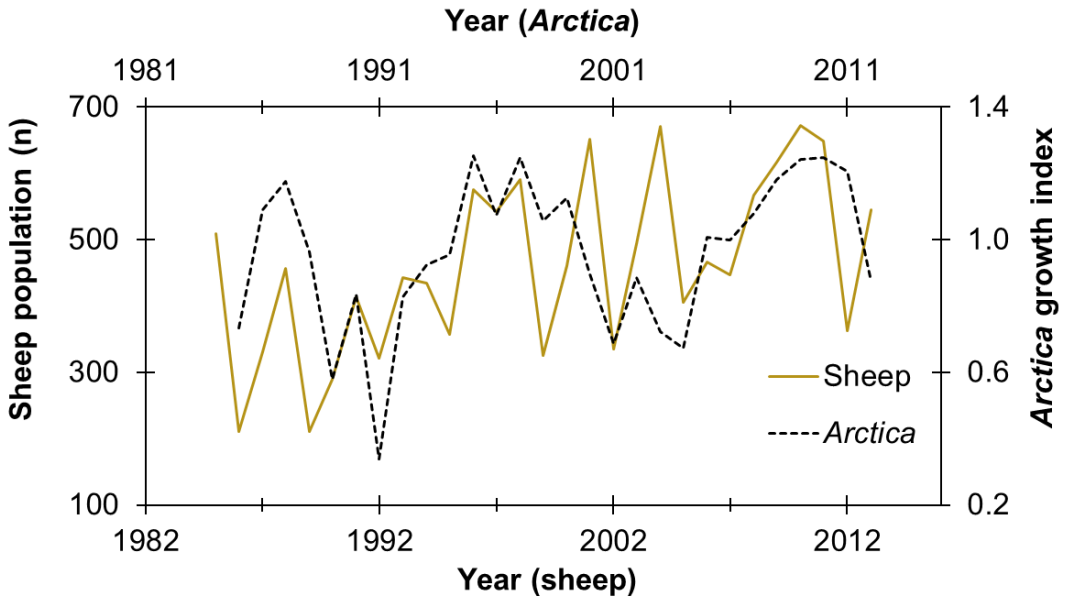

Figure 7.11: *Arctica* growth index (dashed black line) compared to the population size of Soay sheep on Hirta (solid brown line), St Kilda. Please note the different x-axes for the two series (top and bottom). The *Arctica* growth record is leading by one year (top x-axis); e.g., year 2011 in the *Arctica* chronology correlates with year 2012 in the sheep population.

The growth chronology was compared to population size data of the feral Soay sheep on Hirta, St Kilda (Figure 7.11). The two records correlate positively with each other (r = 0.46, p = 0.01) at a lag of −1 year (*Arctica* leading).

7.2 *Arctica* annual oxygen isotope series

An annually resolved $\delta^{18}O_c$ series was constructed by averaging the replicated $\delta^{18}O_c$ in two *A. islandica* shells. Several samples were lost during the technical analysis due to electrostatic issues. The resulting series spans 1887–2012 CE with ten individual years missing in different places (Figure 7.12).

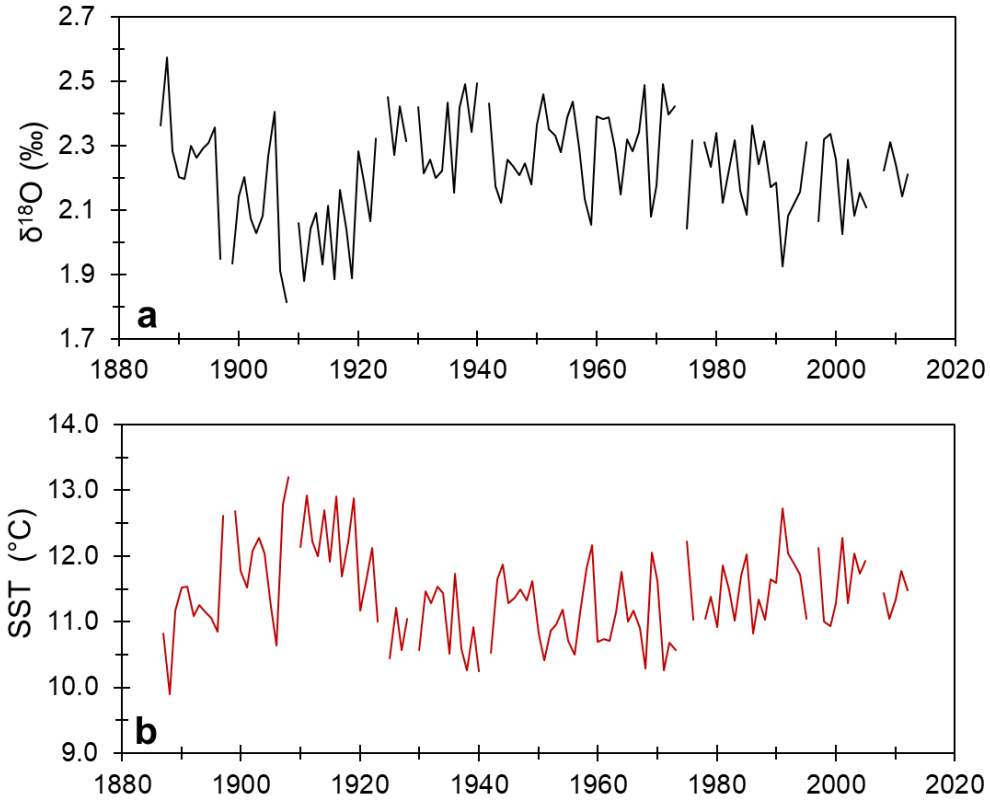

Figure 7.12: (a) Annual $\delta^{18}O_c$ values obtained from two *A. islandica* shells. (b) Annual $\delta^{18}O_c$-derived *in-situ* SSTs.

The first ca. 30 years of the $\delta^{18}O_c$ series are characterized by a rapid decrease and subsequent rapid increase in $\delta^{18}O_c$ values (Figure 7.12a), similarly to the growth chronology (Figure 6.10). The $\delta^{18}O_c$ series is in fact positively correlated with the growth chronology throughout the

length of the chronology ($p < 0.001$, $r = 0.43$). Figure 7.13 shows the $\delta^{18}O_c$-derived *in-situ* temperatures compared to the growth chronology after a 5-yr moving average filter has been applied.

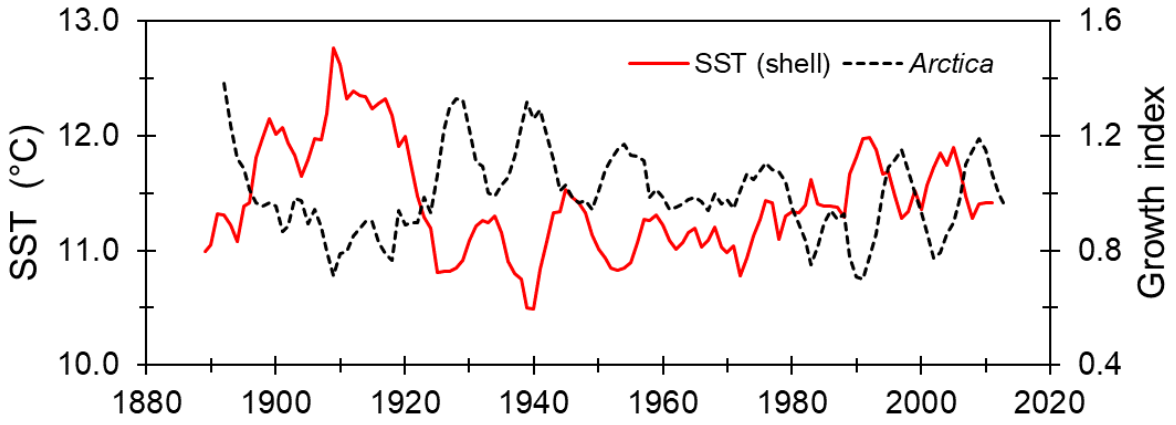

Figure 7.13: $\delta^{18}O_c$-derived SSTs (red solid line) and *Arctica* growth chronology (black dashed line). A 5-point moving average filter has been applied to both series.

The *in-situ* temperatures calculated from $\delta^{18}O_c$ data correlate with regional spring SSTs, with the strongest correlation in May (Table 7.3). There is no significant correlation between the $\delta^{18}O_c$ series and the phytocolour index ($p = 0.34$; $r = -0.14$). Spatial correlation analysis shows a positive correlation between the $\delta^{18}O_c$-derived *in-situ* temperatures and regional sea surface salinity (SSS) and SSTs on the Scottish shelf and upstream towards the North Sea and the Norwegian Sea (Figure 7.14).

Table 7.3: Pearson cross-correlation between the annual $\delta^{18}O_c$-derived *in-situ* temperatures and the regional HadISST data (Lat: 57.00–58.00° N, Long: 08.00–09.00° W) by month for the time interval 1890–2012 CE.

	r	***p***
March	**0.22**	**0.02**
April	**0.26**	**0.01**
May	**0.27**	**0.004**
June	0.17	0.08
July	0.04	0.70
August	0.00	0.93
September	-0.05	0.58

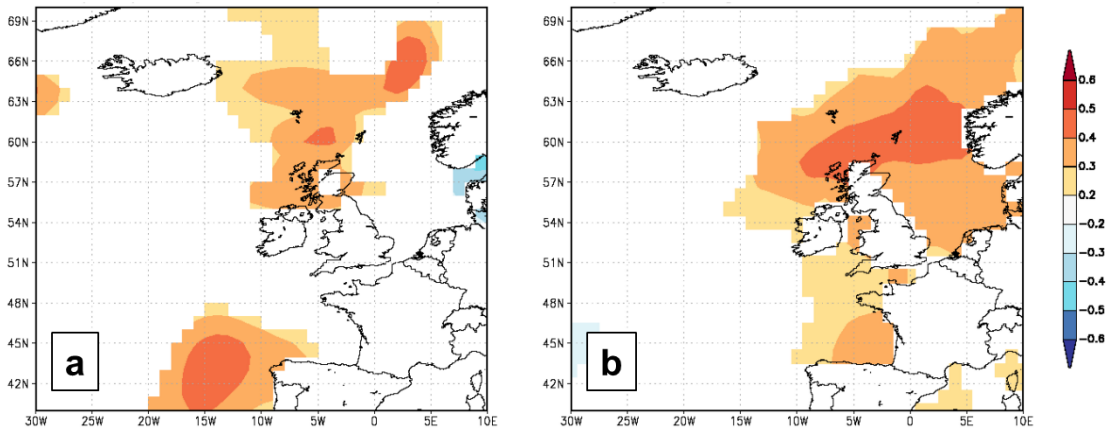

Figure 7.14: Spatial correlations between the $\delta^{18}O_c$-derived *in-situ* SSTs at St Kilda and (a) EN4.2.1 SSS and (b) HadISST1 SSTs from April to September, calculated over the time interval 1950–2012. Correlation coefficients are indicated by colour and defined in the legend to the right. $p < 0.1$. Calculated with KNMI Climate Explorer (Trouet and Van Oldenborgh, 2013).

7.3 Discussion

7.3.1 *Arctica* growth, temperature, and primary production

Shell growth variability is most commonly attributed to food availability and quality. Previous studies have linked *Arctica* shell growth to food supply (1) directly, through positive correlation with primary production (e.g., Bonitz et al., 2017), or (2) indirectly, through correlation with copepods (Wanamaker Jr. et al., 2009; Witbaard et al., 2003) or with climate indices and temperature changes (e.g., Schöne et al., 2003), which in turn influence production and food web dynamics. It has been postulated that *Arctica islandica* are selective feeders who choose fresh phytoplankton over older, dead organic matter (Erlenkeuser, 1976), and that their growth variability should therefore be closely linked to primary productivity (Bonitz et al., 2017; Marali and Schöne, 2015). Like other filter-feeding bivalves, *Arctica* may also be selective among different types of phytoplankton, choosing certain species while rejecting others (Shumway et al., 1985).

Growth variability in *Arctica* specimens from St Kilda showed a significant correlation with phytocolour — a proxy for primary productivity (Figure 7.1). The correlation is positive for the entire length of the phytocolour series, apart from four short-lived negative excursions (Figure 7.2). These inversions of the relationship could not be linked to changes in climate indices or regional data and remain without explanation. It should be noted, however, that the CPR data span a relatively large area (see Methods section 3.3.5.2) and will therefore show limited skill in capturing local conditions in the upwelling system at St Kilda. This could also be one explanation for the lack of correlations between *Arctica* growth and taxonomic groups of phyto- and zooplankton.

Apart from food supply, temperature may also have a direct effect on shell growth. In a tank experiment with juvenile specimens of *Arctica islandica*, Witbaard et al. (1997b) observed an increase in growth rates with increasing temperature; this influence was strongest at the lowest temperature range (1–6° C). However, in their discussion, the authors note that the effect of temperature on *in-situ* growth is likely small and overruled by other factors (Witbaard et al., 1997b; see also Witbaard et al., 1997a). Some field studies have found a direct relationship between temperature and shell growth in *Arctica*; however, these were all from high latitudes,

where winter seawater temperatures drop below 4 °C (Schöne et al., 2005; Weidman et al., 1994). On the outer western Scottish shelf, annual SSTs range generally from ca. 8 °C to 15 °C and reach optimum temperatures for spawning and larval survival in the summer (Mann, 1982; Mann and Wolf, 1983). It is therefore unlikely that *Arctica* experience thermal stress at this location (see also Butler et al., 2010).

In-situ temperatures at St Kilda were calculated from annual $\delta^{18}O_c$ and showed a significant anticorrelation with annual growth rates throughout the chronology (Figure 7.13). Inverse relationships between shell growth and *in-situ* temperatures have previously been observed in Arctic specimens of *Ciliatocardium ciliatum* (Carroll et al., 2014) and *A. islandica* (Mette et al., 2016) at shallow depths. Carroll et al. (2014) hypothesised that warmer temperatures at their study site in the Barents Sea correspond to more Atlantic inflow, retreating Arctic water, and less sea-ice formation, which favours primary production and grazing activity. It is a common hypothesis that colder temperatures have a favourable effect on food availability and food quality to bivalves, because there are fewer zooplankton and therefore grazing activity decreases (Carroll et al., 2014; and references therein). Conversely, higher temperatures lead to a higher abundance of copepods, which replace fresh phytoplankton with faecal pellets. Negative correlations between copepod abundance and shell growth have previously been reported in *G. glycymeris* on the western Scottish shelf (David J. Reynolds et al., 2017) and *A. islandica* in the North Sea (Witbaard et al., 2003). Another hypothesis for the anticorrelation with temperature is that metabolic costs increase in warmer water, which leaves the animal with less energy to invest in shell growth if food supply remains constant. This has been reported for scallop species in the Arctic (Blicher et al., 2010) and in subtropical waters (Kirby-Smith and Barber, 1974), and was considered a viable explanation for *A. islandica* in northern Norway (Mette et al., 2016). Lastly, a negative correlation between *in-situ* temperatures and shell growth rates was also found in *A. islandica* collected at 100 m depth on the Faroe shelf (Bonitz et al., 2017). The authors attributed this observation to the inverse relationship between temperatures and phytoplankton abundance below the thermocline (Bonitz et al., 2017).

The studies cited above were undertaken in conditions that differ significantly from those at St Kilda. Firstly, the *A. islandica* at Village Bay lived in well-mixed surface water throughout the year, unlike the specimens in the study on the Faroe shelf (Bonitz et al., 2017). Secondly, the region is entirely free from sea ice. Thirdly, temperatures during the growth season range from 9 °C to 15 °C (see Chapter 6), which should have a positive effect on shell growth according

to tank experiments (Witbaard et al., 1997b). The difference between colder and warmer years at St Kilda is usually smaller than 2 °C (Figure 7.12) and well within the temperature tolerance of *A. islandica* (Golikov and Scarlato, 1973; Winter, 1969). A direct negative effect of temperature on shell growth at this location is therefore unlikely (see also Bonitz et al., 2017). Changes in copepod abundance could be responsible for the inverse relationship, but there is no clear evidence supporting this hypothesis based on the available CPR data. Similarly, neither can it be ruled out nor proven that the colder temperatures are indicative of changes in water mass, i.e., of increased Atlantic inflow. Atlantic water is richer in nutrients and phytoplankton than Scottish coastal water, and carries phytoplankton communities that are taxonomically distinct from those on the shelf (Siemering et al., 2016). There is also evidence of an inverse relationship between water temperature and nutrient concentration on the western Scottish shelf (Siemering et al., 2016). However, temperature is an unreliable tracer of water mass origin in this region (Jones et al., 2018; Jones, 2016); therefore, the $\delta^{18}O_c$ series cannot be used to estimate changes in Atlantic water vs shelf water dominance. Finally, colder temperatures at St Kilda are likely linked to local upwelling (see Chapter 2). Upwelling brings colder, nutrient-rich bottom water to the surface, which stimulates primary productivity and ultimately leads to favourable conditions for both pelagic and benthic organisms, including *Arctica islandica*.

7.3.2 *Arctica* growth, climate indices, and spatial correlations

As discussed in the previous section, growth variability in *Arctica* at St Kilda is most likely linked to changes in food availability and quality. However, apart from a positive correlation with phytocolour (Figure 7.1), no significant correlations with regional plankton data were found. A possible explanation for this is that the spatial and temporal resolution of the CPR data are not meshed finely enough to capture temporal and local variability at St Kilda. Indeed, it is often the case that large-scale climate indices achieve better results than regional data in predicting ecological processes (e.g., Mette et al., 2016). Hallett et al. (2004) explain this "paradox" with the fact that averages of local data — where available — fail to capture the complicated and temporally variable interactions between local environment and ecological processes. Climate paradigms like the NAO, on the other hand, incorporate the variability and interconnections of a suite of components.

The results in sections 7.1.3 and 7.1.4 show that the *Arctica* chronology reflects broad climate variability in the North Atlantic. While the correlation with winter NAO was weak (Table 7.2; Figure 7.6), there was a relatively strong and significant negative correlation between the growth chronology and (1) zonal wind stress at 200 mbar, which is consistent with the jet stream (Figure 7.10a), as well as with (2) the dipole-like pattern of sea level pressure variability that corresponds to the pressure systems associated with the NAO (Figure 7.10b). This suggests that shell growth decreases during intervals with positive winter NAO conditions, which are associated with strong westerly winds, precipitation, and milder temperatures in northwest Europe. The *Arctica* growth series lags the wind stress series by one year, which may be due to a lagged response of nutrient supply and plankton to temperature changes (Fromentin and Planque, 1996). A positive winter NAO is also associated with increased, storm-driven inflow of oceanic water onto the western Scottish shelf (see Chapter 2; Jones et al., 2020). Storms increase mixing, which can bring nutrients to the surface and enhance phytoplankton growth. However, storms can also cause a sharp decline in primary production or a delay in phytoplankton blooms due to increased turbidity and suspended particulate matter in surface water (Siemering et al., 2016, and references therein).

The growth chronology largely covaries with the AMO, which is thought to be related to variations in the strength of Atlantic overturning circulation (Knight et al., 2006). While the mechanisms of AMO-related variability are not fully understood, it is commonly accepted that the AMO at least in part reflects natural internal variations in the AMOC (Drinkwater et al., 2014; but see Clement et al., 2015). The covariance between the *Arctica* growth index and the AMO index is strongest in the first half of the 20th century CE, where a pronounced multidecadal trend in the chronology is present. Between 1900 and 1920 CE, *Arctica* experienced lower-than average growth, which concurred with a negative AMO index (Figure 7.4), low regional SSTs (Figure 7.3), and higher-than-average *in-situ* temperatures at St Kilda (Figure 7.12). At around 1920 CE, shell growth rates and regional SSTs show a rapid increase. This increase coincides with a regime shift in the North Atlantic that resulted in a considerable warming of the northern North Atlantic Ocean and a subsequent drastic increase in phytoplankton and zooplankton production, as well as changes in migration patterns of species at various trophic levels (Drinkwater, 2006).

7.3.3 *Arctica* growth, Soay sheep survival, and marine-terrestrial connectivity

The significant correlation between the *Arctica* growth chronology and population size fluctuation of Soay sheep on Hirta indicates that the terrestrial and marine environments at St Kilda are closely linked (Figure 7.11). A strong marine-terrestrial connectivity at this site is not unexpected, given its exposed location on the outer shelf. However, accurately characterising and quantifying this relationship and the complex interactions, connections, and common responses of marine and terrestrial organisms is a far from trivial task.

The overarching question is whether Soay sheep and *Arctica islandica* are (1) responding to common environmental factors, (2) responding to different environmental factors that are connected with one another, or (3) indirectly impacting each other. A fourth option is that the correlation is spurious and not does not represent a connection between the two series. This possibility is worth consideration, given the relatively short overlap in time (1985–2013) and the fact that the EPS is at its lowest in this part of the *Arctica* growth chronology (see Chapter 6). However, as will be detailed below, there is good reason not to dismiss the correlation between the two series. Indeed, a "real-world" connection between the sheep on Hirta and bivalves at Village Bay seems likely when all environmental influences are taken into account.

7.3.3.1 Population ecology, physical environment, and large-scale weather patterns

As with *Arctica* growth variability, sheep population size fluctuation cannot be attributed to any single factor, but a suite of drivers, and sheep fitness is influenced by cumulative effects over time. The population fluctuates drastically and experiences population crashes at irregular intervals (Clutton-Brock and Pemberton, 2004) (Figure 7.12). These population crashes have been described as a nonlinear interaction between population density, weather, and population structure (Coulson et al., 2001). In other words, the drastic changes in population size are caused both by density-dependent intrinsic processes (i.e. competition for food among sheep) and by extrinsic factors such as weather. In what way these different processes impact each individual, in turn, depends on the age and sex of the animal. The major cause of death in Soay sheep is starvation, which results from the energetic cost of thermoregulation in extreme weather conditions and/or diminished food availability (Gulland, 1992; Hallett et al., 2004).

Sheep of different age and sex classes expend different amounts of energy at different times of the year, and thus respond differently to weather and population density (Coulson et al., 2001).

Numerous studies have shown a link between the NAO and population dynamics in Soay sheep (e.g., Catchpole et al., 2000; Simmonds and Coulson, 2015) or other ungulates in the Northern Hemisphere (e.g., Post and Forchhammer, 2002; Post and Stenseth, 1998). Windy and wet winters during a positive NAO phase negatively affects Soay sheep in two ways — (1) by increasing energetic costs, particularly in weak individuals, and (2) by regulating plant productivity and thus food availability on the island (Hallett et al., 2004). Figure 7.15 shows a strong negative correlation between jet stream strength during winter and Soay sheep population size, which further supports the finding that sheep fitness is negatively impacted by wet and windy winters. *Arctica* growth variability shows a similar negative correlation with wind stress (see Figure 7.10 and Section 7.3.2). Previous studies have linked bivalve growth variability to variability in other marine and terrestrial organisms. *Arctica islandica* and Scots pine from northern Norway showed synchronized growth patterns in years with strongly negative winter NAO or strongly positive summer NAO (Helama et al., 2007). Similarly, Black (2009) found that growth patterns in Pacific geoduck and two Pacific rockfish species related to tree-ring chronologies in western North America, which he attributed to a shared sensitivity to climatic variability.

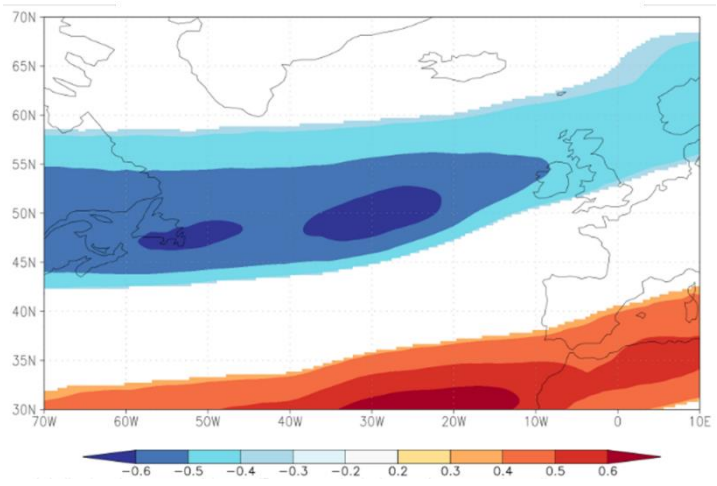

Figure 7.15: Spatial correlations between ERA5 zonal wind stress at 200 mbar from 1985 to 2013 in winter (Dec–Feb) and the Soay sheep population size. Correlation coefficients are indicated by colour and defined in the legend below each figure. $p < 0.1$. Calculated with KNMI Climate Explorer (Trouet and Van Oldenborgh, 2013).

Despite the reported negative correlation between Soay sheep population size and winter NAO, the NAO index does not code the severity and energetic cost of winter weather in Soay sheep efficiently (Hallett et al., 2004). A negative NAO phase can also reflect challenging winter weather (e.g., colder temperatures), which will negatively affect sheep fitness (Hallett et al., 2004; Hurrell et al., 2003). Moreover, the timing of severe weather events within the winter season determines the impact on sheep population size (Hallett et al., 2004). For example, a mortality pulse caused by a storm in the early winter implies that weak sheep are killed off early; the remaining population has a higher chance to survive the rest of the winter because there is less competition for food (Hallett et al., 2004). Survival rates and mortality in Soay sheep are thus influenced by temporally variable associations between local climate and population density. As discussed in Chapter 6, bivalve growth rates are influenced by similarly complex associations of multiple drivers, for which there are not sufficient instrumental data at St Kilda.

In summary, both Soay sheep population dynamics and *Arctica* growth are likely linked to local environmental factors that are partially reflected in the NAO index.

The Soay sheep series lags the *Arctica* growth series by one year (Figure 7.12). However, treating the two series as equally resolved annual data is misleading; they represent different seasons and timings. Mortality searches for Soay sheep are performed throughout the year, but they are particularly frequent (daily) during winter months because that is when the major mortality pulses occur (Hunter et al., 2018). Thus, annual Soay sheep population size is mainly associated with conditions of the preceding winter. The *Arctica* growth chronology, on the other hand, represents spring and summer conditions (see Chapter 6). In both species, cumulative effects on fitness over time have to be considered. Thus, the lag between the series may be reflective of differences in sampling resolution, seasonality, and response time to environmental change, rather than any direct lead–lag relationships between the atmosphere and the ocean.

7.3.3.2 Food-web dynamics and land–water nutrient exchange

There are several major conduits through which organic material and nutrients are transferred from islands to the marine environment, and vice versa. An important source of nutrients from the land is through soil runoff, which plays a major role in promoting productivity in coastal waters (Polis et al., 1997, and references therein). Terrestrial mammals can play an important

role in bringing nutrients to aquatic systems through detritus transport and defecation (Polis et al., 1997). Hence, Soay sheep population size could potentially impact *Arctica* growth indirectly through the transfer of nutrients from land to water via sheep droppings. In a year with a high number of sheep, more faeces will be produced, which may lead to more nutrients leaching into the surrounding sea, promoting primary productivity. Sclerochronological studies on deep-water corals (Prouty et al., 2014; Williams et al., 2007) and bivalves (Black et al., 2017; Thibault et al., 2020) have shown that enrichment in skeletal or shell $\delta^{15}N$ can be used to measure terrestrial runoff and waste input into waterways. Moreover, Gillikin et al. (2017) demonstrated that $\delta^{15}N$ in bivalve shell can be sampled at a very high resolution (i.e. up to weekly). In a recent study using shells from various locations in the Northeast Atlantic, Schöne and Huang (2021) emphasised the remarkable potential of $\delta^{15}N$ in *A. islandica* for the study of trophic ecology and pollution, provided that ontogenetic trends in nitrate utilisation and fractionation are first removed from the data.

Whether $\delta^{15}N$ profiles of *A. islandica* at Village Bay could be related to Soay sheep population size on Hirta, is unclear. A highly resolved nitrogen series could be analysed with consideration of mortality pulses and other big events in Soay sheep. However, the relatively low freshwater input from Hirta, and the highly dynamic and stormy conditions at St Kilda, would most likely mask or dampen any fertilising effect of sheep faeces on the marine environment. Moreover, as will be discussed below, any fertilising effect by sheep faeces and carcasses may be "outperformed" by a more significant actor in the St Kildan food web: seabirds.

Conversely to the land-to-water flux of nutrients, nutrients may be transported from the sea to terrestrial ecosystems in sea spray and seafoam (Swan, 1963). It has been shown that the salts in sea spray enrich the soil on the islands of St Kilda and thus promote productivity (Scottish Executive, 2003). Algal wrack and carrion are other important marine sources of nutrients in coastal terrestrial ecosystems (Polis et al., 1997). Small islands are particularly suitable study sites for biotic connectivity, because the terrestrial island ecosystem often receives more biomass from marine drift than it produces via *in-situ* primary productivity (Polis and Hurd, 1996). It may, however, be the case that the most important actors linking the marine and terrestrial ecosystems at St Kilda are seabirds. It has been clearly demonstrated that seabirds play a significant role in fertilising soil on islands, as well as marine coastal ecosystems (Croll et al., 2005; Frederiksen et al., 2006; Fukami et al., 2006; Mulder et al., 2011; Polis and Hurd, 1996). Seabirds feed in the sea or the open ocean, and enrich coastal ecosystems with nutrients

such as nitrogen and phosphorus by leaving behind guano, feathers, and carcasses (Polis et al., 1997; Shatova et al., 2016). Guano is a powerful fertiliser and enhances primary production on land (Fukami et al., 2006), and in adjacent marine ecosystems, which subsequently affects higher trophic levels (Graham et al., 2018; McCauley et al., 2012; Shatova et al., 2016). As described in Chapter 2, St Kilda is an important seabird breeding site, with up to a million seabirds present at the height of the season; their impact on productivity at this location is considerable (Scottish Executive, 2003).

Numerous studies have linked breeding success and survival rates in seabirds to the winter NAO index (Drinkwater et al., 2003b; Grosbois and Thompson, 2005, and references therein). The most common explanation for this link is that the NAO affects food availability and quality (e.g., Thompson and Ollason, 2001). Similarly, increasing SSTs, due to climate change, leads to changes in foraging behaviour and diet diversification in seabirds, which may impact population dynamics (Howells et al., 2017). This, in turn, may have knock-on effects on food web stability and productivity at various trophic levels at St Kilda.

As outlined above, Soay sheep and *Arctica* are both part of a complex web of physical, biological, and chemical interplay across spheres and systems, and their survival and growth rates may be linked through various pathways. Even though this chapter provides only a limited glimpse into these interactions, it highlights their complexity and the need for integrating data and knowledge about all "pieces" of the puzzle. Natural systems are open, and interdependency of different habitats can be relatively important compared to within-habitat effects (Huxel and McCann, 1998; Polis and Hurd, 1996). It is crucial to keep this in mind when interpreting data from the focal area and target species of a study, while trying to disentangle biological responses to natural environmental variability and human disturbance.

Chapter 8

General discussion

Chapter 8 — General discussion

8.1 Summary of findings

This thesis investigated past hydrographic variability at St Kilda, a volcanic archipelago on the outer western Scottish shelf, using sclerochronological methods. Three bivalve chronologies were presented: two floating chronologies constructed with fossil *Glycymeris glycymeris* shells from the 4th millennium BP, and one modern chronology built with live-collected and dead-collected shells of *Arctica islandica*. A brief overview of the results chapters is given in the following paragraphs and the main findings are visualised in Figure 8.1.

Chapter 4 explored the available instrumental temperature data from the western Scottish shelf. *In-situ* temperature data are scarce; however, the available data from the shelf break, outer shelf, and inner shelf still showed a clear horizontal gradient in temperature and salinity — the inner shelf is more variable and fresher than the outer shelf. These findings are in good accordance with the existing literature introduced in Chapter 2. In the second part of Chapter 4, three gridded data products (HadISST1, ERSSTv.5, OISST V2) were compared to an ensemble of *in-situ* data to test how well each data product represents the environment on the outer

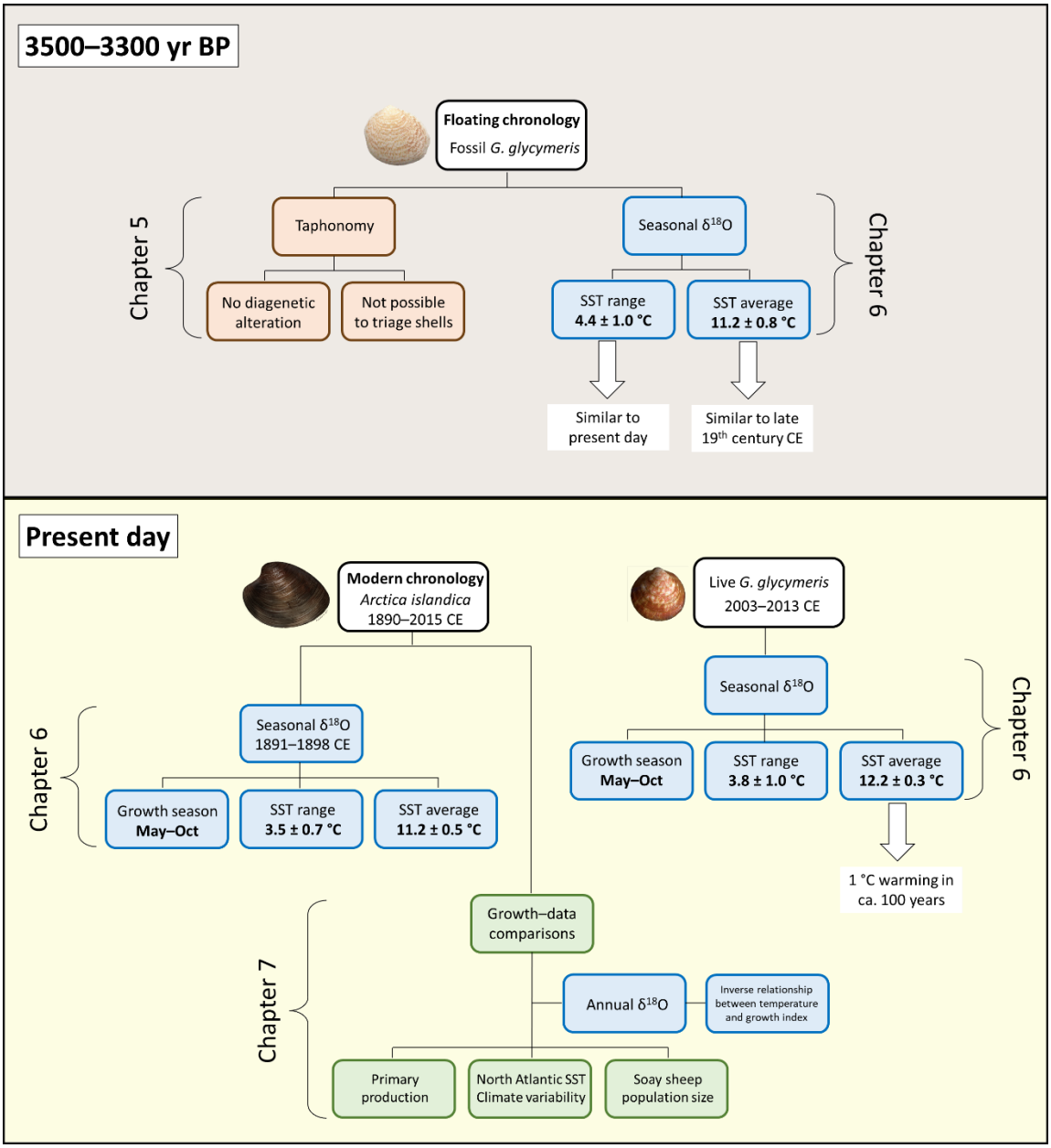

Figure 8.1: Schematic overview of the results presented in chapters 5, 6, and 7.

western Scottish shelf. Skill scores for each gridded data product were calculated following the methods outlined in Hughes et al. (2009). ERSST v.5 achieved the highest Skill score; however, the results were based on intermittent *in-situ* data and the difference between Skill scores of the three data products was relatively small. Moreover, ERSST v.5 had the highest RMSE; this reduced the significance of its Skill score. Previous studies recommended HadISST1 for similar environments (Boehme et al., 2014; Hughes et al., 2009), which also achieved the lowest RMSE in the present work. Therefore, HadISST1 was used in the subsequent chapters for proxy–temperature comparisons.

Chapter 5 laid the foundation for the subsequent chronology chapters by presenting the shell material. The condition of live-collected and dead-collected *G. glycymeris* and *A. islandica* shells was assessed using a taphonomic scoring system (see also Butler et al., 2020). The focus of this chapter was on the fossil *G. glycymeris* shell material. Raman spectroscopy showed no diagenetic alteration in the fossil material, indicating that the shells were solely composed of aragonite. This was important to test, since aragonite-to-calcite transformation may have changed the $\delta^{18}O_c$ composition of the shell and therefore distorted the temperature reconstructions (Dettman et al., 1999; Martín-García et al., 2019; Pederson et al., 2019). The dead-collected *G. glycymeris* shells that had been radiocarbon dated (n = 14) or crossmatched with live-collected specimens (n = 1) were placed into different age groups and further evaluated. Scores of the taphonomic variables (periostracum, ligament, margin, bioeorosion, nacre) did not show any significant trends related to how much time had passed since the death of the animal. In other words, shell condition indicated how the shells had been preserved in the sea, rather than for how long. These results are consistent with previous studies that investigated the relationship between passage of time and *in-situ* shell preservation (Butler et al., 2020; Rogalla and Amler, 2007).

Chapter 6 introduced the fossil and modern chronologies as well as sub-annual oxygen isotope profiles. Sub-annual $\delta^{18}O_c$ data from modern *G. glycymeris* and *A. islandica* showed that both species mainly grow from May to September/October.

Wavelet spectrum analysis showed significant periods of 2–6 years throughout the fossil *St Kilda Seven* chronology and the modern *Arctica* chronology. Similar patterns have been observed in *A. islandica* at various sites across the North Atlantic and have been speculated to represent NAO-type forcing (Schöne et al., 2005; Wanamaker Jr. et al., 2009). However, both the NAO record and growth chronologies are (weakly) autocorrelated, which enhances the risk of "false positive" covariance between the series (Wunsch, 1999). Therefore, frequency domain studies should be treated with considerable caution.

Bayesian modelling of the radiocarbon dates produced high-density peaks at 3500–300 cal yr BP, most likely placing the *St Kilda Seven* floating chronology in this time range. This period coincides with regional climatic shifts on the British Isles from dry to wet conditions (Charman, 2010).

Temperature reconstructions based on $\delta^{18}O_c$ indicated similar conditions in the 4th millennium BP and the present day — like their modern counterparts, the fossil *G. glycymeris* specimens lived in mixed surface water. Average temperatures calculated for the 4th millennium BP (fossil *G. glycymeris*) and the late 19th century (modern *A. islandica*) were similar to each other and 1 °C colder than today (Figure 8.1). Thus, the fossil shells showed no evidence for a pronounced SST cooling in the 4th millennium BP, in contrast to proxy records from several other sites in the Northeast Atlantic (Orme et al., 2018, and references therein). However, the shell record represents only a short time window; a longer time series would be needed to answer the question whether a pronounced cooling took place at this location.

Lastly, **Chapter 7** provided a more in-depth analysis of the modern *Arctica* growth chronology by comparing it to biological and environmental data and climate indices. Growth variability is likely influenced by local changes in food availability, which, in turn, are linked to large-scale variability in atmospheric and ocean circulation. This link is also visible in the significant correlation between the chronology and the AMO, regional SSTs, zonal wind stress, and sea level pressure. *Arctica* growth variability at St Kilda thus reflects broad climate variability.

Based on the growth index series, an annual $\delta^{18}O_c$ record was obtained and used for temperature reconstruction. Interestingly, this *in-situ* temperature record had an inverse relationship with growth variability, which further supports the hypothesis that growth at this location is primarily driven by food supply rather than directly by temperatures. Lower temperatures may indicate increased local upwelling processes, causing higher primary productivity. Colder

conditions could also result in lower grazing pressure by zooplankton in spring (Planque and Fromentin, 1996). The annual $\delta^{18}O_c$ series shows a strong warming trend in the early 20th century, and a rapid decrease in temperature at around 1920 CE. This is contrary to the basin-wide regime shift, which saw a strong warming trend in air and sea temperatures in the 1920s and 1930s, due to a spatial shift in the atmospheric pressure systems, causing increased heat transfer from low to high latitudes (Drinkwater, 2006; Rogers, 1985). However, from 1950 CE onwards, the *in-situ* temperatures at St Kilda correlate positively with regional SSTs on the western Scottish shelf (Figure 7.14). The *Arctica* growth index series, on the other hand, shows no significant correlations with regional SSTs on the Scottish shelf, but instead correlates positively with SSTs in the wider North Atlantic, including the subpolar gyre (Figure 7.9). These findings provide further evidence that *Arctica* growth is not directly influenced by temperature, but by changes in food supply, storminess, and ocean circulation.

A positive correlation was found between the *Arctica* growth chronology and Soay sheep population size, which indicates a tight coupling of the marine and terrestrial environments at St Kilda.

8.2 Limitations of using $\delta^{18}O_c$ in temperature reconstructions

An important and well-known caveat of $\delta^{18}O_c$ temperature reconstructions is that $\delta^{18}O_w$ needs to be known or estimated. The $\delta^{18}O_w$ composition of seawater is controlled by fractionation processes in the hydrological cycle such as evaporation, precipitation, vapour transport, and changes in sea ice; it is thus linked to changes in salinity (Rohling, 2013, and references therein). Furthermore, $\delta^{18}O_w$ varies based on the mixing and advection of water masses with specific $\delta^{18}O_w$ signatures. Large-scale changes in North Atlantic Ocean circulation as well as wind-driven regional processes on the Scottish shelf will contribute to salinity and $\delta^{18}O_w$ variability at St Kilda. However, no local measurements of $\delta^{18}O_w$ are available for either of the two time periods discussed in this study, and no regional salinity–$\delta^{18}O_w$ relationship has yet been formulated. Therefore, the $\delta^{18}O_w$ value for surface water from the closest available location in the open ocean was applied to both the modern and the fossil shell-derived temperature series.

At St Kilda, terrestrial freshwater input is negligible and the region was fully deglaciated by the early Holocene (Austin and Kroon, 1996), ruling these factors out as local influences on $\delta^{18}O_w$ variability. Instrumental measurements along the Ellett line since 1975 show that the station closest and most similar to St Kilda (station 15G), has an average salinity of 35.2 ± 0.2 (Jones et al., 2018). How much changes in salinity affect the $\delta^{18}O_w$, and consequently the reconstructed temperature, can be estimated with a salinity–$\delta^{18}O_w$ mixing line. However, as mentioned above, no such mixing line has been developed for the outer western Scottish shelf. Austin et al. (2006) recommend using the equation $\delta^{18}O_w = 0.5972 \times S - 20.6850$ for the Outer Hebrides, which is a modified version of the equation developed by Frew et al. (2000) for the northern North Atlantic. Following this recommendation, a standard deviation of ± 0.2 in salinity would result in a fluctuation of ± 0.5 °C in reconstructed temperature. However, the applicability of this equation to St Kilda remains uncertain, given that St Kilda is influenced both by oceanic and by coastal waters, as well as local dynamics such as cold-water upwelling.

8.3 Novelty of this study and main conclusions

This work presented the first floating bivalve chronology from the Scottish shelf, and the first floating chronology built with *G. glycymeris* shells. As discussed in Chapter 5, shell lags can contain specimens with age differences of thousands of years (Flessa et al., 1993; Butler et al., 2009), and taphonomic variables do not reliably indicate for how long shells have been buried in sediment (Butler et al., 2020). Instead, radiometric dating is commonly used to constrain ages of fossil shells — provided that the necessary funding is available. While archaeological shell middens may provide more stratigraphic information than shell lags, they usually consist of short-lived species, which are unsuitable for crossmatching (Andrus, 2011). Given these challenges, floating bivalve chronologies remain rare, however, published examples do exist both for shell lags (e.g., Scourse et al., 2006) and shell middens (Helama and Hood, 2011). Finding alternative sampling strategies that help constrain ages in the fossil record has been raised as a priority research question in a recent horizon-scanning survey in the field of sclerochronology (Trofimova et al., 2020). Alternatively, new technologies and methodologies that reduce the time needed for measuring and crossmatching shell increments could facilitate the use of fossil material.

The results in Chapter 6 show that the fossil *G. glycymeris* shells experienced a similar growth season and temperature range as the modern shells, which can be attributed to similar boundary conditions in this region. The age uncertainty and short time frame of the $\delta^{18}O_c$ series are limiting factors that prevent conclusions being drawn on the presence or timing of a distinct summer SST cooling event or cold interval. However, the average $\delta^{18}O_c$ of the fossil specimens indicate that late-spring and summer SSTs on the Scottish shelf were cooler in the fourth millennium BP than they are today, and comparable to SSTs in the early 20th century. Thus, an extension of the chronology, accompanied by an annually resolved $\delta^{18}O_c$ record, is needed to address the question whether this region was affected by a cold interval. This would also provide more insight into a time that saw a climate shift to wetter conditions on the British Isles, in which the role of the ocean is uncertain. Such an extension of the chronology would be challenging and require additional funding; however, it is feasible.

Attempts were made to correlate the fossil chronologies with proxy data from speleothems in NW Scotland (Baker et al., 2002), tree-ring growth in England (Boswijk, 2002), and multi-proxy peatland water table data (Swindles et al., 2013), but no significant results were found (results not included in this thesis). With no instrumental or proxy data to compare the chronologies to, there is no direct evidence to show which environmental drivers are represented in the growth indices. Hypotheses may be inferred based on modern chronologies, but drivers of growth are not necessarily constant over time. Consequently, the floating growth chronologies are currently not "readable" as climate proxies per se. They do, however, provide an annually resolved, replicated template for $\delta^{18}O_c$ sampling. As was shown in Chapter 6, $\delta^{18}O_c$ in *G. glycymeris* and *A. islandica* provide accurate records of temperature at St Kilda. However, low sampling resolution or changes in salinity may mask the true temperature signal. Offsets between individual specimens and outliers are another potential source of error (Mette et al., 2018). Therefore, $\delta^{18}O_c$ series should be replicated across coeval specimens from the same population where possible. Potential limitations of $\delta^{18}O_c$ as a temperature proxy are discussed in Section 8.2.

Due to their high resolution and capacity for replication, sclerochronological archives are exceptionally well suited to study variability in the coupled ocean–atmosphere climate system (Reynolds et al., 2016) and responses in the coupled marine–terrestrial ecosystem (Black et al., 2014). However, only few studies have investigated the relationship between marine sclerochronologies and terrestrial proxy data directly (Black, 2009; Black et al., 2014; Helama et al., 2007; Ong et al., 2016). To my knowledge, the present work is the first to report synchrony between bivalve growth variability and population dynamics in terrestrial mammals. The common variability in *Arctica* shell growth and Soay sheep population size is a product of the remote location of St Kilda. Direct human disturbance is negligible at this location; thus, organisms on the islands and in the surrounding sea show an unmediated response to their natural physical, biological, and chemical environment. Storms are a common occurrence on the outer western Scottish shelf and, perhaps unsurprisingly, both Soay sheep mortality and *Arctica islandica* growth are influenced by broad climate variability of the North Atlantic, which, in turn, determines the frequency and scale of severe weather events.

In summary, St Kilda is appropriately sited to study the variability of North Atlantic inflow and large-scale climatic variability as it is an offshore location close to the shelf margin, with negligible freshwater input. The *A. islandica* growth chronology likely reflects changes in food availability and quality, which are associated with changes in temperature and ocean circulation. The good fit between gridded SSTs and seasonal $\delta^{18}O_c$-derived *in-situ* temperatures in Chapter 6 further confirms the applicability of *G. glycymeris* and *A. islandica* shells from St Kilda as proxies for temperature. However, St Kilda is also influenced by the Scottish Coastal Current and, due to its island topography, local upwelling processes must be considered.

8.4 Outlook and future work

Chapter 6 provides a discussion on the potential of extending the fossil *G. glycymeris* chronology. Linking the two floating chronologies with each other would provide a multicentennial record within the fourth millennium BP, allowing further analysis of trends and variability during that time. In addition, extending the chronology or incorporating more shells into the series — in combination with additional radiocarbon dating — would provide more data to further constrain the dates of the floating chronology with Bayesian modelling.

Another possibility to constrain the dates of the floating chronology is by linking the growth index series to major events with known dates, like the Minoan Eruption of Thera at ca. 3600 yrs BP, via other proxy records, such as tree rings (Pearson et al., 2020). However, it is impossible to reliably base any such connection on the growth index series alone, and geochemical sampling is indispensable for further exploration of possible correlations.

It is not clear whether the modern *Arctica* chronology can be extended back in time with the shell material collected in the 2016 diving campaign. The divers collected shells that were in relatively close proximity to each other, of equal size, and that were either alive or had died recently. The seven shells currently incorporated into the master chronology all settled within a few years of each other. However, regardless of whether the chronology can be considerably extended in time, future work would benefit from incorporating more shells into the series. Particularly for the years 1980–2015, a higher replication may increase the statistical

robustness and improve the EPS (expressed population signal), i.e. the skill of the chronology to predict environmental variability.

G. glycymeris and *A. islandica* at St Kilda share the same growth season (May–October); thus, both species experience environmental variability during the same time of year. Unfortunately, all *G. glycymeris* specimens collected in 2014 were very young (<30 years), and the subsequent diving campaign had to be abandoned due to stormy conditions before any additional specimens were found. It is therefore not possible to directly compare growth variability in *G. glycymeris* and *A. islandica* from St Kilda. If long-lived, modern *G. glycymeris* specimens were collected at Village Bay in a future campaign, the resulting chronology could be combined with *A. islandica* to form an inter-species growth series. Combining different sclerochronologies into a composite record can significantly increase their skill at reconstructing climate variability (Reynolds et al., 2017). In addition, the St Kilda records could be combined with sclerochronologies from other locations in the North Atlantic in a spatial network analysis (Reynolds et al., 2018). Available data include records from other ARAMACC projects (e.g., Bonitz et al., 2017) and other published and unpublished records from various locations in the Northeast Atlantic, for example in northern Norway (e.g., Mette et al., 2021), the northern North Sea (e.g., Butler et al., 2009a), northern Iceland (e.g., Butler et al., 2013). Such a spatial network of highly resolved and absolutely dated chronologies provides a powerful tool to investigate spatial patterns of marine variability on decadal-to-centennial scales and the role of the ocean in climate variability (Reynolds et al., 2018).

Another exciting avenue for future work is a more comprehensive study of marine–terrestrial connectivity at St Kilda. The correlation between Soay sheep population size and *Arctica* growth width variability demonstrates the tight coupling of the marine and terrestrial ecosystem at this location. In addition to population size and mortality, the St Kilda Soay sheep project assesses lamb mass (e.g., Hunter et al., 2018) and horn growth rates every year (Alastair Wilson, University of Exeter, 2018, pers. communication), which may be incorporated into further analyses. Future work should also include analysis of seabird breeding and site occupation, grazing pressure and plant cover on Hirta, and records of mid-trophic fish species such as sandeels and mackerels. Seabird data are collected and made available by the Joint

Nature Conservation Committee (JNCC; https://jncc.gov.uk/about-jncc/corporate-information/open-data/); however, these data are intermittent.

A transdisciplinary study considering all these different actors and variables, as well as sub-annually resolved $\delta^{15}N$ data sampled in the *Arctica* chronology, may provide complementary insight into marine–terrestrial exchange and food-web dynamics at this near-pristine location.

References

References

Adams, C.E., Godfrey, J.D., Dodd, J.A., Maitland, P.S., 2013. Is proximity to the North Atlantic Drift and the Continental Shelf Current sustaining freshwater European eel populations in western Scotland? Freshw. Biol. 58, 1–9. https://doi.org/10.1111/fwb.12021

Aiken, J., Bruce, R.H., Lindley, J.A., 1977. Ecological investigations with the Undulating Oceanographic Recorder: The hydrography and plankton of the waters adjacent to the Orkney and Shetland Islands. Mar. Biol. 39, 77–91.

Alexandroff, S.J., Butler, P.G., Hollyman, P.R., Schöne, B.R., Scourse, J.D., 2021. Late Holocene seasonal temperature variability of the western Scottish shelf (St Kilda) recorded in fossil shells of the bivalve *Glycymeris glycymeris*. Palaeogeogr. Palaeoclimatol. Palaeoecol. 562, 110146. https://doi.org/10.1016/j.palaeo.2020.110146

Andrus, C.F.T., 2011. Shell midden sclerochronology. Quat. Sci. Rev. 30, 2892–2905. https://doi.org/10.1016/j.quascirev.2011.07.016

Aristotle, 350 BCE [1910 transl. edn]. History of Animals. Translated by D.W. Thompson. Clarendon Press, Oxford

Ascough, P.L., Church, M.J., Cook, G.T., 2016. Marine Radiocarbon Reservoir Effects for the Mesolithic and Medieval Periods in the Western Isles of Scotland. Radiocarbon 59, 17–31. https://doi.org/10.1063/1.2756072

Ascough, P.L., Cook, G.T., Dugmore, A.J., Barber, J., Higney, E., Scott, E.M., 2004. Holocene Variations in the Scottish Marine Radiocarbon Reservoir Effect. Radiocarbon 46, 611–620.

Ascough, P.L., Cook, G.T., Dugmore, A.J., Scott, E.M., 2007. The North Atlantic marine reservoir effect in the Early Holocene: Implications for defining and understanding MRE values. Nucl. Instruments Methods Phys. Res. Sect. B Beam Interact. with Mater. Atoms 259, 438–447. https://doi.org/10.1016/j.nimb.2007.01.185

Austin, W.E.N., Cage, A.G., Scourse, J.D., 2006. Mid-latitude shelf seas: a NW European perspective on the seasonal dynamics of temperature, salinity and oxygen isotopes. The Holocene 16, 937–947. https://doi.org/10.1177/0959683606hl985rp

Austin, W.E.N., Kroon, D., 1996. Late glacial sedimentology, foraminifera and stable isotope stratigraphy of the Hebridean Continental Shelf, northwest Scotland, in: Andrews, J.T., Austin, W.E.N., Bergsten, H., Jennings, A.E. (Eds.), Late Quaternary Palaeoceanography of the North Atlantic Margin. Geological Society Special Publication 111, pp. 187–213. https://doi.org/10.1144/GSL.SP.1996.111.01.13

Austin, W.E.N., Scourse, J.D., 1997. Evolution of seasonal stratification in the Celtic Sea during the Holocene. J. Geol. Soc. London. 154, 249–256.

Bailey, M., Bailey, D., Bellini, L., Fernandes, P., Fox, C., Heymans, S., Holmes, S., Howe, J., Hughes, S., Magill, S., McIntyre, D., McKee, D., Ryan, M., Smith, I., Tyldsley, G., Watret, R., Turrell, W., 2011. The west of Scotland marine ecosystem: A review of scientific knowledge. Fish. Res. 292.

Baker, A., Proctor, C., Barnes, W., 2002. Northwest Scotland Stalagmite Data to 3600 BP, IGBP PAGES/World Data Center A for Paleoclimatology Data Contribution Series #2002-028. NOAA/NGDC Paleoclimatology Program, Boulder CO, USA

Ballesta-Artero, I., Witbaard, R., Carroll, M.L., van der Meer, J., 2017. Environmental factors regulating gaping activity of the bivalve *Arctica islandica* in Northern Norway. Mar. Biol. 164. https://doi.org/10.1007/s00227-017-3144-7

Barber, K.E., Charman, D.J., 2003. Holocene palaeoclimate records from peatlands., in: Mackay, A.W., Battarbee, R.W., Birks, H.J.B., Oldfield, F. (Eds.), Global Change in the Holocene. Edward Arnold, London, pp. 210–226.

Berner, K.S., Koc, N., Divine, D., Godtliebsen, F., Moros, M., 2008. A decadal-scale Holocene sea surface temperature record from the subpolar North Atlantic constructed using diatoms and statistics and its relation to other climate parameters. Paleobiology 23. https://doi.org/10.1029/2006PA001339

Bersch, M., 2002. North Atlantic Oscillation–induced changes of the upper layer circulation in the northern North Atlantic Ocean. J. Geophys. Res. 107. https://doi.org/10.1029/2001jc000901

Berthou, P., Blanchard, M., Noel, P., Vergnaud-Grazzini, C., 1986. The analysis of stable isotopes of the shell applied to the determination of the age of four bivalves of the "Normano-Breton" Gulf, Western Channel. ICES K 16.

Black, B.A., 2009. Climate-driven synchrony across tree, bivalve, and rockfish growth-increment chronologies of the northeast Pacific. Mar. Ecol. Prog. Ser. 378, 37–46. https://doi.org/10.3354/meps07854

Black, B.A., Andersson, C., Butler, P.G., Carroll, M.L., DeLong, K.L., Reynolds, D.J., Schöne, B.R., Scourse, J.D., van der Sleen, P., Wanamaker, A.D., Witbaard, R., 2019. The revolution of crossdating in marine palaeoecology and palaeoclimatology. Biol. Lett. 15, 20180665.

Black, B.A., Copenheaver, C.A., Frank, D.C., Stuckey, M.J., Kormanyos, R.E., 2009. Multi-proxy reconstructions of northeastern Pacific sea surface temperature data from trees and Pacific geoduck. Palaeogeogr. Palaeoclimatol. Palaeoecol. 278, 40–47. https://doi.org/10.1016/j.palaeo.2009.04.010

Black, B.A., Griffin, D., van der Sleen, P., Wanamaker, Jr., A.D., Speer, J.H., Frank, D.C., Stahle, D.W., Pederson, N., Copenheaver, C.A., Trouet, V., Griffin, S., Gillanders, B.M., 2016. The value of crossdating to retain high-frequency variability, climate signals, and extreme events in environmental proxies. Glob. Chang. Biol. 22, 2582–2595. https://doi.org/10.1111/gcb.13256

Black, B.A., Sydeman, W.J., Frank, D.C., Griffin, D., Stahle, D.W., García-Reyes, M., Rykaczewski, R.R., Bograd, S.J., Peterson, W.T., 2014. Six centuries of variability and extremes in a coupled marine-terrestrial ecosystem. Science 345, 1498–1502.

Black, H.D., Andrus, C.F.T., Lambert, W.J., Rick, T.C., Gillikin, D.P., 2017. $\delta^{15}N$ values in *Crassostrea virginica* shells provides early direct evidence for nitrogen loading to Chesapeake Bay. Sci. Rep. 7. https://doi.org/10.1038/srep44241

Blake, C.B., 2005. Use of maerl as a biogenic archive. Queen's University Belfast.

Blicher, M.E., Rysgaard, S., Sejr, M.K., 2010. Seasonal growth variation in *Chlamys islandica* (Bivalvia) from sub-arctic Greenland is linked to food availability and temperature. Mar. Ecol. Prog. Ser. 407, 71–86. https://doi.org/10.3354/meps08536

Boehme, L., Lonergan, M., Todd, C.D., 2014. Comparison of gridded sea surface temperature datasets for marine ecosystem studies. Mar. Ecol. Prog. Ser. 516, 7–22. https://doi.org/10.3354/meps11023

Böhm, C.F., Demmert, B., Harris, J., Fey, T., Marin, F., Wolf, S.E., 2016. Structural commonalities and deviations in the hierarchical organization of crossed-lamellar shells: A case study on the shell of the bivalve *Glycymeris glycymeris*. J. Mater. Res. 31, 536–546. https://doi.org/10.1557/jmr.2016.46

Bonitz, F.G.W., Andersson, C., Trofimova, T., Hátún, H., 2017. Links between phytoplankton dynamics and shell growth of *Arctica islandica* on the Faroe Shelf. J. Mar. Syst. 179, 72–87. https://doi.org/10.1016/j.jmarsys.2017.11.005

Boswijk, G., 2002. NOAA/WDS Paleoclimatology - Boswijk - Thorne Moors GM02 T51 - PISY - ITRDB BRIT039. NOAA National Centers for Environmental Information. https://doi.org/10.25921/sx13-tf51

Bowen, D.Q., Rose, J., McCabe, A.M., Sutherland, D.G., 1986. Correlation of Quaternary glaciations in England, Ireland, Scotland and Wales. Quat. Sci. Rev. 5, 299–340. https://doi.org/10.1016/0277-3791(86)90194-0

Box, G.E.P., Jenkins, G.M., Reinsel, G.C., 1994. Time Series Analysis: Forecasting and Control, 3rd ed. Prentice-Hall, New Jersey.

Boyd, J.M., Doney, J.M., Gunn, R.G., Jewell, P.A., 1964. The Soay sheep of the island of Hirta, St. Kilda. A study of a feral population. Proc. Zool. Soc. London 142, 129–163.

Briffa, K.R., Jones, P.D., Bartholin, T.S., Eckstein, D., Schweingruber, F.H., Karlén, W., Zetterberg, P., Eronen, M., 1992. Fennoscandian summers from ad 500: temperature changes on short and long timescales. Clim. Dyn. 7, 111–119. https://doi.org/10.1007/BF00211153

Brinza, L., Schofield, P. F., Mosselmans, J. F. W., Donner, E., Lombi, E., Paterson, D., & Hodson, M. E., 2014. Can earthworm secreted calcium carbonate immobilise Zn in contaminated soils? Soil Biol. and Biochem., 74, 1−10. https://doi.org/10.1016/j.soilbio.2014.01.012

Brocas, W.M., Reynolds, D.J., Butler, P.G., Richardson, C.A., Scourse, J.D., Ridgway, I.D., Ramsay, K., 2013. The dog cockle, *Glycymeris glycymeris* (L.), a new annually-resolved sclerochronological archive for the Irish Sea. Palaeogeogr. Palaeoclimatol. Palaeoecol. 373, 133–140. https://doi.org/10.1016/j.palaeo.2012.03.030

Bronk Ramsey, C., 2009. Bayesian analysis of radiocarbon dates. Radiocarbon 51, 337–360. https://doi.org/10.2458/azu_js_rc.v51i1.3494

Bronk Ramsey, C., 2021. OxCal 4.4.4 calibration program. https://c14.arch.ox.ac.uk/oxcal/OxCal.html

Bronk Ramsey, C., van der Plicht, J., Weninger, B., 2001. 'Wiggle matching' radiocarbon dates. Radiocarbon 43, 381–389. https://doi.org/https://doi.org/10.1017/S0033822200038248

Buckley, M.W., Marshall, J., 2015. Observations, inferences, and mechanisms of the Atlantic Meridional Overturning Circulation: A review. Rev. Geophys. 54, 5–63. https://doi.org/10.1002/2015RG000493

Buddemeier, R.W., Maragos, J.E., Knutson, D.W., 1974. Radiographic studies of reef coral exoskeletons: Rates and patterns of coral growth. J. Exp. Mar. Bio. Ecol. 14, 179–199. https://doi.org/10.1016/0022-0981(74)90024-0

Buras, A., 2017. A comment on the expressed population signal. Dendrochronologia 44, 130–132. https://doi.org/10.1016/j.dendro.2017.03.005

Burrows, M., Thorpe, S.A., 1999. Drifter observations of the Hebrides slope current and nearby circulation patterns. Ann. Geophys. 17, 280–302. https://doi.org/10.1007/s005850050757

Burrows, M., Thorpe, S.A., Meldrum, D.T., 1999. Dispersion over the Hebridean and Shetland shelves and slopes. Cont. Shelf Res. 19, 49–55. https://doi.org/10.1016/S0278-4343(98)00082-X

Bušelić, I., Peharda, M., Reynolds, D.J., Butler, P.G., González, A.R., Ezgeta-Balić, D., Vilibić, I., Grbec, B., Hollyman, P., Richardson, C.A., 2015. *Glycymeris bimaculata* (Poli, 1795) - A new sclerochronological archive for the Mediterranean? J. Sea Res. 95, 139–148. https://doi.org/10.1016/j.seares.2014.07.011

Butler, P.G., Fraser, N.M., Scourse, J.D., Richardson, C.A., Bryant, C., Heinemeier, J., 2020. Is there a reliable taphonomic clock in the temperate North Atlantic? An example from a North Sea population of the mollusc *Arctica islandica*. Palaeogeogr. Palaeoclimatol. Palaeoecol. 560, 109975. https://doi.org/10.1016/j.palaeo.2020.109975

Butler, P.G., Richardson, C. A., Scourse, J.D., Wanamaker, Jr., A.D., Shammon, T.M., Bennell, J.D., 2010. Marine climate in the Irish Sea: analysis of a 489-year marine master chronology derived from growth increments in the shell of the clam *Arctica islandica*. Quat. Sci. Rev. 29, 1614–1632. https://doi.org/10.1016/j.quascirev.2009.07.010

Butler, P.G., Richardson, C.A., Scourse, J.D., Witbaard, R., Schöne, B.R., Fraser, N.M., Wanamaker, Jr., A.D., Bryant, C.L., Harris, I., Robertson, I., 2009a. Accurate increment identification and the spatial extent of the common signal in five *Arctica islandica* chronologies from the Fladen Ground, northern North Sea. Paleoceanography 24, PA2210. https://doi.org/10.1029/2008PA001715

Butler, P.G., Scourse, J.D., Richardson, C. A., Wanamaker, A.D.J., Bryant, C.L., Bennell, J.D., 2009b. Continuous marine radiocarbon reservoir calibration and the ^{13}C Suess effect in the Irish Sea: Results from the first multi-centennial shell-based marine master chronology. Earth Planet. Sci. Lett. 279, 230–241. https://doi.org/10.1016/j.epsl.2008.12.043

Butler, P.G., Wanamaker, A.D.J., Scourse, J.D., Richardson, C.A., Reynolds, D.J., 2013. Variability of marine climate on the North Icelandic Shelf in a 1357-year proxy archive based on growth increments in the bivalve *Arctica islandica*. Palaeogeogr. Palaeoclimatol. Palaeoecol. 373, 141–151. https://doi.org/10.1016/j.palaeo.2012.01.016

Cabral, J.P., Martins, J.M.S., 2016. Archaeological *Glycymeris glycymeris* shells perforated at the umbo: Natural or man-made holes? J. Archaeol. Sci. Reports 10, 474–482. https://doi.org/10.1016/j.jasrep.2016.11.008

Caesar, L., Mccarthy, G.D., Thornalley, D.J.R., Cahill, N., Rahmstorf, S., 2021. Current Atlantic Meridional Overturning Circulation weakest in last millennium. Nat. Geosci. 14, 118–121. https://doi.org/10.1038/s41561-021-00699-z

Cage, A.G., Austin, W.E.N., 2010. Marine climate variability during the last millennium: The Loch Sunart record, Scotland, UK. Quat. Sci. Rev. 29, 1633–1647. https://doi.org/10.1016/j.quascirev.2010.01.014

Campana, S.E., 1999. Chemistry and composition of fish otoliths: pathways, mechanisms and applications. Mar. Ecol. Prog. Ser. 188, 263–297.

Lo Giudice Cappelli, E., Austin, W.E.N., 2020. Marine Bivalve Feeding Strategies and Radiocarbon Ages in Northeast Atlantic Coastal Waters. Radiocarbon 62, 107–125. https://doi.org/10.1017/RDC.2019.68Carroll, M.L., Ambrose, W.G., Locke V, W.L., Ryan, S.K., Johnson, B.J., 2014. Bivalve growth rate and isotopic variability across the Barents Sea Polar Front. J. Mar. Syst. 130, 167–180. https://doi.org/10.1016/j.jmarsys.2013.10.006

Cartwright, D.E., 1969. Extraordinary Tidal Currents near St Kilda. Nature 223, 928–932.

Cartwright, D.E., Huthnance, J.M., Spencer, R., Vassie, J.M., 1980. On the St Kilda shelf tidal regime. Deep Sea Res. Part A, Oceanogr. Res. Pap. 27, 61–70. https://doi.org/10.1016/0198-0149(80)90072-2

Catchpole, E.A., Morgan, B.J.T., Coulson, T.N., Freeman, S.N., Albon, S.D., 2000. Factors influencing Soay sheep survival. J. R. Stat. Soc. Ser. C (Applied Stat.) 49, 453–472.

Charman, D.J., 2010. Centennial climate variability in the British Isles during the mid-late Holocene. Quat. Sci. Rev. 29, 1539–1554. https://doi.org/10.1016/j.quascirev.2009.02.017

Charman, D.J., McCarroll, D., 2010. Climate variability of the British Isles and adjoining seas. Quat. Sci. Rev. 29, 1503–1506. https://doi.org/10.1016/j.quascirev.2010.05.001

Chen, C.-T.A., Huang, T.-H., Chen, Y.-C., Bai, Y., He, X., Kang, Y., 2013. Air–sea exchanges of CO_2 in the world's coastal seas. Biogeosciences 10, 6509–6544. https://doi.org/10.5194/bg-10-6509-2013

Cheung, W.W.L., Lam, V.W.Y., Sarmiento, J.L., Kearney, K., Watson, R., Zeller, D., Pauly, D., 2010. Large-scale redistribution of maximum fisheries catch potential in the global ocean under climate change. Glob. Chang. Biol. 16, 24–35. https://doi.org/10.1111/j.1365-2486.2009.01995.x

Clark, G.R., 1968. Mollusk shell: daily growth lines. Science 161, 800–802. https://doi.org/10.1126/science.161.3843.800

Clark, P.U., Dyke, A.S., Shakun, J.D., Carlson, A.E., Clark, J., Wohlfarth, B., Mitrovica, J.X., Hostetler, S.W., McCabe, A.M., 2009. The Last Glacial Maximum. Science 325, 710–714. https://doi.org/10.1126/science.1172873

Clement, A., Bellomo, K., Murphy, L.N., Cane, M.A., Mauritsen, T., Stevens, B., 2015. The Atlantic Multidecadal Oscillation without a role for ocean circulation. Science 350, 320–324.

Clement, A., Cane, M.A., Murphy, L.N., Bellomo, K., Mauritsen, T., Stevens, B., 2016. Response to Comment on "The Atlantic Multidecadal Oscillation without a role for ocean circulation." Science 352, 1527-b.

Clutton-Brock, T.H., Pemberton, J.M., 2004. Soay Sheep: Dynamics and Selection in an Island Population. Cambridge University Press, Cambridge. https://doi.org/10.1644/05-mamm-r-364.1

Cochran, J.K., Kallenberg, K., Landman, N.H., Harries, P.J., Weinreb, D., Turekian, K.K., Beck, A., Cobban, W.A., 2010. Effect of diagenesis on the Sr, O, and C isotope composition of late cretaceous mollusks from the western interior seaway of North America. Am. J. Sci. 310, 69–88. https://doi.org/10.2475/02.2010.01

Cook, E.R., 1985. A time series analysis approach to tree ring standardization. Unpubl. PhD Thesis. University of Arizona, Tucson, USA.

Cook, E.R., Briffa, K.R., Meko, D.M., Graybill, D.A., Funkhouser, G., 1995. The 'segment length curse' in long tree-ring chronology development for palaeoclimatic studies. The Holocene 5, 229–237. https://doi.org/10.1177/095968369500500211

Cook, E.R., Krusic, P.J., 2005. Program ARSTAN: A tree-ring standardization program based on detrending and autoregressive time series modeling, with interactive graphics. Tree-Ring Laboratory Lamont Doherty Earth Observatory of Columbia University Palisades, NY.

Cook, E.R., Shiyatov, S.G., Mazepa, V.S., 1990. Tree-ring standardization and growth-trend estimation, in: Cook, E.R., Kairiukstis, L.A. (Eds.), Methods of Dendrochronology: Applications in the Environmental Sciences. Springer Science+Business Media, Dordrecht, pp. 104–123.

Coulson, T., Catchpole, E.A., Albon, S.D., Morgan, B.J.T., Pemberton, J.M., Clutton-Brock, T.H., Crawley, M.J., Grenfell, B.T., 2001. Age, sex, density, winter weather, and population crashes in Soay sheep. Science 292, 1528–1532.

Crippa, G., 2013. The shell ultrastructure of the genus *Glycymeris* Da Costa, 1778: A comparison between fossil and recent specimens. Riv. Ital. di Paleontol. e Stratigr. 119, 387–399.

Croll, D.A., Maron, J.L., Estes, J.A., Danner, E.M., Byrd, G. V., 2005. Introduced predators transform subarctic islands from grassland to tundra. Science 307, 1959–1961. https://doi.org/10.1126/science.1108485

Cunningham, L.K., Austin, W.E.N., Knudsen, K.L., Eiríksson, J., Scourse, J.D., Wanamaker, Jr., A.D., Butler, P.G., Cage, A.G., Richter, T., Husum, K., Hald, M., Andersson, C., Zorita, E., Linderholm, H.W., Gunnarson, B.E., Sicre, M.-A., Sejrup, H.P., Jiang, H., Wilson, R.J.S., 2013. Reconstructions of surface ocean conditions from the northeast Atlantic and Nordic seas during the last millennium. The Holocene 23, 921–935. https://doi.org/10.1177/0959683613479677

Curry, R.G., McCartney, M.S., 2001. Ocean gyre circulation changes associated with the North Atlantic Oscillation. J. Phys. Oceanogr. 31, 3374–3400. https://doi.org/10.1175/1520-0485(2001)031<3374:OGCCAW>2.0.CO;2

da Vinci, L., 1510 [1970 transl. edn]. *Codex Leicester* (1510) in The Notebooks of Leonardo da Vinci. Translated by J.P. Richter (original translation 1883).

De La Pierre, M., Carteret, C., Maschio, L., André, E., Orlando, R., Dovesi, R., 2014. The Raman spectrum of $CaCO_3$ polymorphs calcite and aragonite: A combined experimental and computational study. J. Chem. Phys. 140. https://doi.org/10.1063/1.4871900

Defant, A., 1929. Dynamische Ozeanographie. Springer, Berlin. https://doi.org/10.1097/00000658-190001000-00036

Department of Energy and Climate Change, 2016. UK Offshore Energy Strategic Environmental Assessment 3 (OESEA3). Appendix A1a.6 Birds.

Dettman, D., Lohmann, K., 1995. Microsampling carbonates for stable and minor element analysis: Physical separation on a 20 micrometer scale. J. Sediment. Res. A65, 566–569. https://doi.org/10.1306/D426813F-2B26-11D7-8648000102C1865D

Dettman, D.L., Reische, A.K., Lohmann, K.C., 1999. Controls on the stable isotope composition of seasonal growth bands in aragonitic fresh-water bivalves (Unionidae). Geochim. Cosmochim. Acta 63, 1049–1057.

Devereux, I., 1967. Temperature measeurements from oxygen isotope ratios of fish otoliths. Science 155, 1683–1685.

Doty, M.S., Oguri, M., 1956. The island mass effect. ICES J. Mar. Sci. 22, 33–37. https://doi.org/https://doi.org/10.1093/icesjms/22.1.33

Drinkwater, K.F., 2006. The regime shift of the 1920s and 1930s in the North Atlantic. Prog. Oceanogr. 68, 134–151. https://doi.org/10.1016/j.pocean.2006.02.011

Drinkwater, K.F., Belgrano, A., Borja, A., Conversi, A., Edwards, M., Greene, C.H., Ottersen, G., Pershing, A.J., Walker, H., 2003. The response of marine ecosystems to climate variability associated with the North Atlantic Oscillation, in: Hurrell, J.W., Kushnir, Y., Ottersen, G., Visbeck, M. (Eds.), The North Atlantic Oscillation: Climatic Significance and Environmental Impact. Geophysical Monograph Series 134. pp. 211–234.

Drinkwater, K.F., Miles, M., Medhaug, I., Otterå, O.H., Kristiansen, T., Sundby, S., Gao, Y., 2014. The Atlantic Multidecadal Oscillation: Its manifestations and impacts with special emphasis on the Atlantic region north of 60°N. J. Mar. Syst. 133, 117–130. https://doi.org/10.1016/j.jmarsys.2013.11.001

Driscoll, E.G., 1970. Selective bivalve shell destruction in marine environments, a field study. J. Sediment. Petrol. 40, 898–905.

Driscoll, E.G., 1967. Experimental field study of shell abrasion. J. Sediment. Petrol. 37, 1117–1123.

Edwards, M., Helaouet, P., Alhaija, R.A., Batten, S., Beaugrand, G., Chiba, S., Horaeb, R.R., Hosie, G., Mcquatters-Gollop, A., Ostle, C., Richardson, A.J., Rochester, W., Skinner, J., Stern, R., Takahashi, K., Taylor, C., Verheye, H.M., Wootton, M., 2016. Global Marine Ecological Status Report: results from the global CPR Survey 2014/2015. SAHFOS Technical Report.

Ellett, D.J., 1979. Some oceanographic features of Hebridean waters. Proc. R. Soc. Edinburgh 77B, 61–74.

Ellett, D.J., Edwards, A., 1983. Oceanography and inshore hydrography of the Inner Hebrides. Proc. R. Soc. Edinburgh 83B, 143–160.

Elliot, M., Welsh, K., Chilcott, C., McCulloch, M., Chappell, J., Ayling, B., 2009. Profiles of trace elements and stable isotopes derived from giant long-lived *Tridacna gigas* bivalves: Potential applications in paleoclimate studies. Palaeogeogr. Palaeoclimatol. Palaeoecol. 280, 132–142. https://doi.org/10.1016/j.palaeo.2009.06.007

Elliott, A.J., Clarke, T., Li, Z., 1991. Monthly distributions of surface and bottom temperatures in the northwest European shelf seas. Cont. Shelf Res. 11, 453–466. https://doi.org/10.1016/0278-4343(91)90053-9

Ellis, J.R., Cadman, P.S., Piertney, S.B., Geiger, D.L., 1995. The marine fauna of the St. Kilda archipelago. Scottish Nat. 107, 53–70.

Ellis, J.R., Milligan, S., Readdy, L., South, A., Taylor, N., Brown, M., 2010. MB5301 Mapping spawning and nursery areas of species to be considered in Marine Protected Areas (Marine Conservation Zones). Report No 1: Final Report on development of derived data layers for 40 mobile species considered to be of conservation importance.

Epstein, S., Buchsbaum, R., Lowenstam, H.A., Urey, H.C., 1953. Revised carbonate-water isotopic temperature scale. Bull. Geol. Soc. Am. 64, 1315–1326.

Erlenkeuser, H., 1976. 14C and13C Isotope concentration in modern marine mussels from sedimentary habitats. Naturwissenschaften 63, 338. https://doi.org/10.1007/BF00597312

Esper, J., Cook, E.R., Krusic, P.J., Peters, K., Schweingruber, F.H., 2003. Tests of the RCS method for preserving low-frequency variability in long tree-ring chronologies. Tree-Ring Res. 59, 81–98.

Featherstone, A.M., Butler, P.G., Schöne, B.R., Peharda, M., Thébault, J., 2020. A 45-year sub-annual reconstruction of seawater temperature in the Bay of Brest, France, using the shell oxygen isotope composition of the bivalve *Glycymeris glycymeris*. Holocene 30, 3–12. https://doi.org/10.1177/0959683619865592

Fleming, A., 1995. St Kilda: stone tools, dolerite quarries and long-term survival. Antiquity 69, 25–35. https://doi.org/10.1017/S0003598X00064279

Flessa, K.W., Cutler, A.H., Meldahl, K.H., 1993. Time and taphonomy: Quantitative estimates of time-averaging and stratigraphic disorder in a shallow marine habitat. Paleobiology 19, 266–286.

Foukal, N.P., Lozier, M.S., 2017. Assessing variability in the size and strength of the North Atlantic subpolar gyre. J. Geophys. Res. Ocean. 122, 6295–6308. https://doi.org/10.1002/2017JC012798

Frederiksen, M., Edwards, M., Richardson, A.J., Halliday, N.C., Wanless, S., 2006. From plankton to top predators: Bottom-up control of a marine food web across four trophic levels. J. Anim. Ecol. 75, 1259–1268. https://doi.org/10.1111/j.1365-2656.2006.01148.x

Frew, R.D., Dennis, P.F., Heywood, K.J., Meredith, M.P., Boswell, S.M., 2000. The oxygen isotope composition of water masses in the northern North Atlantic. Deep. Res. I 47, 2265–2286. https://doi.org/10.1016/S0967-0637(00)00023-6

Fromentin, J.M., Planque, B., 1996. *Calanus* and environment in the eastern North Atlantic. II. Influence of the North Atlantic Oscillation on *C. finmarchicus* and *C. helgolandicus*. Mar. Ecol. Prog. Ser. 134, 111–118. https://doi.org/10.3354/meps134101

Fukami, T., Wardle, D.A., Bellingham, P.J., Mulder, C.P.H., Towns, D.R., Yeates, G.W., Bonner, K.I., Durrett, M.S., Grant-Hoffman, M.N., Williamson, W.M., 2006. Above- and below-ground impacts of introduced predators in seabird-dominated island ecosystems. Ecol. Lett. 9, 1299–1307. https://doi.org/10.1111/j.1461-0248.2006.00983.x

Gámiz-Fortis, S.R., Pozo-Vázquez, D., Esteban-Parra, M.J., Castro-Díez, Y., 2002. Spectral characteristics and predictability of the NAO assessed through Singular Spectral Analysis. J. Geophys. Res. 107, 4685. https://doi.org/10.1029/2001JD001436

Gehrels, W.R., 2010. Late Holocene land- and sea-level changes in the British Isles: Implications for future sea-level predictions. Quat. Sci. Rev. 29, 1648–1660. https://doi.org/10.1016/j.quascirev.2009.09.015

Gilbertson, D.D., Schwenninger, J.-L., Kemp, R.A., Rhodes, E.J., 1999. Sand-drift and soil formation along an exposed North Atlantic Coastline: 14,000 years of diverse geomorphological, climatic and human impacts. J. Archaeol. Sci. 26, 439–469. https://doi.org/10.1006/JASC.1998.0360

Gillikin, D.P., Lorrain, A., Jolivet, A., Kelemen, Z., Chauvaud, L., Bouillon, S., 2017. High-resolution nitrogen stable isotope sclerochronology of bivalve shell carbonate-bound organics. Geochim. Cosmochim. Acta 200, 55–66. https://doi.org/10.1016/j.gca.2016.12.008

Golikov, A.N., Scarlato, O.A., 1973. Method for indirectly defining optimum temperatures of inhabitancy for marine cold-blooded animals. Mar. Biol. 20, 1–5. https://doi.org/10.1007/BF00387667

Gonfiantini, R., Stichler, W., Rozanski, K., 1995. Reference and intercomparison materials for stable isotopes of light elements. IAEA TECDOC 825, 67–74.

Good, S.A., Martin, M.J., Rayner, N.A., 2013. EN4: Quality controlled ocean temperature and salinity profiles and monthly objective analyses with uncertainty estimates. J. Geophys. Res. Ocean. 118, 6704–6716. https://doi.org/10.1002/2013JC009067

Goslin, J., Fruergaard, M., Sander, L., Gałka, M., Menviel, L., Monkenbusch, J., Thibault, N., Clemmensen, L.B., 2018. Holocene centennial to millennial shifts in North-Atlantic storminess and ocean dynamics. Sci. Rep. 8, 12778. https://doi.org/10.1038/s41598-018-29949-8

Gowen, R.J., Raine, R., Dickey-Collas, M., White, M., 1998. Plankton distributions in relation to physical oceanographic features on the southern Malin Shelf , August 1996. ICES J. Mar. Sci. 55, 1095–1111.

Graham, N.A.J., Wilson, S.K., Carr, P., Hoey, A.S., Jennings, S., MacNeil, M.A., 2018. Seabirds enhance coral reef productivity and functioning in the absence of invasive rats. Nature 559, 250–253. https://doi.org/10.1038/s41586-018-0202-3

Grosbois, V., Thompson, P.M., 2005. North Atlantic climate variation influences survival in adult fulmars. Oikos 109, 273–290.

Grossman, E.L., Ku, T.-L., 1986. Oxygen and carbon isotope fractionation in biogenic aragonite: Temperature effects. Chem. Geol. (Isotope Geosci. Sect. 59, 59–74.

Gulland, F.M.D., 1992. The role of nematode parasites in Soay sheep (*Ovis aries* L.) mortality during a population crash. Parasitology 105, 493–503. https://doi.org/10.1017/S0031182000074679

Halfar, J., Zack, T., Kronz, A., Zachos, J.C., 2000. Growth and high-resolution paleoenvironmental signals of rhodoliths (coralline red algae): A new biogenic archive. J. Geophys. Res. 105, 22,107-22,116.

Hallett, T.B., Coulson, T., Pilkington, J.G., Pemberton, J.M., Grenfell, B.T., 2004. Why large-scale climate indices seem to predict ecological processes better than local weather. Nature 430, 71–75. https://doi.org/10.1038/nature02638.1.

Hammer, Ø., Harper, D., Ryan, P., 2001. PAST: Paleontological statistics software package for education and data analysis. Palaeontol. Electron. 4, 9 pp.

Harkness, D.D., 1983. The extent of the natural ^{14}C deficiency in the coastal environment of the United Kingdom. J. Eur. Study Gr. Phys. Chem. Math. Tech. Appl. to Archaeol. PACT 8, 351–364.

Harris, D.B., Moore, C.G., Porter, J.S., Sanderson, W.G., Ware, F.J., Kamphausen, L., 2018. The establishment of site condition monitoring of the sea caves of the St Kilda and North Rona Special Areas of Conservation with supplementary data from Loch Eriboll, Scottish Natural Heritage Research Report No. 1044.

Harris, M.P., Murray, S., 1989. Birds of St Kilda, Institute of Terrestrial Ecology & Natural Environmental Research Council, UK.

Hátún, H., Sandø, A.B., Drange, H., Hansen, B., Valdimarsson, H., 2005. Influence of the Atlantic subpolar gyre on the thermohaline circulation. Science 309, 1841–1844. https://doi.org/10.1126/science.1114777

Hayward, P.J., Ryland, J.S. (Eds.), 1995. Handbook on the Marine Fauna of North-West Europe. Oxford University Press.

Heaton, T.J., Köhler, P., Butzin, M., Bard, E., Reimer, R.W., Austin, W.E.N., Ramsey, C.B., Grootes, P.M., Hughen, K.A., Kromer, B., Reimer, P.J., Adkins, J., Burke, A., Cook, M.S., Olsen, J., Skinner, L.C., 2020. Marine20 – The marine radiocarbon age calibration curve (0-55,000 cal BP). Radiocarbon 62, 779–820. https://doi.org/10.1017/RDC.2020.68

Helama, S., Hood, B.C., 2011. Stone Age midden deposition assessed by bivalve sclerochronology and radiocarbon wiggle-matching of *Arctica islandica* shell increments. J. Archaeol. Sci. 38, 452–460. https://doi.org/10.1016/j.jas.2010.09.029

Helama, S., Melvin, T.M., Briffa, K.R., 2017. Regional curve standardization: State of the art. The Holocene 27, 172–177. https://doi.org/10.1177/0959683616652709

Helama, S., Schöne, B.R., Kirchhefer, A.J., Nielsen, J.K., Rodland, D.L., Janssen, R., 2007. Compound response of marine and terrestrial ecosystems to varying climate: pre-anthropogenic perspective from bivalve shell growth increments and tree-rings. Mar. Environ. Res. 63, 185–99. https://doi.org/10.1016/j.marenvres.2006.08.003

Hersbach, H., Bell, B., Berrisford, P., Hirahara, S., Horányi, A., Muñoz-Sabater, J., Nicolas, J., Peubey, C., Radu, R., Schepers, D., Simmons, A., Soci, C., Abdalla, S., Abellan, X., Balsamo, G., Bechtold, P., Biavati, G., Bidlot, J., Bonavita, M., De Chiara, G., Dahlgren, P., Dee, D., Diamantakis, M., Dragani, R., Flemming, J., Forbes, R., Fuentes, M., Geer, A., Haimberger, L., Healy, S., Hogan, R.J., Hólm, E., Janisková, M., Keeley, S., Laloyaux, P., Lopez, P., Lupu, C., Radnoti, G., de Rosnay, P., Rozum, I., Vamborg, F., Villaume, S., Thépaut, J.-N., 2020. The ERA5 global reanalysis. Q. J. R. Meteorol. Soc. 146, 1999–2049. https://doi.org/10.1002/qj.3803

Hill, A.E., Horsburgh, K.J., Garvine, R.W., Gillibrand, P.A., Slesser, G., Turrell, W.R., Adams, R.D., 1997. Observations of a density-driven recirculation of the Scottish Coastal Current in the Minch. Estuar. Coast. Shelf Sci. 45, 473–484.

Holliday, N.P., 2003. Air-sea interaction and circulation changes in the northeast Atlantic. J. Geophys. Res. 108, 1–11. https://doi.org/10.1029/2002jc001344

Holliday, N.P., Gary, S., 2014. State of the eastern North Atlantic subpolar gyre: The Extended Ellett Line Programme Annual Report No. 2, Research & Consultancy Report No. 43, National Oceanography Centre.

Holliday, N.P., Hughes, S.L., Bacon, S., Beszczynska-Möller, A., Hansen, B., Lavín, A., Loeng, H., Mork, K.A., Østerhus, S., Sherwin, T., Walczowski, W., 2008. Reversal of the 1960s to 1990s freshening trend in the northeast North Atlantic and Nordic Seas. Geophys. Res. Lett. 35. https://doi.org/10.1029/2007GL032675

Holliday, N.P., Pollard, R.T., Read, J.F., Leach, H., Penny Holliday, N., Pollard, R.T., Read, J.F., Leach, H., 2000. Water mass properties and fluxes in the Rockall Trough,1975-1998. Deep. Res. 47, 1303–1332. https://doi.org/10.1016/S0967-0637(99)00109-0

Holligan, P.M., 1986. Phytoplankton distributions along the shelf break. Proc. R. Soc. Edinburgh 88B, 239–263.

Hollyman, P.R., Leng, M.J., Chenery, S.R.N., Laptikhovsky, V. V, Richardson, C.A., 2018. Statoliths of the whelk *Buccinum undatum*: a novel age determination tool. Mar. Ecol. Prog. Ser. 598, 261–272. https://doi.org/10.3354/meps12119

Holme, N.A., 1966. The bottom fauna of the English Channel. Part II. J. Mar. Biol. Assoc. United Kingdom 46, 401–493. https://doi.org/10.1017/S0025315400027193

Holmes, R.L., 1983. Computer-assisted quality control in tree-ring dating and measurement. Tree-Ring Bull. 43, 69–78.

Holt, J., Wakelin, S., Huthnance, J., 2009. Down-welling circulation of the northwest European continental shelf: A driving mechanism for the continental shelf carbon pump. Geophys. Res. Lett. 36. https://doi.org/10.1029/2009GL038997

Howells, R.J., Burthe, S.J., Green, J.A., Harris, M.P., Newell, M.A., Butler, A., Johns, D.G., Carnell, E.J., Wanless, S., Daunt, F., 2017. From days to decades: Short-and long-term variation in environmental conditions affect offspring diet composition of a marine top predator. Mar. Ecol. Prog. Ser. 583, 227–242. https://doi.org/10.3354/meps12343

Huang, B., Thorne, P.W., Banzon, V.F., Boyer, T., Chepurin, G., Lawrimore, J.H., Menne, M.J., Smith, T.M., Vose, R.S., Zhang, H.-M., 2017. Extended Reconstructed Sea Surface Temperature, Version 5 (ERSSTv5): Upgrades , Validations , and Intercomparisons. J. Clim. 30, 8179–8205. https://doi.org/10.1175/JCLI-D-16-0836.1

Hudson, J.H., Shinn, E.A., Halley, R.B., Lidz, B., 1976. Sclerochronology: A tool for interpreting past environments. Geology 4, 361–364. https://doi.org/10.1130/0091-7613(1976)4<361:SATFIP>2.0.CO;2

Hughes, S.L., Holliday, N.P., Colbourne, E., Ozhigin, V., Valdimarsson, H., Østerhus, S., Wiltshire, K., 2009. Comparison of *in situ* time-series of temperature with gridded sea surface temperature datasets in the north Atlantic. ICES J. Mar. Sci. 66, 1467–1479. https://doi.org/10.1093/icesjms/fsp041

Hughes, S.L., Holliday, N.P., Gaillard, F., 2012. Variability in the ICES/NAFO region between 1950 and 2009: Observations from the ICES Report on Ocean Climate. ICES J. Mar. Sci. 69, 706–719. https://doi.org/10.1093/icesjms/fss044

Hughes, S.L., Tinker, J., Dye, S., Andres, O., Berry, D.I., Hermanson, L., Hewitt, H., Holliday, N.P., Kent, E.C., Kennington, K., Inall, M., Smyth, T., 2017. Temperature. Mar. Clim. Chang. Impacts Partnersh. Sci. Rev. 22–41. https://doi.org/10.14465/2017.arc10.003.tem

Hunter, D.C., Pemberton, J.M., Pilkington, J.G., Morrissey, M.B., 2018. Quantification and decomposition of environment-selection relationships. Evolution (N. Y). 72, 851–866. https://doi.org/10.1111/evo.13461

Hurrell, J.W., Kushnir, Y., Ottersen, G., Visbeck, M., 2003. An overview of the North Atlantic Oscillation, in: Hurrell, J.W., Kushnir, Y., Ottersen, G., Visbeck, M. (Eds.), The North Atlantic Oscillation: Climatic Significance and Environmental Impact, Geophysical Monograph Series Vol. 134. AGU, Washington, DC, pp. 1–35. https://doi.org/10.1029/134GM01

Huthnance, J.M., 1992. Extensive slope currents and the ocean-shelf boundary. Prog. Oceanogr. 29, 161–196. https://doi.org/10.1016/0079-6611(92)90023-S

Huthnance, J.M., 1984. Slope Currents and "JEBAR." J. Phys. Oceanogr. 14, 795–810.

Huxel, G.R., McCann, K., 1998. Food web stability: The influence of trophic flows across habitats. Am. Nat. 152, 460–469. https://doi.org/10.1086/286182

Inall, M., Gillibrand, P., Griffiths, C., MacDougal, N., Blackwell, K., 2009. On the oceanographic variability of the North-West European Shelf to the West of Scotland. J. Mar. Syst. 77, 210–226. https://doi.org/10.1016/j.jmarsys.2007.12.012

IOC-UNESCO, 2021. Ocean Knowledge for a Sustainable Ocean Economy: Synergies between the Ocean Decade and the Outcomes of the Ocean Panel.

IPCC, 2022. Summary for Policymakers [H.-O. Pörtner, D.C. Roberts, E.S. Poloczanska, K. Mintenbeck, M. Tignor, A. Alegría, M. Craig, S. Langsdorf, S. Löschke, V. Möller, A. Okem (eds.)], in: H.-O. Pörtner, Roberts, D.C., Tignor, M., Poloczanska, E.S., Mintenbeck, K., Alegría, A., Craig, M., Langsdorf, S., Löschke, S., Möller, V., Okem, A., Rama, B. (Eds.), Climate Change 2022: Impacts, Adaptation, and Vulnerability. Contribution of Working Group II to the Sixth Assessment Report of the Intergovernmental Panel on Climate Change. Cambridge University Press, Cambridge.

Johns, D., Marine Biological Association of the UK, 2021. Selected CPR taxa data from standard areas C4 and C5. The Archive for Marine Species and Habitats Data (DASSH). Dataset. https://doi.org/10.17031/1757

Johnson, C., Inall, M., Häkkinen, S., 2013. Declining nutrient concentrations in the northeast Atlantic as a result of a weakening Subpolar Gyre. Deep. Res. Part I Oceanogr. Res. Pap. 82, 95–107. https://doi.org/10.1016/j.dsr.2013.08.007

Jones, D.S., 1983. Sclerochronology: reading the record of the molluscan shell. Am. Sci. 71, 384–391.

Jones, D.S., 1981. Annual growth increments in shells of *Spisula solidissima* record marine temperature variability. Science 211, 165–1687. https://doi.org/10.1126/science.211.4478.165

Jones, D.S., 1980. Annual cycle of shell growth increment formation in two continental shelf bivalves and its paleoecologic significance. Paleobiology 6, 331–340.

Jones, D.S., Thompson, I., Ambrose, W., 1978. Age and growth rate determinations for the Atlantic surf clam *Spisula solidissima* (Bivalvia: Mactracea), based on internal growth lines in shell cross-sections. Mar. Biol. 47, 63–70. https://doi.org/10.1007/BF00397019

Jones, S., Cottier, F., Inall, M., Griffiths, C., 2018. Decadal variability on the Northwest European continental shelf. Prog. Oceanogr. 161, 131–151. https://doi.org/10.1016/j.pocean.2018.01.012

Jones, S., Inall, M., Porter, M., Graham, J.A., Cottier, F., 2020. Storm-driven across-shelf oceanic flows into coastal waters. Ocean Sci. 16, 389–403. https://doi.org/10.5194/os-16-389-2020

Jones, S., 2016. Shelf edge exchange and the influence on coastal oceanography. PhD Thesis, University of Aberdeen, UK

Karney, G.B., Butler, P.G., Scourse, J.D., Richardson, C. a, Lau, K.H., Czernuszka, J.T., Grovenor, C.R.M., 2011. Identification of growth increments in the shell of the bivalve mollusc *Arctica islandica* using backscattered electron imaging. J. Microsc. 241, 29–36. https://doi.org/10.1111/j.1365-2818.2010.03403.x

Kendon, M., McCarthy, M., Jevrejeva, S., Matthews, A., Legg, T., 2019. State of the UK climate 2018. Int. J. Climatol. 39, 1–55. https://doi.org/10.1002/joc.6213

Kennish, M.J., Lutz, R.A., Rhoads, D.C., 1980. Preparation of acetate peels and fractured sections for observation of growth patterns within the bivalve shell, in: Rhoads, D.C., Lutz, R.A. (Eds.), Skeletal Growth of Aquatic Organisms: Biological Records of Environmental Change. Plenum Press, New York, pp. 597–601.

Kilbourne, K.H., Wanamaker, A.D., Moffa-Sanchez, P., Reynolds, D.J., Amrhein, D.E., Butler, P.G., Gebbie, G., Goes, M., Jansen, M.F., Little, C.M., Mette, M., Moreno-Chamarro, E., Ortega, P., Otto-Bliesner, B.L., Rossby, T., Scourse, J., Whitney, N.M., 2022. Atlantic circulation change still uncertain. Nat. Geosci. 15, 165–167. https://doi.org/10.1038/s41561-022-00896-4

Killam, D.E., Clapham, M.E., 2018. Identifying the ticks of bivalve shell clocks: seasonal growth in relation to temperature and food supply. Palaios 33, 228–236. https://doi.org/10.2110/palo.2017.072

Kirby-Smith, W.W., Barber, R.T., 1974. Suspension-feeding aquaculture systems: Effects of phytoplankton concentration and temperature on growth of the bay scallop. Aquaculture 3, 135–145. https://doi.org/10.1016/0044-8486(74)90108-2

Knight, J.R., Folland, C.K., Scaife, A.A., 2006. Climate impacts of the Atlantic Multidecadal Oscillation. Geophys. Res. Lett. 33, 2–5. https://doi.org/10.1029/2006GL026242

Knutson, D.W., Buddemeier, R.W., Smith, S. V., 1972. Coral chronometers: Seasonal growth bands in reef corals. Science 177, 270–272. https://doi.org/10.1126/science.177.4045.270

Kober, K., Webb, A., Win, I., Lewis, M., O'Brien, S., Wilson, L.J., Reid, J.B., 2010. An analysis of the numbers and distribution of seabirds within the British Fishery Limit aimed at identifying areas that qualify as possible marine SPAs, JNCC Report No. 431.

Kuhlbrodt, T., Griesel, A., Montoya, M., Levermann, A., Hofmann, M., Rahmstorf, S., 2007. On the driving processes of the Atlantic meridional overturning circulation. Rev. Geophys. 45. https://doi.org/10.1029/2004RG000166

Lees, J.M., Park, J., 1995. Multiple-taper spectral analysis: A stand-alone C-subroutine. Comput. Geosci. 21, 199–236. https://doi.org/10.1016/0098-3004(94)00067-5

Lescinsky, H., Titus, B., Hubbard, D., 2011. Live coral cover in the fossil record: an example from Holocene reefs of the Dominican Republic. Coral Reefs 31, 335–346. https://doi.org/10.1007/s00338-011-0863-y

Linnaeus, C., 1758. Systema Naturae per Regna Tria Naturae, Secundum Classes, Ordines, Genera, Species, Cum Characteribus, Differentiis, Synonymis, Locis, Editio decima, Reformata. Holmiae: Laurentius Salvius.

Linnaeus C., 1767. Caroli Linnaei...Systema Naturae per Regna Tria Naturae: Secundum Classes, Ordines, Genera, Species, Cum Characteribus, Differentiis, Synonymis, Locis, Editio duodecima. 1. Regnum Animale. 1 & 2 Holmiae, Laurentii Salvii. Holmiae [Stockholm]: Laurentii Salvii, 1–532 [1766], 533–1327 [1767].

Lozier, M.S., Owens, W.B., Curry, R.G., 1995. The climatology of the North Atlantic. Prog. Oceanogr. 36, 1–44. https://doi.org/10.1016/0079-6611(95)00013-5

Lynch-Stieglitz, J., Adkins, J.F., Curry, W.B., Dokken, T., Hall, I.R., Herguera, J.C., Hirschi, J.J.-M., Ivanova, E. V, Kissel, C., Marchal, O., Marchitto, T.M., McCave, I.N., McManus, J.F., Mulitza, S., Ninnemann, U., Peeters, F., Yu, E.-F., Zahn, R., 2007. Atlantic meridional overturning circulation during the Last Glacial Maximum. Science 316, 66–69. https://doi.org/10.1126/science.1137127

Mann, R., 1982. The seasonal cycle of gonadal development in *Arctica islandica* from the Southern New England Shelf. Fish. Bull. 80, 315–326.

Mann, R., Wolf, C.C., 1983. Swimming behaviour of larvae of the ocean quahog *Arctica islandica* in response to pressure and temperature. Mar. Ecol. Prog. Ser. 13, 211–218. https://doi.org/10.3354/meps013211

Marali, S., Schöne, B.R., 2015. Oceanographic control on shell growth of *Arctica islandica* (Bivalvia) in surface waters of Northeast Iceland - Implications for paleoclimate reconstructions. Palaeogeogr. Palaeoclimatol. Palaeoecol. 420, 138–149. https://doi.org/10.1016/j.palaeo.2014.12.016

Marchal, O., Cacho, I., Stocker, T.F., Grimalt, J.O., Calvo, E., Martrat, B., Shackleton, N., Vautravers, M., Cortijo, E., Van Kreveld, S., Andersson, C., Koç, N., Chapman, M., Sbaffi, L., Duplessy, J.C., Sarnthein, M., Turon, J.L., Duprat, J., Jansen, E., 2002. Apparent long-term cooling of the sea surface in the northeast Atlantic and Mediterranean during the Holocene. Quat. Sci. Rev. 21, 455–483. https://doi.org/10.1016/S0277-3791(01)00105-6

Marchitto, T.M., Jones, G.A., Goodfriend, G.A., Weidman, C.R., 2000. Precise temporal correlation of Holocene mollusk shells using sclerochronology. Quat. Res. 53, 236–246. https://doi.org/10.1006/qres.1999.2107

Marret, F., Scourse, J., Austin, W., 2004. Holocene shelf-sea seasonal stratification dynamics: a dinoflagellate cyst record from the Celtic Sea, NW European shelf. The Holocene 5, 689–696.

Martin, M., 1698 [1753 edn]. A Voyage to St Kilda. D. Brown & L. Davis, London.

Martín-García, R., Alonso-Zarza, A.M., Frisia, S., Rodríguez-Berriguete, Á., Drysdale, R., Hellstrom, J., 2019. Effect of aragonite to calcite transformation on the geochemistry and dating accuracy of speleothems. An example from Castañar Cave, Spain. Sediment. Geol. 383, 41–54. https://doi.org/10.1016/j.sedgeo.2019.01.014

McCauley, D.J., Desalles, P.A., Young, H.S., Dunbar, R.B., Dirzo, R., Mills, M.M., Micheli, F., 2012. From wing to wing: The persistence of long ecological interaction chains in less-disturbed ecosystems. Sci. Rep. 2. https://doi.org/10.1038/srep00409

Mette, M.J., Wanamaker Jr., A.D., Carroll, M.L., Ambrose Jr., W.G., Retelle, M.J., 2016. Linking large-scale climate variability with *Arctica islandica* shell growth and geochemistry in northern Norway. Limnol. Oceanogr. 61, 748–764. https://doi.org/10.1002/lno.10252

Mette, M.J., Wanamaker Jr., A.D., Retelle, M.J., Carroll, M.L., Andersson, C., Ambrose Jr., W.G., 2021. Persistent multidecadal variability since the 15th century in the southern Barents Sea derived from annually resolved shell-based records. J. Geophys. Res. Ocean. 126. https://doi.org/10.1029/2020JC017074

Mette, M.J., Whitney, N.M., Ballew, J., Wanamaker, Jr., A.D., 2018. Unexpected isotopic variability in biogenic aragonite: A user issue or proxy problem? Chem. Geol. 483, 286–294. https://doi.org/10.1016/j.chemgeo.2018.02.027

Moffa-Sánchez, P., Born, A., Hall, I.R., Thornalley, D.J.R., Barker, S., 2014. Solar forcing of North Atlantic surface temperature and salinity over the past millennium. Nat. Geosci. 7, 275–278. https://doi.org/10.1038/ngeo2094

Morton, B., 2011. The biology and functional morphology of *Arctica islandica* (Bivalvia: Arcticidae) – A gerontophilic living fossil. Mar. Biol. Res. 7, 540–553. https://doi.org/10.1080/17451000.2010.535833

Mulder, C.P.H., Jones, H.P., Kameda, K., Palmborg, C., Schmidt, S., Ellis, J.C., Orrock, J.L., Alexander Wait, D., Wardle, D.A., Yang, L.H., Young, H., Croll, D.A., Vidal, E., 2011. Impacts of seabirds on plant and soil properties. Seab. Islands Ecol. Invasion, Restor. https://doi.org/10.1093/acprof:osobl/9780199735693.003.0005

National Trust for Scotland, 2012. St Kilda world heritage site management plan 2012-2017.

Ninnemann, U.S., Thornalley, D.J.R., 2016. Recent natural variability of the Iceland Scotland Overflows on decadal to millennial timescales: Clues from the ooze. US Clivar Var. 14, 1–7.

Olsen, J., Anderson, N.J., Knudsen, M.F., 2012. Variability of the North Atlantic Oscillation over the past 5,200 years. Nat. Geosci. 5, 808–812. https://doi.org/10.1038/ngeo1589

Olsson, I.U., 1980. Content of ^{14}C in marine mammals from Northern Europe. Radiocarbon 22, 662–675.

Ong, J.J.L., Rountrey, A.N., Zinke, J., Meeuwig, J.J., Grierson, P.F., O'Donnell, A.J., Newman, S.J., Lough, J.M., Trougan, M., Meekan, M.G., 2016. Evidence for climate-driven synchrony of marine and terrestrial ecosystems in northwest Australia. Glob. Chang. Biol. 22, 2776–2786. https://doi.org/10.1111/gcb.13239

Orme, L.C., Charman, D.J., Reinhardt, L., Jones, R.T., Mitchell, F.J.G., Stefanini, B.S., Barkwith, A., Ellis, M.A., Grosvenor, M., 2017. Past changes in the North Atlantic storm track driven by insolation and sea-ice forcing. Geology 45, 335–338. https://doi.org/10.1130/G38521.1

Orme, L.C., Miettinen, A., Divine, D., Husum, K., Pearce, C., Van Nieuwenhove, N., Born, A., Mohan, R., Seidenkrantz, M.-S., 2018. Subpolar North Atlantic sea surface temperature since 6 ka BP: Indications of anomalous ocean-atmosphere interactions at 4-2 ka BP. Quat. Sci. Rev. 194, 128–142. https://doi.org/10.1016/j.quascirev.2018.07.007

Orme, L.C., Reinhardt, L., Jones, R.T., Charman, D.J., Barkwith, A., Ellis, M.A., 2016. Aeolian sediment reconstructions from the Scottish Outer Hebrides: Late Holocene storminess and the role of the North Atlantic Oscillation. Quat. Sci. Rev. 132, 15–25. https://doi.org/10.1016/j.quascirev.2015.10.045

Oschmann, W., 2009. Sclerochronology: editorial. Int. J. Earth Sci. 98, 1–2. https://doi.org/10.1007/s00531-008-0403-3

Östlund, H.G.; Grall, C., 2001. Part of the global seawater delta oxygen-18 database from reference Östlund 1993. PANGAEA, https://doi.org/10.1594/PANGAEA.58084

Ottersen, G., Planque, B., Belgrano, A., Post, E., Reid, P.C., Stenseth, N.C., 2001. Ecological effects of the North Atlantic Oscillation 1770, 1–14. https://doi.org/10.1007/s004420100655

Paillard, D., Labeyrie, L., Yiou, P., 1996. AnalySeries 1.0: a Macintosh software for the analysis of geophysical time-series. Eos, Trans. AGU 77, 379.

Painter, S.C., Hartman, S.E., Kivimae, C., Salt, L.A., Clargo, N.M., Bozec, Y., Daniels, C.J., Jones, S.C., Hemsley, V.S., Munns, L.R., Allen, S.R., 2016. Carbon exchange between a shelf sea and the ocean: The Hebrides Shelf, west of Scotland. J. Geophys. Res. Ocean. 121, 4522–4544. https://doi.org/10.1002/2015JC011599

Parker, J.E., Thompson, S.P., Lennie, A.R., Potter, J., Tang, C.C., 2010. A study of the aragonite-calcite transformation using Raman spectroscopy, synchrotron powder diffraction and scanning electron microscopy. CrystEngComm 12, 1590–1599. https://doi.org/10.1039/B921487A

Pearson, C., Salzer, M., Wacker, L., Brewer, P., Sookdeo, A., Kuniholm, P., 2020. Securing timelines in the ancient Mediterranean using multiproxy annual tree-ring data. Proc. Natl. Acad. Sci. 117. https://doi.org/10.1073/pnas.1917445117

Pederson, C., Mavromatis, V., Dietzel, M., Rollion-Bard, C., Nehrke, G., Jöns, N., Jochum, K.P., Immenhauser, A., 2019. Diagenesis of mollusc aragonite and the role of fluid reservoirs. Earth Planet. Sci. Lett. 514, 130–142. https://doi.org/10.1016/j.epsl.2019.02.038

Pingree, R.D., Holligan, P.M., Mardell, G.T., 1978. The effects of vertical stability on phytoplankton distributions in the summer on the northwest European Shelf. Deep. Res. 25. https://doi.org/10.1016/0146-6291(78)90584-2

Pingree, R.D., Sinha, B., Griffiths, C.R., 1999. Seasonality of the European slope current (Goban Spur) and ocean margin exchange. Cont. Shelf Res. 19, 929–975.

Planque, B., Fromentin, J.-M., 1996. *Calanus* and environment in the eastern North Atlantic. I. Spatial and temporal patterns of *C. finmarchicus* and *C. helgolandicus*. Mar. Ecol. Prog. Ser. 134, 101–109.

Polis, G.A., Anderson, W.B., Holt, R.D., 1997. Toward an integration of landscape and food web ecology: The dynamics of spatially subsidized food webs. Annu. Rev. Ecol. Syst. 28, 289–316. https://doi.org/10.1146/annurev.ecolsys.28.1.289

Polis, G.A., Hurd, S.D., 1996. Linking marine and terrestrial food webs: allochthonous input from the ocean supports high secondary productivity on small islands and coastal land communities. Am. Nat. 147, 396–423.

Porter, M., Dale, A.C., Jones, S., Siemering, B., Inall, M.E., 2018. Cross-slope flow in the Atlantic Inflow Current driven by the on-shelf deflection of a slope current. Deep. Res. Part I Oceanogr. Res. Pap. 140, 173–185. https://doi.org/10.1016/j.dsr.2018.09.002

Post, E., Forchhammer, M.C., 2002. Synchronization of animal population dynamics by large-scale climate. Nature 420, 168–171. https://doi.org/10.1038/nature01064

Post, E., Stenseth, N.C.H.R., 1998. Large-Scale climatic fluctuation and population dynamics of moose and white-tailed deer. J. Anim. Ecol. 67, 537–543.

Proctor, R., Holt, J.T., Allen, J.I., Blackford, J., 2003. Nutrient fluxes and budgets for the North West European Shelf from a three-dimensional model. Sci. Total Environ. 314–316, 769–785. https://doi.org/10.1016/S0048-9697(03)00083-4

Prouty, N.G., Roark, E.B., Koenig, A.E., Demopoulos, A.W.J., Batista, F.C., Kocar, B.D., Selby, D., McCarthy, M.D., Mienis, F., Ross, S.W., 2014. Deep-sea coral record of human impact on watershed quality in the Mississippi River Basin. Global Biogeochem. Cycles 28, 29–43. https://doi.org/10.1002/2013GB004754.Received

Rahmstorf, S., 2015. Thermohaline Circulation. Ref. Modul. Earth Syst. Environ. Sci. 1–12. https://doi.org/10.1016/b978-0-12-409548-9.09514-2

Rayner, N.A., Parker, D.E., Horton, E.B., Folland, C.K., Alexander, L. V., Rowell, D.P., Kent, E.C., Kaplan, A., 2003. Global analyses of sea surface temperature, sea ice, and night marine air temperature since the late nineteenth century. J. Geophys. Res. 108, 4407. https://doi.org/10.1029/2002JD002670

Reid, P.C., Colebrook, J.M., Matthews, J.B.L., Aiken, J., 2003. The Continuous Plankton Recorder: concepts and history, from Plankton Indicator to undulating recorders. Prog. Oceanogr. 58, 117–173. https://doi.org/10.1016/j.pocean.2003.08.002

Reid, P.C., Holliday, N.P., Smyth, T.J., 2001. Pulses in the eastern margin current and warmer water off the north west European shelf linked to North Sea ecosystem changes. Mar. Ecol. Prog. Ser. 215, 283–287.

Reimer, P., Hoper, S., McDonald, J., Reimer, R., Svyatko, S., Thompson, M., 2015. Laboratory Protocols Used for AMS Radiocarbon Dating at the ^{14}Chrono Centre, Research Report Series.

Reimer, P.J., McCormac, F.G., Moore, J., McCormick, F., Murray, E. V, 2002. Marine radiocarbon reservoir corrections for the mid- to late Holocene in the eastern subpolar North Atlantic. Holocene 12, 129–135. https://doi.org/10.1191/0959683602h1528rpReynolds, D.J., Butler, P.G., Williams, S.M., Scourse, J.D., Richardson, C.A., Wanamaker Jr., A.D., Austin, W.E.N., Cage, A.G., Sayer, M.D.J., 2013. A multiproxy reconstruction of Hebridean (NW Scotland) spring sea surface temperatures between AD 1805 and 2010. Palaeogeogr. Palaeoclimatol. Palaeoecol. 386, 275–285. https://doi.org/10.1016/j.palaeo.2013.05.029

Reynolds, D.J., Hall, I.R., Slater, S.M., Mette, M.J., Wanamaker, A.D., Scourse, J.D., Garry, F.K., Halloran, P.R., 2018. Isolating and reconstructing key components of North Atlantic Ocean variability from a sclerochronological spatial network. Paleoceanogr. Paleoclimatology 33, 1086–1098. https://doi.org/10.1029/2018PA003366

Reynolds, D.J., Hall, I.R., Slater, S.M., Scourse, J.D., Halloran, P.R., Sayer, M.D.J., 2017. Reconstructing past seasonal to multicentennial-scale variability in the NE Atlantic Ocean using the long-lived marine bivalve mollusk *Glycymeris glycymeris*. Paleoceanography 32. https://doi.org/10.1002/2017PA003154

Reynolds, D.J., Richardson, C.A., Scourse, J.D., Butler, P.G., Hollyman, P., Román-González, A., Hall, I.R., 2017. Reconstructing North Atlantic marine climate variability using an absolutely-dated sclerochronological network. Palaeogeogr. Palaeoclimatol. Palaeoecol. 465, 333–346. https://doi.org/10.1016/j.palaeo.2016.08.006

Reynolds, D.J., Scourse, J.D., Halloran, P.R., Nederbragt, A.J., Wanamaker, A.D.J., Butler, P.G., Richardson, C.A., Heinemeier, J., Eiríksson, J., Knudsen, K.L., Hall, I.R., 2016. Annually resolved North Atlantic marine climate over the last millennium. Nat. Commun. 7:13502. https://doi.org/10.1038/ncomms13502

Reynolds, R.W., Rayner, N.A., Smith, T.M., Stokes, D.C., Wang, W., 2002. An improved *in situ* and satellite SST analysis for climate. J. Clim. 15, 1609–1625.

Richardson, A.J., Walne, A.W., John, A.W.G., Jonas, T.D., Lindley, J.A., Sims, D.W., Stevens, D., Witt, M., 2006. Using continuous plankton recorder data. Prog. Oceanogr. 68, 27–74. https://doi.org/10.1016/j.pocean.2005.09.011

Richardson, C.A., 2001. Molluscs as archives of environmental change. Oceanogr. Mar. Biol. an Annu. Rev. 39, 103–164.

Rienecker, M.M., Suarez, M.J., Gelaro, R., Todling, R., Bacmeister, J., Liu, E., Bosilovich, M.G., Schubert, S.D., Takacs, L., Kim, G.-K., Bloom, S., Chen, J., Collins, D., Conaty, A., da Silva, A., Gu, W., Joiner, J., Koster, R.D., Lucchesi, R., Molod, A., Owens, T., Pawson, S., Pegion, P., Redder, C.R., Reichle, R., Robertson, F.R., Ruddick, A.G., Sienkiewicz, M., Woollen, J., 2011. MERRA : NASA's Modern-Era Retrospective Analysis for Research and Applications. J. Clim. 24, 3624–3648. https://doi.org/10.1175/JCLI-D-11-00015.1

Robson, J., Hodson, D., Hawkins, E., Sutton, R., 2014. Atlantic overturning in decline? Nat. Geosci. 7, 2–3. https://doi.org/10.1038/ngeo2050

Rogalla, N.S., Amler, M.R.W., 2007. Statistic approach on taphonomic phenomena in shells of *Glycymeris glycymeris* (Bivalvia: Glycymerididae) and its significance in the fossil record. Paläontologische Zeitschrift 81, 334–355.

Rogers, J.C., 1985. Atmospheric circulation changes associated with the warming over the northern North Atlantic in the 1920s. J. Clim. Appl. Meteorol. 24, 1303–1310.

Rohling, E.J., 2013. Oxygen isotope composition of seawater, in: Elias, S.A. (Ed.), The Encyclopedia of Quaternary Science. Amsterdam: Elsevier, pp. 915–922. https://doi.org/10.1016/B978-0-444-53643-3.00293-4

Ropes, J.W., 1987. Preparation of acetate peels of valves from the ocean quahog, *Arctica islandica*, for age determinations. NOAA Tech. Rep. NMFS 50 1–5.

Rossby, T., 1996. The North Atlantic Current and surrounding waters: at the crossroads. Rev. Geophys. 34, 463–481.

Royer, C., Thébault, J., Chauvaud, L., Olivier, F., 2013. Structural analysis and paleoenvironmental potential of dog cockle shells (*Glycymeris glycymeris*) in Brittany, northwest France. Palaeogeogr. Palaeoclimatol. Palaeoecol. 373, 123–132. https://doi.org/10.1016/j.palaeo.2012.01.033

Russell, N., Cook, G.T., Ascough, P.L., Scott, E.M., 2015. A period of calm in Scottish seas: A comprehensive study of δR values for the northern British Isles coast and the consequent implications for archaeology and oceanography. Quat. Geochronol. 30, 34–41. https://doi.org/10.1016/j.quageo.2015.08.001

Schlitzer, R., 2020. Ocean Data View, http://odv.awi.de

Schmidt, G.A., Bigg, G.R., Rohling, E.J., 1999. Global seawater oxygen-18 database – v1.22. https://data.giss.nasa.gov/o18data/

Schmitt, R.W., 2018. The ocean's role in climate. Oceanography 31, 32–40. https://doi.org/10.5670/oceanog.2018.225

Schöne, B.R., 2013. *Arctica islandica* (Bivalvia): A unique paleoenvironmental archive of the northern North Atlantic Ocean. Glob. Planet. Change 111, 199–225. https://doi.org/10.1016/j.gloplacha.2013.09.013

Schöne, B.R., Fiebig, J., 2009. Seasonality in the North Sea during the Allerød and Late Medieval Climate Optimum using bivalve sclerochronology. Int. J. Earth Sci. 98, 83–98. https://doi.org/10.1007/s00531-008-0363-7

Schöne, B.R., Fiebig, J., Pfeiffer, M., Gleß, R., Hickson, J., Johnson, A.L.A., Dreyer, W., Oschmann, W., 2005. Climate records from a bivalved Methuselah (*Arctica islandica*, Mollusca; Iceland). Palaeogeogr. Palaeoclimatol. Palaeoecol. 228, 130–148. https://doi.org/10.1016/j.palaeo.2005.03.049

Schöne, B.R., Gillikin, D.P., 2013. Unraveling environmental histories from skeletal diaries - Advances in sclerochronology. Palaeogeogr. Palaeoclimatol. Palaeoecol. 373, 1–5. https://doi.org/10.1016/j.palaeo.2012.11.026

Schöne, B.R., Goodwin, D.H., Flessa, K.W., Dettman, D.L., Roopnarine, P.D., 2002. Sclerochronology and growth of the bivalve mollusks *Chione* (Chionista) *fluctifraga* and *C.* (Chionista) *cortezi* in the northern Gulf of California, Mexico. Veliger 45, 45–54.

Schöne, B.R., Huang, Q., 2021. Ontogenetic $\delta^{15}N$ trends and multidecadal variability in shells of the bivalve mollusk, *Arctica islandica*. Front. Mar. Sci. 8, 1–15. https://doi.org/10.3389/fmars.2021.748593

Schöne, B.R., Oschmann, W., Rössler, J., Freyre Castro, A.D., Houk, S.D., Kröncke, I., Dreyer, W., Janssen, R., Rumohr, H., Dunca, E., 2003. North Atlantic Oscillation dynamics recorded in shells of a long-lived bivalve mollusk. Geology 31, 1037–1040. https://doi.org/10.1130/G20013.1

Scott, A., 1960. The fauna of the sandy beach, Village Bay, St. Kilda: A dynamical relationship. Oikos 11, 153–160.

Scottish Executive, 2003. Revised Nomination of St Kilda for inclusion in the World Heritage Site List. Scottish Executive, Edinburgh.

Scourse, J., Richardson, C., Forsythe, G., Harris, I., Heinemeier, J., Fraser, N., Briffa, K., Jones, P., 2006. First cross-matched floating chronology from the marine fossil record: data from growth lines of the long-lived bivalve mollusc *Arctica islandica*. The Holocene 16, 967–974. https://doi.org/10.1177/0959683606hl987rp

Scourse, J.D., Austin, W.E.N., Long, B.T., Assinder, D.J., Huws, D., 2002. Holocene evolution of seasonal stratification in the Celtic Sea: Refined age model, mixing

depths and foraminiferal stratigraphy. Mar. Geol. 191, 119–145. https://doi.org/10.1016/S0025-3227(02)00528-5

Scourse, J.D., Wanamaker Jr, A.D., Weidman, C., Heinemeier, J., Reimer, P.J., Butler, P.G., Witbaard, R., Richardson, C.A., 2012. The marine radiocarbon bomb pulse across the temperate North Atlantic: A compilation of $\Delta^{14}C$ time histories from *Arctica islandica* growth increments. Radiocarbon 54, 165–186. https://doi.org/10.2458/azu_js_rc.v54i2.16026

Seager, R., Battisti, D.S., Yin, J., Gordon, N., Naik, N., Clement, A.C., Cane, M.A., 2002. Is the Gulf Stream responsible for Europe's mild winters? Q. J. R. Meteorol. Soc. 128, 2563–2586. https://doi.org/10.1256/qj.01.128

Shapiro, G.I., Hill, A.E., 1997. Dynamics of dense water cascades at the shelf edge. J. Phys. Oceanogr. 27, 2381–2394.

Shapiro, G.I., Huthnance, J.M., Ivanov, V. V, 2003. Dense water cascading off the continental shelf. J. Geophys. Res. 108. https://doi.org/10.1029/2002JC001610

Shatova, O., Wing, S.R., Gault-Ringold, M., Wing, L., Hoffmann, L.J., 2016. Seabird guano enhances phytoplankton production in the Southern Ocean. J. Exp. Mar. Bio. Ecol. 483, 74–87. https://doi.org/10.1016/j.jembe.2016.07.004

Shumway, S.E., Cucci, T.L., Newell, R.C., Yentsch, C.M., 1985. Particle selection, ingestion, and absorption in filter-feeding bivalves. J. Exp. Mar. Bio. Ecol. 91, 77–92. https://doi.org/10.1016/0022-0981(85)90222-9

Siemering, B., Bresnan, E., Painter, S.C., Daniels, C.J., Inall, M., Davidson, K., 2016. Phytoplankton distribution in relation to environmental drivers on the North West European Shelf sea. PLoS One 11, e0164482. https://doi.org/10.1371/journal.pone.0164482

Simmonds, E.G., Coulson, T., 2015. Analysis of phenotypic change in relation to climatic drivers in a population of Soay sheep *Ovis aries*. Oikos 124, 543–552. https://doi.org/10.1111/oik.01727

Simpson, J.H., 1997. Physical processes in the ROFI regime. J. Mar. Syst. 12, 3–15.

Simpson, J.H., Edelsten, D.J., Edwards, A., Morris, N.C.G., Tett, P.B., 1979. The Islay Front: Physical structure and phytoplankton distribution. Estuar. Coast. Mar. Sci. 9, 713–726.

Simpson, J.H., Hill, A.E., 1986. The Scottish Coastal Current, in: Skreslet, S. (Ed.), The Role of Freshwater Outflow in Coastal Marine Ecosystems. NATO ASI Series (Series G: Ecological Sciences), Vol. 7. Springer, Berlin, Heidelberg, pp. 295–308. https://doi.org/10.1007/978-3-642-70886-2_21

Simpson, J.H., McCandliss, R.R., 2013. "The Ekman Drain": a conduit to the deep ocean for shelf material. Ocean Dyn. 1063–1072. https://doi.org/10.1007/s10236-013-0644-y

Simpson, J.H., Tett, P.B., 1986. Island stirring effects on phytoplankton growth, in: Bowman, J., Yentsch, M., Peterson, W.T. (Eds.), Tidal Mixing and Plankton Dynamics.

Lecture Notes on Coastal and Estuarine Studies. Springer Berlin Heidelberg, pp. 41–76.

Smeed, D.A., Josey, S.A., Beaulieu, C., Johns, W.E., Moat, B.I., Frajka-Williams, E., Rayner, D., Meinen, C.S., Baringer, M.O., Bryden, H.L., McCarthy, G.D., 2018. The North Atlantic Ocean is in a state of reduced overturning. Geophys. Res. Lett. 45, 1527–1533. https://doi.org/10.1002/2017GL076350

Smith, A.F., Fryer, R.J., Webster, L., Berx, B., Taylor, A., Walsham, P., Turrell, W.R., 2014. Setting background nutrient levels for coastal waters with oceanic influences. Estuar. Coast. Shelf Sci. 145, 69–79. https://doi.org/10.1016/j.ecss.2014.04.006

Smith, T.M., Reynolds, R.W., Peterson, T.C., Lawrimore, J., 2008. Improvements to NOAA's historical merged land-ocean surface temperature analysis (1880-2006). J. Clim. 21, 2283–2296. https://doi.org/10.1175/2007JCLI2100.1

Solignac, S., Grelaud, M., de Vernal, A., Giraudeau, J., Moros, M., McCave, I.N., Hoogakker, B., 2008. Reorganization of the upper ocean circulation in the mid-Holocene in the northeastern Atlantic. Can. J. Earth Sci. 45, 1417–1433. https://doi.org/10.1139/E08-061

Souza, A.J., Simpson, J.H., Harikrishnan, M., Malarkey, J., 2001. Flow structure and seasonality in the Hebridean slope current. Oceanol. Acta 24, 63–76. https://doi.org/10.1016/S0399-1784(00)01103-8

Steel, T., 1975 [2011 edn]. The Life and Death of St Kilda. HarperPress, London, 304 pp.

Steinhilber, F., Abreu, J.A., Beer, J., Brunner, I., Christl, M., Fischer, H., Heikkilä, U., Kubik, P.W., Mann, M., McCracken, K.G., Miller, H., Miyahara, H., Oerter, H., Wilhelms, F., 2012. 9,400 years of cosmic radiation and solar activity from ice cores and tree rings. Proc. Natl. Acad. Sci. U. S. A. 109, 5967–5971. https://doi.org/10.1073/pnas.1118965109

Steinhilber, F., Beer, J., Fröhlich, C., 2009. Total solar irradiance during the Holocene. Geophys. Res. Lett. 36, L19704.

Strom, A., Francis, R.C., Mantua, N.J., Miles, E.L., Peterson, D.L., 2005. Preserving low-frequency climate signals in growth records of geoduck clams (*Panopea abrupta*). Palaeogeogr. Palaeoclimatol. Palaeoecol. 228, 167–178. https://doi.org/10.1016/j.palaeo.2005.03.048

Stuiver, M., Braziunas, T.F., 1993. Modeling atmospheric ^{14}C influences and ^{14}C ages of marine samples to 10,000 BC. Radiocarbon 35, 137–189. https://doi.org/10.1017/S0033822200013874Surge, D., Wang, T., Gutiérrez-Zugasti, I.G., Kelley, P.H., 2013. Isotope sclerochronology and season of annual growth line formation in limpet shells (*Patella vulgata*) from warm- and cold-temperate zones in the eastern North Atlantic. Palaios 28, 386–393. https://doi.org/10.2110/palo.2012.p12-038r

Sutherland, D.G., 1984. The submerged landforms of the St. Kilda archipelago, western Scotland. Mar. Geol. 58, 435–442.

Sutherland, D.G., Ballantyne, C.K., Walker, M.J.C., 1984. Late Quaternary glaciation and environmental change on St. Kilda, Scotland, and their palaeoclimatic significance. Boreas 13, 261–272.

Swan, L.W., 1963. Aeolian zone. Science 140, 77–78. https://doi.org/10.1126/science.140.3562.78

Swindles, G.T., Lawson, I.T., Matthews, I.P., Blaauw, M., Daley, T.J., Charman, D.J., Roland, T.P., Plunkett, G., Schettler, G., Gearey, B.R., Turner, T.E., Rea, H.A., Roe, H.M., Amesbury, M.J., Chambers, F.M., Holmes, Jonathan, Mitchell, F.J.G., Blackford, J., Blundell, A., Branch, N., Holmes, Jane, Langdon, P., McCarroll, J., McDermott, F., Oksanen, P.O., Pritchard, O., Stastney, P., Stefanini, B., Young, D., Wheeler, J., Becker, K., Armit, I., 2013. Centennial-scale climate change in Ireland during the Holocene. Earth-Science Rev. 126, 300–320. https://doi.org/10.1016/j.earscirev.2013.08.012

Taylor, A.C., 1976. Burrowing behaviour and anaerobiosis in the bivalve *Arctica islandica* (L.). J. Mar. Biol. Assoc. United Kingdom 56, 95–109. https://doi.org/10.1017/S0025315400020464

Taylor, A.H., Stephens, J.A., 1998. The North Atlantic Oscillation and the latitude of the Gulf Stream. Tellus A Dyn. Meteorol. Oceanogr. 50, 134–142. https://doi.org/10.3402/tellusa.v50i1.14517

Taylor, K.E., 2001. Summarizing multiple aspects of model performance in a single diagram. J. Geophys. Res. 106, 7183–7192. https://doi.org/10.1029/2000JD900719

Tebble, N., 1966. British bivalve seashells. British Museum (Natural History), London, 212 pp.

Thibault, M., Duprey, N., Gillikin, D.P., Thébault, J., Douillet, P., Chauvaud, L., Amice, E., Munaron, J.M., Lorrain, A., 2020. Bivalve $\delta^{15}N$ isoscapes provide a baseline for urban nitrogen footprint at the edge of a World Heritage coral reef. Mar. Pollut. Bull. 152, 110870. https://doi.org/10.1016/j.marpolbul.2019.110870

Thomas, R.D.K., 1975. Functional morphology, ecology, and evolutionary conservatism in the Glycymerididae (Bivalvia). Palaeontology 18, 217–254.

Thompson, I., Jones, D.S., 1977. The ocean quahog, *Arctica islandica*, "tree" of the north Atlantic shelf. Annual Meeting of the Geological Society of America Abstracts 9, 1199.

Thompson, I., Jones, D.S., Dreibelbis, D., 1980. Annual internal growth banding and life history of the ocean quahog *Arctica islandica* (Mollusca: Bivalvia). Marine Biology 57, 25–34.

Thompson, P.M., Ollason, J.C., 2001. Lagged effects of ocean climate change on fulmar population dynamics. Nature 413, 417–420. https://doi.org/10.1038/35096558

Thomson, D.J., 1982. Spectrum estimation and harmonic analysis. Proc. IEEE 70, 1055–1096. https://doi.org/10.1109/PROC.1982.12433

Thórarinsdóttir, G.G., Einarsson, S.T., 1996. Distribution, abundance, population structure and meat yield of the ocean quahog, *Arctica islandica*, in Icelandic waters. J. Mar. Biol. Assoc. United Kingdom 76, 1107–1114. https://doi.org/10.1017/s0025315400040996

Toggweiler, J.R., Key, R.M., 2001. Thermohaline Circulation. Encycl. Ocean Sci. 2941–2947. https://doi.org/10.1006/rwos.2001.0111

Torrence, C., Compo, G.P., 1998. A Practical Guide to Wavelet Analysis. Bull. Am. Meteorol. Soc. 79, 61–78. https://doi.org/10.1175/1520-0477(1998)079<0061:APGTWA>2.0.CO;2

Trenberth, K.E., Fasullo, J.T., Balmaseda, M.A., 2014. Earth's energy imbalance. J. Clim. 27, 3129–3144. https://doi.org/10.1175/JCLI-D-13-00294.1

Trofimova, T., Alexandroff, S.J., Mette, M.J., Tray, E., Butler, P.G., Campana, S.E., Harper, E.M., Johnson, A.L.A., Morrongiello, J.R., Peharda, M., Schöne, B.R., Andersson, C., Andrus, C.F.T., Black, B.A., Burchell, M., Carroll, M.L., DeLong, K.L., Gillanders, B.M., Grønkjær, P., Killam, D., Prendergast, A.L., Reynolds, D.J., Scourse, J.D., Shirai, K., Thébault, J., Trueman, C., de Winter, N., 2020. Fundamental questions and applications of sclerochronology: Community-defined research priorities. Estuar. Coast. Shelf Sci. 245, 106977. https://doi.org/10.1016/j.ecss.2020.106977

Trofimova, T., Milano, S., Andersson, C., Bonitz, F.G.W., Schöne, B.R., 2018. Oxygen isotope composition of *Arctica islandica* aragonite in the context of shell architectural organization: Implications for paleoclimate reconstructions. Geochemistry, Geophys. Geosystems 19. https://doi.org/10.1002/2017GC007239

Trouet, V., Van Oldenborgh, G.J., 2013. KNMI climate explorer: A web-based research tool for high-resolution paleoclimatology. Tree-Ring Res. 69, 3–13. https://doi.org/10.3959/1536-1098-69.1.3

Turrell, W.R., Slesser, G., Payne, R., Adams, R.D., Gillibrand, P.A., 1996. Hydrography of the East Shetland Basin in relation to decadal North Sea variability. ICES J. Mar. Sci. 53, 899–916. https://doi.org/10.1006/jmsc.1996.0112

Uehara, K., Scourse, J.D., Horsburgh, K.J., Lambeck, K., Purcell, A.P., 2006. Tidal evolution of the northwest European shelf seas from the Last Glacial Maximum to the present. J. Geophys. Res. Ocean. 111, C09025. https://doi.org/10.1029/2006JC003531

UNFCCC, 2021. Nationally determined contributions under the Paris Agreement: Synthesis report by the secretariat. English 1–42.

Urey, H.C., 1947. The Thermodynamic properties of isotopic substances. J. Chem. Soc. 562–581.

Urey, H.C., Lowenstam, H.A., Epstein, S., McKinney, C.R., 1951. Measurement of paleotemperatures and temperatures of the upper Cretaceous of England, Denmark, and the southeastern United States. Bull. Geol. Soc. Am. 62, 399–416. https://doi.org/10.1130/0016-7606(1951)62[399:MOPATO]2.0.CO;2

Van Nieuwenhove, N., Pearce, C., Knudsen, M.F., Røy, H., Seidenkrantz, M.-S., 2018. Meltwater and seasonality influence on Subpolar Gyre circulation during the Holocene. Palaeogeogr. Palaeoclimatol. Palaeoecol. 502, 104–118. https://doi.org/10.1016/j.palaeo.2018.05.002

Vaughan, S., Bailey, R.J., Smith, D.G., 2011. Detecting cycles in stratigraphic data: Spectral analysis in the presence of red noise. Paleoceanography 26, 1–15. https://doi.org/10.1029/2011PA002195

Vautard, R., Yiou, P., Ghil, M., 1992. Singular-spectrum analysis: A toolkit for short, noisy chaotic signals. Phys. D Nonlinear Phenom. 58, 95–126. https://doi.org/10.1016/0167-2789(92)90103-T

Visbeck, M., Chassignet, E.P., Curry, R.G., Delworth, T.L., Dickson, R.R., Krahmann, G., 2003. The ocean's response to North Atlantic Oscillation variability, in: The North Atlantic Oscillation: Climatic Significance and Environmental Impact. Geophysical Monograph Series. https://doi.org/10.1029/134GM06

Vogel, J.S., Southon, J.R., Nelson, D.E., Brown, T.A., 1984. Performance of catalytically condensed carbon for use in accelerator mass spectrometry. Nucl. Inst. Methods Phys. Res. B 5, 289–293. https://doi.org/10.1016/0168-583X(84)90529-9

Vogel, K., Gektidis, M., Golubic, S., Kiene, W.E., Radtke, G., 2000. Experimental studies on microbial bioerosion at Lee Stocking Island, Bahamas and One Tree Island, Great Barrier Reef, Australia: Implications for paleoecological reconstructions. Lethaia 33, 190–204. https://doi.org/10.1080/00241160025100053

Wakelin, S.L., Holt, J.T., Blackford, J.C., Allen, J.I., Butenschön, M., Artioli, Y., 2012. Modeling the carbon fluxes of the northwest European continental shelf: Validation and budgets. J. Geophys. Res. Ocean. 117, C05020. https://doi.org/10.1029/2011JC007402

Wanamaker, Jr., A.D., Hetzinger, S., Halfar, J., 2011. Reconstructing mid- to high-latitude marine climate and ocean variability using bivalves, coralline algae, and marine sediment cores from the Northern Hemisphere. Palaeogeogr. Palaeoclimatol. Palaeoecol. 302, 1–9. https://doi.org/10.1016/j.palaeo.2010.12.024

Wanamaker, A.D.J., Kreutz, K.J., Schöne, B.R., Introne, D.S., 2011. Gulf of Maine shells reveal changes in seawater temperature seasonality during the Medieval Climate Anomaly and the Little Ice Age. Palaeogeogr. Palaeoclimatol. Palaeoecol. 302, 43–51. https://doi.org/10.1016/j.palaeo.2010.06.005

Wanamaker Jr., A.D., Kreutz, K.J., Schöne, B.R., Maasch, K.A., Pershing, A.J., Borns, H.W., Introne, D.S., Feindel, S., 2009. A late Holocene paleo-productivity record in the western Gulf of Maine, USA, inferred from growth histories of the long-lived ocean quahog (*Arctica islandica*). Int. J. Earth Sci. 98, 19–29. https://doi.org/10.1007/s00531-008-0318-z

Wanner, H., Beer, J., Bütikofer, J., Crowley, T.J., Cubasch, U., Flückiger, J., Goosse, H., Grosjean, M., Joos, F., Kaplan, J.O., Küttel, M., Müller, S.A., Prentice, I.C., Solomina, O., Stocker, T.F., Tarasov, P., Wagner, M., Widmann, M., 2008. Mid- to

Late Holocene climate change: an overview. Quat. Sci. Rev. 27, 1791–1828. https://doi.org/10.1016/j.quascirev.2008.06.013

Ward, S.L., Neill, S.P., Scourse, J.D., Bradley, S.L., Uehara, K., 2016. Sensitivity of palaeotidal models of the northwest European shelf seas to glacial isostatic adjustment since the Last Glacial Maximum. Quat. Sci. Rev. 151, 198–211. https://doi.org/10.1016/j.quascirev.2016.08.034

Warter, V., Müller, W., 2017. Daily growth and tidal rhythms in Miocene and modern giant clams revealed via ultra-high resolution LA-ICPMS analysis — A novel methodological approach towards improved sclerochemistry. Palaeogeogr. Palaeoclimatol. Palaeoecol. 465, 362–375. https://doi.org/10.1016/j.palaeo.2016.03.019

Watling, R., Irvine, L.M., Norton, T.A., 1970. The marine algae of St. Kilda. Trans. Bot. Soc. Edinburgh 41, 31–41. https://doi.org/10.1080/03746607008685197

Wehrmeister, U., Soldati, A. L., Jacob, D. E., Häger, T., & Hofmeister, W. (2010) Raman spectroscopy of synthetic, geological and biological vaterite: a Raman spectroscopic study. J. Raman Spectr., 41, 193–201. https://doi.org/10.1002/jrs.2438

Weidman, C.R., Jones, G.A., Lohmann, K.C., 1994. The long-lived mollusc *Arctica islandica*: A new paleoceanographic tool for the reconstruction of bottom temperatures for the continental shelves of the northern North Atlantic Ocean. J. Geophys. Res. 99, 18,305-18,314. https://doi.org/10.1029/94JC01882

Whyte, C., Swan, S., Davidson, K., 2014. Changing wind patterns linked to unusually high Dinophysis blooms around the Shetland Islands, Scotland. Harmful Algae 39, 365–373. https://doi.org/10.1016/j.hal.2014.09.006

Wigley, T.M.L., Briffa, K.R., Jones, P.D., 1984. On the average value of correlated time series, with applications in dendroclimatology and hydrometeorology. J. Clim. Appl. Meteorol. 23, 201–213.

Wijffels, S., Roemmich, D., Monselesan, D., Church, J., Gilson, J., 2016. Ocean temperatures chronicle the ongoing warming of Earth. Nat. Clim. Chang. 6, 116–118. https://doi.org/10.1038/nclimate2924

Williams, B., Risk, M.J., Ross, S.W., Sulak, K.J., 2007. Stable isotope data from deep-water Antipatharians: 400-year records from the southeastern coast of the United States of America. Bull. Mar. Sci. 81, 437–447.

Winter, J.E., 1969. Über den Einfluß der Nahrungskonzentration und anderer Faktoren auf Filtrierleistung und Nahrungsausnutzung der Muscheln *Arctica islandica* und *Modiolus modiolus*. Mar. Biol. 4, 87–135. https://doi.org/10.1007/BF00347037

Witbaard, R., Duineveld, G.C.A., de Wilde, P.A.W.J., 1997a. A long-term growth record derived from *Arctica islandica* (Mollusca, Bivalvia) from the Fladen Ground (northern North Sea). J. Mar. Biol. Assoc. United Kingdom 77, 801–816.

Witbaard, R., Franken, R., Visser, B., 1997b. Growth of juvenile *Arctica islandica* under experimental conditions. Helgoländer Meeresuntersuchungen 51, 417–431.

Witbaard, R., Jansma, E., Sass Klaassen, U., 2003. Copepods link quahog growth to climate. J. Sea Res. 50, 77–83. https://doi.org/10.1016/S1385-1101(03)00040-6

Witbaard, R., Jenness, M.I., Van Der Borg, K., Ganssen, G., 1994. Verification of annual growth increments in *Arctica islandica* L. from the North Sea by means of oxygen and carbon isotopes. Netherlands J. Sea Res. 33, 91–101. https://doi.org/10.1016/0077-7579(94)90054-X

Wunsch, C., 1999. The interpretation of short climate records, with comments on the North Atlantic and Southern Oscillations. Bull. Am. Meteorol. Soc. 80, 245–255. https://doi.org/10.1175/1520-0477(1999)080<0245:TIOSCR>2.0.CO;2

Young, E.F., Holt, J.T., 2007. Prediction and analysis of long-term variability of temperature and salinity in the Irish Sea. J. Geophys. Res. Ocean. 112. https://doi.org/10.1029/2005JC003386

Zhang, R., Sutton, R., Danabasoglu, G., Delworth, T.L., Kim, W.M., Robson, J., Yeager, S.G., 2016. Comment on "The Atlantic Multidecadal Oscillation without a role for ocean circulation." Science 352, 1527-a. https://doi.org/10.1126/science.aaf1660

Adams, C.E., Godfrey, J.D., Dodd, J.A., Maitland, P.S., 2013. Is proximity to the North Atlantic Drift and the Continental Shelf Current sustaining freshwater European eel populations in western Scotland ? Freshw. Biol. 58, 1–9. https://doi.org/10.1111/fwb.12021

Aiken, J., Bruce, R.H., Lindley, J.A., 1977. Ecological investigations with the Undulating Oceanographic Recorder: The hydrography and plankton of the waters adjacent to the Orkney and Shetland Islands. Mar. Biol. 39, 77–91.

Alexandroff, S.J., Butler, P.G., Hollyman, P.R., Schöne, B.R., Scourse, J.D., 2021. Late Holocene seasonal temperature variability of the western Scottish shelf (St Kilda) recorded in fossil shells of the bivalve Glycymeris glycymeris. Palaeogeogr. Palaeoclimatol. Palaeoecol. 562, 110146. https://doi.org/10.1016/j.palaeo.2020.110146

Andrus, C.F.T., 2011. Shell midden sclerochronology. Quat. Sci. Rev. 30, 2892–2905. https://doi.org/10.1016/j.quascirev.2011.07.016

Ascough, P.L., Church, M.J., Cook, G.T., 2016. Marine Radiocarbon Reservoir Effects for the Mesolithic and Medieval Periods in the Western Isles of Scotland. Radiocarbon 59, 17–31. https://doi.org/10.1063/1.2756072

Ascough, P.L., Cook, G.T., Dugmore, A.J., Barber, J., Higney, E., Scott, E.M., 2004. Holocene Variations in the Scottish Marine Radiocarbon Reservoir Effect. Radiocarbon 46, 611–620.

Ascough, P.L., Cook, G.T., Dugmore, A.J., Scott, E.M., 2007. The North Atlantic marine reservoir effect in the Early Holocene: Implications for defining and understanding MRE values. Nucl. Instruments Methods Phys. Res. Sect. B Beam Interact. with Mater. Atoms 259, 438–447. https://doi.org/10.1016/j.nimb.2007.01.185

Austin, W.E.N., Cage, A.G., Scourse, J.D., 2006. Mid-latitude shelf seas: a NW European perspective on the seasonal dynamics of temperature, salinity and oxygen isotopes. The Holocene 16, 937–947. https://doi.org/10.1177/0959683606hl985rp

Austin, W.E.N., Kroon, D., 1996. Late glacial sedimentology, foraminifera and stable isotope stratigraphy of the Hebridean Continental Shelf, northwest Scotland, in: Andrews, J.T., Austin, W.E.N., Bergsten, H., Jennings, A.E. (Eds.), Late Quaternary Palaeoceanography of the North Atlantic Margin. Geological Society Special Publication 111, pp. 187–213. https://doi.org/10.1144/GSL.SP.1996.111.01.13

Austin, W.E.N., Scourse, J.D., 1997. Evolution of seasonal stratification in the Celtic Sea during the Holocene. J. Geol. Soc. London. 154, 249–256.

Bailey, M., Bailey, D., Bellini, L., Fernandes, P., Fox, C., Heymans, S., Holmes, S., Howe, J., Hughes, S., Magill, S., McIntyre, D., McKee, D., Ryan, M., Smith, I., Tyldsley, G., Watret, R., Turrell, W., 2011. The west of Scotland marine ecosystem: A review of scientific knowledge. Fish. Res. 292.

Ballesta-Artero, I., Witbaard, R., Carroll, M.L., van der Meer, J., 2017. Environmental factors regulating gaping activity of the bivalve Arctica islandica in Northern Norway. Mar. Biol. 164. https://doi.org/10.1007/s00227-017-3144-7

Berner, K.S., Koc, N., Divine, D., Godtliebsen, F., Moros, M., 2008. A decadal-scale Holocene sea surface temperature record from the subpolar North Atlantic constructed using diatoms and statistics and its relation to other climate parameters. Paleobiology 23. https://doi.org/10.1029/2006PA001339

Bersch, M., 2002. North Atlantic Oscillation–induced changes of the upper layer circulation in the northern North Atlantic Ocean. J. Geophys. Res. 107. https://doi.org/10.1029/2001jc000901

Berthou, P., Blanchard, M., Noel, P., Vergnaud-Grazzini, C., 1986. The analysis of stable isotopes of the shell applied to the determination of the age of four bivalves of the "Normano-Breton" Gulf, Western Channel. ICES K 16.

Black, B.A., 2009. Climate-driven synchrony across tree, bivalve, and rockfish growth-increment chronologies of the northeast Pacific. Mar. Ecol. Prog. Ser. 378, 37–46. https://doi.org/10.3354/meps07854

Black, B.A., Andersson, C., Butler, P.G., Carroll, M.L., DeLong, K.L., Reynolds, D.J., Schöne, B.R., Scourse, J.D., van der Sleen, P., Wanamaker, A.D., Witbaard, R., 2019. The revolution of crossdating in marine palaeoecology and palaeoclimatology. Biol. Lett. 15, 20180665.

Black, B.A., Copenheaver, C.A., Frank, D.C., Stuckey, M.J., Kormanyos, R.E., 2009. Multi-proxy reconstructions of northeastern Pacific sea surface temperature data from trees and Pacific geoduck. Palaeogeogr. Palaeoclimatol. Palaeoecol. 278, 40–47. https://doi.org/10.1016/j.palaeo.2009.04.010

Black, B.A., Griffin, D., van der Sleen, P., Wanamaker, Jr., A.D., Speer, J.H., Frank, D.C., Stahle, D.W., Pederson, N., Copenheaver, C.A., Trouet, V., Griffin, S., Gillanders, B.M., 2016. The value of crossdating to retain high-frequency variability, climate signals, and extreme events in environmental proxies. Glob. Chang. Biol. 22, 2582–2595. https://doi.org/10.1111/gcb.13256

Black, B.A., Sydeman, W.J., Frank, D.C., Griffin, D., Stahle, D.W., García-Reyes, M., Rykaczewski, R.R., Bograd, S.J., Peterson, W.T., 2014. Six centuries of variability and extremes in a coupled marine-terrestrial ecosystem. Science (80-.). 345, 1498–1502.

Black, H.D., Andrus, C.F.T., Lambert, W.J., Rick, T.C., Gillikin, D.P., 2017. δ15N values in Crassostrea virginica shells provides early direct evidence for nitrogen loading to Chesapeake Bay. Sci. Rep. 7. https://doi.org/10.1038/srep44241

Blicher, M.E., Rysgaard, S., Sejr, M.K., 2010. Seasonal growth variation in Chlamys islandica (Bivalvia) from sub-arctic Greenland is linked to food availability and temperature. Mar. Ecol. Prog. Ser. 407, 71–86. https://doi.org/10.3354/meps08536

Boehme, L., Lonergan, M., Todd, C.D., 2014. Comparison of gridded sea surface temperature datasets for marine ecosystem studies. Mar. Ecol. Prog. Ser. 516, 7–22. https://doi.org/10.3354/meps11023

Böhm, C.F., Demmert, B., Harris, J., Fey, T., Marin, F., Wolf, S.E., 2016. Structural commonalities and deviations in the hierarchical organization of crossed-lamellar shells: A case study on the shell of the bivalve Glycymeris glycymeris. J. Mater. Res. 31, 536–546. https://doi.org/10.1557/jmr.2016.46

Bonitz, F.G.W., Andersson, C., Trofimova, T., Hátún, H., 2017. Links between phytoplankton dynamics and shell growth of Arctica islandica on the Faroe Shelf. J. Mar. Syst. 179, 72–87. https://doi.org/10.1016/j.jmarsys.2017.11.005

Bowen, D.Q., Rose, J., McCabe, A.M., Sutherland, D.G., 1986. Correlation of Quaternary glaciations in England, Ireland, Scotland and Wales. Quat. Sci. Rev. 5, 299–340. https://doi.org/10.1016/0277-3791(86)90194-0

Box, G.E.P., Jenkins, G.M., Reinsel, G.C., 1994. Time Series Analysis: Forecasting and Control, 3rd ed. Prentice-Hall, New Jersey.

Boyd, J.M., Doney, J.M., Gunn, R.G., Jewell, P.A., 1964. The Soay sheep of the island of Hirta, St. Kilda. A study of a feral population. Proc. Zool. Soc. London 142, 129–163.

Briffa, K.R., Jones, P.D., Bartholin, T.S., Eckstein, D., Schweingruber, F.H., Karlén, W., Zetterberg, P., Eronen, M., 1992. Fennoscandian summers from ad 500: temperature changes on short and long timescales. Clim. Dyn. 7, 111–119. https://doi.org/10.1007/BF00211153

Brocas, W.M., Reynolds, D.J., Butler, P.G., Richardson, C.A., Scourse, J.D., Ridgway, I.D., Ramsay, K., 2013. The dog cockle, Glycymeris glycymeris (L.), a new annually-resolved sclerochronological archive for the Irish Sea. Palaeogeogr. Palaeoclimatol. Palaeoecol. 373, 133–140. https://doi.org/10.1016/j.palaeo.2012.03.030

Bronk Ramsey, C., 2009. Bayesian analysis of radiocarbon dates. Radiocarbon 51, 337–360. https://doi.org/10.2458/azu_js_rc.v51i1.3494

Bronk Ramsey, C., van der Plicht, J., Weninger, B., 2001. 'Wiggle matching' radiocarbon dates. Radiocarbon 43, 381–389. https://doi.org/https://doi.org/10.1017/S0033822200038248

Buckley, M.W., Marshall, J., 2015. Observations, inferences, and mechanisms of the Atlantic Meridional Overturning Circulation: A review. Rev. Geophys. 54, 5–63. https://doi.org/10.1002/2015RG000493

Buddemeier, R.W., Maragos, J.E., Knutson, D.W., 1974. Radiographic studies of reef coral exoskeletons: Rates and patterns of coral growth. J. Exp. Mar. Bio. Ecol. 14, 179–199. https://doi.org/10.1016/0022-0981(74)90024-0

Buras, A., 2017. A comment on the expressed population signal. Dendrochronologia 44, 130–132. https://doi.org/10.1016/j.dendro.2017.03.005

Burrows, M., Thorpe, S.A., 1999. Drifter observations of the Hebrides slope current and nearby circulation patterns. Ann. Geophys. 17, 280–302. https://doi.org/10.1007/s005850050757

Burrows, M., Thorpe, S.A., Meldrum, D.T., 1999. Dispersion over the Hebridean and Shetland shelves and slopes. Cont. Shelf Res. 19, 49–55. https://doi.org/10.1016/S0278-4343(98)00082-X

Bušelić, I., Peharda, M., Reynolds, D.J., Butler, P.G., González, A.R., Ezgeta-Balić, D., Vilibić, I., Grbec, B., Hollyman, P., Richardson, C.A., 2015. Glycymeris bimaculata (Poli, 1795) - A new sclerochronological archive for the Mediterranean? J. Sea Res. 95, 139–148. https://doi.org/10.1016/j.seares.2014.07.011

Butler, P.G., Fraser, N.M., Scourse, J.D., Richardson, C.A., Bryant, C., Heinemeier, J., 2020. Is there a reliable taphonomic clock in the temperate North Atlantic? An example from a North Sea population of the mollusc Arctica islandica. Palaeogeogr. Palaeoclimatol. Palaeoecol. 560, 109975. https://doi.org/10.1016/j.palaeo.2020.109975

Butler, P.G., Richardson, C. a., Scourse, J.D., Wanamaker, Jr., A.D., Shammon, T.M., Bennell, J.D., 2010. Marine climate in the Irish Sea: analysis of a 489-year marine master chronology derived from growth increments in the shell of the clam Arctica islandica. Quat. Sci. Rev. 29, 1614–1632. https://doi.org/10.1016/j.quascirev.2009.07.010

Butler, P.G., Richardson, C.A., Scourse, J.D., Witbaard, R., Schöne, B.R., Fraser, N.M., Wanamaker, Jr., A.D., Bryant, C.L., Harris, I., Robertson, I., 2009a. Accurate increment identification and the spatial extent of the common signal in five Arctica islandica chronologies from the Fladen Ground, northern North Sea. Paleoceanography 24, PA2210. https://doi.org/10.1029/2008PA001715

Butler, P.G., Scourse, J.D., Richardson, C. a., Wanamaker, A.D.J., Bryant, C.L., Bennell, J.D., 2009b. Continuous marine radiocarbon reservoir calibration and the 13C Suess effect in the Irish Sea: Results from the first multi-centennial shell-based marine master chronology. Earth Planet. Sci. Lett. 279, 230–241. https://doi.org/10.1016/j.epsl.2008.12.043

Butler, P.G., Wanamaker, A.D.J., Scourse, J.D., Richardson, C.A., Reynolds, D.J., 2013. Variability of marine climate on the North Icelandic Shelf in a 1357-year proxy archive based on growth increments in the bivalve Arctica islandica. Palaeogeogr. Palaeoclimatol. Palaeoecol. 373, 141–151. https://doi.org/10.1016/j.palaeo.2012.01.016

Cabral, J.P., Martins, J.M.S., 2016. Archaeological Glycymeris glycymeris shells perforated at the umbo: Natural or man-made holes? J. Archaeol. Sci. Reports 10, 474–482. https://doi.org/10.1016/j.jasrep.2016.11.008

Caesar, L., Mccarthy, G.D., Thornalley, D.J.R., Cahill, N., Rahmstorf, S., 2021. Current Atlantic Meridional Overturning Circulation weakest in last millennium. Nat. Geosci. 14, 118–121. https://doi.org/10.1038/s41561-021-00699-z

Cage, A.G., Austin, W.E.N., 2010. Marine climate variability during the last millennium: The Loch Sunart record, Scotland, UK. Quat. Sci. Rev. 29, 1633–1647. https://doi.org/10.1016/j.quascirev.2010.01.014

Campana, S.E., 1999. Chemistry and composition of fish otoliths: pathways, mechanisms and applications. Mar. Ecol. Prog. Ser. 188, 263–297.

Carroll, M.L., Ambrose, W.G., Locke V, W.L., Ryan, S.K., Johnson, B.J., 2014. Bivalve growth rate and isotopic variability across the Barents Sea Polar Front. J. Mar. Syst. 130, 167–180. https://doi.org/10.1016/j.jmarsys.2013.10.006

Cartwright, D.E., 1969. Extraordinary Tidal Currents near St Kilda. Nature 223, 928–932.

Cartwright, D.E., Huthnance, J.M., Spencer, R., Vassie, J.M., 1980. On the St Kilda shelf tidal regime. Deep Sea Res. Part A, Oceanogr. Res. Pap. 27, 61–70. https://doi.org/10.1016/0198-0149(80)90072-2

Catchpole, E.A., Morgan, B.J.T., Coulson, T.N., Freeman, S.N., Albon, S.D., 2000. Factors influencing Soay sheep survival. J. R. Stat. Soc. Ser. C (Applied Stat. 49, 453–472.

Charman, D.J., 2010. Centennial climate variability in the British Isles during the mid-late Holocene. Quat. Sci. Rev. 29, 1539–1554. https://doi.org/10.1016/j.quascirev.2009.02.017

Charman, D.J., McCarroll, D., 2010. Climate variability of the British Isles and adjoining seas. Quat. Sci. Rev. 29, 1503–1506. https://doi.org/10.1016/j.quascirev.2010.05.001

Chen, C.-T.A., Huang, T.-H., Chen, Y.-C., Bai, Y., He, X., Kang, Y., 2013. Air–sea exchanges of CO2 in the world's coastal seas. Biogeosciences 10, 6509–6544. https://doi.org/10.5194/bg-10-6509-2013

Cheung, W.W.L., Lam, V.W.Y., Sarmiento, J.L., Kearney, K., Watson, R., Zeller, D., Pauly, D., 2010. Large-scale redistribution of maximum fisheries catch potential in the global ocean under climate change. Glob. Chang. Biol. 16, 24–35. https://doi.org/10.1111/j.1365-2486.2009.01995.x

Clark, G.R., 1968. Mollusk shell: daily growth lines. Science (80-.). 161, 800–802. https://doi.org/10.1126/science.161.3843.800

Clark, P.U., Dyke, A.S., Shakun, J.D., Carlson, A.E., Clark, J., Wohlfarth, B., Mitrovica, J.X., Hostetler, S.W., McCabe, A.M., 2009. The Last Glacial Maximum. Science (80-.). 325, 710–714. https://doi.org/10.1126/science.1172873

Clement, A., Bellomo, K., Murphy, L.N., Cane, M.A., Mauritsen, T., Stevens, B., 2015. The Atlantic Multidecadal Oscillation without a role for ocean circulation. Science (80-.). 350, 320–324.

Clement, A., Cane, M.A., Murphy, L.N., Bellomo, K., Mauritsen, T., Stevens, B., 2016. Response to Comment on "The Atlantic Multidecadal Oscillation without a role for ocean circulation." Science (80-.). 352, 1527-b.

Clutton-Brock, T.H., Pemberton, J.M., 2004. Soay Sheep: Dynamics and Selection in an Island Population. Cambridge University Press, Cambridge. https://doi.org/10.1644/05-mamm-r-364.1

Cochran, J.K., Kallenberg, K., Landman, N.H., Harries, P.J., Weinreb, D., Turekian, K.K., Beck, A., Cobban, W.A., 2010. Effect of diagenesis on the Sr, O, and C isotope composition of late cretaceous mollusks from the western interior seaway of North America. Am. J. Sci. 310, 69–88. https://doi.org/10.2475/02.2010.01

Cook, E.R., 1985. A time series analysis approach to tree ring standardization. Unpubl. PhD Thesis. University of Arizona, Tucson, USA.

Cook, E.R., Briffa, K.R., Meko, D.M., Graybill, D.A., Funkhouser, G., 1995. The 'segment length curse' in long tree-ring chronology development for palaeoclimatic studies. The Holocene 5, 229–237. https://doi.org/10.1177/095968369500500211

Cook, E.R., Krusic, P.J., 2005. Program ARSTAN: A tree-ring standardization program based on detrending and autoregressive time series modeling, with interactive graphics. Tree-Ring Laboratory Lamont Doherty Earth Observatory of Columbia University Palisades, NY.

Cook, E.R., Shiyatov, S.G., Mazepa, V.S., 1990. Tree-ring standardization and growth-trend estimation, in: Cook, E.R., Kairiukstis, L.A. (Eds.), Methods of Dendrochronology: Applications in the Environmental Sciences. Springer Science+Business Media, Dordrecht, pp. 104–123.

Coulson, T., Catchpole, E.A., Albon, S.D., Morgan, B.J.T., Pemberton, J.M., Clutton-Brock, T.H., Crawley, M.J., Grenfell, B.T., 2001. Age, sex, density, winter weather, and population crashes in Soay sheep. Science (80-.). 292, 1528–1532.

Crippa, G., 2013. The shell ultrastructure of the genus Glycymeris Da Costa, 1778: A comparison between fossil and recent specimens. Riv. Ital. di Paleontol. e Stratigr. 119, 387–399.

Croll, D.A., Maron, J.L., Estes, J.A., Danner, E.M., Byrd, G. V., 2005. Introduced predators transform subarctic islands from grassland to tundra. Science (80-.). 307, 1959–1961. https://doi.org/10.1126/science.1108485

Cunningham, L.K., Austin, W.E.N., Knudsen, K.L., Eiríksson, J., Scourse, J.D., Wanamaker, Jr., A.D., Butler, P.G., Cage, A.G., Richter, T., Husum, K., Hald, M., Andersson, C., Zorita, E., Linderholm, H.W., Gunnarson, B.E., Sicre, M.-A., Sejrup, H.P., Jiang, H., Wilson, R.J.S., 2013. Reconstructions of surface ocean conditions from the northeast Atlantic and Nordic seas during the last millennium. The Holocene 23, 921–935. https://doi.org/10.1177/0959683613479677

Curry, R.G., McCartney, M.S., 2001. Ocean gyre circulation changes associated with the North Atlantic Oscillation. J. Phys. Oceanogr. 31, 3374–3400. https://doi.org/10.1175/1520-0485(2001)031<3374:OGCCAW>2.0.CO;2

da Vinci, L., 1970. The Notebooks of Leonardo da Vinci (Translated by J.P. Richter. Original translation in 1883.). Dover Publications, New York.

Dahlgren, T.G., Weinberg, J.R., Halanych, K.M., 2000. Phylogeography of the ocean quahog (Arctica islandica): influences of paleoclimate on genetic diversity and species range. Mar. Biol. 137, 487–495. https://doi.org/10.1007/s002270000342

De La Pierre, M., Carteret, C., Maschio, L., André, E., Orlando, R., Dovesi, R., 2014. The Raman spectrum of CaCO3 polymorphs calcite and aragonite: A combined experimental and computational study. J. Chem. Phys. 140. https://doi.org/10.1063/1.4871900

Defant, A., 1929. Dynamische Ozeanographie. Springer, Berlin. https://doi.org/10.1097/00000658-190001000-00036

Department of Energy and Climate Change, 2016. UK Offshore Energy Strategic Environmental Assessment 3 (OESEA3). Appendix A1a.6 Birds.

Dettman, D., Lohmann, K., 1995. Microsampling carbonates for stable and minor element analysis: Physical separation on a 20 micrometer scale. J. Sediment. Res. A65, 566–569. https://doi.org/10.1306/D426813F-2B26-11D7-8648000102C1865D

Dettman, D.L., Reische, A.K., Lohmann, K.C., 1999. Controls on the stable isotope composition of seasonal growth bands in aragonitic fresh-water bivalves (Unionidae). Geochim. Cosmochim. Acta 63, 1049–1057.

Devereux, I., 1967. Temperature measeurements from oxygen isotope ratios of fish otoliths. Science (80-.). 155, 1683–1685.

Doty, M.S., Oguri, M., 1956. The island mass effect. ICES J. Mar. Sci. 22, 33–37. https://doi.org/https://doi.org/10.1093/icesjms/22.1.33

Drinkwater, K.F., 2006. The regime shift of the 1920s and 1930s in the North Atlantic. Prog. Oceanogr. 68, 134–151. https://doi.org/10.1016/j.pocean.2006.02.011

Drinkwater, K.F., Belgrano, A., Borja, A., Conversi, A., Edwards, M., Greene, C.H., Ottersen, G., Pershing, A.J., Walker, H., 2003. The response of marine ecosystems to climate variability associated with the North Atlantic Oscillation, in: Hurrell, J.W., Kushnir, Y., Ottersen, G., Visbeck, M. (Eds.), The North Atlantic Oscillation: Climatic Significance and Environmental Impact. Geophysical Monograph Series 134. pp. 211–234.

Drinkwater, K.F., Miles, M., Medhaug, I., Otterå, O.H., Kristiansen, T., Sundby, S., Gao, Y., 2014. The Atlantic Multidecadal Oscillation: Its manifestations and impacts with special emphasis on the Atlantic region north of 60°N. J. Mar. Syst. 133, 117–130. https://doi.org/10.1016/j.jmarsys.2013.11.001

Driscoll, E.G., 1970. Selective bivalve shell destruction in marine environments, a field study. J. Sediment. Petrol. 40, 898–905.

Driscoll, E.G., 1967. Experimental field study of shell abrasion. J. Sediment. Petrol. 37, 1117–1123.

Edwards, M., Helaouet, P., Alhaija, R.A., Batten, S., Beaugrand, G., Chiba, S., Horaeb, R.R., Hosie, G., Mcquatters-Gollop, A., Ostle, C., Richardson, A.J., Rochester, W., Skinner, J., Stern, R., Takahashi, K., Taylor, C., Verheye, H.M., Wootton, M., 2016. Global Marine Ecological Status Report: results from the global CPR Survey 2014/2015. SAHFOS Technical Report.

Ellett, D.J., 1979. Some oceanographic features of Hebridean waters. Proc. R. Soc. Edinburgh 77B, 61–74.

Ellett, D.J., Edwards, A., 1983. Oceanography and inshore hydrography of the Inner Hebrides. Proc. R. Soc. Edinburgh 83B, 143–160.

Elliot, M., Welsh, K., Chilcott, C., McCulloch, M., Chappell, J., Ayling, B., 2009. Profiles of trace elements and stable isotopes derived from giant long-lived Tridacna gigas bivalves: Potential applications in paleoclimate studies. Palaeogeogr. Palaeoclimatol. Palaeoecol. 280, 132–142. https://doi.org/10.1016/j.palaeo.2009.06.007

Elliott, A.J., Clarke, T., Li, Z., 1991. Monthly distributions of surface and bottom temperatures in the northwest European shelf seas. Cont. Shelf Res. 11, 453–466. https://doi.org/10.1016/0278-4343(91)90053-9

Ellis, J.R., Cadman, P.S., Piertney, S.B., Geiger, D.L., 1995. The marine fauna of the St. Kilda archipelago. Scottish Nat. 107, 53–70.

Ellis, J.R., Milligan, S., Readdy, L., South, A., Taylor, N., Brown, M., 2010. MB5301 Mapping spawning and nursery areas of species to be considered in Marine Protected Areas (Marine Conservation Zones). Report No 1: Final Report on development of derived data layers for 40 mobile species considered to be of conservation importance.

Epstein, S., Buchsbaum, R., Lowenstam, H.A., Urey, H.C., 1953. Revised carbonate-water isotopic temperature scale. Bull. Geol. Soc. Am. 64, 1315–1326.

Erlenkeuser, H., 1976. 14C and13C Isotope concentration in modern marine mussels from sedimentary habitats. Naturwissenschaften 63, 338. https://doi.org/10.1007/BF00597312

Esper, J., Cook, E.R., Krusic, P.J., Peters, K., Schweingruber, F.H., 2003. Tests of the RCS method for preserving low-frequency variability in long tree-ring chronologies. Tree-Ring Res. 59, 81–98.

Fleming, A., 1995. St Kilda: stone tools, dolerite quarries and long-term survival. Antiquity 69, 25–35. https://doi.org/10.1017/S0003598X00064279

Flessa, K.W., Cutler, A.H., Meldahl, K.H., 1993. Time and taphonomy: Quantitative estimates of time-averaging and stratigraphic disorder in a shallow marine habitat. Paleobiology 19, 266–286.

Foukal, N.P., Lozier, M.S., 2017. Assessing variability in the size and strength of the North Atlantic subpolar gyre. J. Geophys. Res. Ocean. 122, 6295–6308. https://doi.org/10.1002/2017JC012798

Frederiksen, M., Edwards, M., Richardson, A.J., Halliday, N.C., Wanless, S., 2006. From plankton to top predators: Bottom-up control of a marine food web across four trophic levels. J. Anim. Ecol. 75, 1259–1268. https://doi.org/10.1111/j.1365-2656.2006.01148.x

Frew, R.D., Dennis, P.F., Heywood, K.J., Meredith, M.P., Boswell, S.M., 2000. The oxygen isotope composition of water masses in the northern North Atlantic. Deep. Res. I 47, 2265–2286. https://doi.org/10.1016/S0967-0637(00)00023-6

Fromentin, J.M., Planque, B., 1996. Calanus and environment in the eastern North Atlantic. II. Influence of the North Atlantic Oscillation on C. finmarchicus and C. helgolandicus. Mar. Ecol. Prog. Ser. 134, 111–118. https://doi.org/10.3354/meps134101

Fukami, T., Wardle, D.A., Bellingham, P.J., Mulder, C.P.H., Towns, D.R., Yeates, G.W., Bonner, K.I., Durrett, M.S., Grant-Hoffman, M.N., Williamson, W.M., 2006. Above- and below-ground impacts of introduced predators in seabird-dominated island ecosystems. Ecol. Lett. 9, 1299–1307. https://doi.org/10.1111/j.1461-0248.2006.00983.x

Gámiz-Fortis, S.R., Pozo-Vázquez, D., Esteban-Parra, M.J., Castro-Díez, Y., 2002. Spectral characteristics and predictability of the NAO assessed through Singular Spectral Analysis. J. Geophys. Res. 107, 4685. https://doi.org/10.1029/2001JD001436

Gehrels, W.R., 2010. Late Holocene land- and sea-level changes in the British Isles: Implications for future sea-level predictions. Quat. Sci. Rev. 29, 1648–1660. https://doi.org/10.1016/j.quascirev.2009.09.015

Gilbertson, D.D., Schwenninger, J.-L., Kemp, R.A., Rhodes, E.J., 1999. Sand-drift and soil formation along an exposed North Atlantic Coastline: 14,000 years of diverse

geomorphological, climatic and human impacts. J. Archaeol. Sci. 26, 439–469. https://doi.org/10.1006/JASC.1998.0360

Gillikin, D.P., Lorrain, A., Jolivet, A., Kelemen, Z., Chauvaud, L., Bouillon, S., 2017. High-resolution nitrogen stable isotope sclerochronology of bivalve shell carbonate-bound organics. Geochim. Cosmochim. Acta 200, 55–66. https://doi.org/10.1016/j.gca.2016.12.008

Golikov, A.N., Scarlato, O.A., 1973. Method for indirectly defining optimum temperatures of inhabitancy for marine cold-blooded animals. Mar. Biol. 20, 1–5. https://doi.org/10.1007/BF00387667

Good, S.A., Martin, M.J., Rayner, N.A., 2013. EN4: Quality controlled ocean temperature and salinity profiles and monthly objective analyses with uncertainty estimates. J. Geophys. Res. Ocean. 118, 6704–6716. https://doi.org/10.1002/2013JC009067

Goslin, J., Fruergaard, M., Sander, L., Gałka, M., Menviel, L., Monkenbusch, J., Thibault, N., Clemmensen, L.B., 2018. Holocene centennial to millennial shifts in North-Atlantic storminess and ocean dynamics. Sci. Rep. 8, 12778. https://doi.org/10.1038/s41598-018-29949-8

Gowen, R.J., Raine, R., Dickey-Collas, M., White, M., 1998. Plankton distributions in relation to physical oceanographic features on the southern Malin Shelf , August 1996. ICES J. Mar. Sci. 55, 1095–1111.

Graham, N.A.J., Wilson, S.K., Carr, P., Hoey, A.S., Jennings, S., MacNeil, M.A., 2018. Seabirds enhance coral reef productivity and functioning in the absence of invasive rats. Nature 559, 250–253. https://doi.org/10.1038/s41586-018-0202-3

Grosbois, V., Thompson, P.M., 2005. North Atlantic climate variation influences survival in adult fulmars. Oikos 109, 273–290.

Grossman, E.L., Ku, T.-L., 1986. Oxygen and carbon isotope fractionation in biogenic aragonite: Temperature effects. Chem. Geol. (Isotope Geosci. Sect. 59, 59–74.

Gulland, F.M.D., 1992. The role of nematode parasites in Soay sheep (Ovis aries L.) mortality during a population crash. Parasitology 105, 493–503. https://doi.org/10.1017/S0031182000074679

Halfar, J., Zack, T., Kronz, A., Zachos, J.C., 2000. Growth and high-resolution paleoenvironmental signals of rhodoliths (coralline red algae): A new biogenic archive. J. Geophys. Res. 105, 22,107-22,116.

Hallett, T.B., Coulson, T., Pilkington, J.G., Pemberton, J.M., Grenfell, B.T., 2004. Why large-scale climate indices seem to predict ecological processes better than local weather. Nature 430, 71–75. https://doi.org/10.1038/nature02638.1.

Hammer, Ø., Harper, D., Ryan, P., 2001. PAST: Paleontological statistics software package for education and data analysis. Palaeontol. Electron. 4, 9 pp.

Harkness, D.D., 1983. The extent of the natural 14C deficiency in the coastal environment of the United Kingdom. J. Eur. Study Gr. Phys. Chem. Math. Tech. Appl. to Archaeol. PACT 8, 351–364.

Harris, D.B., Moore, C.G., Porter, J.S., Sanderson, W.G., Ware, F.J., Kamphausen, L., 2018. The establishment of site condition monitoring of the sea caves of the St Kilda and

North Rona Special Areas of Conservation with supplementary data from Loch Eriboll, Scottish Natural Heritage Research Report No. 1044.

Harris, M.P., Murray, S., 1989. Birds of St Kilda, Institute of Terrestrial Ecology & Natural Environmental Research Council, UK.

Hátún, H., Sandø, A.B., Drange, H., Hansen, B., Valdimarsson, H., 2005. Influence of the Atlantic subpolar gyre on the thermohaline circulation. Science 309, 1841–1844. https://doi.org/10.1126/science.1114777

Helama, S., Hood, B.C., 2011. Stone Age midden deposition assessed by bivalve sclerochronology and radiocarbon wiggle-matching of Arctica islandica shell increments. J. Archaeol. Sci. 38, 452–460. https://doi.org/10.1016/j.jas.2010.09.029

Helama, S., Melvin, T.M., Briffa, K.R., 2017. Regional curve standardization: State of the art. The Holocene 27, 172–177. https://doi.org/10.1177/0959683616652709

Helama, S., Schöne, B.R., Kirchhefer, A.J., Nielsen, J.K., Rodland, D.L., Janssen, R., 2007. Compound response of marine and terrestrial ecosystems to varying climate: pre-anthropogenic perspective from bivalve shell growth increments and tree-rings. Mar. Environ. Res. 63, 185–99. https://doi.org/10.1016/j.marenvres.2006.08.003

Hersbach, H., Bell, B., Berrisford, P., Hirahara, S., Horányi, A., Muñoz-Sabater, J., Nicolas, J., Peubey, C., Radu, R., Schepers, D., Simmons, A., Soci, C., Abdalla, S., Abellan, X., Balsamo, G., Bechtold, P., Biavati, G., Bidlot, J., Bonavita, M., De Chiara, G., Dahlgren, P., Dee, D., Diamantakis, M., Dragani, R., Flemming, J., Forbes, R., Fuentes, M., Geer, A., Haimberger, L., Healy, S., Hogan, R.J., Hólm, E., Janisková, M., Keeley, S., Laloyaux, P., Lopez, P., Lupu, C., Radnoti, G., de Rosnay, P., Rozum, I., Vamborg, F., Villaume, S., Thépaut, J.-N., 2020. The ERA5 global reanalysis. Q. J. R. Meteorol. Soc. 146, 1999–2049. https://doi.org/10.1002/qj.3803

Hill, A.E., Horsburgh, K.J., Garvine, R.W., Gillibrand, P.A., Slesser, G., Turrell, W.R., Adams, R.D., 1997. Observations of a density-driven recirculation of the Scottish Coastal Current in the Minch. Estuar. Coast. Shelf Sci. 45, 473–484.

Holliday, N.P., 2003. Air-sea interaction and circulation changes in the northeast Atlantic. J. Geophys. Res. 108, 1–11. https://doi.org/10.1029/2002jc001344

Holliday, N.P., Gary, S., 2014. State of the eastern North Atlantic subpolar gyre: The Extended Ellett Line Programme Annual Report No . 2, Research & Consultancy Report No. 43, National Oceanography Centre.

Holliday, N.P., Hughes, S.L., Bacon, S., Beszczynska-Möller, A., Hansen, B., Lavín, A., Loeng, H., Mork, K.A., Østerhus, S., Sherwin, T., Walczowski, W., 2008. Reversal of the 1960s to 1990s freshening trend in the northeast North Atlantic and Nordic Seas. Geophys. Res. Lett. 35. https://doi.org/10.1029/2007GL032675

Holliday, N.P., Pollard, R.T., Read, J.F., Leach, H., Penny Holliday, N., Pollard, R.T., Read, J.F., Leach, H., 2000. Water mass properties and fluxes in the Rockall Trough,1975-1998. Deep. Res. 47, 1303–1332. https://doi.org/10.1016/S0967-0637(99)00109-0

Holligan, P.M., 1986. Phytoplankton distributions along the shelf break. Proc. R. Soc. Edinburgh 88B, 239–263.

Hollyman, P.R., Leng, M.J., Chenery, S.R.N., Laptikhovsky, V. V, Richardson, C.A., 2018. Statoliths of the whelk Buccinum undatum: a novel age determination tool. Mar. Ecol.

Prog. Ser. 598, 261–272. https://doi.org/10.3354/meps12119

Holme, N.A., 1966. The bottom fauna of the English Channel. Part II. J. Mar. Biol. Assoc. United Kingdom 46, 401–493. https://doi.org/10.1017/S0025315400027193

Holmes, R.L., 1983. Computer-assisted quality control in tree-ring dating and measurement. Tree-Ring Bull. 43, 69–78.

Holt, J., Wakelin, S., Huthnance, J., 2009. Down-welling circulation of the northwest European continental shelf: A driving mechanism for the continental shelf carbon pump. Geophys. Res. Lett. 36. https://doi.org/10.1029/2009GL038997

Howells, R.J., Burthe, S.J., Green, J.A., Harris, M.P., Newell, M.A., Butler, A., Johns, D.G., Carnell, E.J., Wanless, S., Daunt, F., 2017. From days to decades: Short-and long-term variation in environmental conditions affect offspring diet composition of a marine top predator. Mar. Ecol. Prog. Ser. 583, 227–242. https://doi.org/10.3354/meps12343

Huang, B., Thorne, P.W., Banzon, V.F., Boyer, T., Chepurin, G., Lawrimore, J.H., Menne, M.J., Smith, T.M., Vose, R.S., Zhang, H.-M., 2017. Extended Reconstructed Sea Surface Temperature , Version 5 (ERSSTv5): Upgrades , Validations , and Intercomparisons. J. Clim. 30, 8179–8205. https://doi.org/10.1175/JCLI-D-16-0836.1

Hudson, J.H., Shinn, E.A., Halley, R.B., Lidz, B., 1976. Sclerochronology: A tool for interpreting past environments. Geology 4, 361–364. https://doi.org/10.1130/0091-7613(1976)4<361:SATFIP>2.0.CO;2

Hughes, S.L., Holliday, N.P., Colbourne, E., Ozhigin, V., Valdimarsson, H., Østerhus, S., Wiltshire, K., 2009. Comparison of in situ time-series of temperature with gridded sea surface temperature datasets in the north Atlantic. ICES J. Mar. Sci. 66, 1467–1479. https://doi.org/10.1093/icesjms/fsp041

Hughes, S.L., Holliday, N.P., Gaillard, F., 2012. Variability in the ICES/NAFO region between 1950 and 2009: Observations from the ICES Report on Ocean Climate. ICES J. Mar. Sci. 69, 706–719. https://doi.org/10.1093/icesjms/fss044

Hughes, S.L., Tinker, J., Dye, S., Andres, O., Berry, D.I., Hermanson, L., Hewitt, H., Holliday, N.P., Kent, E.C., Kennington, K., Inall, M., Smyth, T., 2017. Temperature. Mar. Clim. Chang. Impacts Partnersh. Sci. Rev. 22–41. https://doi.org/10.14465/2017.arc10.003.tem

Hunter, D.C., Pemberton, J.M., Pilkington, J.G., Morrissey, M.B., 2018. Quantification and decomposition of environment-selection relationships. Evolution (N. Y). 72, 851–866. https://doi.org/10.1111/evo.13461

Hurrell, J.W., Kushnir, Y., Ottersen, G., Visbeck, M., 2003. An Overview of the North Atlantic Oscillation, in: Hurrell, J.W., Kushnir, Y., Ottersen, G., Visbeck, M. (Eds.), The North Atlantic Oscillation: Climatic Significance and Environmental Impact, Geophysical Monograph Series Vol. 134. AGU, Washington, DC, pp. 1–35. https://doi.org/10.1029/134GM01

Huthnance, J.M., 1992. Extensive slope currents and the ocean-shelf boundary. Prog. Oceanogr. 29, 161–196. https://doi.org/10.1016/0079-6611(92)90023-S

Huthnance, J.M., 1984. Slope Currents and “JEBAR.” J. Phys. Oceanogr. 14, 795–810.

Huxel, G.R., McCann, K., 1998. Food web stability: The influence of trophic flows across

habitats. Am. Nat. 152, 460–469. https://doi.org/10.1086/286182

Inall, M., Gillibrand, P., Griffiths, C., MacDougal, N., Blackwell, K., 2009. On the oceanographic variability of the North-West European Shelf to the West of Scotland. J. Mar. Syst. 77, 210–226. https://doi.org/10.1016/j.jmarsys.2007.12.012

IOC-UNESCO, 2021. Ocean Knowledge for a Sustainable Ocean Economy: Synergies between the Ocean Decade and the Outcomes of the Ocean Panel.

IPCC, 2022. Summary for Policymakers [H.-O. Pörtner, D.C. Roberts, E.S. Poloczanska, K. Mintenbeck, M. Tignor, A. Alegría, M. Craig, S. Langsdorf, S. Löschke, V. Möller, A. Okem (eds.)], in: H.-O. Pörtner, Roberts, D.C., Tignor, M., Poloczanska, E.S., Mintenbeck, K., Alegría, A., Craig, M., Langsdorf, S., Löschke, S., Möller, V., Okem, A., Rama, B. (Eds.), Climate Change 2022: Impacts, Adaptation, and Vulnerability. Contribution of Working Group II to the Sixth Assessment Report of the Intergovernmental Panel on Climate Change. Cambridge University Press, Cambridge.

Johnson, C., Inall, M., Häkkinen, S., 2013. Declining nutrient concentrations in the northeast Atlantic as a result of a weakening Subpolar Gyre. Deep. Res. Part I Oceanogr. Res. Pap. 82, 95–107. https://doi.org/10.1016/j.dsr.2013.08.007

Jones, D.S., 1983. Sclerochronology: reading the record of the molluscan shell. Am. Sci. 71, 384–391.

Jones, D.S., 1981. Annual growth increments in shells of Spisula solidissima record marine temperature variability. Science (80-.). 211, 165–1687. https://doi.org/10.1126/science.211.4478.165

Jones, D.S., 1980. Annual cycle of shell growth increment formation in two continental shelf bivalves and its paleoecologic significance. Paleobiology 6, 331–340.

Jones, D.S., Thompson, I., Ambrose, W., 1978. Age and growth rate determinations for the Atlantic surf clam Spisula solidissima (Bivalvia: Mactracea), based on internal growth lines in shell cross-sections. Mar. Biol. 47, 63–70. https://doi.org/10.1007/BF00397019

Jones, S., Cottier, F., Inall, M., Griffiths, C., 2018. Decadal variability on the Northwest European continental shelf. Prog. Oceanogr. 161, 131–151. https://doi.org/10.1016/j.pocean.2018.01.012

Jones, S., Inall, M., Porter, M., Graham, J.A., Cottier, F., 2020. Storm-driven across-shelf oceanic flows into coastal waters. Ocean Sci. 16, 389–403. https://doi.org/10.5194/os-16-389-2020

Jones, S.C., 2016. Shelf edge exchange and the influence on coastal oceanography.

Karney, G.B., Butler, P.G., Scourse, J.D., Richardson, C. a, Lau, K.H., Czernuszka, J.T., Grovenor, C.R.M., 2011. Identification of growth increments in the shell of the bivalve mollusc Arctica islandica using backscattered electron imaging. J. Microsc. 241, 29–36. https://doi.org/10.1111/j.1365-2818.2010.03403.x

Kendon, M., McCarthy, M., Jevrejeva, S., Matthews, A., Legg, T., 2019. State of the UK climate 2018. Int. J. Climatol. 39, 1–55. https://doi.org/10.1002/joc.6213

Kennish, M.J., Lutz, R.A., Rhoads, D.C., 1980. Preparation of acetate peels and fractured sections for observation of growth patterns within the bivalve shell, in: Rhoads, D.C., Lutz, R.A. (Eds.), Skeletal Growth of Aquatic Organisms: Biological Records of

Environmental Change. Plenum Press, New York, pp. 597–601.

Kilbourne, K.H., Wanamaker, A.D., Moffa-Sanchez, P., Reynolds, D.J., Amrhein, D.E., Butler, P.G., Gebbie, G., Goes, M., Jansen, M.F., Little, C.M., Mette, M., Moreno-Chamarro, E., Ortega, P., Otto-Bliesner, B.L., Rossby, T., Scourse, J., Whitney, N.M., 2022. Atlantic circulation change still uncertain. Nat. Geosci. 15, 165–167. https://doi.org/10.1038/s41561-022-00896-4

Killam, D.E., Clapham, M.E., 2018. Identifying the ticks of bivalve shell clocks: seasonal growth in relation to temperature and food supply. Palaios 33, 228–236. https://doi.org/10.2110/palo.2017.072

Kirby-Smith, W.W., Barber, R.T., 1974. Suspension-feeding aquaculture systems: Effects of phytoplankton concentration and temperature on growth of the bay scallop. Aquaculture 3, 135–145. https://doi.org/10.1016/0044-8486(74)90108-2

Knight, J.R., Folland, C.K., Scaife, A.A., 2006. Climate impacts of the Atlantic Multidecadal Oscillation. Geophys. Res. Lett. 33, 2–5. https://doi.org/10.1029/2006GL026242

Knutson, D.W., Buddemeier, R.W., Smith, S. V., 1972. Coral chronometers: Seasonal growth bands in reef corals. Science (80-.). 177, 270–272. https://doi.org/10.1126/science.177.4045.270

Kober, K., Webb, A., Win, I., Lewis, M., O'Brien, S., Wilson, L.J., Reid, J.B., 2010. An analysis of the numbers and distribution of seabirds within the British Fishery Limit aimed at identifying areas that qualify as possible marine SPAs, JNCC Report No. 431.

Kuhlbrodt, T., Griesel, A., Montoya, M., Levermann, A., Hofmann, M., Rahmstorf, S., 2007. On the driving processes of the Atlantic meridional overturning circulation. Rev. Geophys. 45. https://doi.org/10.1029/2004RG000166

Lees, J.M., Park, J., 1995. Multiple-taper spectral analysis: A stand-alone C-subroutine. Comput. Geosci. 21, 199–236. https://doi.org/10.1016/0098-3004(94)00067-5

Lescinsky, H., Titus, B., Hubbard, D., 2011. Live coral cover in the fossil record: an example from Holocene reefs of the Dominican Republic. Coral Reefs 31, 335–346. https://doi.org/10.1007/s00338-011-0863-y

Lozier, M.S., Owens, W.B., Curry, R.G., 1995. The climatology of the North Atlantic. Prog. Oceanogr. 36, 1–44. https://doi.org/10.1016/0079-6611(95)00013-5

Lynch-Stieglitz, J., Adkins, J.F., Curry, W.B., Dokken, T., Hall, I.R., Herguera, J.C., Hirschi, J.J.-M., Ivanova, E. V, Kissel, C., Marchal, O., Marchitto, T.M., McCave, I.N., McManus, J.F., Mulitza, S., Ninnemann, U., Peeters, F., Yu, E.-F., Zahn, R., 2007. Atlantic meridional overturning circulation during the Last Glacial Maximum. Science 316, 66–69. https://doi.org/10.1126/science.1137127

Mann, R., 1982. The seasonal cycle of gonadal development in Arctica islandica from the Southern New England Shelf. Fish. Bull. 80, 315–326.

Mann, R., Wolf, C.C., 1983. Swimming behaviour of larvae of the ocean quahog Arctica islandica in response to pressure and temperature. Mar. Ecol. Prog. Ser. 13, 211–218. https://doi.org/10.3354/meps013211

Marali, S., Schöne, B.R., 2015. Oceanographic control on shell growth of Arctica islandica (Bivalvia) in surface waters of Northeast Iceland - Implications for paleoclimate

reconstructions. Palaeogeogr. Palaeoclimatol. Palaeoecol. 420, 138–149. https://doi.org/10.1016/j.palaeo.2014.12.016

Marchal, O., Cacho, I., Stocker, T.F., Grimalt, J.O., Calvo, E., Martrat, B., Shackleton, N., Vautravers, M., Cortijo, E., Van Kreveld, S., Andersson, C., Koç, N., Chapman, M., Sbaffi, L., Duplessy, J.C., Sarnthein, M., Turon, J.L., Duprat, J., Jansen, E., 2002. Apparent long-term cooling of the sea surface in the northeast Atlantic and Mediterranean during the Holocene. Quat. Sci. Rev. 21, 455–483. https://doi.org/10.1016/S0277-3791(01)00105-6

Marchitto, T.M., Jones, G.A., Goodfriend, G.A., Weidman, C.R., 2000. Precise temporal correlation of Holocene mollusk shells using sclerochronology. Quat. Res. 53, 236–246. https://doi.org/10.1006/qres.1999.2107

Marret, F., Scourse, J., Austin, W., 2004. Holocene shelf-sea seasonal stratification dynamics: a dinoflagellate cyst record from the Celtic Sea, NW European shelf. The Holocene 5, 689–696.

Martín-García, R., Alonso-Zarza, A.M., Frisia, S., Rodríguez-Berriguete, Á., Drysdale, R., Hellstrom, J., 2019. Effect of aragonite to calcite transformation on the geochemistry and dating accuracy of speleothems. An example from Castañar Cave, Spain. Sediment. Geol. 383, 41–54. https://doi.org/10.1016/j.sedgeo.2019.01.014

McCauley, D.J., Desalles, P.A., Young, H.S., Dunbar, R.B., Dirzo, R., Mills, M.M., Micheli, F., 2012. From wing to wing: The persistence of long ecological interaction chains in less-disturbed ecosystems. Sci. Rep. 2. https://doi.org/10.1038/srep00409

Mette, M.J., Wanamaker Jr., A.D., Carroll, M.L., Ambrose Jr., W.G., Retelle, M.J., 2016. Linking large-scale climate variability with Arctica islandica shell growth and geochemistry in northern Norway. Limnol. Oceanogr. 61, 748–764. https://doi.org/10.1002/lno.10252

Mette, M.J., Wanamaker Jr., A.D., Retelle, M.J., Carroll, M.L., Andersson, C., Ambrose Jr., W.G., 2021. Persistent multidecadal variability since the 15th century in the southern Barents Sea derived from annually resolved shell-based records. J. Geophys. Res. Ocean. 126. https://doi.org/10.1029/2020JC017074

Mette, M.J., Whitney, N.M., Ballew, J., Wanamaker, Jr., A.D., 2018. Unexpected isotopic variability in biogenic aragonite: A user issue or proxy problem? Chem. Geol. 483, 286–294. https://doi.org/10.1016/j.chemgeo.2018.02.027

Moffa-Sánchez, P., Born, A., Hall, I.R., Thornalley, D.J.R., Barker, S., 2014. Solar forcing of North Atlantic surface temperature and salinity over the past millennium. Nat. Geosci. 7, 275–278. https://doi.org/10.1038/ngeo2094

Morton, B., 2011. The biology and functional morphology of Arctica islandica (Bivalvia: Arcticidae) – A gerontophilic living fossil. Mar. Biol. Res. 7, 540–553. https://doi.org/10.1080/17451000.2010.535833

Mulder, C.P.H., Jones, H.P., Kameda, K., Palmborg, C., Schmidt, S., Ellis, J.C., Orrock, J.L., Alexander Wait, D., Wardle, D.A., Yang, L.H., Young, H., Croll, D.A., Vidal, E., 2011. Impacts of seabirds on plant and soil properties. Seab. Islands Ecol. Invasion, Restor. https://doi.org/10.1093/acprof:osobl/9780199735693.003.0005

National Trust for Scotland, 2012. St Kilda world heritage site management plan 2012-2017.

Ninnemann, U.S., Thornalley, D.J.R., 2016. Recent natural variability of the Iceland Scotland Overflows on decadal to millennial timescales: Clues from the ooze. US Clivar Var. 14, 1–7.

Olsen, J., Anderson, N.J., Knudsen, M.F., 2012. Variability of the North Atlantic Oscillation over the past 5,200 years. Nat. Geosci. 5, 808–812. https://doi.org/10.1038/ngeo1589

Ong, J.J.L., Rountrey, A.N., Zinke, J., Meeuwig, J.J., Grierson, P.F., O'Donnell, A.J., Newman, S.J., Lough, J.M., Trougan, M., Meekan, M.G., 2016. Evidence for climate-driven synchrony of marine and terrestrial ecosystems in northwest Australia. Glob. Chang. Biol. 22, 2776–2786. https://doi.org/10.1111/gcb.13239

Orme, L.C., Charman, D.J., Reinhardt, L., Jones, R.T., Mitchell, F.J.G., Stefanini, B.S., Barkwith, A., Ellis, M.A., Grosvenor, M., 2017. Past changes in the North Atlantic storm track driven by insolation and sea-ice forcing. Geology 45, 335–338. https://doi.org/10.1130/G38521.1

Orme, L.C., Miettinen, A., Divine, D., Husum, K., Pearce, C., Van Nieuwenhove, N., Born, A., Mohan, R., Seidenkrantz, M.-S., 2018. Subpolar North Atlantic sea surface temperature since 6 ka BP: Indications of anomalous ocean-atmosphere interactions at 4-2 ka BP. Quat. Sci. Rev. 194, 128–142. https://doi.org/10.1016/j.quascirev.2018.07.007

Orme, L.C., Reinhardt, L., Jones, R.T., Charman, D.J., Barkwith, A., Ellis, M.A., 2016. Aeolian sediment reconstructions from the Scottish Outer Hebrides: Late Holocene storminess and the role of the North Atlantic Oscillation. Quat. Sci. Rev. 132, 15–25. https://doi.org/10.1016/j.quascirev.2015.10.045

Oschmann, W., 2009. Sclerochronology: editorial. Int. J. Earth Sci. 98, 1–2. https://doi.org/10.1007/s00531-008-0403-3

Ottersen, G., Planque, B., Belgrano, A., Post, E., Reid, P.C., Stenseth, N.C., 2001. Ecological effects of the North Atlantic Oscillation 1770, 1–14. https://doi.org/10.1007/s004420100655

Paillard, D., Labeyrie, L., Yiou, P., 1996. AnalySeries 1.0: a Macintosh software for the analysis of geophysical time-series. Eos, Trans. AGU 77, 379.

Painter, S.C., Hartman, S.E., Kivimae, C., Salt, L.A., Clargo, N.M., Bozec, Y., Daniels, C.J., Jones, S.C., Hemsley, V.S., Munns, L.R., Allen, S.R., 2016. Carbon exchange between a shelf sea and the ocean: The Hebrides Shelf, west of Scotland. J. Geophys. Res. Ocean. 121, 4522–4544. https://doi.org/10.1002/2015JC011599

Pearson, C., Salzer, M., Wacker, L., Brewer, P., Sookdeo, A., Kuniholm, P., 2020. Securing timelines in the ancient Mediterranean using multiproxy annual tree-ring data. Proc. Natl. Acad. Sci. 117. https://doi.org/10.1073/pnas.1917445117

Pederson, C., Mavromatis, V., Dietzel, M., Rollion-Bard, C., Nehrke, G., Jöns, N., Jochum, K.P., Immenhauser, A., 2019. Diagenesis of mollusc aragonite and the role of fluid reservoirs. Earth Planet. Sci. Lett. 514, 130–142. https://doi.org/10.1016/j.epsl.2019.02.038

Pingree, R.D., Holligan, P.M., Mardell, G.T., 1978. The effects of vertical stability on phytoplankton distributions in the summer on the northwest European Shelf. Deep. Res. 25. https://doi.org/10.1016/0146-6291(78)90584-2

Pingree, R.D., Sinha, B., Griffiths, C.R., 1999. Seasonality of the European slope current (Goban Spur) and ocean margin exchange. Cont. Shelf Res. 19, 929–975.

Planque, B., Fromentin, J.-M., 1996. Calanus and environment in the eastern North Atlantic. I. Spatial and temporal patterns of C. finmarchicus and C. helgolandicus. Mar. Ecol. Prog. Ser. 134, 101–109.

Polis, G.A., Anderson, W.B., Holt, R.D., 1997. Toward an integration of landscape and food web ecology: The dynamics of spatially subsidized food webs. Annu. Rev. Ecol. Syst. 28, 289–316. https://doi.org/10.1146/annurev.ecolsys.28.1.289

Polis, G.A., Hurd, S.D., 1996. Linking marine and terrestrial food webs: allochthonous input from the ocean supports high secondary productivity on small islands and coastal land communities. Am. Nat. 147, 396–423.

Porter, M., Dale, A.C., Jones, S., Siemering, B., Inall, M.E., 2018. Cross-slope flow in the Atlantic Inflow Current driven by the on-shelf deflection of a slope current. Deep. Res. Part I Oceanogr. Res. Pap. 140, 173–185. https://doi.org/10.1016/j.dsr.2018.09.002

Post, E., Forchhammer, M.C., 2002. Synchronization of animal population dynamics by large-scale climate. Nature 420, 168–171. https://doi.org/10.1038/nature01064

Post, E., Stenseth, N.C.H.R., 1998. Large-Scale climatic fluctuation and population dynamics of moose and white-tailed deer. J. Anim. Ecol. 67, 537–543.

Proctor, R., Holt, J.T., Allen, J.I., Blackford, J., 2003. Nutrient fluxes and budgets for the North West European Shelf from a three-dimensional model. Sci. Total Environ. 314–316, 769–785. https://doi.org/10.1016/S0048-9697(03)00083-4

Prouty, N.G., Roark, E.B., Koenig, A.E., Demopoulos, A.W.J., Batista, F.C., Kocar, B.D., Selby, D., McCarthy, M.D., Mienis, F., Ross, S.W., 2014. Deep-sea coral record of human impact on watershed quality in the Mississippi River Basin. Global Biogeochem. Cycles 28, 29–43. https://doi.org/10.1002/2013GB004754.Received

Rahmstorf, S., 2015. Thermohaline Circulation. Ref. Modul. Earth Syst. Environ. Sci. 1–12. https://doi.org/10.1016/b978-0-12-409548-9.09514-2

Rayner, N.A., Parker, D.E., Horton, E.B., Folland, C.K., Alexander, L. V., Rowell, D.P., Kent, E.C., Kaplan, A., 2003. Global analyses of sea surface temperature, sea ice, and night marine air temperature since the late nineteenth century. J. Geophys. Res. 108, 4407. https://doi.org/10.1029/2002JD002670

Reid, P.C., Colebrook, J.M., Matthews, J.B.L., Aiken, J., 2003. The Continuous Plankton Recorder: concepts and history, from Plankton Indicator to undulating recorders. Prog. Oceanogr. 58, 117–173. https://doi.org/10.1016/j.pocean.2003.08.002

Reid, P.C., Holliday, N.P., Smyth, T.J., 2001. Pulses in the eastern margin current and warmer water off the north west European shelf linked to North Sea ecosystem changes. Mar. Ecol. Prog. Ser. 215, 283–287.

Reimer, P., Hoper, S., McDonald, J., Reimer, R., Svyatko, S., Thompson, M., 2015. Laboratory Protocols Used for AMS Radiocarbon Dating at the 14Chrono Centre, Research Report Series.

Reimer, P.J., Bard, E., Bayliss, A., Beck, W.J., Blackwell, P.G., Bronk Ramsey, C., Buck, C.E., Cheng, H., Edwards, R.L., Friedrich, M., Grootes, P.M., Guilderson, T.P.,

Haflidason, H., Hajdas, I., Hatté, C., Heaton, T.J., Hoffmann, D.L., Hogg, A.G., Hughen, K.A., Kaiser, K.F., Kromer, B., Manning, S.W., Niu, M., Reimer, R.W., Richards, D.A., Scott, E.M., Southon, J.R., Staff, R.A., Turney, C.S.M., van der Plicht, J., 2013. Intcal13 and Marine13 radiocarbon age calibration curves 0–50,000 years cal BP. Radiocarbon 55, 1869–1887.

Reimer, P.J., McCormac, F.G., Moore, J., McCormick, F., Murray, E. V, 2002. Marine radiocarbon reservoir corrections for the mid- to late Holocene in the eastern subpolar North Atlantic. Holocene 12, 129–135. https://doi.org/10.1191/0959683602h1528rp

Reynolds, D.J., Butler, P.G., Williams, S.M., Scourse, J.D., Richardson, C.A., Wanamaker Jr., A.D., Austin, W.E.N., Cage, A.G., Sayer, M.D.J., 2013. A multiproxy reconstruction of Hebridean (NW Scotland) spring sea surface temperatures between AD 1805 and 2010. Palaeogeogr. Palaeoclimatol. Palaeoecol. 386, 275–285. https://doi.org/10.1016/j.palaeo.2013.05.029

Reynolds, D.J., Hall, I.R., Slater, S.M., Mette, M.J., Wanamaker, A.D., Scourse, J.D., Garry, F.K., Halloran, P.R., 2018. Isolating and reconstructing key components of North Atlantic Ocean variability from a sclerochronological spatial network. Paleoceanogr. Paleoclimatology 33, 1086–1098. https://doi.org/10.1029/2018PA003366

Reynolds, David J., Hall, I.R., Slater, S.M., Scourse, J.D., Halloran, P.R., Sayer, M.D.J., 2017. Reconstructing past seasonal to multicentennial-scale variability in the NE Atlantic Ocean using the long-lived marine bivalve mollusk Glycymeris glycymeris. Paleoceanography 32. https://doi.org/10.1002/2017PA003154

Reynolds, D. J., Richardson, C.A., Scourse, J.D., Butler, P.G., Hollyman, P., Rom??n-Gonz??lez, A., Hall, I.R., 2017. Reconstructing North Atlantic marine climate variability using an absolutely-dated sclerochronological network. Palaeogeogr. Palaeoclimatol. Palaeoecol. 465, 333–346. https://doi.org/10.1016/j.palaeo.2016.08.006

Reynolds, D.J., Scourse, J.D., Halloran, P.R., Nederbragt, A.J., Wanamaker, A.D.J., Butler, P.G., Richardson, C.A., Heinemeier, J., Eiríksson, J., Knudsen, K.L., Hall, I.R., 2016. Annually resolved North Atlantic marine climate over the last millennium. Nat. Commun. 7:13502. https://doi.org/10.1038/ncomms13502

Reynolds, R.W., Rayner, N.A., Smith, T.M., Stokes, D.C., Wang, W., 2002. An improved in situ and satellite SST analysis for climate. J. Clim. 15, 1609–1625.

Richardson, A.J., Walne, A.W., John, A.W.G., Jonas, T.D., Lindley, J.A., Sims, D.W., Stevens, D., Witt, M., 2006. Using continuous plankton recorder data. Prog. Oceanogr. 68, 27–74. https://doi.org/10.1016/j.pocean.2005.09.011

Richardson, C.A., 2001. Molluscs as archives of environmental change. Oceanogr. Mar. Biol. an Annu. Rev. 39, 103–164.

Rienecker, M.M., Suarez, M.J., Gelaro, R., Todling, R., Bacmeister, J., Liu, E., Bosilovich, M.G., Schubert, S.D., Takacs, L., Kim, G.-K., Bloom, S., Chen, J., Collins, D., Conaty, A., da Silva, A., Gu, W., Joiner, J., Koster, R.D., Lucchesi, R., Molod, A., Owens, T., Pawson, S., Pegion, P., Redder, C.R., Reichle, R., Robertson, F.R., Ruddick, A.G., Sienkiewicz, M., Woollen, J., 2011. MERRA : NASA's Modern-Era Retrospective Analysis for Research and Applications. J. Clim. 24, 3624–3648. https://doi.org/10.1175/JCLI-D-11-00015.1

Robson, J., Hodson, D., Hawkins, E., Sutton, R., 2014. Atlantic overturning in decline? Nat.

Geosci. 7, 2–3. https://doi.org/10.1038/ngeo2050

Rogalla, N.S., Amler, M.R.W., 2007. Statistic approach on taphonomic phenomena in shells of Glycymeris glycymeris (Bivalvia: Glycymerididae) and its significance in the fossil record. Paläontologische Zeitschrift 81, 334–355.

Rogers, J.C., 1985. Atmospheric circulation changes associated with the warming over the northern North Atlantic in the 1920s. J. Clim. Appl. Meteorol. 24, 1303–1310.

Rohling, E.J., 2013. Oxygen isotope composition of seawater, in: Elias, S.A. (Ed.), The Encyclopedia of Quaternary Science. Amsterdam: Elsevier, pp. 915–922. https://doi.org/10.1016/B978-0-444-53643-3.00293-4

Ropes, J.W., 1987. Preparation of acetate peels of valves from the ocean quahog, Arctica islandica, for age determinations. NOAA Tech. Rep. NMFS 50 1–5.

Rossby, T., 1996. The North Atlantic Current and surrounding waters: at the crossroads. Rev. Geophys. 34, 463–481.

Royer, C., Thébault, J., Chauvaud, L., Olivier, F., 2013. Structural analysis and paleoenvironmental potential of dog cockle shells (Glycymeris glycymeris) in Brittany, northwest France. Palaeogeogr. Palaeoclimatol. Palaeoecol. 373, 123–132. https://doi.org/10.1016/j.palaeo.2012.01.033

Russell, N., Cook, G.T., Ascough, P.L., Scott, E.M., 2015. A period of calm in Scottish seas: A comprehensive study of δR values for the northern British Isles coast and the consequent implications for archaeology and oceanography. Quat. Geochronol. 30, 34–41. https://doi.org/10.1016/j.quageo.2015.08.001

Schmitt, R.W., 2018. The ocean's role in climate. Oceanography 31, 32–40. https://doi.org/10.5670/oceanog.2018.225

Schöne, B.R., 2013. Arctica islandica (Bivalvia): A unique paleoenvironmental archive of the northern North Atlantic Ocean. Glob. Planet. Change 111, 199–225. https://doi.org/10.1016/j.gloplacha.2013.09.013

Schöne, B.R., Fiebig, J., 2009. Seasonality in the North Sea during the Allerød and Late Medieval Climate Optimum using bivalve sclerochronology. Int. J. Earth Sci. 98, 83–98. https://doi.org/10.1007/s00531-008-0363-7

Schöne, B.R., Fiebig, J., Pfeiffer, M., Gleß, R., Hickson, J., Johnson, A.L.A., Dreyer, W., Oschmann, W., 2005. Climate records from a bivalved Methuselah (Arctica islandica, Mollusca; Iceland). Palaeogeogr. Palaeoclimatol. Palaeoecol. 228, 130–148. https://doi.org/10.1016/j.palaeo.2005.03.049

Schöne, B.R., Gillikin, D.P., 2013. Unraveling environmental histories from skeletal diaries - Advances in sclerochronology. Palaeogeogr. Palaeoclimatol. Palaeoecol. 373, 1–5. https://doi.org/10.1016/j.palaeo.2012.11.026

Schöne, B.R., Goodwin, D.H., Flessa, K.W., Dettman, D.L., Roopnarine, P.D., 2002. Sclerochronology and growth of the bivalve mollusks Chione (Chionista) fluctifraga and C. (Chionista) cortezi in the northern Gulf of California, Mexico. Veliger 45, 45–54.

Schöne, B.R., Huang, Q., 2021. Ontogenetic δ15N trends and multidecadal variability in shells of the bivalve mollusk, Arctica islandica. Front. Mar. Sci. 8, 1–15. https://doi.org/10.3389/fmars.2021.748593

Schöne, B.R., Oschmann, W., Rössler, J., Freyre Castro, A.D., Houk, S.D., Kröncke, I., Dreyer, W., Janssen, R., Rumohr, H., Dunca, E., 2003. North Atlantic Oscillation dynamics recorded in shells of a long-lived bivalve mollusk. Geology 31, 1037–1040. https://doi.org/10.1130/G20013.1

Scott, A., 1960. The fauna of the sandy beach, Village Bay, St. Kilda: A dynamical relationship. Oikos 11, 153–160.

Scottish Executive, 2003. Revised Nomination of St Kilda for inclusion in the World Heritage Site List. Scottish Executive, Edinburgh.

Scourse, J., Richardson, C., Forsythe, G., Harris, I., Heinemeier, J., Fraser, N., Briffa, K., Jones, P., 2006. First cross-matched floating chronology from the marine fossil record: data from growth lines of the long-lived bivalve mollusc Arctica islandica. The Holocene 16, 967–974. https://doi.org/10.1177/0959683606hl987rp

Scourse, J.D., Austin, W.E.N., Long, B.T., Assinder, D.J., Huws, D., 2002. Holocene evolution of seasonal stratification in the Celtic Sea: Refined age model, mixing depths and foraminiferal stratigraphy. Mar. Geol. 191, 119–145. https://doi.org/10.1016/S0025-3227(02)00528-5

Scourse, J.D., Wanamaker Jr, A.D., Weidman, C., Heinemeier, J., Reimer, P.J., Butler, P.G., Witbaard, R., Richardson, C.A., 2012. The marine radiocarbon bomb pulse across the temperate North Atlantic: A compilation of Δ14C time histories from Arctica islandica growth increments. Radiocarbon 54, 165–186. https://doi.org/10.2458/azu_js_rc.v54i2.16026

Seager, R., Battisti, D.S., Yin, J., Gordon, N., Naik, N., Clement, A.C., Cane, M.A., 2002. Is the Gulf Stream responsible for Europe's mild winters? Q. J. R. Meteorol. Soc. 128, 2563–2586. https://doi.org/10.1256/qj.01.128

Shapiro, G.I., Hill, A.E., 1997. Dynamics of dense water cascades at the shelf edge. J. Phys. Oceanogr. 27, 2381–2394.

Shapiro, G.I., Huthnance, J.M., Ivanov, V. V, 2003. Dense water cascading off the continental shelf. J. Geophys. Res. 108. https://doi.org/10.1029/2002JC001610

Shatova, O., Wing, S.R., Gault-Ringold, M., Wing, L., Hoffmann, L.J., 2016. Seabird guano enhances phytoplankton production in the Southern Ocean. J. Exp. Mar. Bio. Ecol. 483, 74–87. https://doi.org/10.1016/j.jembe.2016.07.004

Shumway, S.E., Cucci, T.L., Newell, R.C., Yentsch, C.M., 1985. Particle selection, ingestion, and absorption in filter-feeding bivalves. J. Exp. Mar. Bio. Ecol. 91, 77–92. https://doi.org/10.1016/0022-0981(85)90222-9

Siemering, B., Bresnan, E., Painter, S.C., Daniels, C.J., Inall, M., Davidson, K., 2016. Phytoplankton distribution in relation to environmental drivers on the North West European Shelf sea. PLoS One 11, e0164482. https://doi.org/10.1371/journal.pone.0164482

Simmonds, E.G., Coulson, T., 2015. Analysis of phenotypic change in relation to climatic drivers in a population of Soay sheep Ovis aries. Oikos 124, 543–552. https://doi.org/10.1111/oik.01727

Simpson, J.H., 1997. Physical processes in the ROFI regime. J. Mar. Syst. 12, 3–15.

Simpson, J.H., Edelsten, D.J., Edwards, A., Morris, N.C.G., Tett, P.B., 1979. The Islay Front: Physical structure and phytoplankton distribution. Estuar. Coast. Mar. Sci. 9, 713–726.

Simpson, J.H., Hill, A.E., 1986. The Scottish Coastal Current, in: Skreslet, S. (Ed.), The Role of Freshwater Outflow in Coastal Marine Ecosystems. NATO ASI Series (Series G: Ecological Sciences), Vol. 7. Springer, Berlin, Heidelberg, pp. 295–308. https://doi.org/10.1007/978-3-642-70886-2_21

Simpson, J.H., McCandliss, R.R., 2013. "The Ekman Drain": a conduit to the deep ocean for shelf material. Ocean Dyn. 1063–1072. https://doi.org/10.1007/s10236-013-0644-y

Simpson, J.H., Tett, P.B., 1986. Island stirring effects on phytoplankton growth, in: Bowman, J., Yentsch, M., Peterson, W.T. (Eds.), Tidal Mixing and Plankton Dynamics. Lecture Notes on Coastal and Estuarine Studies. Springer Berlin Heidelberg, pp. 41–76.

Smeed, D.A., Josey, S.A., Beaulieu, C., Johns, W.E., Moat, B.I., Frajka-Williams, E., Rayner, D., Meinen, C.S., Baringer, M.O., Bryden, H.L., McCarthy, G.D., 2018. The North Atlantic Ocean is in a state of reduced overturning. Geophys. Res. Lett. 45, 1527–1533. https://doi.org/10.1002/2017GL076350

Smith, A.F., Fryer, R.J., Webster, L., Berx, B., Taylor, A., Walsham, P., Turrell, W.R., 2014. Setting background nutrient levels for coastal waters with oceanic influences. Estuar. Coast. Shelf Sci. 145, 69–79. https://doi.org/10.1016/j.ecss.2014.04.006

Smith, T.M., Reynolds, R.W., Peterson, T.C., Lawrimore, J., 2008. Improvements to NOAA's historical merged land-ocean surface temperature analysis (1880-2006). J. Clim. 21, 2283–2296. https://doi.org/10.1175/2007JCLI2100.1

Solignac, S., Grelaud, M., de Vernal, A., Giraudeau, J., Moros, M., McCave, I.N., Hoogakker, B., 2008. Reorganization of the upper ocean circulation in the mid-Holocene in the northeastern Atlantic. Can. J. Earth Sci. 45, 1417–1433. https://doi.org/10.1139/E08-061

Souza, A.J., Simpson, J.H., Harikrishnan, M., Malarkey, J., 2001. Flow structure and seasonality in the Hebridean slope current. Oceanol. Acta 24, 63–76. https://doi.org/10.1016/S0399-1784(00)01103-8

Steinhilber, F., Abreu, J.A., Beer, J., Brunner, I., Christl, M., Fischer, H., Heikkilä, U., Kubik, P.W., Mann, M., McCracken, K.G., Miller, H., Miyahara, H., Oerter, H., Wilhelms, F., 2012. 9,400 years of cosmic radiation and solar activity from ice cores and tree rings. Proc. Natl. Acad. Sci. U. S. A. 109, 5967–5971. https://doi.org/10.1073/pnas.1118965109

Steinhilber, F., Beer, J., Fröhlich, C., 2009. Total solar irradiance during the Holocene. Geophys. Res. Lett. 36, L19704.

Strom, A., Francis, R.C., Mantua, N.J., Miles, E.L., Peterson, D.L., 2005. Preserving low-frequency climate signals in growth records of geoduck clams (Panopea abrupta). Palaeogeogr. Palaeoclimatol. Palaeoecol. 228, 167–178. https://doi.org/10.1016/j.palaeo.2005.03.048

Stuiver, M., Braziunas, T.F., 1993. Modeling atmospheric 14C influences and 14C ages of marine samples to 10,000 BC. Radiocarbon 35, 137–189. https://doi.org/10.1017/S0033822200013874

Surge, D., Wang, T., Gutiérrez-Zugasti, I.G., Kelley, P.H., 2013. Isotope sclerochronology

and season of annual growth line formation in limpet shells (Patella vulgata) from warm- and cold-temperate zones in the eastern North Atlantic. Palaios 28, 386–393. https://doi.org/10.2110/palo.2012.p12-038r

Sutherland, D.G., 1984. The submerged landforms of the St. Kilda archipelago, western Scotland. Mar. Geol. 58, 435–442.

Sutherland, D.G., Ballantyne, C.K., Walker, M.J.C., 1984. Late Quaternary glaciation and environmental change on St. Kilda, Scotland, and their palaeoclimatic significance. Boreas 13, 261–272.

Swan, L.W., 1963. Aeolian zone. Science (80-.). 140, 77–78. https://doi.org/10.1126/science.140.3562.78

Swindles, G.T., Lawson, I.T., Matthews, I.P., Blaauw, M., Daley, T.J., Charman, D.J., Roland, T.P., Plunkett, G., Schettler, G., Gearey, B.R., Turner, T.E., Rea, H.A., Roe, H.M., Amesbury, M.J., Chambers, F.M., Holmes, Jonathan, Mitchell, F.J.G., Blackford, J., Blundell, A., Branch, N., Holmes, Jane, Langdon, P., McCarroll, J., McDermott, F., Oksanen, P.O., Pritchard, O., Stastney, P., Stefanini, B., Young, D., Wheeler, J., Becker, K., Armit, I., 2013. Centennial-scale climate change in Ireland during the Holocene. Earth-Science Rev. 126, 300–320. https://doi.org/10.1016/j.earscirev.2013.08.012

Taylor, A.C., 1976. Burrowing behaviour and anaerobiosis in the bivalve arctica islandica (L.). J. Mar. Biol. Assoc. United Kingdom 56, 95–109. https://doi.org/10.1017/S0025315400020464

Taylor, A.H., Stephens, J.A., 1998. The North Atlantic Oscillation and the latitude of the Gulf Stream. Tellus A Dyn. Meteorol. Oceanogr. 50, 134–142. https://doi.org/10.3402/tellusa.v50i1.14517

Taylor, K.E., 2001. Summarizing multiple aspects of model performance in a single diagram. J. Geophys. Res. 106, 7183–7192. https://doi.org/10.1029/2000JD900719

Thibault, M., Duprey, N., Gillikin, D.P., Thébault, J., Douillet, P., Chauvaud, L., Amice, E., Munaron, J.M., Lorrain, A., 2020. Bivalve δ15N isoscapes provide a baseline for urban nitrogen footprint at the edge of a World Heritage coral reef. Mar. Pollut. Bull. 152, 110870. https://doi.org/10.1016/j.marpolbul.2019.110870

Thomas, R.D.K., 1975. Functional morphology, ecology, and evolutionary conservatism in the Glycymerididae (Bivalvia). Palaeontology 18, 217–254.

Thompson, P.M., Ollason, J.C., 2001. Lagged effects of ocean climate change on fulmar population dynamics. Nature 413, 417–420. https://doi.org/10.1038/35096558

Thomson, D.J., 1982. Spectrum estimation and harmonic analysis. Proc. IEEE 70, 1055–1096. https://doi.org/10.1109/PROC.1982.12433

Thórarinsdóttir, G.G., Einarsson, S.T., 1996. Distribution, abundance, population structure and meat yield of the ocean quahog, Arctica islandica, in Icelandic waters. J. Mar. Biol. Assoc. United Kingdom 76, 1107–1114. https://doi.org/10.1017/s0025315400040996

Toggweiler, J.R., Key, R.M., 2001. Thermohaline Circulation. Encycl. Ocean Sci. 2941–2947. https://doi.org/10.1006/rwos.2001.0111

Torrence, C., Compo, G.P., 1998. A Practical Guide to Wavelet Analysis. Bull. Am. Meteorol. Soc. 79, 61–78. https://doi.org/10.1175/1520-

0477(1998)079<0061:APGTWA>2.0.CO;2

Trenberth, K.E., Fasullo, J.T., Balmaseda, M.A., 2014. Earth's energy imbalance. J. Clim. 27, 3129–3144. https://doi.org/10.1175/JCLI-D-13-00294.1

Trofimova, T., Alexandroff, S.J., Mette, M.J., Tray, E., Butler, P.G., Campana, S.E., Harper, E.M., Johnson, A.L.A., Morrongiello, J.R., Peharda, M., Schöne, B.R., Andersson, C., Andrus, C.F.T., Black, B.A., Burchell, M., Carroll, M.L., DeLong, K.L., Gillanders, B.M., Grønkjær, P., Killam, D., Prendergast, A.L., Reynolds, D.J., Scourse, J.D., Shirai, K., Thébault, J., Trueman, C., de Winter, N., 2020. Fundamental questions and applications of sclerochronology: Community-defined research priorities. Estuar. Coast. Shelf Sci. 245, 106977. https://doi.org/10.1016/j.ecss.2020.106977

Trofimova, T., Milano, S., Andersson, C., Bonitz, F.G.W., Schöne, B.R., 2018. Oxygen isotope composition of Arctica islandica aragonite in the context of shell architectural organization: Implications for paleoclimate reconstructions. Geochemistry, Geophys. Geosystems 19. https://doi.org/10.1002/2017GC007239

Trouet, V., Van Oldenborgh, G.J., 2013. KNMI climate explorer: A web-based research tool for high-resolution paleoclimatology. Tree-Ring Res. 69, 3–13. https://doi.org/10.3959/1536-1098-69.1.3

Turrell, W.R., Slesser, G., Payne, R., Adams, R.D., Gillibrand, P.A., 1996. Hydrography of the East Shetland Basin in relation to decadal North Sea variability. ICES J. Mar. Sci. 53, 899–916. https://doi.org/10.1006/jmsc.1996.0112

Uehara, K., Scourse, J.D., Horsburgh, K.J., Lambeck, K., Purcell, A.P., 2006. Tidal evolution of the northwest European shelf seas from the Last Glacial Maximum to the present. J. Geophys. Res. Ocean. 111, C09025. https://doi.org/10.1029/2006JC003531

UNFCCC, 2021. Nationally determined contributions under the Paris Agreement: Synthesis report by the secretariat. English 1–42.

Urey, H.C., 1947. The Thermodynamic properties of isotopic substances. J. Chem. Soc. 562–581.

Urey, H.C., Lowenstam, H.A., Epstein, S., McKinney, C.R., 1951. Measurement of paleotemperatures and temperatures of the upper Cretaceous of England, Denmark, and the southeastern United States. Bull. Geol. Soc. Am. 62, 399–416. https://doi.org/10.1130/0016-7606(1951)62[399:MOPATO]2.0.CO;2

Van Nieuwenhove, N., Pearce, C., Knudsen, M.F., Røy, H., Seidenkrantz, M.-S., 2018. Meltwater and seasonality influence on Subpolar Gyre circulation during the Holocene. Palaeogeogr. Palaeoclimatol. Palaeoecol. 502, 104–118. https://doi.org/10.1016/j.palaeo.2018.05.002

Vaughan, S., Bailey, R.J., Smith, D.G., 2011. Detecting cycles in stratigraphic data: Spectral analysis in the presence of red noise. Paleoceanography 26, 1–15. https://doi.org/10.1029/2011PA002195

Vautard, R., Yiou, P., Ghil, M., 1992. Singular-spectrum analysis: A toolkit for short, noisy chaotic signals. Phys. D Nonlinear Phenom. 58, 95–126. https://doi.org/10.1016/0167-2789(92)90103-T

Visbeck, M., Chassignet, E.P., Curry, R.G., Delworth, T.L., Dickson, R.R., Krahmann, G., 2003. The ocean's response to North Atlantic Oscillation variability, in: The North

Atlantic Oscillation: Climatic Significance and Environmental Impact. Geophysical Monograph Series. https://doi.org/10.1029/134GM06

Vogel, J.S., Southon, J.R., Nelson, D.E., Brown, T.A., 1984. Performance of catalytically condensed carbon for use in accelerator mass spectrometry. Nucl. Inst. Methods Phys. Res. B 5, 289–293. https://doi.org/10.1016/0168-583X(84)90529-9

Vogel, K., Gektidis, M., Golubic, S., Kiene, W.E., Radtke, G., 2000. Experimental studies on microbial bioerosion at Lee Stocking Island, Bahamas and One Tree Island, Great Barrier Reef, Australia: Implications for paleoecological reconstructions. Lethaia 33, 190–204. https://doi.org/10.1080/00241160025100053

Wakelin, S.L., Holt, J.T., Blackford, J.C., Allen, J.I., Butenschön, M., Artioli, Y., 2012. Modeling the carbon fluxes of the northwest European continental shelf: Validation and budgets. J. Geophys. Res. Ocean. 117, C05020. https://doi.org/10.1029/2011JC007402

Wanamaker, Jr., A.D., Hetzinger, S., Halfar, J., 2011. Reconstructing mid- to high-latitude marine climate and ocean variability using bivalves, coralline algae, and marine sediment cores from the Northern Hemisphere. Palaeogeogr. Palaeoclimatol. Palaeoecol. 302, 1–9. https://doi.org/10.1016/j.palaeo.2010.12.024

Wanamaker, A.D.J., Kreutz, K.J., Schöne, B.R., Introne, D.S., 2011. Gulf of Maine shells reveal changes in seawater temperature seasonality during the Medieval Climate Anomaly and the Little Ice Age. Palaeogeogr. Palaeoclimatol. Palaeoecol. 302, 43–51. https://doi.org/10.1016/j.palaeo.2010.06.005

Wanamaker Jr., A.D., Kreutz, K.J., Schöne, B.R., Maasch, K.A., Pershing, A.J., Borns, H.W., Introne, D.S., Feindel, S., 2009. A late Holocene paleo-productivity record in the western Gulf of Maine, USA, inferred from growth histories of the long-lived ocean quahog (Arctica islandica). Int. J. Earth Sci. 98, 19–29. https://doi.org/10.1007/s00531-008-0318-z

Wanner, H., Beer, J., Bütikofer, J., Crowley, T.J., Cubasch, U., Flückiger, J., Goosse, H., Grosjean, M., Joos, F., Kaplan, J.O., Küttel, M., Müller, S.A., Prentice, I.C., Solomina, O., Stocker, T.F., Tarasov, P., Wagner, M., Widmann, M., 2008. Mid- to Late Holocene climate change: an overview. Quat. Sci. Rev. 27, 1791–1828. https://doi.org/10.1016/j.quascirev.2008.06.013

Ward, S.L., Neill, S.P., Scourse, J.D., Bradley, S.L., Uehara, K., 2016. Sensitivity of palaeotidal models of the northwest European shelf seas to glacial isostatic adjustment since the Last Glacial Maximum. Quat. Sci. Rev. 151, 198–211. https://doi.org/10.1016/j.quascirev.2016.08.034

Warter, V., Müller, W., 2017. Daily growth and tidal rhythms in Miocene and modern giant clams revealed via ultra-high resolution LA-ICPMS analysis — A novel methodological approach towards improved sclerochemistry. Palaeogeogr. Palaeoclimatol. Palaeoecol. 465, 362–375. https://doi.org/10.1016/j.palaeo.2016.03.019

Watling, R., Irvine, L.M., Norton, T.A., 1970. The marine algae of St. Kilda. Trans. Bot. Soc. Edinburgh 41, 31–41. https://doi.org/10.1080/03746607008685197

Weidman, C.R., Jones, G.A., Lohmann, K.C., 1994. The long-lived mollusc Arctica islandica: A new paleoceanographic tool for the reconstruction of bottom temperatures for the continental shelves of the northern North Atlantic Ocean. J. Geophys. Res. 99, 18,305-18,314. https://doi.org/10.1029/94JC01882

Whyte, C., Swan, S., Davidson, K., 2014. Changing wind patterns linked to unusually high Dinophysis blooms around the Shetland Islands , Scotland. Harmful Algae 39, 365–373. https://doi.org/10.1016/j.hal.2014.09.006

Wigley, T.M.L., Briffa, K.R., Jones, P.D., 1984. On the average value of correlated time series, with applications in dendroclimatology and hydrometeorology. J. Clim. Appl. Meteorol. 23, 201–213.

Wijffels, S., Roemmich, D., Monselesan, D., Church, J., Gilson, J., 2016. Ocean temperatures chronicle the ongoing warming of Earth. Nat. Clim. Chang. 6, 116–118. https://doi.org/10.1038/nclimate2924

Williams, B., Risk, M.J., Ross, S.W., Sulak, K.J., 2007. Stable isotope data from deep-water Antipatharians : 400-year records from the southeastern coast of the United States of America. Bull. Mar. Sci. 81, 437–447.

Winter, J.E., 1969. Über den Einfluß der Nahrungskonzentration und anderer Faktoren auf Filtrierleistung und Nahrungsausnutzung der Muscheln Arctica islandica und Modiolus modiolus. Mar. Biol. 4, 87–135. https://doi.org/10.1007/BF00347037

Witbaard, R., Duineveld, G.C.A., de Wilde, P.A.W.J., 1997a. A long-term growth record derived from Arctica islandica (Mollusca, Bivalvia) from the Fladen Ground (northern North Sea). J. Mar. Biol. Assoc. United Kingdom 77, 801–816.

Witbaard, R., Franken, R., Visser, B., 1997b. Growth of juvenile Arctica islandica under experimental conditions. Helgoländer Meeresuntersuchungen 51, 417–431.

Witbaard, R., Jansma, E., Sass Klaassen, U., 2003. Copepods link quahog growth to climate. J. Sea Res. 50, 77–83. https://doi.org/10.1016/S1385-1101(03)00040-6

Witbaard, R., Jenness, M.I., Van Der Borg, K., Ganssen, G., 1994. Verification of annual growth increments in Arctica islandica L. from the North Sea by means of oxygen and carbon isotopes. Netherlands J. Sea Res. 33, 91–101. https://doi.org/10.1016/0077-7579(94)90054-X

Wunsch, C., 1999. The interpretation of short climate records, with comments on the North Atlantic and Southern Oscillations. Bull. Am. Meteorol. Soc. 80, 245–255. https://doi.org/10.1175/1520-0477(1999)080<0245:TIOSCR>2.0.CO;2

Young, E.F., Holt, J.T., 2007. Prediction and analysis of long-term variability of temperature and salinity in the Irish Sea. J. Geophys. Res. Ocean. 112. https://doi.org/10.1029/2005JC003386

Zhang, R., Sutton, R., Danabasoglu, G., Delworth, T.L., Kim, W.M., Robson, J., Yeager, S.G., 2016. Comment on “The Atlantic Multidecadal Oscillation without a role for ocean circulation.” Science (80-.). 352, 1527. https://doi.org/10.1126/science.aaf1660

Appendix A1, A2, B

Appendix A1 — *Glycymeris* measurements and shell conditions

Glycymeris reference #	*Locality*	*Valve (Right / Left / Articulated)*	*Length (mm)*	*Height (mm)*	*Max Height (mm)*	*Width (mm)*	*Mass of a single valve (g)*	*Periostracum (1-5)*	*Ligament (1-4)*	*Shell margin (1-4)*	*Bioerosion (1-4)*	*Nacre (1-3)*
14G0VB001	St Kilda	N	64.84	58.67	60.01	19.04	28.0	1	1	2	4	2
14G0VB002	St Kilda	N	57.34	51.91	52.71	16.49	22.6	1	1	2	4	2
14G0VB003	St Kilda	N	79.09	70.65	72.81	21.25	48.9	1	1	2	4	1
14G0VB004	St Kilda	N	68.78	65.65	66.21	18.91	38.3	1	1	2	4	2
14G0VB005	St Kilda	N	72.43	66.30	72.51	20.76	46.8	1	1	2	4	2
14G0VB006	St Kilda	N	69.67	62.29	65.17	18.91	36.0	1	1	2	4	1
14G0VB007	St Kilda	N	59.23	53.32	53.84	17.02	21.8	1	1	2	4	2
14G0VB008	St Kilda	N	66.05	60.08	61.28	17.03	29.0	1	1	2	4	2
14G0VB009	St Kilda	N	58.55	52.37	52.56	15.92	20.7	1	1	2	4	2
14G0VB010	St Kilda	N	60.47	55.36	56.45	17.73	20.9	1	1	2	4	2
14G0VB011	St Kilda	N	52.60	50.45	52.38	15.41	18.8	1	1	2	4	2
14G0VB012	St Kilda	N	52.36	50.92	51.90	15.95	20.5	1	1	2	4	2
14G0VB013	St Kilda	N	53.48	51.49	53.34	15.43	16.0	1	1	2	4	2
14G0VB014	St Kilda	N	48.15	46.34	46.34	16.49	16.7	1	1	2	4	2
14G0VB015	St Kilda	N	40.59	37.19	37.29	10.91	6.6	1	1	2	4	2
14G0VB016	St Kilda	N	46.87	43.26	43.64	12.63	10.3	1	1	2	4	2
14G0VB017	St Kilda	N	45.36	44.94	45.51	13.87	12.1	1	1	2	4	2
14G0VB018	St Kilda	N	43.54	41.45	41.45	10.17	6.9	1	1	2	4	2
14G0VB019	St Kilda	N	71.01	64.86	67.19	19.58	40.1	1	1	2	4	3

Glycymeris reference #	*Locality*	*Valve (Right / Left / Articulated)*	*Length (mm)*	*Height (mm)*	*Max Height (mm)*	*Width (mm)*	*Mass of a single valve (g)*	*Periostracum (1-5)*	*Ligament (1-4)*	*Shell margin (1-4)*	*Bioerosion (1-4)*	*Nacre (1-3)*
14G0VB020	St Kilda	N	72.49	67.90	70.27	20.97	44.0	1	1	1	4	2
14G0VB021	St Kilda	N	68.07	64.12	65.59	19.01	33.6	1	1	2	4	3
14G0VB022	St Kilda	N	63.40	58.26	59.77	19.80	31.6	1	1	2	4	2
14G0VB023	St Kilda	N	59.09	56.46	58.06	18.02	27.5	1	1	2	4	2
14G0VB024	St Kilda	N	64.33	56.37	60.24	18.30	27.9	1	1	1	4	2
14G0VB025	St Kilda	N	59.01	52.68	53.13	15.51	22.3	1	1	1	4	2
14G0VB026	St Kilda	N	57.36	53.55	55.07	15.40	22.0	1	1	1	4	2
14G0VB027	St Kilda	N	58.91	53.24	56.59	17.69	24.0	1	1	1	4	2
14G0VB028	St Kilda	N	58.07	57.36	58.23	18.36	27.7	1	1	1	4	1
14G0VB029	St Kilda	N	55.64	55.40	55.95	17.33	23.1	1	1	1	4	1
14G0VB030	St Kilda	N	57.07	52.87	53.26	14.20	16.3	1	1	2	4	2
14G0VB031	St Kilda	N	55.49	53.90	55.21	17.28	21.5	1	1	1	4	1
14G0VB032	St Kilda	N	55.12	52.22	53.59	15.59	15.7	1	1	1	4	1
14G0VB033	St Kilda	N	54.76	51.56	52.23	17.72	16.4	1	1	2	4	3
14G0VB034	St Kilda	N	52.70	47.96	48.47	13.37	11.9	1	1	2	4	3
14G0VB035	St Kilda	N	54.68	49.48	49.76	15.01	15.5	1	1	2	4	3
14G0VB036	St Kilda	N	49.22	47.67	47.67	13.50	14.0	1	1	2	4	3
14G0VB037	St Kilda	N	54.27	51.61	52.92	15.93	16.8	1	1	2	4	3
14G0VB038	St Kilda	N	48.98	47.78	47.78	14.17	16.5	1	1	2	4	3
14G0VB039	St Kilda	N	45.23	45.65	45.85	13.35	10.2	1	1	2	4	3
14G0VB040	St Kilda	N	36.05	33.95	34.24	9.28	5.1	1	1	2	4	3
14G0VB041	St Kilda	N	44.02	42.67	43.49	11.70	10.0	1	1	2	4	3

Glycymeris reference #	*Locality*	*Valve (Right / Left / Articulated)*	*Length (mm)*	*Height (mm)*	*Max Height (mm)*	*Width (mm)*	*Mass of a single valve (g)*	*Periostracum (1-5)*	*Ligament (1-4)*	*Shell margin (1-4)*	*Bioerosion (1-4)*	*Nacre (1-3)*
14G0VB042	St Kilda	N	72.46	70.36	71.16	18.15	45.6	1	1	1	4	1
14G0VB043	St Kilda	N	64.82	62.31	63.06	18.78	40.2	1	1	1	4	2
14G0VB044	St Kilda	N	61.42	59.46	60.45	17.65	29.5	1	1	1	4	3
14G0VB045	St Kilda	N	56.52	53.73	54.30	15.23	20.5	1	1	1	4	3
14G0VB046	St Kilda	N	57.56	53.65	54.23	15.11	19.6	1	1	1	4	3
14G0VB047	St Kilda	N	33.03	30.46	30.46	7.78	3.9	1	1	1	4	3
14G0VB048	St Kilda	N	57.05	53.28	53.28	n.a.	n.a.	1	1	1	4	3
14G0VB049	St Kilda	N	58.27	55.20	55.20	16.38	23.0	1	1	2	4	2
14G0VB050	St Kilda	N	58.03	60.09	60.09	18.44	31.6	1	1	2	4	2
14G0VB051	St Kilda	N	54.70	56.41	56.41	17.06	24.9	1	1	1	2	2
14G0VB052	St Kilda	N	49.80	49.04	49.04	12.89	14.5	1	1	1	2	2
14G0VB053	St Kilda	N	48.30	50.33	50.33	14.22	17.7	1	1	1	2	2
14G0VB054	St Kilda	N	55.12	55.88	55.88	14.92	19.4	1	1	1	2	2
14G0VB055	St Kilda	N	38.60	37.66	37.66	10.84	7.5	1	1	1	2	2
14G0VB056	St Kilda	N	54.19	51.15	51.15	13.24	16.8	1	1	1	2	2
14G0VB057	St Kilda	N	55.36	56.72	56.72	17.26	21.3	1	1	1	2	2
14G0VB058	St Kilda	N	62.79	62.52	62.52	16.48	25.6	1	1	1	2	1
14G0VB059	St Kilda	N	59.38	56.96	56.96	17.01	22.0	1	1	1	3	1
14G0VB060	St Kilda	N	55.14	52.77	52.77	14.33	16.3	1	1	1	3	1
14G0VB061	St Kilda	N	40.10	39.39	39.39	10.19	9.4	1	1	1	3	1
14G0VB062	St Kilda	N	42.59	43.70	43.70	12.36	9.3	1	1	1	3	1
14G0VB063	St Kilda	N	40.81	39.18	39.18	9.82	7.0	1	1	1	3	1

Glycymeris reference #	*Locality*	*Valve (Right / Left / Articulated)*	*Length (mm)*	*Height (mm)*	*Max Height (mm)*	*Width (mm)*	*Mass of a single valve (g)*	*Periostracum (1-5)*	*Ligament (1-4)*	*Shell margin (1-4)*	*Bioerosion (1-4)*	*Nacre (1-3)*
14G0VB064	St Kilda	N	46.04	43.87	43.87	12.65	10.6	1	1	1	3	1
14G0VB065	St Kilda	N	43.90	42.68	42.68	12.12	10.6	1	1	1	3	1
14G0VB066	St Kilda	N	41.10	40.19	40.19	11.12	8.9	1	1	1	3	1
14G0VB067	St Kilda	N	47.40	48.38	48.38	13.10	14.4	1	1	1	3	1
14G0VB068	St Kilda	N	43.22	41.76	41.76	11.45	8.0	1	1	1	3	1
14G0VB069	St Kilda	N	40.56	39.95	39.95	11.56	8.0	1	1	1	3	1
14G0VB070	St Kilda	N	55.62	54.15	54.78	14.69	22.9	1	1	1	3	1
14G0VB071	St Kilda	N	51.70	49.30	49.30	11.95	12.8	1	1	1	3	1
14G0VB072	St Kilda	N	56.21	53.77	54.31	15.91	22.5	1	1	1	3	1
14G0VB073	St Kilda	N	43.04	41.25	41.47	11.29	10.5	1	1	1	3	1
14G0VB074	St Kilda	N	52.45	52.52	53.09	14.35	18.0	1	1	1	3	1
14G0VB075	St Kilda	N	41.58	40.31	40.31	12.86	7.3	1	1	1	3	1
14G0VB076	St Kilda	N	42.86	40.16	40.40	11.23	8.7	1	1	1	3	1
14G0VB077	St Kilda	N	52.13	50.53	51.00	14.04	16.3	1	1	1	3	1
14G0VB078	St Kilda	N	48.88	49.85	49.95	12.30	12.1	1	1	1	3	1
14G0VB079	St Kilda	N	50.39	49.50	49.67	14.25	16.5	1	1	1	3	1
14G0VB080	St Kilda	N	46.99	46.87	46.99	12.73	9.8	1	1	1	3	1
14G0VB081	St Kilda	N	40.12	41.87	41.89	11.86	8.1	1	1	1	3	1
14G0VB082	St Kilda	N	39.64	37.54	37.54	10.62	7.2	1	1	1	3	1
14G0VB083	St Kilda	N	59.64	58.14	58.49	14.53	17.3	1	1	1	3	1
14G0VB084	St Kilda	N	62.50	59.27	60.55	16.43	20.5	1	1	1	3	1
14G0VB085	St Kilda	N	48.91	47.30	47.53	10.86	10.9	1	1	1	3	1

Glycymeris reference #	*Locality*	*Valve (Right / Left / Articulated)*	*Length (mm)*	*Height (mm)*	*Max Height (mm)*	*Width (mm)*	*Mass of a single valve (g)*	*Periostracum (1-5)*	*Ligament (1-4)*	*Shell margin (1-4)*	*Bioerosion (1-4)*	*Nacre (1-3)*
14G0VB086	St Kilda	N	52.44	52.32	52.37	14.59	17.5	1	1	1	3	1
14G0VB087	St Kilda	N	63.30	63.08	64.06	16.48	24.0	1	1	1	1	1
14G0VB088	St Kilda	N	59.82	58.53	58.83	16.64	27.7	1	1	1	3	1
14G0VB089	St Kilda	N	64.08	62.64	63.80	16.77	24.0	1	1	1	3	1
14G0VB090	St Kilda	N	55.88	52.31	53.62	13.77	14.8	1	1	1	3	1
14G0VB091	St Kilda	N	52.02	49.62	49.62	14.45	15.5	1	1	1	3	1
14G0VB092	St Kilda	N	53.36	51.65	51.68	14.33	16.1	1	1	1	3	1
14G0VB093	St Kilda	N	50.03	49.63	49.63	12.47	15.5	1	1	1	3	1
14G0VB094	St Kilda	N	50.64	45.91	46.21	11.78	10.2	1	1	1	3	1
14G0VB095	St Kilda	N	52.78	50.34	50.34	12.72	15.1	1	1	1	3	1
14G0VB096	St Kilda	N	49.50	n.a.	n.a.	14.55	18.6	1	1	1	3	1
14G0VB097	St Kilda	N	49.57	48.12	48.23	13.38	14.8	1	1	1	3	1
14G0VB098	St Kilda	N	43.31	41.76	41.76	11.61	9.0	1	1	1	3	1
14G0VB099	St Kilda	N	43.13	40.10	40.10	11.27	9.8	1	1	1	3	1
14G0VB100	St Kilda	N	53.26	51.52	51.76	12.97	14.8	1	1	2	4	2
14G0VB101	St Kilda	N	41.47	38.41	38.49	12.01	8.8	1	1	2	4	2
14G0VB102	St Kilda	N	50.17	48.08	48.08	14.44	17.6	1	1	2	4	2
14G0VB103	St Kilda	N	50.38	47.64	48.07	13.75	17.3	1	1	2	4	2
14G0VB104	St Kilda	N	51.50	51.21	51.70	14.62	17.4	1	1	2	4	2
14G0VB105	St Kilda	N	45.35	44.11	44.28	14.20	15.7	1	1	2	4	2
14G0VB106	St Kilda	N	43.03	42.08	42.22	11.38	9.3	1	1	2	4	2
14G0VB107	St Kilda	N	47.58	46.67	46.75	11.96	11.3	1	1	2	4	2

Glycymeris reference #	*Locality*	*Valve (Right / Left / Articulated)*	*Length (mm)*	*Height (mm)*	*Max Height (mm)*	*Width (mm)*	*Mass of a single valve (g)*	*Periostracum (1-5)*	*Ligament (1-4)*	*Shell margin (1-4)*	*Bioerosion (1-4)*	*Nacre (1-3)*
14G0VB108	St Kilda	N	41.92	39.72	40.12	10.64	8.7	1	1	2	4	2
14G0VB109	St Kilda	N	53.92	53.58	54.15	14.74	18.9	1	1	1	3	2
14G0VB110	St Kilda	N	56.86	54.10	54.22	13.52	17.4	1	1	1	2	1
14G0VB111	St Kilda	N	54.04	50.62	50.66	14.16	12.6	1	1	1	2	1
14G0VB112	St Kilda	N	44.45	44.62	44.92	12.21	9.8	1	1	1	2	1
14G0VB113	St Kilda	N	46.87	48.47	48.51	14.38	14.6	1	1	1	2	1
14G0VB114	St Kilda	N	58.47	56.32	56.32	16.36	25.5	1	1	2	4	2
14G0VB115	St Kilda	N	56.24	55.11	55.11	15.11	22.4	1	1	1	4	1
14G0VB116	St Kilda	N	51.92	54.81	54.95	14.05	17.9			3	4	2
14G0VB117	St Kilda	N	52.09	52.85	52.92	14.07	18.9			2	3	2
14G0VB118	St Kilda	N	59.48	57.81	57.83	16.24	18.9			2	2	2
14G0VB119	St Kilda	N	58.72	57.21	57.77	14.75	20.9			2	3	2
14G0VB120	St Kilda	N	60.71	59.77	60.25	16.41	27.3			1	2	2
14G0VB121	St Kilda	N	52.47	50.89	51.28	13.84	16.6			2	3	3
14G0VB122	St Kilda	N	50.78	52.32	52.55	12.94	15.5			2	2	2
14G0VB123	St Kilda	N	47.83	48.55	48.82	13.54	14.8			3	3	2
14G0VB124	St Kilda	N	57.81	56.00	56.34	13.86	20.7			3	2	2
14G0VB125	St Kilda	N	58.25	57.56	57.87	16.13	22.4			2	2	2
14G0VB126	St Kilda	N	49.35	49.33	49.79	13.63	13.1			1	2	2
14G0VB127	St Kilda	N	44.07	41.59	41.93	10.85	7.4			2	3	2
14G0VB128	St Kilda	N	48.42	47.81	47.81	12.52	10.4			2	2	2
14G0VB129	St Kilda	N	54.02	52.70	52.87	15.21	21.1			1	3	1

Glycymeris reference #	*Locality*	*Valve (Right / Left / Articulated)*	*Length (mm)*	*Height (mm)*	*Max Height (mm)*	*Width (mm)*	*Mass of a single valve (g)*	*Periostracum (1-5)*	*Ligament (1-4)*	*Shell margin (1-4)*	*Bioerosion (1-4)*	*Nacre (1-3)*
14G0VB130	St Kilda	N	56.49	54.97	55.32	13.56	9.6			1	1	1
14G0VB131	St Kilda	N	53.28	50.10	50.85	13.90	13.1			2	2	2
14G2VB132	St Kilda	Y	30.23	28.33	28.33	16.52	3.2	5	4	4	4	3
14G2VB133	St Kilda	Y	25.97	24.93	24.93	13.78	1.8	5	4	4	4	3
14G2VB134	St Kilda	Y	26.55	25.67	25.67	13.46	1.9	5	4	4	4	3
14G2VB135	St Kilda	Y	25.05	24.18	24.18	14.09	1.9	5	4	4	4	3
14G2VB136	St Kilda	Y	22.00	19.59	19.59	13.64	1.4	5	4	4	4	3
14G2VB137	St Kilda	Y	25.29	23.72	23.72	14.92	2.2	5	4	4	4	3
14G2VB138	St Kilda	Y	n.a.	n.a.	n.a.	n.a.	n.a.	5	4	n.a.	4	3
14G0VB139	St Kilda	N	60.71	57.18	58.65	16.28	19.9			1	1	2
14G0VB140	St Kilda	N	48.54	49.60	49.60	14.31	17.6			2	4	3
14G0VB141	St Kilda	N	45.34	45.35	45.35	13.91	13.5			2	4	3
14G0VB142	St Kilda	N	50.46	46.81	46.81	13.77	13.6			2	2	2
14G0VB143	St Kilda	N	40.48	38.23	38.23	11.17	7.4			3	4	2
14G0VB144	St Kilda	N	47.12	47.58	47.58	12.41	9.2			1	1	1
14G0VB145	St Kilda	N	45.57	45.36	45.36	12.36	9.0			2	2	2
14G0VB146	St Kilda	N	56.46	55.39	56.66	15.83	17.4			1	1	2
14G0VB147	St Kilda	N	44.90	45.46	45.46	12.14	7.0			1	2	2
14G0VB148	St Kilda	N	45.21	43.93	43.93	12.63	9.6			2	3	2
14G0VB149	St Kilda	N	42.10	43.06	43.06	12.11	10.5			2	3	2
14G0VB150	St Kilda	N	45.58	45.57	45.68	12.45	10.1			2	2	2
14G0VB151	St Kilda	N	45.93	60.39	60.47	15.18	14.5			1	2	2

Glycymeris reference #	*Locality*	*Valve (Right / Left / Articulated)*	*Length (mm)*	*Height (mm)*	*Max Height (mm)*	*Width (mm)*	*Mass of a single valve (g)*	*Periostracum (1-5)*	*Ligament (1-4)*	*Shell margin (1-4)*	*Bioerosion (1-4)*	*Nacre (1-3)*
14G0VB152	St Kilda	N	47.31	45.44	45.72	10.44	8.7			2	2	2
14G0VB153	St Kilda	N	55.36	48.62	50.91	14.35	21.0			2	4	3
14G0VB154	St Kilda	N	40.58	40.09	40.55	12.40	10.6			3	4	3
14G0VB155	St Kilda	N	40.25	n.a.	n.a.	10.67	n.a.			3	4	3
14G0VB156	St Kilda	N	35.89	34.27	34.27	8.36	4.3			3	4	3
14G0VB157	St Kilda	N	64.25	59.26	59.41	17.16	39.7			1	4	2
14G0VB158	St Kilda	N	51.46	48.67	48.98	15.12	19.2			3	4	3
14G0VB159	St Kilda	N	49.59	44.64	47.00	13.01	13.7			2	4	3
14G0VB160	St Kilda	N	42.05	42.60	42.60	11.97	10.7			3	4	3
14G0VB161	St Kilda	N	42.81	42.59	42.89	11.09	8.7			2	4	3
14G0VB162	St Kilda	N	42.25	39.10	39.20	10.24	8.6			3	4	3
14G0VB163	St Kilda	N	45.79	42.12	42.88	11.03	8.6			2	4	3
14G0VB164	St Kilda	N	41.86	39.84	39.84	10.59	8.5			2	4	3
14G0VB165	St Kilda	N	47.61	44.81	47.05	13.57	15.7			3	4	3
14G0VB166	St Kilda	N	40.56	38.02	38.43	10.84	9.2			3	4	3
14G0VB167	St Kilda	N	45.14	42.32	42.58	12.45	8.7			3	4	3
14G0VB168	St Kilda	N	39.38	37.82	38.01	9.91	6.1			3	4	3
14G0VB169	St Kilda	N	38.80	37.09	37.09	9.41	5.3			3	4	3
14G2SN001	Skye	Y	57.95	55.62	55.62	30.08	17.6	5	4	4	4	3
14G2SN002	Skye	Y	52.32	53.19	53.19	30.01	18.5	5	4	4	4	3
14G2SN003	Skye	Y	55.37	54.58	54.58	31.24	20.0	5	4	4	4	3
14G0RH001	Rhum	N	65.46	60.01	60.71	20.39	39.7			2	4	2

Glycymeris reference #	*Locality*	*Valve (Right / Left / Articulated)*	*Length (mm)*	*Height (mm)*	*Max Height (mm)*	*Width (mm)*	*Mass of a single valve (g)*	*Periostracum (1-5)*	*Ligament (1-4)*	*Shell margin (1-4)*	*Bioerosion (1-4)*	*Nacre (1-3)*
14G0RH002	Rhum	N	64.95	65.91	66.50	20.37	46.6			1	4	1
14G0RH003	Rhum	N	63.19	64.63	64.63	17.44	34.7			1	4	1
14G0RH004	Rhum	N	59.03	62.23	62.52	18.80	38.1			3	4	2
14G0RH005	Rhum	N	60.48	60.73	61.76	18.35	31.0			1	3	1
14G0RH006	Rhum	N	59.75	60.02	60.96	18.44	38.2			2	4	1
14G0RH007	Rhum	N	58.33	58.36	58.51	17.30	33.3			2	4	2
14G0RH008	Rhum	N	58.40	57.52	57.76	15.25	30.4			1	4	1
14G0RH009	Rhum	N	57.66	53.83	54.23	14.09	18.7			2	4	1
14G0RH010	Rhum	N	54.75	53.65	53.65	14.55	18.0			2	4	1
14G0RH011	Rhum	N	48.44	50.99	50.99	13.67	17.6			1	4	2
14G0RH012	Rhum	N	47.97	49.96	49.96	13.72	16.0			2	3	1
14G0RH013	Rhum	N	57.23	57.10	57.10	16.80	17.4			1	1	1
14G0RH014	Rhum	N	45.45	45.58	45.58	13.09	14.6			3	4	2
14G0RH015	Rhum	N	46.80	45.31	45.31	11.19	10.0			3	3	1
14G0VB170	St Kilda	N	67.18	67.10	67.37	19.87				1	1	1
14G0VB171	St Kilda	N	60.30	57.13	57.54	18.84				2	1	4
14G0VB172	St Kilda	N	56.84	55.50	56.12	16.70				1	1	1
14G0SN004	Skye	N	62.93	63.45	63.45	19.19		1	3	4	2	4
14G0SN005	Skye	N	53.59	51.86	52.16	16.00		1		2	2	2

Appendix A2 — *Arctica* measurements and shell condition

Arctica reference #	*Locality*	*Live (Y/N)*	*Length (mm)*	*Height (mm)*	*Max Height (mm)*	*Width (mm)*	*Mass of a single valve (g)*	*Periostracum preservation (1-5)*	*Ligament preservation (1-4)*	*Shell margin (1-4)*	*Bioerosion (1-4)*	*Condition of nacre w/in pallial line (1-3)*
16A2VB001	St Kilda	Y	100.05	87.29	95.45	59.28	201.2					
16A2VB002	St Kilda	Y	100.00	85.34	96.03	60.23	228.2					
16A2VB003	St Kilda	Y	97.87	88.33	91.98	64.99	230.4					
16A2VB004	St Kilda	Y	97.63	88.97	97.12	62.20	244.0					
16A2VB005	St Kilda	Y	103.77	87.90	96.98	60.92	202.3					
16A2VB006	St Kilda	Y	93.89	79.90	89.74	52.55	164.6					
16A2VB007	St Kilda	Y	101.66	84.81	96.07	62.86	222.0					
16A2VB008	St Kilda	Y	102.85	89.45	96.58	61.94	212.5					
16A2VB009	St Kilda	Y	99.79	84.28	96.18	60.15	206.6					
16A2VB010	St Kilda	Y	95.67	79.16	90.74	58.70	219.7					
16A2VB011	St Kilda	Y	93.17	83.56	90.55	58.53	187.0					
16A2VB012	St Kilda	Y	92.97	82.16	87.92	58.62	167.8					
16A2VB013	St Kilda	Y	90.65	78.40	84.07	52.50	144.8					
16A0VB014	St Kilda	N	103.48	95.13	100.85	31.81	107.1			4	4	3
16A0VB015	St Kilda	N	101.24	87.78	95.12	30.04	114.1			4	4	3

Arctica reference #	*Locality*	*Live (Y/N)*	*Length (mm)*	*Height (mm)*	*Max Height (mm)*	*Width (mm)*	*Mass of a single valve (g)*	*Periostracum preservation (1-5)*	*Ligament preservation (1-4)*	*Shell margin (1-4)*	*Bioerosion (1-4)*	*Condition of nacre w/in pallial line (1-3)*
16A0VB016	St Kilda	N	96.36	91.31	94.49	56.97	87.8			3	4	1
16A0VB017	St Kilda	N	96.78	89.05	95.46	58.15	97.8			4	4	3
16A0VB018	St Kilda	N	101.97	80.62	96.02	29.59	86.4			3	4	3
16A0VB019	St Kilda	N	93.51	79.50	90.85	26.89	68.7			3	4	3
16A0VB020	St Kilda	N	93.45	78.93	91.71	29.46	93.2			3	4	2
16A2VB021	St Kilda	Y	106.48	87.91	104.79	34.81	121.8					
16A2VB022	St Kilda	Y	102.53	82.74	98.13	29.44	94.9					
16A2VB023	St Kilda	Y	99.40	86.49	92.40	29.95	87.4					
16A2VB024	St Kilda	Y	97.31	86.11	93.75	32.23	106.5					
16A2VB025	St Kilda	Y	100.40	79.10	97.89	32.68	104.0					
16A2VB026	St Kilda	Y	98.93	78.31	94.05	28.60	98.5					
16A2VB027	St Kilda	Y	107.98	84.87	100.65	28.68	96.7					
16A2VB028	St Kilda	Y	98.41	81.42	95.65	29.42	80.9					
16A2VB029	St Kilda	Y	95.89	80.50	94.06	31.27	91.5					
16A2VB030	St Kilda	Y	95.01	76.53	88.98	26.03	87.9					
16A2VB031	St Kilda	Y	95.24	74.59	93.12	27.81	81.4					
16A2VB032	St Kilda	Y	95.99	79.70	89.75	25.19	71.9					
16A2VB033	St Kilda	Y	91.18	77.23	87.25	29.66	79.9					

Arctica reference #	*Locality*	*Live (Y/N)*	*Length (mm)*	*Height (mm)*	*Max Height (mm)*	*Width (mm)*	*Mass of a single valve (g)*	*Periostracum preservation (1-5)*	*Ligament preservation (1-4)*	*Shell margin (1-4)*	*Bioerosion (1-4)*	*Condition of nacre w/in pallial line (1-3)*
16A2VB034	St Kilda	Y	97.98	88.20	96.12	28.18	104.0					
16A0VB035	St Kilda	N	89.00	75.00	82.00	25.00	75.0	2	3	4	4	2
16A0VB036	St Kilda	N	97.50	76.00	81.00	21.50	57.4	3	2	2	4	1
16A0VB037	St Kilda	N	91.50	79.00	82.50	26.00	81.1	2	2	3	4	3
16A0VB038	St Kilda	N	97.00	85.00	92.00	260.00	83.4	2	3	4	4	3
16A0VB039	St Kilda	N	98.00	86.00	93.00	26.30	95.6	3	3	4	4	3
16A0VB040	St Kilda	N	93.28	88.80	104.50	25.60	90.9	2	2	3	4	3
16A0VB041	St Kilda	N	98.00	86.50	93.50	29.50	114.5	3	3	4	4	3
16A0VB042	St Kilda	N	92.60	80.10	84.90	24.80	74.3	2	2	3	4	1
16A0VB043	St Kilda	N	93.00	83.90	88.80	26.2	81.80	2	1	2	4	1
16A0VB044	St Kilda	N	93.00	79.00	92.00	23.00	91.5	3	4	4	4	3
16A0VB045	St Kilda	N	91.97	85.30	87.60	21.50	66.0	3	2	3	4	1
16A0VB046	St Kilda	N	90.00	79.50	85.30	27.20	86.7	2	3	2	4	3
16A0VB047	St Kilda	N	86.60	73.20	82.30	25.60	69.5	2	4	2	4	1
16A0VB048	St Kilda	N	91.50	89.10	89.30	29.90	82.5	4	3	3	4	1
16A0VB049	St Kilda	N	87.60	73.73	85.21	29.00	78.7	2	1	3	4	1
16A0VB050	St Kilda	N	80.24	71.83	75.74	26.30	43.4	2	1	2	4	2
16A0VB051	St Kilda	N	78.08	68.60	74.72	24.17	33.8	2	1	2	4	1
16A0VB052	St Kilda	N	85.94	73.66	80.90	25.53	43.9	2	1	2	4	1
16A0VB053	St Kilda	N	92.00	84.20	86.00	27.80	81.5	3	2	3	4	3
16A0VB054	St Kilda	N	86.80	76.80	81.10	24.30	65.8	3	3	3	4	3

Arctica reference #	*Locality*	*Live (Y/N)*	*Length (mm)*	*Height (mm)*	*Max Height (mm)*	*Width (mm)*	*Mass of a single valve (g)*	*Periostracum preservation (1-5)*	*Ligament preservation (1-4)*	*Shell margin (1-4)*	*Bioerosion (1-4)*	*Condition of nacre w/in pallial line (1-3)*
16A0VB055	St Kilda	N	92.30	80.80	87.20	23.10	86.0	3	2	3	4	3
16A0VB056	St Kilda	N	54.70	49.60	52.60	14.50	13.6	2	1	4	4	1
16A2VB057	St Kilda	Y	101.60	87.10	97.70	32.40	103.6	4	4	4	4	3
16A2VB058	St Kilda	Y	100.90	90.80	96.70	33.60	117.0	2	3	4	4	3
16A2VB059	St Kilda	Y	99.40	90.90	99.40	32.00	128.8	3	5	4	4	3
16A2VB060	St Kilda	Y	99.90	86.90	97.30	27.80	100.2	2	5	4	4	3
16A2VB061	St Kilda	Y	105.00	86.20	95.90	31.90	103.0	3	2	4	4	3
16A2VB062	St Kilda	Y	101.80	88.40	95.20	31.20	96.9	3	3	4	4	3
16A2VB063	St Kilda	Y	97.50	83.70	91.60	32.30	92.3	3	4	4	4	3
16A2VB064	St Kilda	Y	99.40	89.80	96.10	29.10	109.4	2	4	4	4	3
16A2VB065	St Kilda	Y	95.50	86.10	94.50	29.20	92.6	3	4	4	4	3
16A0VB066	St Kilda	N	85.20	74.80	77.50	24.20	46.7	1	1	1	4	2
14A2SN001	Skye North	Y	82.62	72.88	75.64	48.02	44.5	4	4	4	4	3
14A2SN002	Skye North	Y	93.17	73.35	84.86	52.59	60.2	3	4	4	4	3
14A2SN003	Skye North	Y	97.42	81.53	95.18	56.99	70.8	4	4	4	4	3
14A2SN004	Skye North	Y	98.21	78.06	84.13	51.99	63.1	4	4	4	4	3
14A2SN005	Skye North	Y	86.14	76.75	85.25	51.71	58.6	4	4	4	4	3
14A2CN001	Canna North	Y	80.73	70.03	75.23	45.49	44	4	4	4	4	3
14A2CN002	Canna North	Y	81.82	74.32	79.44	50.39	45.8	4	4	4	4	3

Arctica reference #	*Locality*	*Live (Y/N)*	*Length (mm)*	*Height (mm)*	*Max Height (mm)*	*Width (mm)*	*Mass of a single valve (g)*	*Periostracum preservation (1-5)*	*Ligament preservation (1-4)*	*Shell margin (1-4)*	*Bioerosion (1-4)*	*Condition of nacre w/in pallial line (1-3)*
14A2CN003	Canna North	Y	84.75	71.88	80.63	48.17	48.1	4	4	4	4	3
14A2CN004	Canna North	Y	77.93	65.15	72.39	44.02	34.7	4	4	4	4	3
14A2CN005	Canna North	Y	83.14	70.44	77.55	46.66	45.8	4	4	4	4	3
14A2RH001	Rhum	Y	82.1	71.34	76.98	46.72	46.9	3	4	4	4	3
14A2RH002	Rhum	Y	88.88	77.4	84.46	50.04	56.1	3	4	4	4	3
14A2RH003	Rhum	Y	86.85	73.41	83.59	49.78	64.4	2	4	4	4	3
14A2RH004	Rhum	Y	86.01	75.2	84.24	21.6	47.3	1	4	4	4	3
14A2RH005	Rhum	Y	92.49	80.78	88.1	24.01	61	1	4	4	4	3
14A2CN006	Canna North	Y	81.84	69.32	75.43	46.8	42.6	4	4	4	4	3
14A2SN006	Skye North	Y	88.8	78.61	88.3	53.79	66.5	4	4	4	4	3
14A2SN007	Skye North	Y	78.92	71.36	77.68	49.17	47.3	1	4	4	4	3
14A2SN008	Skye North	Y	83.78	74.91	82.79	52.32	63.8	4	4	4	4	3
14A2SN009	Skye North	Y	99.02	78.01	93.18	55.38	85.7	3	4	4	4	3
14A2SN010	Skye North	Y	83.67	76.54	83.53	50.11	55.2	4	4	4	4	3
14A2SN011	Skye North	Y	84.51	71.72	78.44	49.31	49.5	4	4	4	4	3
14A2SN012	Skye North	Y	89.91	76.43	85.76	53.02	62.8	4	4	4	4	3
14A2SN013	Skye North	Y	85.76	74.2	82.78	48.96	48.3	4	4	4	4	3
14A2SN014	Skye North	Y	82.38	73.17	78.42	47.65	49.2	4	4	4	4	3
14A2SS001	Skye South	Y	99.05	84.61	95.74	59.96	102.5	1	4	4	4	3
14A2SS002	Skye South	Y	98.27	89.24	95.32	61.85	92.9	1	4	4	4	3
14A2RH006	Rhum	Y	80.47	70.9	76.05	48.64	52.4	3	4	4	4	3
14A2CN007	Canna North	Y	85.29	72.62	79.22	46.7	42.6	4	4	4	4	3

Arctica reference #	*Locality*	*Live (Y/N)*	*Length (mm)*	*Height (mm)*	*Max Height (mm)*	*Width (mm)*	*Mass of a single valve (g)*	*Periostracum preservation (1-5)*	*Ligament preservation (1-4)*	*Shell margin (1-4)*	*Bioerosion (1-4)*	*Condition of nacre w/in pallial line (1-3)*
14A2CN008	Canna North	Y	75.96	65.4	72.66	43.21	32.7	4	4	4	4	3
14A2CN009	Canna North	Y	73.04	66.14	68.97	42.53	33.1	4	4	4	4	3
14A2CN010	Canna North	Y	76.79	67.56	72.25	44.28	35.4	4	4	4	4	3
14A2CN011	Canna North	Y	81.95	74.45	81.09	49.36	47.9	4	4	4	4	3
14A2CN012	Canna North	Y	82.49	71.21	78.94	44.13	41	4	4	4	4	3
14A2CN013	Canna North	Y	82.61	68.18	76.45	43.07	35.2	4	4	4	4	3
14A2CN014	Canna North	Y						4	4	4	4	3
14A2CN015	Canna North	Y	79.16	68.23	72.36			3	4	4	4	3
14A2SN015	Skye North	Y						4	4	4	4	3
14A2CN016	Canna North	Y	78.79	64.94	73.81	45.26	36.7	4	4	4	4	3
14A2CN017	Canna North	Y	82.64	70.9	78.97	51.92	52.5	4	4	4	4	3
14A2RH007	Rhum	Y	96.91	79.48	88.02	24.33	79.3	1	3	4	4	3
14A2SN016	Skye North	Y	95.83					4	4	4	4	3
14A2SN017	Skye North	Y						3	4	4	4	3
14A2SN018	Skye North	Y							4	4	4	3
14A0VB001	St Kilda	N	94.1	84.61	91.92	24.49	72.2	1	1	2	4	3
14A0RH008	Rhum	N	93.91	86.04	90.19	26.66	66.6	1	1	2	4	1
14A0RH009	Rhum	N	103.14	92.01	98.7	27.93	111.2	1	1	1	4	1
14A0RH010	Rhum	N		83.31	91.33	29.12		1	1	1	4	2
14A0RH011	Rhum	N			85.39			1	1	1	4	2
14A0RH012	Rhum	N							1		1	

Appendix B — Cruise logbook

B/E = Barra, StKB = St Kilda Village Bay, StKp = St Kilda platform, StKn = St Kilda north

Station	*Tow*	*Gear*	*Date*	*Lat*	*Long*	*Lat*	*Long*	*Start*	*End*	*Comments*
1 - B/E	No 1	Sidescan Sonar	28.05.2014	57°01...	7°17...	57°02...	7°16.347	x	19.1	
1 - B/E	Tow 1	Arctica dredge	28.05.2014	57°02.052	7°16.484	57°01.809	7°16.660	32.2	38.7	2 small dead Glycymeris
1 - B/E	Tow 2	Arctica dredge	28.05.2014	57°01.940	7°16.582	57°01.765	7°16.699	35.1	41.1	none (only 2 Venus)
1 - B/E	Tow 3	Arctica dredge	28.05.2014	57°01.776	7°16.059	57°01.648	7°16.749	45.4	63.0	none
1 - B/E	Tow 4	Arctica dredge	28.05.2014	57°01.083	7°16.704	57°01.491	7°16.867	61.5	53.7	2 tiny Glycymeris
1 - B/E	Tow 5	Arctica dredge	28.05.2014	57°01.558	7°16.707	57°01.270	7°17.052	65.9	61.6	none, AD damaged
2 - StKB	No 1	Sidescan Sonar	29.05.2014	57°48.555	8°30.014	57°48.300	8°33.820	63.1	23.0	some patches of bedrock, but mostly free of hazards
2 - StKB	Tow 1	Arctica dredge	29.05.2014	57°48.297	8°33.618	57°48.397	8°32.643	27.0	37.5	empty
2 - StKB	Tow 2	Arctica dredge	29.05.2014	57°48.427	8°32.401	57°48.465	8°31.440	46.2	63.0	2 live, 269 dead Glycymeris
2 - StKB	Tow 3	Arctica dredge	29.05.2014	57°48.471	8°31.26	57°48.456	8°32.135	62.3	53.7	11 dead Glycymeris
2 - StKB	Tow 4	Arctica dredge	29.05.2014	57°48.415	8°32.528	57°48.434	8°31.930	39.8	60.1	empty, dredge didn't stay on bottom
2 - StKB	Tow 5	Arctica dredge	29.05.2014	57°48.470	8°31.705	57°48.415	8°32.515	62.3	40.6	same track as tow 4; 5 dead, 1 articulated Glycymeris
2 - StKB	Tow 6	Arctica dredge	29.05.2014	57°48.544	8°29.997	57°48.499	8°30.782	65.3	62.3	1 live, 32 dead Glycymeris - some big and beautiful ones
2 - StKB	Tow 7	Arctica dredge	29.05.2014	57°48.479	8°30.950	57°48.537	8°30.145	61.7	65.1	8 dead Glycymeris
3 - StKp	No 1	Sidescan Sonar	29.05.2014	57°50.135	8°31.021	57°52.582	8°35.757	68.1	89.1	rocks everywhere

Station	*Tow*	*Gear*	*Date*	*Lat*	*Long*	*Lat*	*Long*	*Start*	*End*	*Comments*
4 - StKn	No 1	Sidescan Sonar	29.05.2014	57°56.495	8°35.337	57°56.325	8°32.966	135.9	127.5	sediment, sand waves
4 - StKn	No 2	Sidescan Sonar	29.05.2014	57°55.758	8°25.477	57°55.608	8°24.152	106.1	104.7	a bit risky, boulders and some bedrock
4 - StKn	No 3	Sidescan Sonar	29.05.2014	57°55.359	8°20.654	57°55.080	8°17.596	132.8	131.6	some sediment, some rocky bits
4 - StKn	Tow 1	Arctica dredge	29.05.2014	57°55.121	8°18.227	57°55.177	8°18.436	138.0	135.9	nothing
4 - StKn	Tow 2	Arctica dredge	29.05.2014	57°55.129	8°18.530	57°55.208	8°19.417	135.1	132.3	2 dead Arctica (1 bag)
2 - StKB	Tow 8	Arctica dredge	29.05.2014	57°48.564	8°30.061	57°48.495	8°30.867	63.7	60.9	1 dead Arctica (1bag), 7 dead Glycymeris (1 bag)
2 - StKB	Tow 9	Arctica dredge	29.05.2014	57°48.574	8°29.993	57°48.500	8°30.774	64.4	61.0	30 dead Glycymeris
2 - StKB	Tow 10	Arctica dredge	29.05.2014	57°48.440	8°31.731	57°48.413	8°32.391	62.3	46.6	2 live Glycymeris (1 bag), 93 dead and 1 articulated Glycymeris
2 - StKB	Tow 11	Arctica dredge	29.05.2014	57°48.453	8°31.743	57°48.436	8°32.313	62.1	48.7	2 live Glycymeris (1 bag), 23 dead and 1 articulated Glycymeris
2 - StKB	No 2	Sidescan Sonar	29.05.2014	57°48.583	8°30.215	x	x	65.1	x	Only sand (one rocky patch)
2 - StKB	Tow 12	Arctica dredge	29.05.2014	57°48.673	8°29.330	57°48.624	8°30.032	70.9	65.1	1 dead Arctica, 16 dead Glycymeris
2 - StKB	No 3	Sidescan Sonar	30.05.2014	57°43.230	8°33.169	57°48.421	8°29.610	34.7	66.9	very rocky, risky, some sandy patches
2 - StKB	No 4	Sidescan Sonar	30.05.2014	57°48.260	8°30.051	57°48.076	8°33.095	65.9	34.4	rocky in 60m depth with occasional sand waves. Good in 40m-section
2 - StKB	Tow 13	Arctica dredge	30.05.2014	57°48.267	8°33.173	57°48.220	8°32.471	32.8	50.9	nothing in dredge. Did not stay on bottom

Station	*Tow*	*Gear*	*Date*	*Lat*	*Long*	*Lat*	*Long*	*Start*	*End*	*Comments*
										because of strong tides
2 - StKB	Tow 14	Arctica dredge	30.05.2014	57°48.289	8°32.908	57°48.676	8°32.399	34.8	47.5	nothing in dredge. Did not stay on bottom because of strong tides
2 - StKB	Tow 15	Arctica dredge	30.05.2014	57°48.704	8°32.157	57°48.143	8°32.338	47.6	58.4	only rocks in dredge. Severe damage to AD. Have to use 2nd dredge.
2 - StKB	Tow 16	Beam Trawl	30.05.2014	57°48.442	8°32.671	57°48.396	8°31.587	37.6	61.2	no shells
2 - StKB	Tow 17	Beam Trawl	30.05.2014	57°48.437	8°31.981	57°48.371	8°33.093	57.0	33.4	1 live Glycymeris, 45 dead Glycymeris
2 - StKB	Tow 18	Beam Trawl	30.05.2014	57°48.374	8°32.982	57°48.491	8°31.667	34.1	60.5	2 dead Glycymeris
2 - StKB	Tow 19	Beam Trawl	30.05.2014	57°48.514	8°30.646	57°48.507	8°29.575	60.6	64.8	4 live Glycymeris, 50 dead Glycymeris
2 - StKB	Tow 20	Beam Trawl	30.05.2014	57°48.595	8°29.497	57°48.530	8°30.767	65.7	59.9	51 dead Glycymeris
5 - Skye north	No 1	Sidescan Sonar	31.05.2014	57°36.999	6°33.160	57°36.548	6°28.230	47.3	65.9	Turned through dog-leg into loch
5 - Skye north	No 2	Sidescan Sonar	31.05.2014	57°36.491	6°28.128	57°34.520	6°28.042	65.1	55.9	Turned through dog-leg into loch
5 - Skye north	No 3	Sidescan Sonar	31.05.2014	57°32.184	6°27.605	57°31.043	6°27.445	77.2	47.5	
5 - Skye north	Tow 1	Arctica dredge	31.05.2014	57°31.104	6°27.451	57°31.418	6°27.471	48.3	74.6	9 dead, 3 damaged Glossus
5 - Skye north	Tow 2	Arctica dredge	31.05.2014	57°32.650	6°27.732	57°33.023	6°27.899	65.1	62.3	broken Arctica, articulated hinge, part of animal attached = live!

Station	*Tow*	*Gear*	*Date*	*Lat*	*Long*	*Lat*	*Long*	*Start*	*End*	*Comments*
5 - Skye north	Tow 3	Arctica dredge	31.05.2014	57°34.773	6°28.037	57°35.152	6°28.013	57.3	60.5	1 articulated Glossus
5 - Skye north	Tow 4	Arctica dredge	31.05.2014	57°35.293	6°27.998	57°35.695	6°27.909	61.6	65.5	empty
5 - Skye north	Tow 5	Arctica dredge	31.05.2014	57°35.845	6°27.876	57°36.224	6°27.872	65.5	69.1	empty
5 - Skye north	Tow 6	Arctica dredge	31.05.2014	57°36.350	6°27.903	57°36.561	6°28.314	69.3	69.4	empty
5 - Skye north	Tow 7	Arctica dredge	31.05.2014	57°36.597	6°28.460	57°36.644	6°28.985	70.5	73.0	empty
5 - Skye north	Tow 8	Arctica dredge	31.05.2014	57°36.799	6°30.896	57°36.856	6°31.421	63.4	55.5	4 live Arctica, 5 broken Arctica, 1 umbo, 6 small Arctica
5 - Skye north	Tow 9	Arctica dredge	31.05.2014	57°36.898	6°31.583	57°36.816	6°31.241	52.6	60.4	1 dead Arctica, 2 damaged Arctica, 2 damaged Glycymeris
5 - Skye north	Tow 10	Arctica dredge	31.05.2014	57°36.805	6°30.921	57°36.892	6°31.606	62.6	51.9	5 live Arctica + 1 live damage umbo, 3 dead Arctica, 5 damaged Arctica, 1 small Arctica
5 - Skye north	Tow 11	Arctica dredge	31.05.2014	57°36.869	6°31.517	57°36.950	6°32.094	52.3	45.9	1 live Arctica, 1 live Glycymeris, 1 dead Arctica, 6 damaged Arctica + bits, 6 damaged Glycymeris, 22 dead Glycymeris
5 - Skye north	Tow 12	Arctica dredge	31.05.2014	57°36.938	6°32.057	57°36.900	6°31.859	46.2	47.6	2 Arctica, 8 Glycymeris

Station	*Tow*	*Gear*	*Date*	*Lat*	*Long*	*Lat*	*Long*	*Start*	*End*	*Comments*
5 - Skye north	Tow 13	Arctica dredge	31.05.2014	57°36.899	6°31.796	57°36.847	6°31.312	48.4	60.5	1 damaged Arctica
5 - Skye north	Tow 14	Arctica dredge	31.05.2014	57°36.826	6°31.273	57°36.881	6°31.764	59.5	48.4	2 live Arctica (1 broken), 2 dead and 3 damaged Arctica, 3 dead and 1 damaged Glycymeris
5 - Skye north	Tow 15	Arctica dredge	31.05.2014	57°36.852	6°31.450	57°36.799	6°31.119	52.1	61.8	1 live Arctica, 12 dead Arctica, 1 broken Arctica
5 - Skye north	Tow 16	Arctica dredge	31.05.2014	57°36.789	6°31.301	57°36.884	6°32.062	54.4	42.6	1 live Glycymeris, 2 dead Arctica, 3 dead Glycymeris
5 - Skye north	Tow 17	Arctica dredge	31.05.2014	57°36.930	6°31.871	57°36.846	6°31.288	45.1	59.4	1 live Arctica, 1 dead Glycymeris
5 - Skye north	Tow 18	Arctica dredge	31.05.2014	57°36.865	6°31.190	57°36.942	6°31.975	64.1	43.8	13 dead Glycymeris, 3 broken Arctica
5 - Skye north	Tow 19	Arctica dredge	31.05.2014	57°36.949	6°31.823	57°36.860	6°31.094	44.4	63.7	2 live Arctica (1 broken), 1 live Glycymeris
6 - Skye south	No 1	Sidescan Sonar	31.05.2014	57°19.194	6°32.055	57°12.9598	6°32.304	69.1	>90	many crazy rocks, steep holes, but also some good sediment parts
6 - Skye south	Tow 1	Arctica dredge	31.05.2014	57°14.625	6°32.296	57°14.892	6°32.351	66.5	73.7	2 dead Arctica + flesh from Arctica on the outside => go back?; Dredge damaged

Station	*Tow*	*Gear*	*Date*	*Lat*	*Long*	*Lat*	*Long*	*Start*	*End*	*Comments*
6 - Skye south	Tow 2	Arctica dredge	31.05.2014	57°16.396	6°32.317	57°16.528	6°32.340	64.8	63.0	(data of end of tow not precise) nothing, only rocks in AD
6 - Skye south	Tow 3	Arctica dredge	31.05.2014	57°17.318	6°32.333	57°17.228	6°32.331	64.8	55.1	1 dead Arctica
6 - Skye south	Tow 4	Arctica dredge	31.05.2014	57°17.305	6°32.334	57°17.191	6°32.302	62.3	54.4	1 live Arctica (broken, removed flesh before bagging) and 6 dead Arctica, 1 dead Glycymeris
6 - Skye south	Tow 5	Arctica dredge	31.05.2014	57°17.297	6°32.324	57°17.174	6°32.322	58.7	54.4	1 live Arctica (broken, removed flesh before bagging), 3 dead Arctica (1 broken in 2 pieces)
6 - Skye south	Tow 6	Arctica dredge	31.05.2014	57°17.104	6°32.312	57°16.923	6°32.292	55.1	60.1	1 dead Arctica, 1 piece of a live Arctica (found flesh)
7 - Canna north	No 1	Sidescan Sonar	01.06.2014	57°03.047	6°25.973	57°03.721	6°28.868	202.4	75.9	surveying started at 3:34 due to depth (57°03.347, 6°27.712)
7 - Canna north	No 2	Sidescan Sonar	01.06.2014	57°03.721	6°28.868	57°04.882	6°28.571	75.9	35.9	
7 - Canna north	Tow 1	Arctica dredge	01.06.2014	57°03.422	6°28.193	57°03.521	6°28.631	74.4	71.6	5 live Arctica, 2 broken dead Arctica

Station	*Tow*	*Gear*	*Date*	*Lat*	*Long*	*Lat*	*Long*	*Start*	*End*	*Comments*
7 - Canna north	Tow 2	Arctica dredge	01.06.2014	57°04.064	6°28.733	57°03.874	6°28.798	119.2	98.0	1 dead Arctica, 1 dead Glycymeris
7 - Canna north	Tow 3	Arctica dredge	01.06.2014	57°03.508	6°28.594	57°03.446	6°28.331	71.2	73.4	empty
7 - Canna north	Tow 4	Arctica dredge	01.06.2014	57°03.486	6°28.460	57°03.403	6°28.080	71.6	74.4	empty
7 - Canna north	Tow 5	Arctica dredge	01.06.2014	57°03.433	6°28.251	57°03.380	6°27.899	75.9	70.1	16 (2 of them broken and put in extra bag) live Arctica, 1 articulated broken Arctica
7 - Canna north	Tow 6	Arctica dredge	01.06.2014	57°03.442	6°28.281	57°03.393	6°27.921	75.9	74.4	7 live Arctica, 3 dead Arctica
7 - Canna north	Tow 7	Arctica dredge	01.06.2014	57°03.447	6°28.291	57°03.372	6°27.943	75.9	74.4	1 live Arctica, 3 dead Arctica
8 - Canna south	No 1	Sidescan Sonar	01.06.2014	57°01.002	6°27.389	57°01.005	6°35.449	78.7	88.7	
8 - Canna south	Tow 1	Arctica dredge	01.06.2014	57°00.992	6°34.306	57°00.994	6°33.832	80.1	79.8	empty
8 - Canna south	Tow 2	Arctica dredge	01.06.2014	57°01.004	6°32.868	57°00.998	6°31.967	81.6	94.4	empty

Station	*Tow*	*Gear*	*Date*	*Lat*	*Long*	*Lat*	*Long*	*Start*	*End*	*Comments*
9 - Rhum NW	No 1	Sidescan Sonar	01.06.2014	57°02.637	6°24.503	57°00.666	6°28.287	64.4	40.0	end coordinates not precise
9 - Rhum NW	Tow 1	Arctica dredge	01.06.2014	57°02.479	6°24.652	57°02.177	6°25.094	53.0	58.8	2 dead Arctica (1 of them broken)
9 - Rhum NW	Tow 2	Arctica dredge	01.06.2014	57°01.889	6°25.658	57°01.630	6°26.326	42.0	91.6	1 broken dead Arctica
9 - Rhum NW	Tow 3	Arctica dredge	01.06.2014	57°01.055	6°27.408	57°00.819	6°27.975	88.7	38.7	6 live Arctica (2 of them broken, removed flesh from one of them), 4 dead Arctica (one of them only umbo, one broken), 20 dead Glycymeris. AD teeth bent
9 - Rhum NW	Tow 4	Arctica dredge	01.06.2014	57°01.088	6°27.327	57°00.887	6°27.883	98.7	44.1	2 live Arctica (both broken) put in separate bags. 1 piece of dead Arctica. AD damaged.
7 - Canna north	Tow 8	Beam Trawl	01.06.2014	57°03.429	6°28.045	57°03.474	6°28.303	75.9	77.3	4 dead Arctica (3 small, 1 piece of big)
7 - Canna north	Tow 9	Beam Trawl	01.06.2014	57°03.445	6°28.202	57°03.459	6°28.065	75.9	77.3	no shells, very muddy sand

Station	*Tow*	*Gear*	*Date*	*Lat*	*Long*	*Lat*	*Long*	*Start*	*End*	*Comments*
7 - Canna north	Tow 10	Beam Trawl	01.06.2014	57°03.425	6°28.306	57°03.312	6°27.594	73.7	78.7	4 dead Arctica (2 small complete, 1 small broken, 1 large articulated broken)
7 - Canna north	Tow 11	Day Grab	01.06.2014	57°03.469	6°28.290	57°03.504	6°28.306	77.3	80.9	one bag of sediment was collected. No shells
7 - Canna north	Tow 12	Day Grab	01.06.2014	57°03.444	6°28.339	57°03.458	6°28.346	73.0	74.4	no shells
7 - Canna north	Tow 13	Day Grab	01.06.2014	57°03.464	6°28.331	57°03.482	6°28.361	75.9	75.9	no shells
10 - Loch Shiel	No 1	Sidescan Sonar	02.06.2014	56°46.700	5°54.173	56°48.672	5°57.727	33.0	65.9	dogleg transect. Rocky for the most part, sediment towards the end
10 - Loch Shiel	No 2	Sidescan Sonar	02.06.2014	56°48.550	5°57.064	56°48.233	5°56.353	55.8	29.8	sediment, then rock
10 - Loch Shiel	Tow 1	Arctica dredge	02.06.2014	56°48.172	5°57.476	56°48.771	5°57.311	52.2	64.4	curved line between these points. Empty
10 - Loch Shiel	No 3	Sidescan Sonar	02.06.2014	56°48.560	5°57.303	56°47.509	6°01.134	59.4	69.4	sediment almost all the way
10 - Loch Shiel	Tow 2	Arctica dredge	02.06.2014	56°47.673	6°00.577	56°47.760	6°00.235	76.6	77.3	empty

Station	*Tow*	*Gear*	*Date*	*Lat*	*Long*	*Lat*	*Long*	*Start*	*End*	*Comments*
10 - Loch Shiel	Tow 3	Arctica dredge	02.06.2014	56°47.787	6°00.083	56°47.917	5°59.458	76.1	69.8	empty
10 - Loch Shiel	Tow 4	Arctica dredge	02.06.2014	56°48.147	5°58.612	56°48.263	5°58.123	45.9	61.6	2 broken Arctica. Dredge damaged